A NON-INVASIVE SPEED AND POSITION SENSOR FOR INDUCTION MACHINES USING EXTERNAL SEARCH COILS

A THESIS SUBMITTED TO
THE GRADUATE SCHOOL OF NATURAL AND APPLIED SCIENCES
OF
MIDDLE EAST TECHNICAL UNIVERSITY

BY

OZAN KEYSAN

IN PARTIAL FULFILMENT OF THE REQUIREMENTS
FOR
THE DEGREE OF MASTER OF SCIENCE
IN
ELECTRICAL AND ELECTRONICS ENGINEERING

DECEMBER 2008

Approval of the thesis

A NON-INVASIVE SPEED AND POSITION SENSOR FOR INDUCTION MACHINES USING EXTERNAL SEARCH COILS

Submitted by **OZAN KEYSAN** in partial fulfilment of the requirements for the degree of **Master of Science in Electrical and Electronics Engineering, Middle East Technical University** by,

Prof. Dr. Canan ÖZGEN
Dean, Graduate School of **Natural and Applied Sciences** _____

Prof. Dr. İsmet ERKMEN
Head of Department, **Electrical and Electronics Engineering** _____

Prof. Dr. H. Bülent ERTAN
Supervisor, **Electrical and Electronics Engineering, METU** _____

Examining Committee Members:

Prof. Dr. Muammer ERMİŞ
Electrical and Electronics Engineering, METU _____

Prof. Dr. H. Bülent ERTAN
Electrical and Electronics Engineering, METU _____

Assoc. Prof. Tolga ÇİLOĞLU
Electrical and Electronics Engineering, METU _____

Assist. Prof. Dr. M. Timur AYDEMİR
Electrical and Electronics Engineering, Gazi University _____

Dr. Erbil NALÇACI
EPDK (Retired) _____

Date: 30**.12.2008**

I hereby declare that all information in this document has been obtained and presented in accordance with academic rules and ethical conduct. I also declare that, as required by these rules and conduct, I have fully cited and referenced all material and results that are not original to this work.

Ozan KEYSAN

ABSTRACT

A NON-INVASIVE SPEED AND POSITION SENSOR FOR INDUCTION MACHINES USING EXTERNAL SEARCH COILS

KEYSAN, OZAN
M.Sc., Department of Electrical and Electronics Engineering
Supervisor: Prof. Dr. H. Bülent ERTAN

December 2008, 214 pages

In industrial drives market, speed and position estimation are one of the most important subjects for accurate motor drives. Vector controlled drives has the best dynamic performance among AC motor drives. Sensorless vector control is one of the most studied one. However, sensorless drive systems fail at low or zero speeds and may not have enough accuracy. For better accuracy and speed range speed sensors or position encoders are usually essential. However, coupling of sensor and sensor prices introduces extra cost on the drive. Thus in order to reduce the cost of the drive a cheap and easy to mount speed sensor is essential.

Throughout this study, a speed and position sensor using an external search coil placed between cooling fins on the frame of an induction machine is proposed. The search coil utilizes the fringing flux outside the frame of induction motor. Using the induced voltage on the external search coil, a new method that estimates the flux and rotor position is proposed.

In this study, the induced voltage on the search coils are investigated with different types of search coils placed on various positions. The frequency domain and

time domain analysis are performed in order to build a model that can estimate machine flux, rotor speed and rotor position.

As a result of this study, a low cost, easy to mount speed and position sensor is designed and implemented. Experiment results are presented.

Keywords: Search coil, speed estimation, position estimation, rotor slot harmonics, fringing flux

ÖZ

ASENKRON MOTORLAR İÇİN HARİCİ BOBİN İLE MODİFİYESİZ HIZ VE POZİSYON ALGILAYICISI

KEYSAN, OZAN
Yüksek Lisans, Elektrik Elektronik Mühendisliği Bölümü
Tez Danışmanı: Prof. Dr. H. Bülent ERTAN

Aralık 2008, 214 sayfa

Endüstriyel sürücü pazarında, hız ve pozisyon kestirimi hassas motor sürücüleri için en önemli konulardan biridir. Vektör kontrollü AC sürücüler diğer sürücüler arasında en iyi dinamik performansa sahiptirler. Duyargasız vektör sürücüleri en çok araştırılan konulardan birisidir. Ancak, duyargasız sürücüler genellikle düşük ve sıfır hızda başarısız olurlar ya da yeterli hassasiyet sağlayamazlar. Daha fazla hassasiyet ve çalışma aralığı için hız veya pozisyon sensörleri genellikle gereklidir. Ancak, sensörlerin montajı ve sensör fiyatları sürücü için ayrıca masraf getirir. Sürücü fiyatını düşürmek için, ucuz ve montajı kolay hız sensörleri gereklidir.

Bu çalışmada, asenkron bir makinenin dışına yerleştirilen harici bir bobin kullanılarak yapılan bir hız ve pozisyon sensörü önerilmiştir. Harici bobin, endüksiyon motorunun dışına taşan akıyı kullanır. Harici bobinde indüklenen gerilim kullanılarak, akı ve rotor pozisyonunu tahmin eden yeni bir metot önerilmiştir.

Bu çalışmada, harici bobinlerde indüklenen gerilim değişik bobinlerle ve çeşitli pozisyonlarda araştırılmıştır. Makinenin aksını, rotor hızını ve rotor pozisyonunu tahmin edecek bir model oluşturabilmek için frekans alanında ve gerçek zamanda analizler yapılmıştır.

Sonuç olarak bu çalışmada, düşük maliyetli ve montajı kolay bir hız ve pozisyon sensörü tasarlanmış ve gerçekleştirilmiştir. Deney sonuçları sunulmuştur.

Anahtar Kelimeler: algılayıcı bobin, hız tahmini, pozisyon tahmini, rotor oluk harmonikleri, taşan akı

ACKNOWLEDGEMENTS

I express sincere appreciation to Prof. Dr. H. Bülent Ertan for his valuable guidance throughout all stages of this study.

I would like to thank Volkan Sezgin and Ahmet Cemal Durgun for their precious suggestions, encouragement and willingness for help in all phases of this study.

I would also like to thank department technicians; Bünyamin Bostan, Hamis Erdem, Hakan Balcı and Zekeriya Özgün for their effort, precious suggestions and help for experiments and hardware setup of this study.

Also I would like to thank my dear wife Asuman Özgür Keysan and my whole family for their encouragement and precious support during my life.

TABLE OF CONTENTS

LIST OF TABLES

LIST OF FIGURES

LIST OF SYMBOLS

A	Amplitude
A_v	Magnitude of v^{th} harmonic component
α	Harmonic order
B	Magnetic Flux density
B_0	Fundamental component of flux density
δ	Angle between search coil magnetic axis and stator phase A magnetic axis.
$\Delta L_{\sigma s}$	Differential stator transient inductance
$\Delta\theta$	Position variation step
E_a	Magnetizing voltage
$\varepsilon(f_r)$	Average error in rotor frequency
$\varepsilon(f_{rsh})$	Average error in rotor slot harmonics
$\varepsilon(f_s)$	Average error in fundamental supply frequency
$\Sigma L_{\sigma s}$	Average stator transient inductance
F_1	Magnitude of MMF fundamental component
f_C	Center frequency of filter
f_h	Frequency of harmonics
f_H	Higher cut off frequency of filter
f_L	Lower cut off frequency of filter
f_R	Rotor slot permeance variation frequency
fr	Rotor electrical speed in Hz
f_{range}	Frequency range of spectral analysis
$f_{resolution}$	Frequency resolution of spectral analysis
f_{rsh}	Frequency of rotor slot harmonics
f_s	Supply frequency
f_{samp}	Sampling frequency
f_{window}	Frequency window interval of spectral analysis
Φ	Flux

Φ_i Phase shift of the i^{th} component

Ψ Phase angle

Ψ_v Phase of the v^{th} harmonic component

h Harmonic order of saliency

h_i Harmonic number of the sinusoidally distributed saliency causing the i^{th} component

I_{cn} Negative sequence component of induced currents

I_{cni} Magnitude of the i^{th} component of the negative sequence current

I_{cp} Positive sequence component of induced currents

I_s Motor phase current

I_{coil} Coil passes from the search

i^s_{qdr} Rotor d-q axis current in stationary reference frame

i^s_{qds} Stator d-q axis current in stationary reference frame

K_1, K_f, K_r Magnitudes of signals

L_{lr} Rotor leakage inductance

L_{ls} Stator leakage inductance

L_m Mutual inductance

L_r Rotor inductance

L_s Stator inductance

$L_{\sigma s}$ Stator transient inductance

λ Stator Flux linkage

λ_{av} Average magnitude of permeance

λ_{var} Magnitude of permeance fluctuation

M_{coil_a}, M_{coil_b}, M_{coil_c} Mutual inductance between search coil and stator windings

N Number of Turns

k, n Positive integer (1,2,3,...)

N Pulse/revolution of encoder

N_1 Turns ratio between leakage branch and the search coil

N_2 Turns ratio between magnetizing branch and the search coil

n_d Order of eccentricity

Nr Rotor speed (RPM)

p Derivative operation

P	Number of pole pairs
r_{coil}	Search coil resistance
r_r	Rotor resistance
r_s	Stator resistance
T	Period of the signal
t	Time
θ	Mechanical angle
θ_{ei} :	Angular position of the sinusoidally distributed saliency causing the i^{th} component
θ_r	Rotor position in electrical degree
v	Stator harmonics of the power supply driving the motor (v=1, 3, 5...)
$V_{induced}$	Induced Search Coil Voltage
v^s_{qdr}	Rotor d-q axis voltage in stationary reference frame
v^s_{qds}	Stator d-q axis voltage in stationary reference frame
V_t	Motor terminal voltage
V_m	Magnetizing voltage
w_c	Carrier signal frequency
w_r	Angular velocity
w_{rshi}	Rotor slot harmonic for an inverter
w_s	Angular velocity of the power supply
Z	Number of rotor slots

CHAPTER 1

INTRODUCTION

1.1 Introduction

In recent years, alternating current motors which can have simple and rugged structure, high maintainability and economy; that are also robust and immune to heavy overloading are widely used in industrial applications. [1]. However, the speed or torque control of induction machines is more difficult than DC motors due to their nonlinear and complex structure.

Field-oriented control techniques have made possible the development of high dynamic performance induction motor drives. Field orientation control can be achieved in two ways, direct flux orientation and indirect field orientation. Direct field orientation is achieved by direct measurement of the flux [1]. Direct field orientation requires Hall probes or other sensors which requires a specially modified machine. Indirect field orientation is usually preferred because the method does not need modification to the machine. On the other hand, indirect field orientation needs machine parameters for correct alignment of dq reference frame with the rotor flux vector [36]. But motor parameters change during the machine operation due to temperature change or flux variation. In order to compensate these variations online parameter identification techniques or adaptive control techniques are used.

Voltage model for indirect field orientation is the most widely used technique; however it faces difficulties in low speeds. This is due to the difficulty in ideal integration with very low voltage signals and difficulty in estimating stator resistance which becomes more dominant at lower frequencies [50].

Current model for indirect field orientation has much better characteristics than voltage model at low speeds. But, flux estimation using the current model needs a

speed sensor. And since rotor position is not same with rotor flux position in an induction machine a flux estimation loop is still necessary. Using this method, satisfactory control can be achieved down to zero speeds. However, using a speed sensor or encoder implies additional electronics, extra wiring, extra spaces and careful mounting, all decreasing the robustness of the drive [3]. Also, for low power drives the cost of sensor is comparable with the cost of the motor [36].

Other rotor flux estimation methods are available only using machine electrical measurements such as, model reference adaptive systems and extended Kalman filters. All these methods are parameter dependent, thus parameter errors can affect accuracy of the methods [37]. However these methods offer fast speed estimation and extended speed range.

To estimate rotor speed and rotor position different techniques may be applied. One method is to superimpose a high frequency sinusoidal signal to acquire a current signal that is related with rotor flux position [7, 9, 10]. In this method, the superimposed signal generates harmonics in the air gap flux thus, in stator phase currents in a voltage source controlled inverter. The frequency of the harmonics is directly related with rotor speed. But in order to obtain a reasonable signal the magnitude of this superimposed signal should be large, which causes torque ripples and increased losses.

Another method is to utilize the existing saliencies for rotor position and speed estimation [2]. Every type of electric machine has some form of saliency present in it. Saliencies provide indirect information about the machine operation such as, saturation, rotor eccentricity, faults etc. Saliencies are generally generates time varying air gap permeance. This permeance variation modulates the air gap flux and they have been detected in many ways in literature. Measuring phase voltage, phase current or neutral point voltage is the most common methods. The most commonly used saliency that all machines have is the slot harmonics caused by the permeance variations of rotor and stator slots. The speed estimation using rotor slot harmonics has the advantage of the estimation will be independent of machine parameters. On the other side, this estimation will need some kind of signal processing as will be explained in following chapters.

To detect saliencies of the machine and estimate position of the rotor flux, the placement of a search coil inside the machine is a known method [43, 44]. However, the modification of the machine for installation of search coil makes this method impractical. In this study, instead of an internal search coil an external search coil which is mounted on the frame of the machine will be used. By measuring the induced voltage on the external search coil valuable information about rotor position, rotor speed and air gap flux can be obtained.

1.2 Brief Introduction of the Proposed Method

In an induction machine, most of the flux generated by the stator windings crosses the air gap and links the stator and rotor windings, which is called mutual flux. Most of this flux flows over the stator core. A small part of the flux also links the stator core and travels through the frame of the motor, which is called fringing mutual flux. In this thesis, a search coil, wrapped around a laminated core is placed on the frame of the machine, between the cooling fins. By placing a search coil on the outside of the frame, some part of fringing mutual flux links the search coil and induces an observable voltage on the search coil. The basic visualization of the method is given in Fig. 1-1.

The induced voltage on a search coil can be expressed using equation (1-1)

$$V_{induced} = \mathrm{r_{coil}}.\mathrm{i_{coil}} + N.\frac{d\Phi}{dt} \qquad (1\text{-}1)$$

Where, Φ is the total flux linking the search coil. The fringing flux linking carries some important information such as; air gap flux magnitude and position, slot harmonics, etc. If no current is drawn from search coil the induced voltage on the search coil is directly related with the fringing flux that links the search coil. In this thesis, the relation between the induced search coil voltage and the machine flux will be studied. It is aimed to find out whether it is possible to detect the stator flux position, rotor speed and rotor position means of some signal processing using the induced voltage on the search coil.

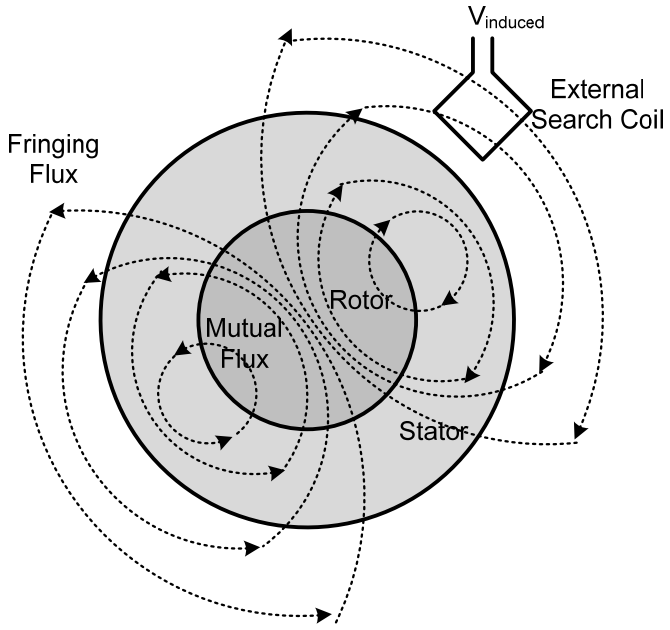

Fig. 1-1 Schematic of the proposed method

In literature, there are few studies that utilizes external search coil. One of the most comprehensive study is "Condition monitoring of squirrel-cage motors by axial magnetic flux measurements" by Voitto Kokko, [45]. In [45], the axial flux is measured by an external search coil and captured data is analyzed for condition monitoring of induction-cage motors. Also M. D. Negrea have studied this subject in [2]. G. A. Capolino, J. F. Brudny, D. Belkhayat has also presented valuable studies in measuring the leakage flux by an external sensor [28, 46, 47]. All these studies aim to improve the condition monitoring for electrical machines. They try to capture harmonics caused by broken rotor bars, worn bearings, etc. by axial or radial leakage flux sensors. But none of them tries to estimate the rotor speed by external sensors.

1.3 Investigation of Rotor Speed Estimation Methods

In this part, some rotor speed estimation methods in the literature will be studied. The studied methods are; methods utilizing asymmetric rotor cage harmonics, estimation using higher frequency carrier signal injection and the methods utilizing rotor slot harmonics. These methods estimate speed from the

saliencies that are present in the machine or may introduce some modifications to create a saliency.

Every type of electric machine has some form of saliency present in it. Saliencies provide indirect information about the machine operation such as, saturation, rotor eccentricity, faults etc. Saliencies can also be used for the estimation of rotor position or flux angle. By this way, rotor speed or position can be estimated from the saliencies measured. Saliencies create some harmonic components in the air gap; these harmonics of an induction motor fed by a sinusoidal voltage source can be classified as [5];

- Stator and rotor magnetomotive force (MMF) harmonics
- Stator and rotor slot permeance harmonics
- Air gap eccentricity harmonics
- Permeance harmonics introduced by saturation.

These harmonics in the air gap appear also in the stator voltage, stator current and leakage flux. Determining saliency harmonics from the stator voltage and current induced harmonics are rather a common method in literature. Other saliency measurement techniques are [5];

- Indirect, static measurements of saliencies can be obtained by using inductance variation as a function of flux or rotor angle.
- Hall Effect sensors or sensing coils.

The purpose of this section is to investigate the saliency measurement methods in literature and to compare the proposed method with the previous studies. The investigated methods in literature can be classified mainly in three groups;

- Methods utilizing asymmetric rotor cage harmonics [6, 7]
- Method of high frequency signal injection [8, 9,10]
- Methods utilizing rotor slot harmonics. [11, 12]

In this chapter, these methods will be compared and mainly stator and rotor permeance harmonics will be studied.

Spectral analysis techniques are mostly used methods. Employing spectral harmonic technique is shown to be useful in obtaining accurate speed estimation along with the above methods. Spectral analysis can be applied by using on one of

the following approaches; [4]

- The analysis of the phase current in a voltage controlled inverter
- The analysis of the phase voltage in a current controlled inverter
- The higher frequency signal injection into PWM signals.

For spectral analysis of the measured data Fast Fourier Transform is used most commonly. In the following chapters experiments are also performed using FFT analysis.

1.3.1 Speed Estimation Utilizing Asymmetric Rotor Cage Harmonics

This approach uses a specially designed rotor with a circumferential variation in rotor leakage inductance [7] or circumferential variation in rotor resistance [6] as stated in [13]. It is obvious that this special rotor design introduces extra cost and modification compared to normal induction motors. The asymmetrical rotor leakage inductance due to rotor geometry, proposed in [7] is given in Fig. 1-2. In this rotor type, the rotor slot opening width varies spatially. The narrow slot openings give higher leakage where wide slot openings give low leakage as shown in Fig. 1-2.

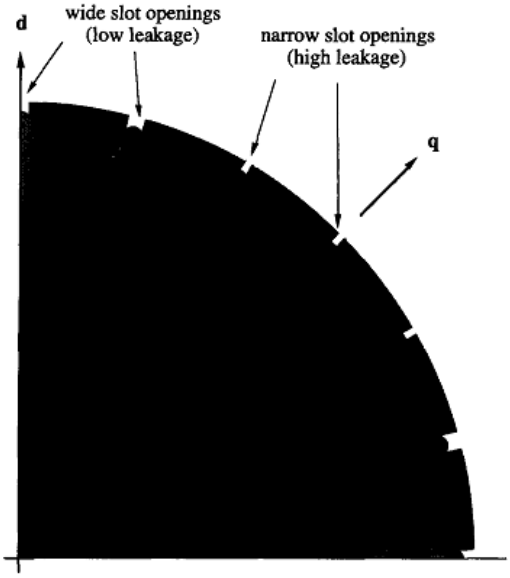

Fig. 1-2 Rotor of a squirrel-cage induction motor with spatially variant rotor leakage inductance created via modulation in the width of the slot openings [7]

Another method is proposed in [6], an asymmetrical rotor resistance is used with a double cage rotor whose cross section is given in Fig. 1-3. In this rotor type, outer cage has higher resistance than the inner. Furthermore, the leakage inductance of the outer cage is significantly lower than the inner section. [6] This asymmetry of the rotor cage will induce rotor position dependent harmonics in the phase currents of the machine. In this study it is shown that, rotor position can be accurately calculated by some means of signal processing and filtering techniques. The disadvantage of this method is; it requires specially designed machine to create position harmonics. Also, small slip frequency currents flow in the outer section giving rise to a small slip-dependent torque ripple.

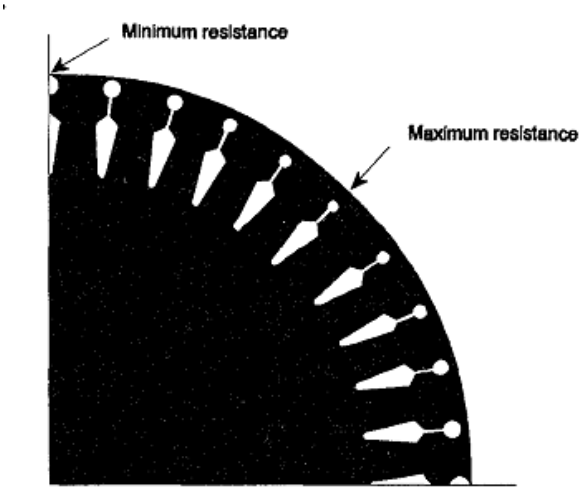

Fig. 1-3 Rotor of a four pole, double cage, induction motor with sinusoidal variation of the outer cage resistance [6]

Another method is to use magnetic asymmetries rather than the mechanical asymmetries. Thus, this method does not require any modification to machine. The saturation in an induction machine is also a parameter that can be used to measure the position of air gap flux. It is stated in [14, 15] that saturation in the machine iron produces a third harmonic component of the flux. In [14], a d-q model is derived

from the conventional constant parameter ac machine model, which is modified to account for the saturation. This modification consists of making the air gap length a function of the air gap flux position and amplitude. It is shown that as a consequence of the saturation, a third harmonic flux component exists, and third harmonic currents are induced in the rotor circuit. An equivalent circuit for the induction machine operating under saturation is developed in [14], the equivalent circuit is given in Fig. 1-4. The derivation of equivalent circuit and saturation elements can be found in [14].

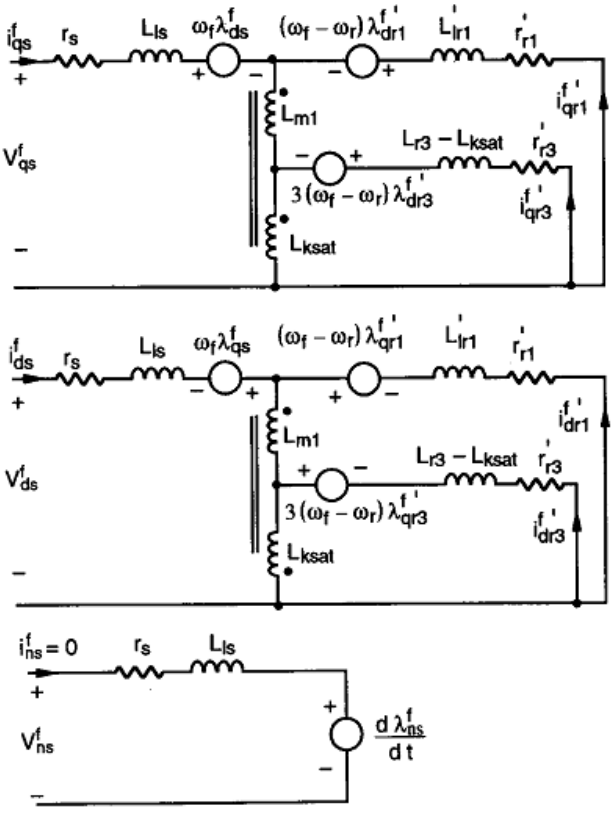

Fig. 1-4 Equivalent circuit for a saturated inductance machine [14]

The third harmonic air gap flux linking the stator spatial winding third harmonic component is responsible for the induction in the stator phases of a zero sequence third harmonic voltage. Since no third harmonic currents will flow in a wye

connected machine. The rotating third harmonic component of the flux links the stator windings. This produces a zero sequence third harmonic voltage in the stator phase voltages. When the three-phase voltages are summed, the fundamental supply harmonics and characteristic harmonics are cancelled and the resultant waveform contains, mainly, a third harmonic voltage signal, which can be used as a means of locating the machine air gap flux.

This model introduces no modification to motor but on the other hand, it needs more than locked rotor and no-load test such as; number of stator turns, rotor, slot stator number, in order to obtain the saturated inductance model. Thus, this method lacks of usage for different machines without obtaining the detailed saturated inductance model for each machine.

1.3.2 Speed Estimation Using High Frequency Signal Injection

The higher frequency signal injection method is one of the most common methods to observe the rotor and flux position. This method relies on; injection of a carrier-signal in addition to the fundamental supply excitation [9]. The injected signal is either voltage or current, produces a carrier-signal current or voltage that contains the desired spatial information. The injection of voltage or current applies with same principles. But, the carrier signal voltage injection has an advantage over carrier signal current injection since it is relatively easy to produce the voltage excitation with a traditional voltage source inverter [10]. In general, higher performance (higher bandwidth) is possible with carrier signal voltage injection since the current regulator does not directly limit its bandwidth.

The well known stator and rotor voltage equations for an induction machine for stationary reference frame is given with equations (1-2) to (1-6) [51].

$$v^s{}_{qds} = r_s . i^s{}_{qds} + p . \lambda^s{}_{qds} \qquad \text{Stator voltage equation} \qquad (1\text{-}2)$$

$$0 = r_r . i^s{}_{qdr} + (p - jw_r) . \lambda^s{}_{qdr} \qquad \text{Rotor voltage equation} \qquad (1\text{-}3)$$

where;

$$\lambda^s{}_{qds} = L_s.i^s{}_{qds} + L_m.i^s{}_{qdr} \quad \text{Stator flux linkage} \qquad (1\text{-}4)$$

$$\lambda^s{}_{qdr} = L_m.i^s{}_{qds} + L_r.i^s{}_{qdr} \quad \text{Rotor flux linkage} \qquad (1\text{-}5)$$

For higher frequency signal injection method, some assumptions will be made on these equations. The principles of the higher frequency signal injection are explained in [9] as follows; at high frequencies, the stator and rotor resistances can be neglected, resulting in the simplified form of rotor voltage equation (1-3);

$$0 \cong (p - jw_r).\lambda^s{}_{qdr} \qquad (1\text{-}6)$$

For a fixed frequency excitation at a carrier frequency w_c, the p (derivative) operator can be replaced with jw_c and the rotor equation can be used to develop an equation between the rotor and stator currents as shown in (1-7)

$$0 \cong j(w_c - w_r).\lambda^s{}_{qdr} \cong j(w_c - w_r).(L_m.i^s{}_{qds} + L_r.i^s{}_{qdr}) \qquad (1\text{-}7)$$

$$i^s{}_{qdr} = -\left(\frac{L_m}{L_r}\right).i^s{}_{qds} \qquad (1\text{-}8)$$

Using equations (1-2) and (1-8);

$$v^s{}_{qds\_c} \cong j.w_c.L_{\sigma s}.i^s{}_{qds\_c} \qquad (1\text{-}9)$$

Where stator transient inductance;

$$L_{\sigma s} = \left(L_s - \frac{{L_m}^2}{L_r}\right) \qquad (1\text{-}10)$$

But, when a rotor-position-dependent saliency (because of rotor-bar slots) exists in the machine, the stator transient inductance is no longer constant. This saliency can be caused generally by rotor stator slot openings. This phenomenon is explained elaborately in Chapter 3. Because of rotor stator slot opening variation the permeance of the machine becomes a function of the rotor position as shown in equation 3.11 [10].

$$L_{\sigma s} = \begin{bmatrix} \Sigma\, L_{\sigma s} + \Delta L_{\sigma s}\cos(h\theta_r) & -\Delta L_{\sigma s}\, sin(h\theta_r) \\ -\Delta L_{\sigma s}\, sin(h\theta_r) & \Sigma\, L_{\sigma s} - \Delta L_{\sigma s}\, cos(h\theta_r) \end{bmatrix} \qquad (1\text{-}11)$$

where;

$\Sigma\, L_{\sigma s} = \frac{1}{2}\left(L_{\sigma qs} + L_{\sigma ds}\right)$ is the average stator transient inductance,

$\Delta L_{\sigma s} = \frac{1}{2}\left(L_{\sigma qs} - L_{\sigma ds}\right)$ is the differential stator transient inductance caused by saliency

$L_{\sigma qs}$, $L_{\sigma ds}$ are the q and d stator transient inductances caused by saliency

h is the harmonic number of saliency,

θ_r is the rotor position in electrical degree

A three phase balanced carrier voltage that produces a constant-amplitude voltage vector that rotates at the carrier frequency is injected to the fundamental excitation. With a machine modelled by equation (1-11), the induced voltage will have a component which has information about the rotor speed. [10]

$$i^s{}_{qds_c} = \begin{bmatrix} i^s{}_{qs_c} \\ i^s{}_{ds_c} \end{bmatrix} = I_{cp}\begin{bmatrix} \sin(w_c t) \\ \cos(w_c t) \end{bmatrix} - I_{cn}\begin{bmatrix} \sin(h\theta_r - w_c t) \\ \cos(h\theta_r - w_c t) \end{bmatrix} \quad (1\text{-}12)$$

$$= -j.I_{cp}.e^{jw_c t} + jI_{cn}e^{j(h\theta_r - w_c t)}$$

$$I_{cp} = \frac{V_{sc}}{w_c.(\Sigma\, L_{\sigma s}{}^2 - \Delta L_{\sigma s}{}^2)}.\Sigma\, L_{\sigma s} \quad (1\text{-}13)$$

$$I_{cn} = \frac{V_{sc}}{w_c.(\Sigma\, L_{\sigma s}{}^2 - \Delta L_{\sigma s}{}^2)}.\Delta L_{\sigma s} \quad (1\text{-}14)$$

I_{cp} and I_{cn} are the positive and negative sequence components of induced currents due to injected carrier signal. The positive sequence is proportional with the average stator transient inductance and this signal contains no spatial information. On the other hand, the negative sequence which is proportional with the differential stator transient inductance contains spatial information in its phase. And utilizing this negative sequence current, rotor position can be detected.

The hardest part of this method is to obtain the spatial information among many other harmonics. The most commonly used method is to use a spectral estimation method like Fast Fourier transform and to filter the harmonics caused by fundamental supply excitation [16]. FFT method is a reliable and accurate method. But, FFT method needs complex calculations. Even more, data should be captured first before spectral analysis introducing lag in estimation and therefore consume some seconds on the processor and are not suitable for using the position information

to obtain good dynamic performance from the drive. Thus, this method should be considered as an offline estimation method.

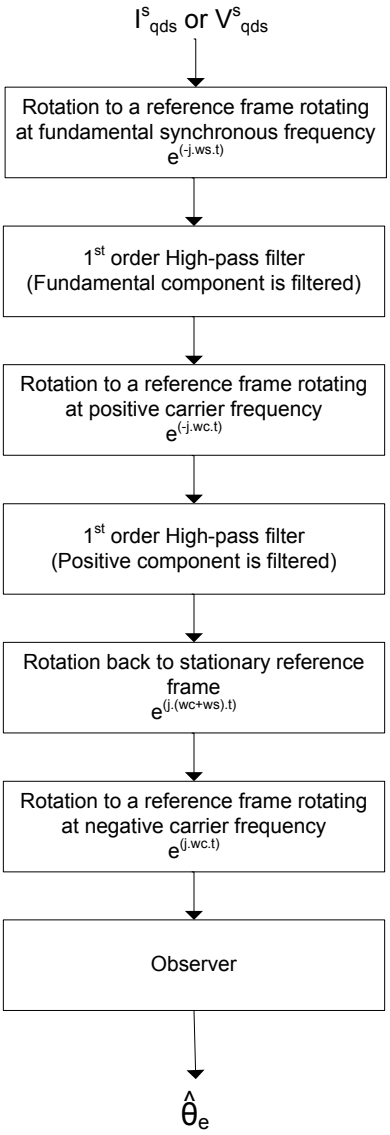

Fig. 1-5 Signal Processing used to extract spatial information from voltage or current carrier signal injection [16]

Some techniques are proposed in system that does not use spectral analysis methods [13]. They estimate rotor speed with some filtering algorithms that should

have varying characteristics in order to follow the variation in rotor speed. In [16], an alternative method that only needs simple low-high pass filters is proposed. This method is called synchronous frame filtering. This method is based on rotating to signals to the rotating reference frame, thus the component that will be filtered becomes a dc quantity and a simple high pass filter is used to obtain the spatial information. The block diagram of the method is given in Fig. 1-5.

The observer given in flowchart in Fig. 1-5 can be used to extract the spatial information contained in the phase of negative sequence component of the filtered data [10, 16], without spectral estimation techniques. Thus, it can be implemented as an online rotor position estimator. The block diagram of the observer is given in Fig. 1-6.

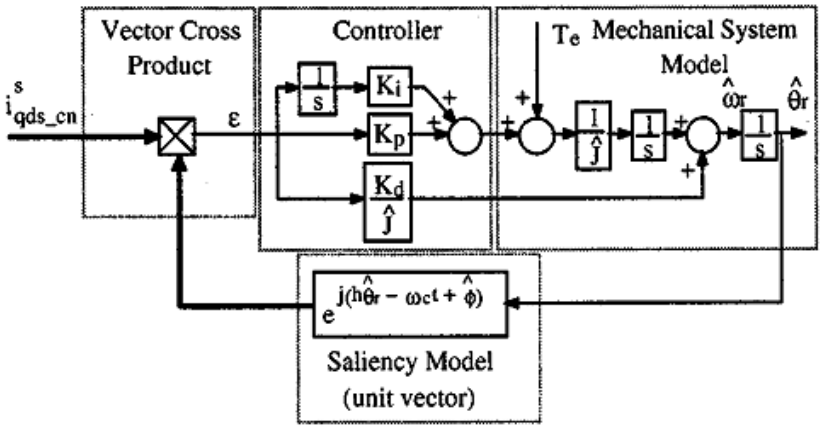

Fig. 1-6 Tracking observer for the estimation of rotor position in a machine with a harmonic saliency [16]

In this observer given in Fig. 1-6, the error signal forces the estimated rotor position to track the actual rotor position (phase locked loop). The error signal is equal to vector cross product of negative sequence carrier signal vector formed by saliency model and the measured negative sequence carrier signal current vector.

(1-15)

In [17], a machine with more than a single sinusoidally distributed saliency or a non-sinusoidal saliency is represented by a Fourier series summation of sinusoidally

distributed saliencies. The generalized model of equation (1-16) for an induced carrier current signal can be represented as;

$$i^{s}{}_{qds_c} = -j.I_{cp}.e^{jw_c t} + j\sum_{i} I_{cni}e^{j(hi\theta_{ei} - w_c t + \phi i)} \quad (1\text{-}16)$$

Where I_{cni} is the magnitude of the i^{th} component of the negative sequence current, h_i is the harmonic number of the sinusoidally distributed saliency causing the i^{th} component, θ_{ei} angular position of the sinusoidally distributed saliency causing the i^{th} component, Φ_i : phase shift of the i^{th} component.

The model given can be used to represent many saliencies such as, stationary saliencies ($h_i = 0$), rotor position dependent saliencies ($\theta_{ei} = \theta_r$), rotor or stator flux position saliencies ($\theta_{ei} = \theta_{rf}$, $\theta_{ei} = \theta_{sf}$) also rotor slot permeance saliency. For a machine that consists of rotor saliency and rotor slotting saliency the negative sequence carrier signal can be expressed as [18];

$$i^{s}{}_{qds\_cn} = I_r.e^{-j(w_c - w_r)t + \phi r)} + I_{slot}e^{-j(w_c - \frac{Z}{P}w_r)t + \phi_{slot})} \quad (1\text{-}17)$$

I_r is the magnitude of the negative carrier signal caused by rotor saliency, and I_{slot} is caused by rotor slot harmonics, w_r is the rotor speed, Z is the number of rotor slots and P is the number of pole pairs.

Using single saliency observer as shown in Fig. 1-6 in a multiple saliency model, may result to estimation errors. The solution to this problem is to use a observer with very narrow bandwidth or to use multiple saliency observers as proposed in [17, 18].

The injection of a separate test carrier has the advantage of this method does not fail in low and zero speeds because of constant magnitude excitation applied. Moreover, since the magnitude of the induced carrier signal has no importance on estimation of the rotor position, this method is not sensitive to machine parameters. The method has the disadvantage that, the fundamental PWM signals of the inverter should be modified in order to superimpose the carrier signal. Moreover, if the injected signal is large, or when the ratio of the injected signals becomes larger (as in the case in low stator frequencies) torque fluctuations are inevitable. In case the motor is small speed fluctuations may be observable [20]. Another issue is the

increasing line current harmonics are transferred to the electrical grid due to injected signal [24].

1.3.3 Speed Estimation Using Rotor Stator Slot Harmonics

These methods directly utilize the harmonics caused by the rotor and stator slot permeance variation without a high frequency signal injection. The permeance variation of the machine because of machine slots was first studied by Ishida and Hayashi [34]. The rotor slot harmonics can be obtained from phase voltages or phase currents, also from the flux of the machine.

As for harmonics caused by the rotor slots; the variation of reluctance caused by the rotor slots may be smoothed by the air-gap viewed from the surface of the stator core. The magnetomotive force wave in the motor is approximately sinusoidal, and the flux distribution B(θ,t) of the air gap can be illustrated as shown in Fig. 1-7 and described by equation (1-18) [4].

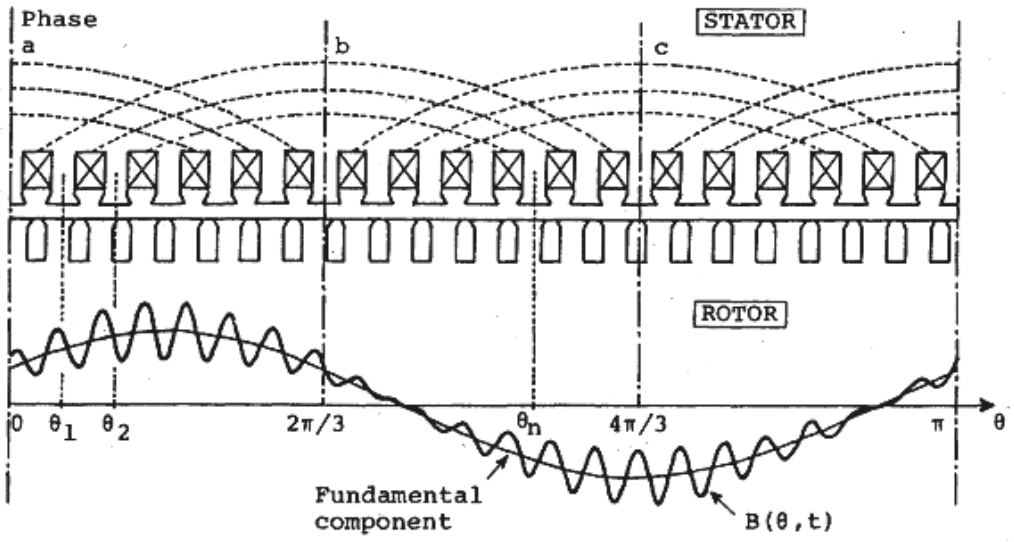

Fig. 1-7 Air-gap structure and air gap flux distribution of induction motor

$$B(\theta,t) = B_0 \cos(w_s t - \theta)[1 + k_H \cos(\frac{Z}{P} w_r t - \theta)] \quad (1\text{-}18)$$

Where; θ angular position on the stator surface ,w_r rotor angular velocity, w_s angular velocity of the power supply, Z number of rotor slots, P number of pole pairs, B_0 magnitude of fundamental component of flux density, k_H ratio of amplitude of the variation to the fundamental component

Supposing a search coil wound around a stator tooth at the angular position θ_n the induced voltage on the search coil is expressed in (1-20) using equations (1-19) and (1-18).

$$v_c(t) = -N.\frac{d\emptyset}{dt} \quad (1\text{-}19)$$

$$v_c(t) = -k.B_0 \sin(w_s t - \theta_n) \quad (1\text{-}20)$$

$$-k_f.B_0 k_H (N_r w_r w_s) \sin[(N_r w_r + w_s)t - (N_r + 1)\theta_n]$$

$$-k_r.B_0 k_H (N_r w_r - w_s)\, sin[(N_r w_r - w_s)t - (N_r - 1)\theta_n]$$

Equation (1-20) is the basic equation used to describe the rotor slot harmonics in an electrical machine. The equation describes the fundamental component and the two components caused by the rotor slot harmonics. The process is the modulation of rotor slots velocity ($N_r w_r$) with the angular velocity of the supply (w_s) resulting in two components rotating at velocity $N_r w_r + w_s$ and $N_r w_r - w_s$.

In an electrical machine, the rotor slots generate air gap permeance disturbance as the rotor slots passes in front of the stator slots. This disturbance is directly related with the number of rotor slots, Z [4, 14]. This permeance change interacts with the fundamental component of the air gap, results a spatial voltage component determined by number of rotor slots and the speed of the rotor. Similar air gap flux harmonics occur from the rotor slot MMF harmonics by the effect of rotor currents with slip frequency interacting with the constant part of the air gap permeance. This variation is directly related with the rotor current for that reason; rotor slot harmonic magnitude is reduced with decreasing load [14].

Equation (1-18) is expressed explicitly in [2]; the net component of the basic rotor slot harmonics of air gap flux is a combination of these two sources, and can be expressed as;

$$B(\theta,t) = B_1 \cos(w_s t - P\theta) + B_f \cos\left[\left(\frac{Z}{P}w_r + w_s\right)t - (P+Z)\theta + \Psi_f\right] + B_r \cos\left[\left(\frac{Z}{P}w_r - w_s\right)t - (P-Z)\theta + \Psi_r\right] \quad (1\text{-}21)$$

Where θ is mechanical angle, t is time, w_0 is the supply angular frequency, P is the number of pole pairs, w_r is the rotor angular frequency and Ψ is phase angle. Equation (1-22) gives the forward (positive sign) and backward (negative sign) slot harmonics [14].

$$w_{rsh} = \frac{Z}{P} w_r \pm w_s \quad (1\text{-}22)$$

It can be clearly seen that rotor slot harmonics contain information about the rotor speed, w_r. Using equation (1-22) by knowing the number of rotor slots, number of pole pairs, supply angular frequency, the rotor speed information can be derived. The details of rotor slot harmonics are explained in Chapter 3 elaborately.

If instead of a purely sinusoidal supply, an inverter is used to drive an induction motor, the inverter itself will introduce new harmonics to the machine, and these harmonics interact with the rotor slotting effect and new harmonics will be created. The slot harmonics in an inverter driven system is expressed in equation (3.4), where α is the time harmonic order [14].

$$w_{rshi} = \frac{Z}{P} w_r \pm \alpha . w_s \quad (1\text{-}23)$$

$$\alpha = 1, 2, 3 \ldots$$

The given equations define the frequencies of the rotor slot harmonics that appear in the air gap flux. But the most important issue is the method of obtaining a measurable signal from the air gap flux. Measuring stator currents is the most common method for measuring the harmonic contents of the air gap flux [21, 22, 23, 24]. In this method, the stator winding of the machine is utilized as search coils and the harmonics in the line currents are measured.

Another method is to use a three phase resistive network to measure the voltage difference between neutral point of stator phases and resistive network as shown in Fig. 1-8. [25]

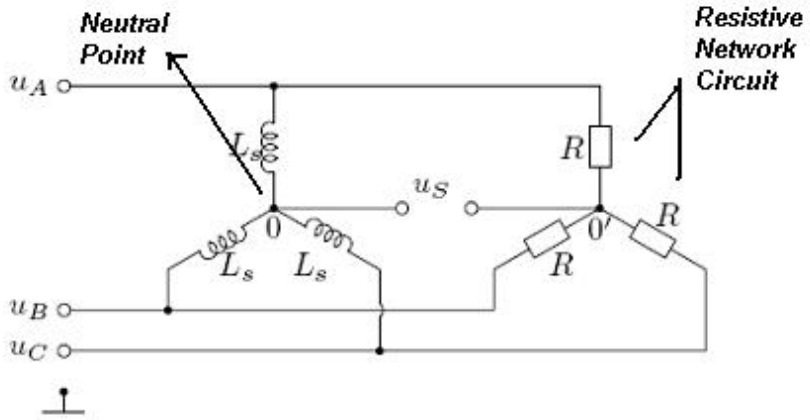

Fig. 1-8 Signal measurement from rotor slot harmonics [25]

By using this method, the fundamental component of the applied voltage and its harmonics can be eliminated in measured voltage (u_s). Thus, the rotor slot harmonics are easier to measure. On the other side, these resistive network will filter the triple harmonics due to its topology and can also filter the rotor slot harmonics if the situations described in [26, 27] occurs. Also, according to [4] in order to obtain rotor slot harmonics in a balanced three phase system, the number of rotor slots should not be a multiple of three as given in the following equation;

$$Z = 3.n \pm 1 \qquad n = 1,2,3 \ldots \qquad (1\text{-}24)$$

After the rotor slot harmonics is obtained, the rotor speed can be calculated as follows. Using equation (1-22) the rotor frequency (f_r) can be expressed as;

$$f_r = \frac{P}{Z}\,(f_{rsh} \pm f_s) \qquad (1\text{-}25)$$

In an induction motor, using the rotor frequency (f_r), number of pole pairs(P), and the rotor speed (N_r) in revolution per-minute (rpm) is given in equation (1-26).

$$N_r = \frac{60\, f_{\mathrm{r}}}{P} \qquad (1\text{-}26)$$

Using equation (1-25) and (1-26) the rotor speed in revolutions per minute (RPM) can be expressed as in equation (1-27) [4], [14].

$$Nr = \frac{60}{Z}(f_{rsh} \pm f_{\mathrm{s}}) \qquad (1\text{-}27)$$

Equation (1-27) is the basic equation that is used to determine the rotor speeds from rotor slot harmonics. Note that, f_s the applied stator voltage frequency is a known parameter. If the frequency of rotor slot harmonics and number of rotor slots can be measured then using equation (1-27) the rotor speed may be estimated. In this thesis, different techniques for determining the rotor slot harmonics frequency and number of rotor slots will be investigated.

1.3.4 Other Harmonics in Electrical Machines

Other harmonics apart from rotor slot harmonics may also occur in an electrical machine. Some of them occur from electrical or mechanical faults. These harmonics are very useful in condition monitoring of electrical machines and widely used. The electrical faults may be a stator-short circuit, unbalance between phases [28, 29] or may be broken rotor bars [29, 30]. Mechanical faults mostly caused by worn bearings resulting in eccentric rotor and asymmetrical air gap [29, 31].

These faults are not the subject of this thesis. In [26], the rotor slot harmonics and the harmonics caused by rotor eccentricity are combined in the generalized equation, which is a very useful equation in speed detection algorithms.

$$f_h = \left[(k.Z \pm n_d).\frac{(1-s)}{P} \pm v\right].f_s \qquad (1\text{-}28)$$

Where; n_d is order of eccentricity (n_d=0; static eccentricity, n_d=1,2..; dynamic eccentricity), k is any positive integer, v is the order of stator harmonics of the power supply driving the motor (v=1, 3, 5...), P is the number of pole pairs.

Note that when v =0 and k=1 in equation (1-28) gives the rotor slot harmonics defined in previous section. If k=2,3... the higher order rotor slot harmonics will be obtained. In the literature the author did not come across any study attempting to

identify rotor position or speed from these harmonics. Rotor speed estimation using higher order rotor slot harmonics will be investigated in Chapter 5.

1.4 Aim of the Thesis

In this chapter, rotor position and estimation methods in literature that use saliencies in electrical machines are discussed previously. These methods can be classified as;

- Methods using specially designed or modified rotor structure [6, 7, 26]
- Inserting a high frequency signal to extract saliency harmonics [8, 9, 10, 37]
- Methods using rotor slot harmonics [11, 12]

For all of these methods, saliencies can be measured and analyzed in many ways like; measuring phase voltages [4, 11, 12, 25] or phase currents [5, 6, 24, 10] or using a resistive network to measure zero sequence voltage [25].

Using an external search coil or an antenna that links the fringing flux is investigated in a few studies. Most of this kind research is focused on detection of faults in the machine such as; worn bearings, broken rotor slots, etc. [2, 28, 29, 30, 31, 45, 46, 47].

For analysis of the rotor slot harmonics or other saliencies data, spectral analysis methods like FFT is mostly used. In [32, 33, 48], some spectral analysis techniques are compared. These studies showed that due to high data acquisition and computation time (up to 2 – 3 seconds); it is very hard to implement these algorithms as an online rotor position estimator. A rotor position/speed estimator is needed in industry that predicts the rotor position in a few hundred μsec. Of course, a non-invasive technique that does not require any modification to the motor and does not introduce extra cost is highly desirable. Thus, the discussed methods may not meet these requirements. But, high frequency signal injection method that utilizes a phase locked loop [10, 16, 37]; can estimate the rotor position down to zero speeds. Thus, this method seems to be the most successful among others. But, injecting a high frequency signal may not be possible for some drives or with small motors where torque ripples may be introduced especially at low speeds.

In this thesis, the focus is on whether it is possible or not to estimate the rotor speed, rotor position and number of rotor slots utilizing the fringing flux out of the machine. Fringing flux is detected with an external search coil placed on the machine frame between cooling fins.

As a first step, the type of external search coil that gives a satisfactory signal is investigated. This is followed by seeking a suitable location for placement of coil on the machine and investigating the characteristics of the induced voltage with frequency, load and flux conditions. Then, after determining the ideal search coil core and position it is discussed that whether it is possible or not to use the induced voltage waveform directly for rotor position estimation. For this purpose, it is attempted to estimate the zero crossings of the induced voltage model that can estimate the position of air gap flux is proposed.

After that, it is observed that the induced external coil voltage contains many harmonics. And these harmonics are analyzed. Then, the study is mainly focussed on the rotor speed estimation using the rotor slot harmonics with FFT method. For rotor speed estimation, the information of rotor slot numbers is needed. To meet this necessity, an algorithm to detect the number of rotor slots is proposed. The next step was the investigation of using rotor slot harmonics for position detection. It is observed that especially when the motor is driven with inverter, the rotor slot harmonics fall into an area of the frequency spectrum where there are many other harmonics. On the other hand, it is found that higher order rotor slot harmonics have a sufficiently high magnitude and they fall into a frequency range where other harmonics are less important. Thus, the higher order rotor slot harmonics is studied without using spectral estimation system. Thus, this method is more suitable for an online implementation or rotor speed/position estimator. In this method, higher order rotor slot harmonics is isolated from the induced search coil voltage using a digital filter. Then, these harmonics are converted to a rotor position data without a data acquisition period. All calculations are performed in time domain at each algorithm cycle. Thus, in this thesis, both frequency and time domain analysis methods will be studied. However, the proposed methods can be implemented as an online rotor

speed and position estimator with some digital filter implementation, this thesis does not cover this implementation.

The following section summarizes the content of the thesis.

1.5 Contents of the Thesis

The summary of the thesis is as follows:

Chapter 1 gives an overview of rotor position estimation methods discussed in the literature. Aim of the thesis is explained.

Chapter 2 discusses the selection of the search coil that will be used for the rest of experiments and the finite element magnetic modelling of the search coils for better understanding of fringing mutual fluxes. Also the radial and axial positioning of the search coil on the frame is investigated. And the designed motor drive hardware is introduced in this chapter.

Chapter 3 is assigned to rotor slot harmonics detection in the induced external search coil voltage with spectral analysis methods. The captured data is analyzed with FFT to verify the existence of rotor slot harmonics. Then these harmonics are used for the estimation of rotor speed. The findings are compared with the speed measurements using an incremental encoder and the accuracy of the predictions is assessed. Also, a new method for the estimation of number of rotor slots is proposed.

Chapter 4 is assigned to time domain analysis of induced voltage in the search coil. In this context internal search coil is also utilized to observe the relationship between the internal and external coil induced voltages. In this context, the relationship of the induced emf's and air gap flux is studied under varying stator frequency, varying flux and varying load conditions with sinusoidal and PWM voltage supplies. The purpose at this stage was to establish a relationship between the external coil emf and the air gap flux. The aim is as indicated above the speed estimation using the zero crossings. It must be noted that such an approach may suffer from in predicting speed at low speeds due to low magnitude of the signals. More over, since the period of signal increases with decreasing frequency, the rotor position update rate may not be sufficient. These problems are discussed in Chapter 4.

Chapter 5 introduces a new method that can identify the high order rotor slot harmonic variation in the induced external coil voltage. In this method, rotor position is estimated without using spectral estimation techniques. This is achieved by some means of digital filtering and demodulation techniques. Once the high order rotor slot harmonics is the zero crossings of the harmonic signal are detected and converted a rotor position data. This is advantageous among other techniques because; it does not need a data capturing period and it can provide much more accurate position estimation.

Chapter 6 is devoted to conclusion, discussion and suggestions for future work.

CHAPTER 2

SELECTION OF SEARCH COIL TYPE AND POSITION

2.1 Introduction

In order to obtain a reasonable signal from the fringing flux of the machine, the type of the search coil and the position of the search coil should be carefully selected. To decide which search coil type and position gives better results different experiments will be performed. The aim of the experiments is to select a search coil shape and position that induces largest voltage from machine fringing flux. The higher induced voltage from the fringing flux of the machine means increased signal to noise ratio on the search coil voltage i.e. reducing noise contents due to other electromagnetic interferences, thus improving the signal quality of the search coil voltage.

The material and the shape of the search coil is an important factor that affects the signal quality. In this chapter, different search coil types are examined to obtain most useful signal. First, finite element analysis for different search coil types positioned on the same place on the motor will be performed to compare the behaviour of fringing flux for each search coil clearly. In finite element modelling ANSOFT Maxwell Student Version is utilized. Then some experiments are performed with the simulated search coils to verify the finite element analysis.

After selecting the type of the search coil, the search coil is placed on various positions across the cooling fins of the motor to compare the induced voltages for each position. The experiments include both radial and axial position variations.

Finally, the designed motor drive hardware to capture the search coil voltage and measure machine electrical parameters is presented.

2.2 Finite Element Model Simulation Method

In this section, finite element analysis software is utilized to verify the operation of search coil and to observe the whole fringing flux across the machine. Finite element analyses are performed with different search coil types placed on the same position on the motor. The induced voltage for each search coil will be simulated and compared.

For finite element analysis, the ANSOFT Maxwell Student Version is used. ANSOFT Maxwell is electromagnetic analysis software that simulates electromagnetic systems from low frequencies to mid-high frequencies in 2D or 3D. The ANSOFT Maxwell has a well developed motor analysis toolbox that provides parametric analysis of many motor types using built-in templates. The student version has limitations as compared to the commercial version such as, 3D analysis, transient analysis, and equivalent circuit export for Simplorer, which are not available in this version.

Since the machine core is symmetrical along the axial line, a 2D electromagnetic analysis will be enough to understand the characteristics of the system.

A 1.1 kW 6-pole (motor #1) and 2.2 kW 2-pole (motor #2) squirrel cage induction machine with the specifications given in Appendix A, are used in experiments. The 2.2 kW 2-pole induction machine (motor #2) with cast iron frame is used for finite element analysis. The machine has 24 stator and 18 rotor slots. The magnetic properties of the materials used in the machine (stator core, rotor core, frame and shaft) are available in Appendix B. The simulations are performed with the following materials; the stator and rotor core with cold rolled steel, the rotor windings with aluminium, the stator windings with copper, and the machine frame with cast iron as shown in Fig. 2-1. All of the experiments and simulations are performed with the iron frame machine. The aluminium frame machine is not considered, because the permeability of the aluminium is much smaller than the iron resulting in a less fringing flux in the aluminium frame machines. This proposition will be supported with experiment result presented in Table 2-2.

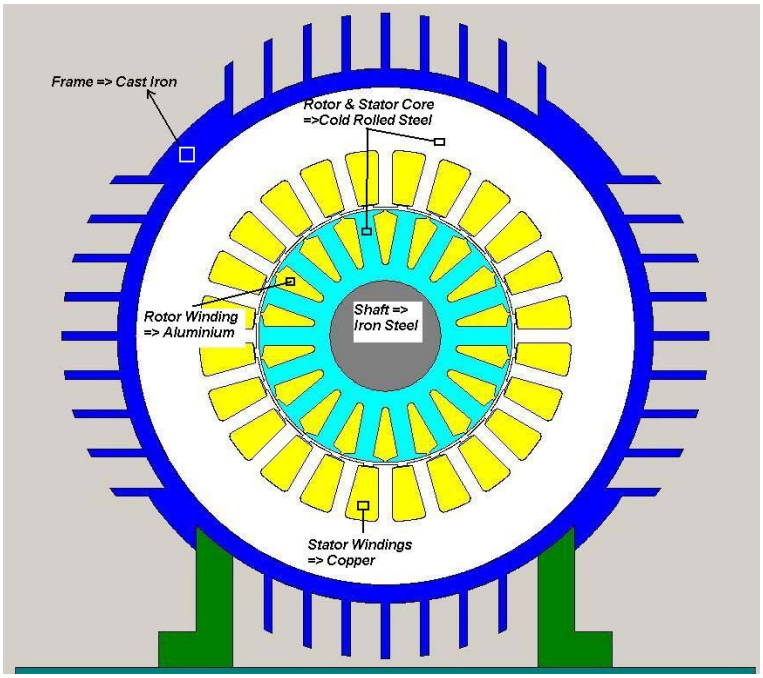

Fig. 2-1 Used material types for finite element analysis

The B-H curves for stator and rotor cores and the motor frame based on [49] is given in Fig. 2-2 and Fig. 2-3.

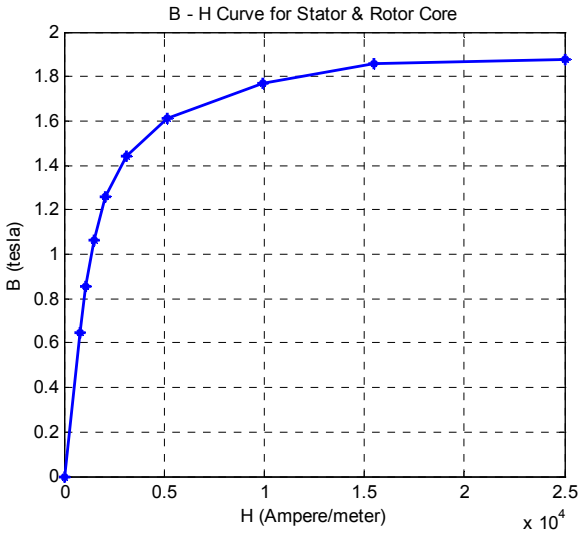

Fig. 2-2 The B-H curve for stator and rotor core (cold rolled steel)

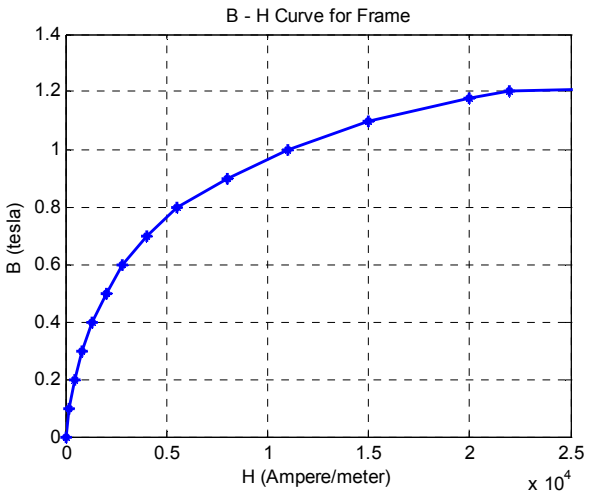

Fig. 2-3 The B-H curve for motor frame (cast iron)

2.3 Finite Element Simulation of Different Search Coils

In this section, different search coil types will be investigated and they will be simulated with the ANSYS Maxwell in order to obtain the magnetic behaviour of the machine with different search coils. In the simulations, the coils of the search coils are not included. The simulations are performed modelling only core of the search coils. It is thought that maximizing the flux linking the search coil core means that larger voltage may be induced for this search coil type. Therefore, the assessment is done on this basis.

The core for the simulated search coils is assumed to be 0.5 mm cold rolled steel core with magnetic properties given in Appendix B. Three different search coil types will be investigated. The search coils used in the experiments are shown in Fig. 2-4.

The search coil core types are as follows;

- U-core (I)
- Horizontally placed straight core (II)
- Vertically placed straight core (III)

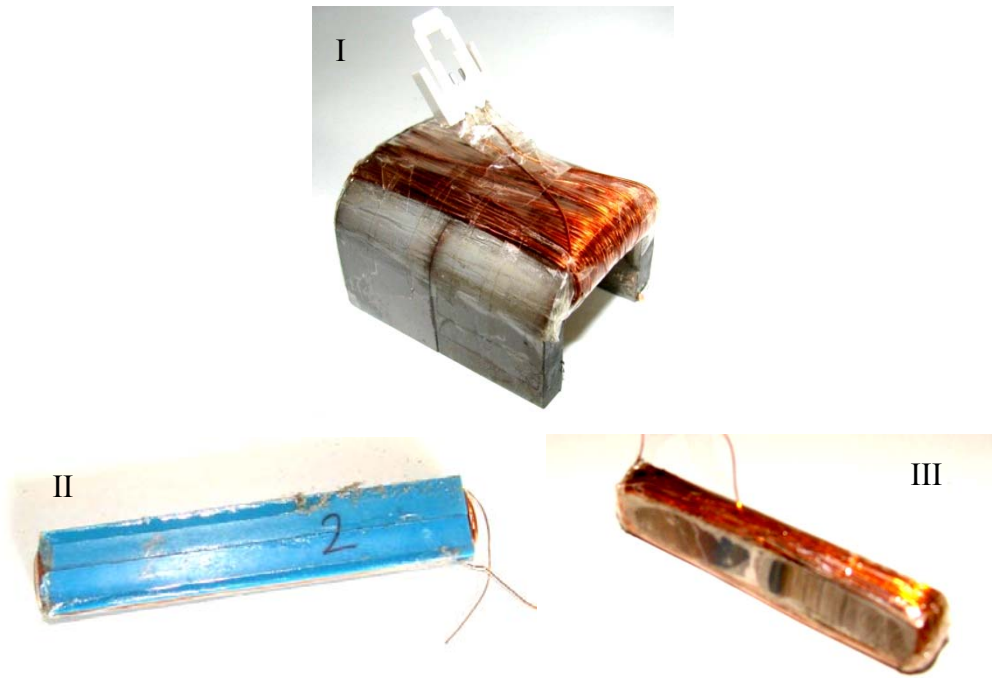

Fig. 2-4 External search coil types used in experiments

The simulations with Maxwell are performed at static conditions. Thus, the simulation does not include eddy currents. The motor #2 with specifications given in Appendix A is simulated using Ansoft Maxwell built-in motor design tool. The three different simulation instants are sufficient to get a rough idea of the behaviour of induced search coil voltage and the fringing flux. The excitations are applied considering the rated operation point of the sample motor.

The current density excitations are applied as follows;

- Phase A: 6 A/mm^2 Phase B: -3 A/mm^2 Phase C: -3 A/mm^2
- Phase A: 3 A/mm^2 Phase B: -6 A/mm^2 Phase C: 3 A/mm^2
- Phase A: 3 A/mm^2 Phase B: 3 A/mm^2 Phase C: -6 A/mm^2

The simulation converges when total potential energy error gets smaller than 0.1 %. The finite element model has a mesh that consists of 12407 triangles. This model may not give accurate solutions for a design, but the simulations are only aiming to get an idea about the fringing flux so this mesh is assumed to be sufficient.

2.3.1 U-Core Search Coil (Type #1)

The simulated search coil is a U-core laminated search coil placed between cooling fins of the motor. The search coil material is cold rolled steel. The position, lamination direction of the core is shown in Fig. 2-5. Also, the coil wound on the core and the expected flux lines in the search coil are shown in same figure.

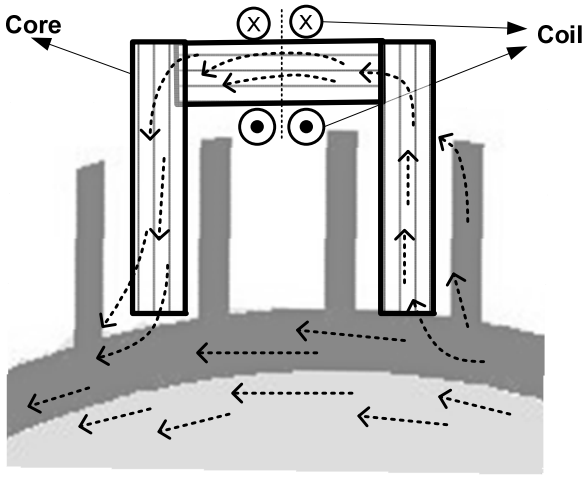

Fig. 2-5 The coil direction and expected flux lines in U-shaped core

The U-shaped search coil, induction motor and the mesh produced in Ansoft Maxwell is given in Fig. 2-6. The boundary is taken as a balloon boundary, in other words, the boundary is assigned by the simulation itself. In the figures, the boundaries of the simulations are not shown. Since, the model can be assumed symmetrical along the horizontal axis only the upper half partition of the model is given in the figures.

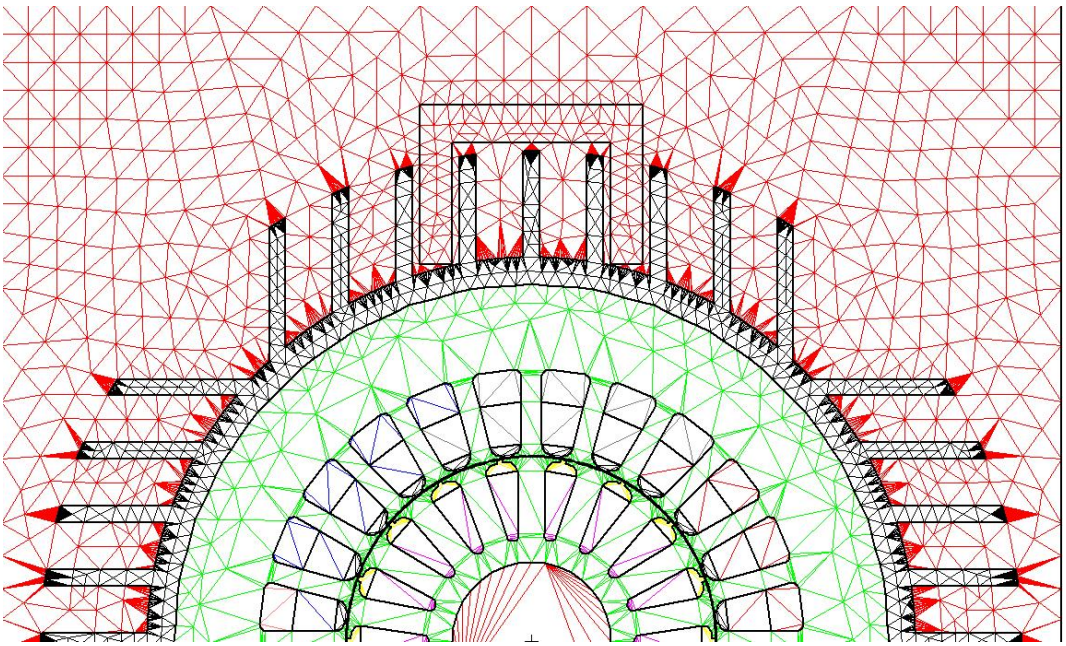

Fig. 2-6 Position of search coil and mesh used in finite element analysis

In the following figures, the rated current excitation is applied and the three phase excitation is simulated with three different excitations at rated current. Since these three different excitations simulate the instants of a rotating magnetic flux, we expect the flux linking the search coil also varies according to these rotating magnetic flux instants.

The three excitations and the induced flux density vectors on the background and the search coil are given in Fig. 2-7, Fig. 2-8, Fig. 2-9 and Fig. 2-10. The flux lines of the stator core and frame are omitted for the sake of simplicity, only the flux on the search coil core and flux out of the frame is shown in figures.

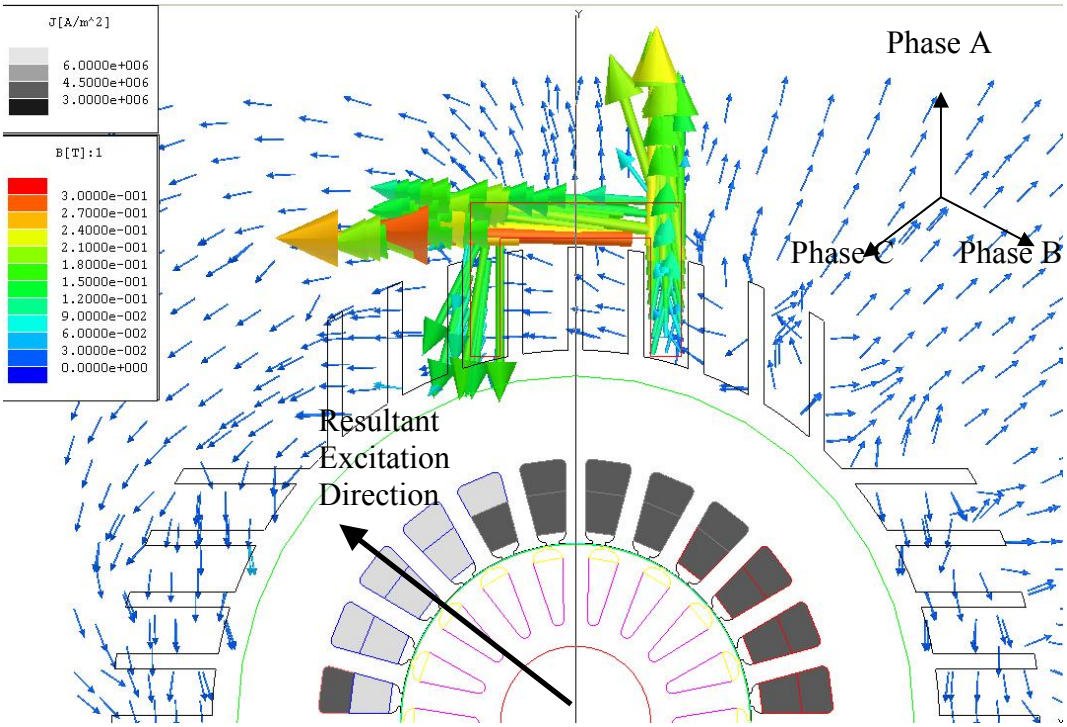

Fig. 2-7 Simulation with excitation centred with the negative magnetic axis of Phase B

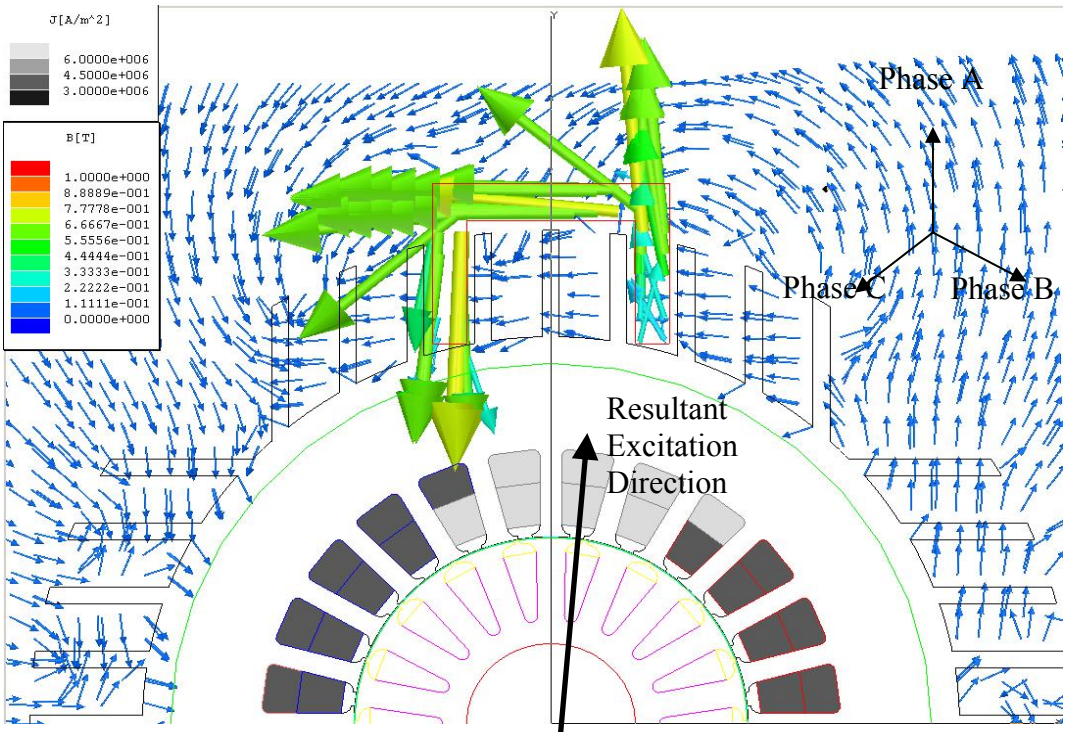

Fig. 2-8 Simulation with excitation centred with the magnetic axis of Phase A

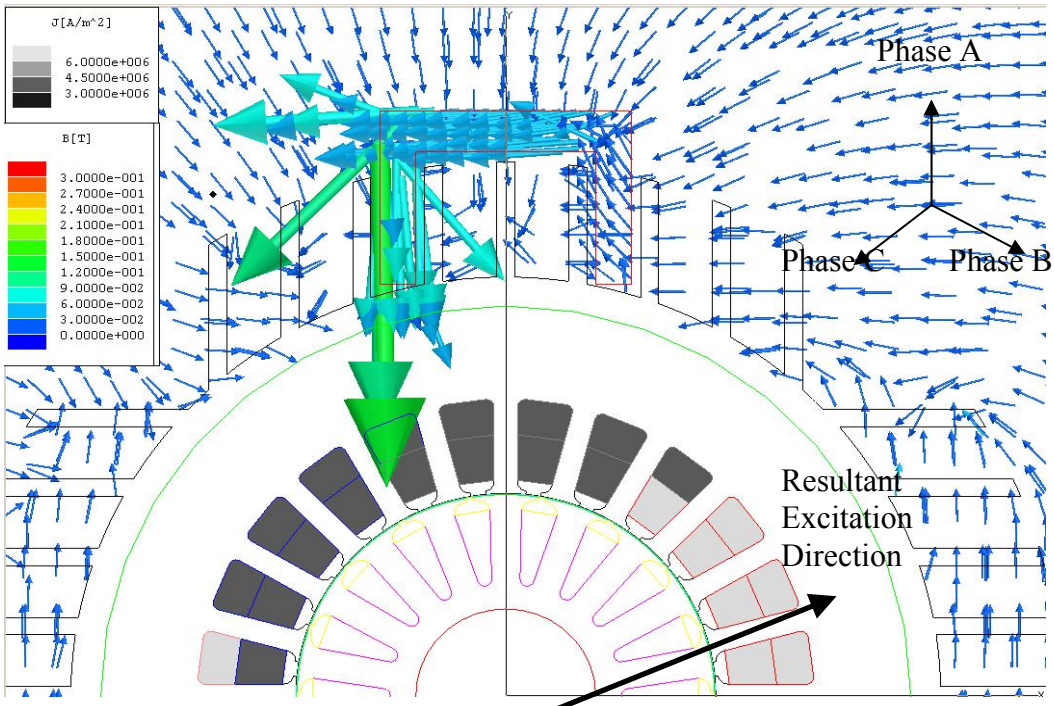

Fig. 2-9 Simulation with excitation centred with the negative magnetic axis of Phase C

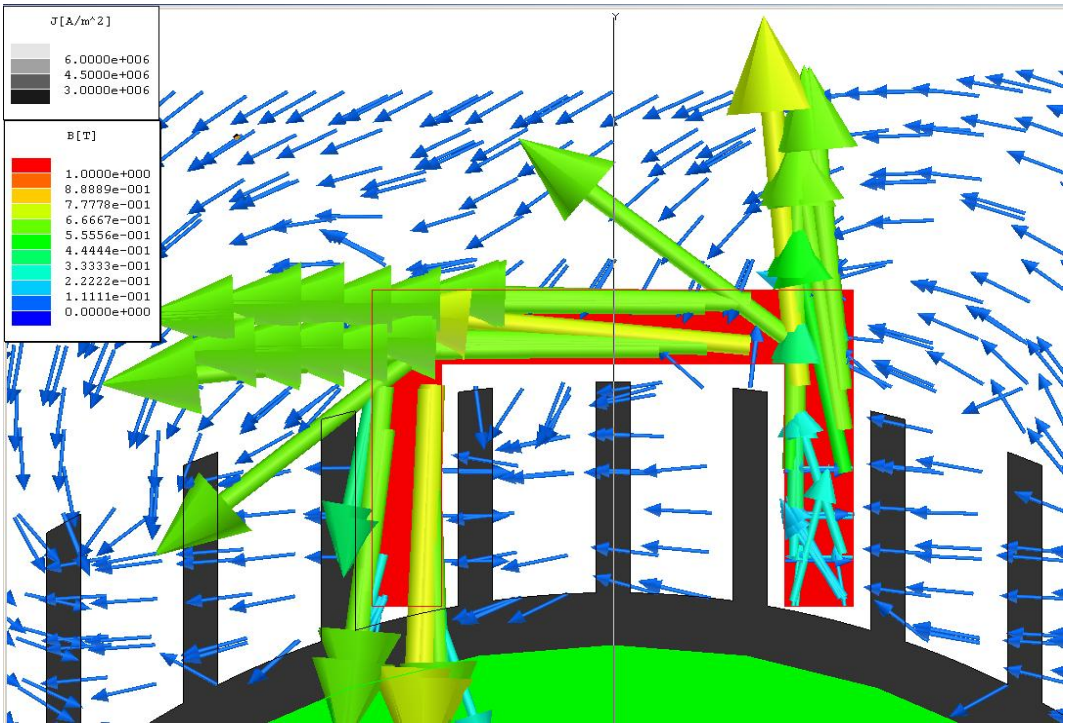

Fig. 2-10 The close-up of the flux density in search coil with the excitation centred to the magnetic axis of Phase A

As seen from the figures above, the magnetic flux density in a U-core shaped search coil rises up to 0.55 T which is a reasonable value to observe the flux inside of the search coil. The total flux in the search coil core can be expressed as;

$$\phi = \int_{s} (\vec{B}.d\vec{s}) \qquad (2\text{-}1)$$

Flux is calculated on the vertical line cutaway (Y-axis) surface of the core as shown in Fig. 2-5, utilizing post process tools of Maxwell software. The flux crosses through this cross-section when the excitation centred with the magnetic axis of Phase A is 0.0675 mWb.

2.3.2 Horizontally Placed Search Coil (Type #2)

Another search coil type that is investigated is a straight core search coil. The search coil is placed horizontally above the cooling fins of the machine. The search coil material is cold rolled steel. The placement of the core and coils are shown in Fig. 2-11. Also the expected flux lines are shown.

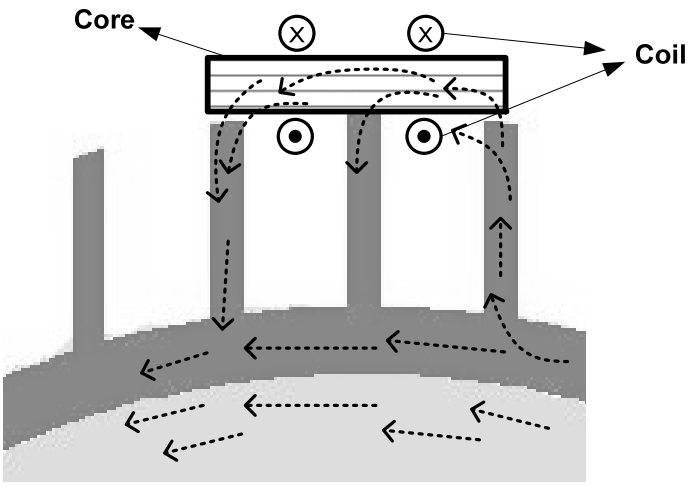

Fig. 2-11 The coil direction and expected flux lines in horizontally placed core

The same procedure with the same excitations is applied as explained in section 2.3. Three static excitations and the induced flux density vectors on the background and the search coil core are given in Fig. 2-12, Fig. 2-13 and Fig. 2-14.

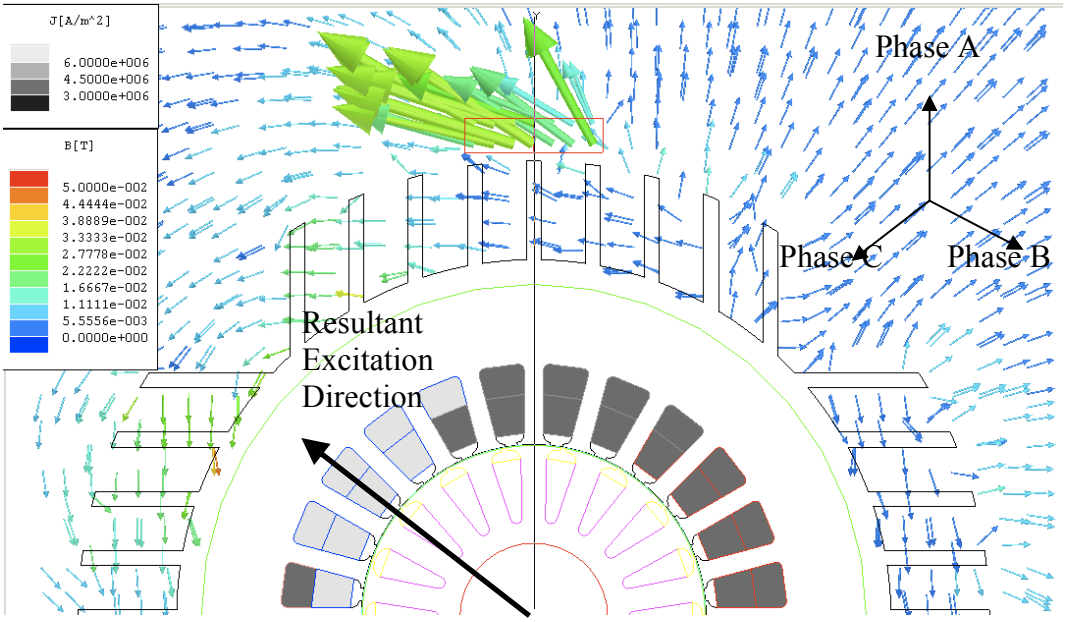

Fig. 2-12 Simulation with excitation centred with the negative magnetic axis of Phase B

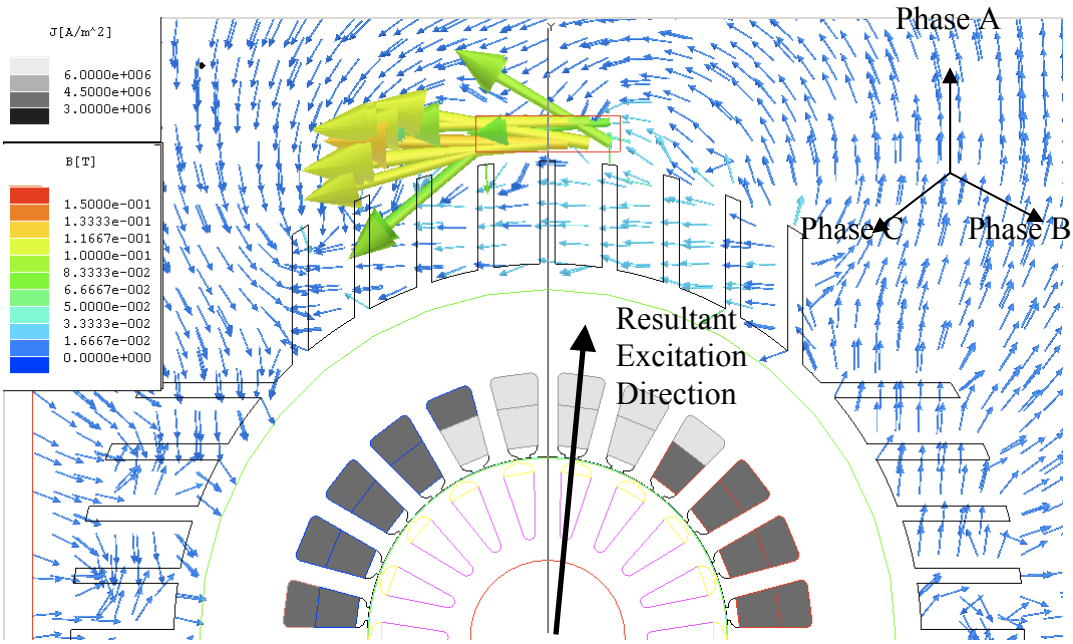

Fig. 2-13 Simulation with excitation centred with the magnetic axis of Phase A

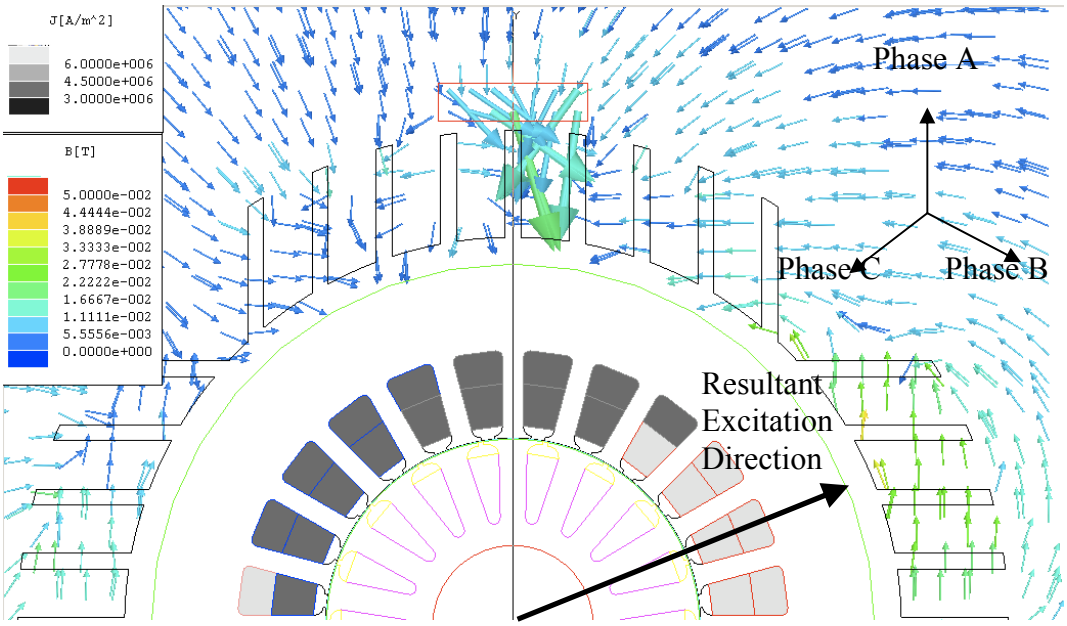

Fig. 2-14 Simulation with excitation centred with the negative magnetic axis of Phase C

The maximum flux density on the horizontal search coil is 0.12 T. The total flux that crosses on the vertical cross-section of the core is calculated as 0.0182 mWb which is smaller than the U-core type search coil.

2.3.3 Vertically Placed Search Coil (Type #3)

The last search coil type that will be investigated is the vertically placed search coil between the cooling fins of the machine. The search coil material and simulation conditions are same with the previous simulations.

The position of the core and coil is shown in Fig. 2-15. Also the expected flux lines in the search coil are shown in same figure.

In the following figures, the rated current excitation is applied and the three phase excitation is simulated with three different excitations at rated current. The three excitations and the induced flux density vectors on the background and the search coil are given in Fig. 2-16, Fig. 2-17 and Fig. 2-18.

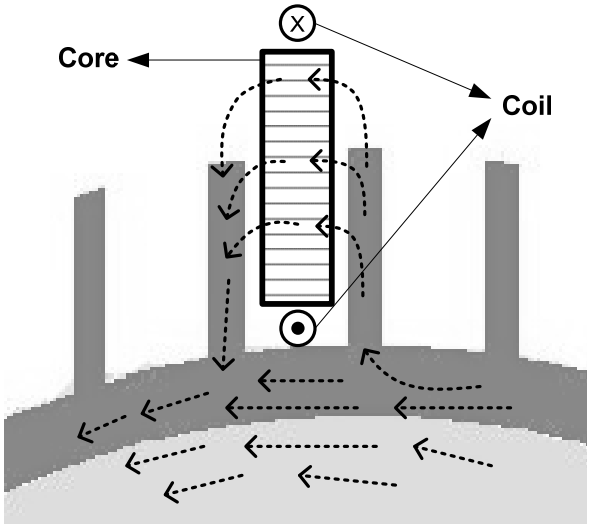

Fig. 2-15 The coil direction and expected flux lines in vertically placed core

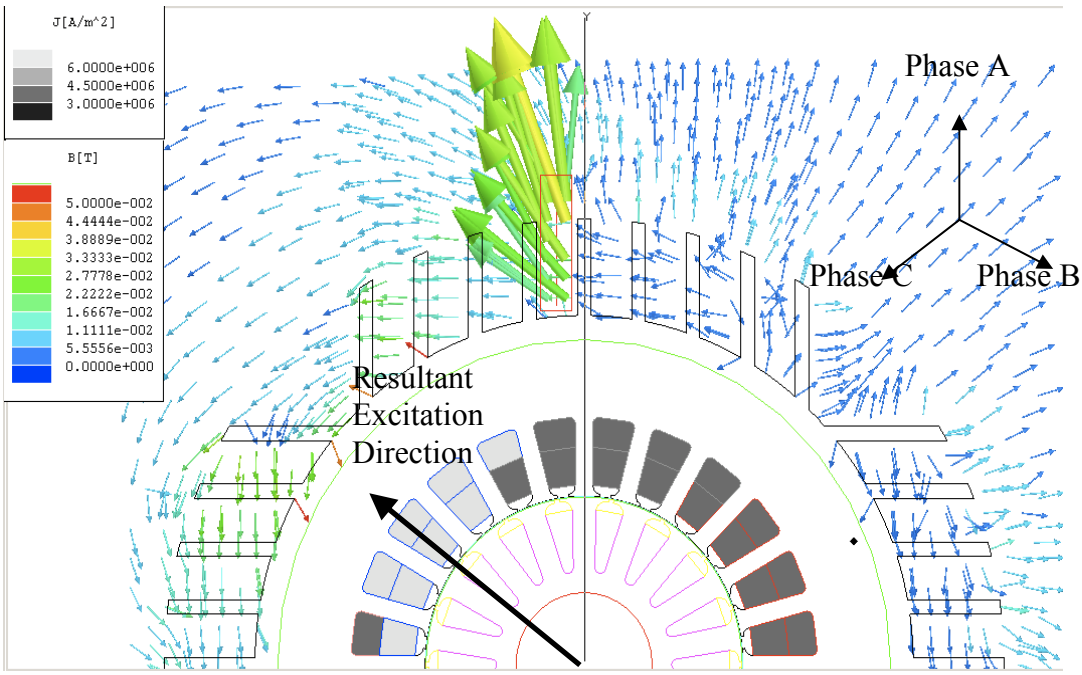

Fig. 2-16 Simulation with excitation centred with the negative magnetic axis of Phase B

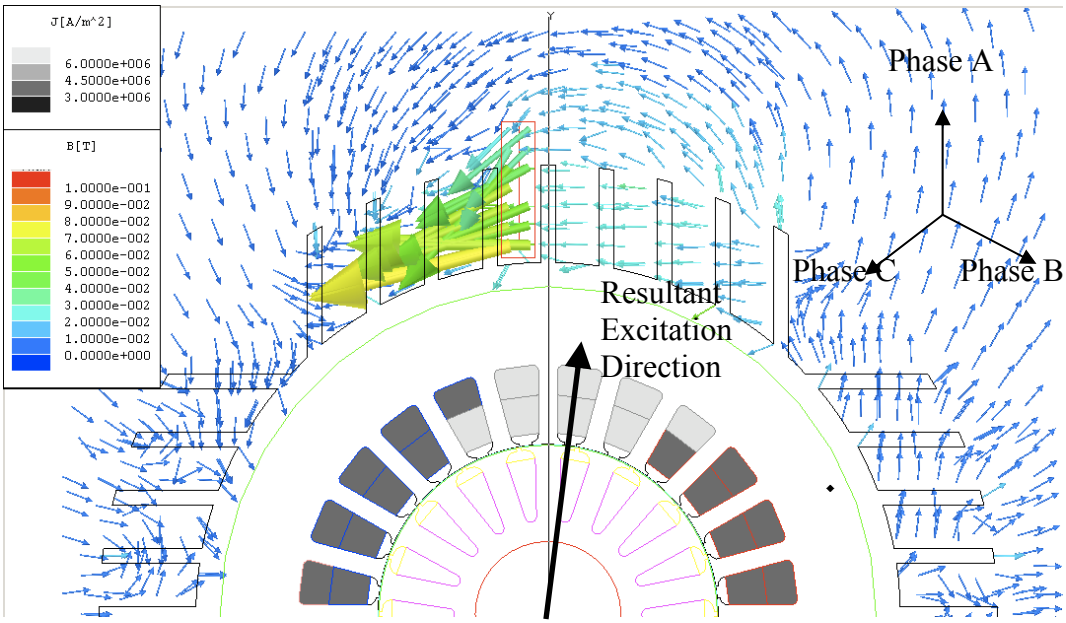

Fig. 2-17 Simulation with excitation centred with the magnetic axis of Phase A

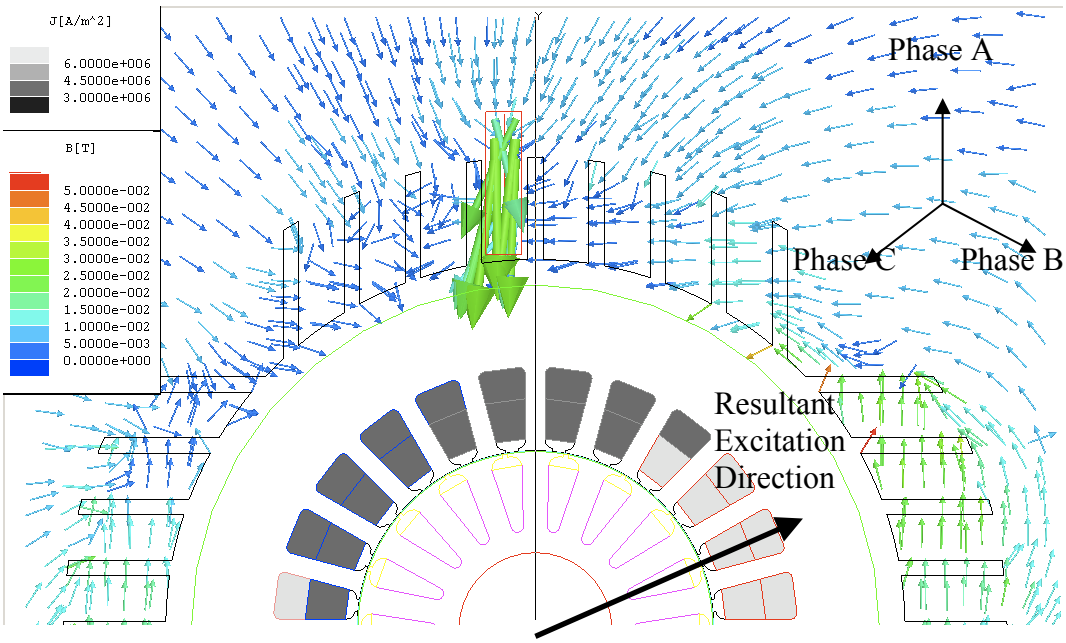

Fig. 2-18 Simulation with excitation centred with the negative magnetic axis of Phase C

The maximum flux density obtained is 0.07 T with the excitation centred with the magnetic axis of Phase A. This type of core has the largest cross-section area along the vertical axis compared with the other type of cores resulting in a flux of 0.0362 mWb which is still smaller than the flux of the U-core shaped core.

2.3.4 Evaluation of Search Coil Cores

The simulations were performed with three different search coil cores with Ansoft Maxwell. Based on these simulation results it is shown that, U-shaped core links the largest flux. The finite element method has given the necessary information about the shape of the coil. But, in order to verify the operation of search coil various experiments are performed with the search coils presented in Fig. 2-4. The induced voltage on each search coil is measured with motor #1 with specifications given in Appendix A. The experiments performed at rated voltage (50 Hz, 220$V_{l\text{-}n}$) at rated load. The induced voltages are presented in Table 2-1.

Table 2-1 Induced voltages for different search coils

Search Coil	Type I (U-shaped core)	Type II (Horizontally Placed)	Type III (Vertically Placed)
Induced Voltage	372 mV	34 mV	131 mV

As seen from the table, experiment results are consistent with the simulations. Based on simulations and experimental results, U-shaped core placed on the frame of the machine induces larger voltage compared to other type of search coils. Thus, for the rest of this study, the search coil with U-shaped core will be used.

An example for placement of external search coil is given in Fig. 2-19.

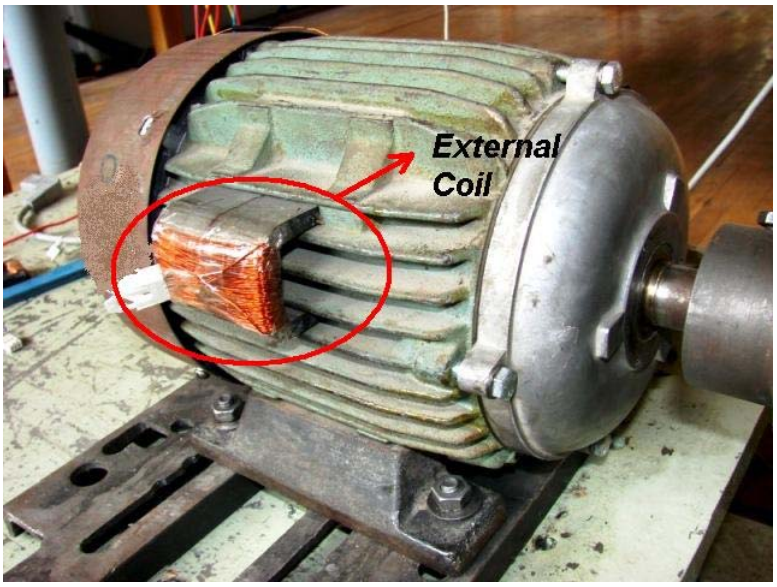

Fig. 2-19 Position of external search coil on the motor #2

To compare the search coil with different motor frame materials, experiments are performed also with an aluminium frame motor. (TEE, 2-pole, 2.2kW, QSL2A-40H, 2860 rpm) The experiment results given in Table 2-2, shows that the induced voltage magnitude on aluminium frame machine is much smaller than one with iron frame machine. However, the ratio of induced voltages may change due to the machine size, stator-rotor slot types, but the experiments results still support our

proposition that, the low permeability of the aluminium frame will causes less fringing flux linking the external search coil.

Table 2-2 Comparison of induced search coil voltage for aluminium frame machine

	Induced External Search Coil Voltage
Iron Frame (Motor #2)	372 mV
Aluminium Frame	67 mV

2.4 Experiments on the Effect of Search Coil Position

Besides, the shape of search coil, another factor affecting the induced voltage on the external search coil is the position of the search coil. In this section, the importance of the position of the search coil will be investigated with some experiments. External search coil may be placed over different places on the frame of the machine. The position variations are investigated in two ways; axial position variation and radial position variation. The applied excitation to the machine is held constant while varying the position of the search coil. The induced voltage is measured for each position of the search coil and the positions where higher voltages are induced are selected as suitable positions. As discussed before, higher induced voltage means higher signal to noise ratio.

Another point that will be investigated is the rotating flux of the induction machine will induce a voltage on the external search coil that shifts as the search coil is moved on radial direction over the machine frame. So actually, we expect that radial placement of the external search coil does not have any importance.

2.4.1 Axial Position Variation

In these experiments the search coil is placed on different position on axial direction. The axial length of the motor is divided into ten parts and the experiments are performed at rated conditions for all positions. The position #1 corresponds to the back side of the machine and the position #10 corresponds to the last position

through the shaft side. The experiment results and the corresponding positions on the motor are given in Fig. 2-20.

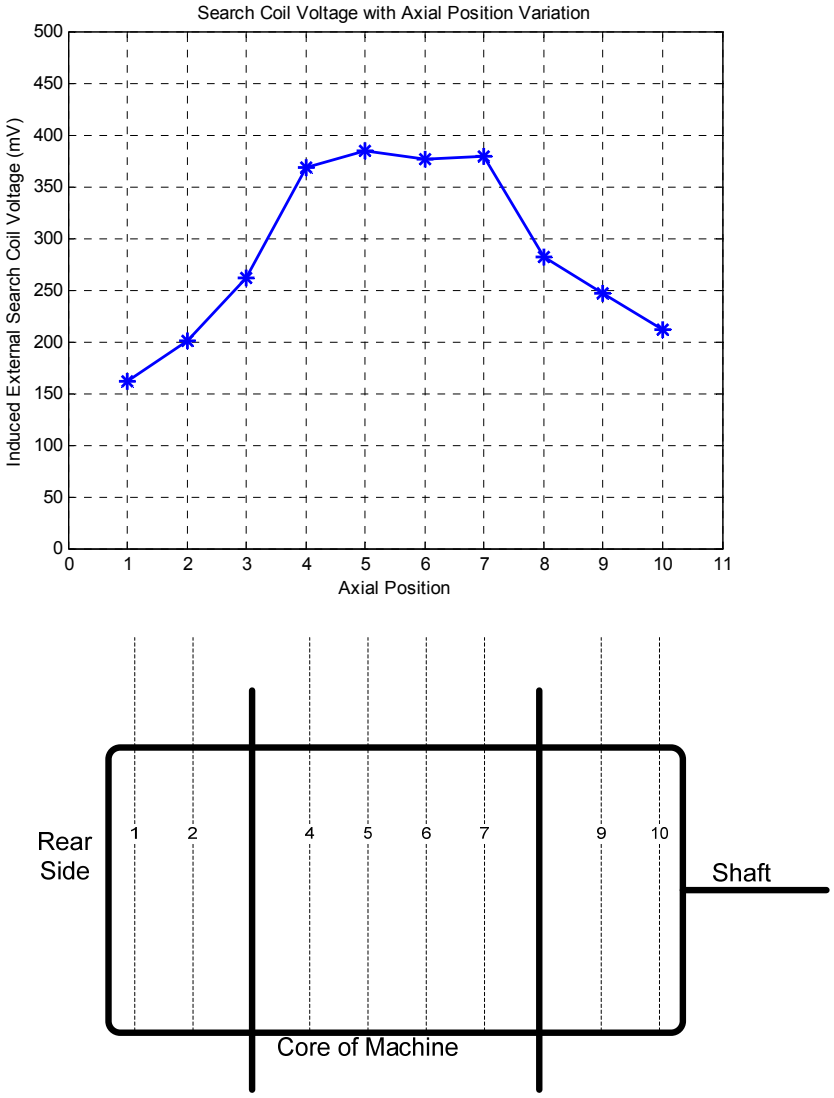

Fig. 2-20 The induced external search coil voltage for various axial positions

The experiment results imply that maximum fringing flux occurs at the middle interval where the stator core and windings lay. The variation of the induced voltage

at the interval of stator core is negligible. Thus, any position is acceptable along the core of the machine.

2.4.2 Radial Position Variation

In these experiments the search coil are placed various positions on the circumference of the machine frame. The search coil is placed on the gaps between the cooling fins. The gaps are labelled as seen in Fig. 2-21.

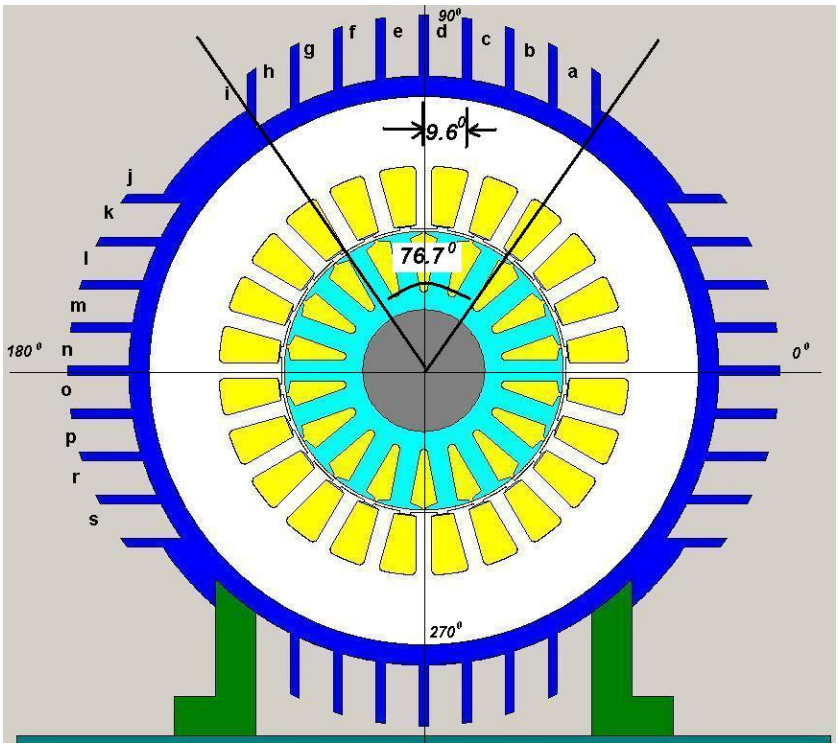

Fig. 2-21 Cooling Fin labels (Front View)

The angle of one set of cooling fins is calculated as 76.7 degrees as shown in Fig. 2-21. And the angle that a single cooling fin spans is 9.6 degrees. Since the machine is a two pole machine, the mechanical angle is identical with the electrical angle. Thus, in a two pole machine, it is expected that the mechanical shift of the search coil should result in equal phase shift on the induced search coil voltage.

The experiments are performed at 50 Hz, 220V applied stator voltage at no load, and the induced voltage on the search coil is recorded for each radial position change.

To use as a reference to the external search coil voltage, an internal search coil placed between stator slots is used. The internal search coil is a coil that is wound on the stator slots and spans one pole pitch of the machine. The position of the internal coil is stationary for all stages of experiments. The internal search coil has 10 turns. The picture of the internal search coil is given in Fig. 2-22. The internal search coil will also be used as a flux observer in following chapters.

Fig. 2-22 Placement of internal search coil

The induced internal and external search coil voltage waveforms are plotted on the same graph for comparison. The experiment results are given in Fig. 2-23. The waveforms showed that, the coil voltage is shifted as the search coil is moved along radial direction. For some positions that search coil does not properly fit to cooling fins, a decrease in the voltage may be seen, but this should be considered as odd case.

The experiment data for some of search coil positions presented in Table 2-3. In the table, the magnitude of the induced search coil voltage and the phase angle normalized with respect to mechanical angle is presented.

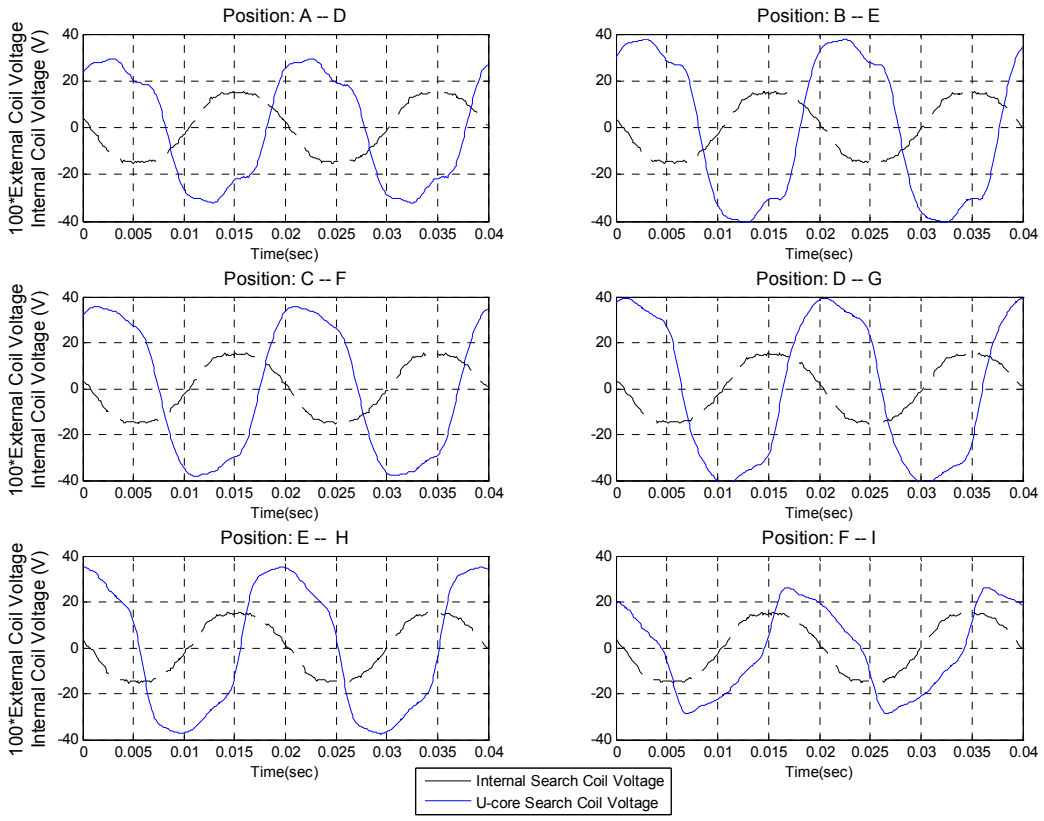

Fig. 2-23 Induced internal and external search coil voltage waveforms for various coil positions.

Table 2-3Induced external search coil voltages and phase angles for various positions

Position	Vcoil (mV) /Phase Angle (degree)	Calculated Mechanical Angle
C-F	410 / 90^0	90^0
D-G	422 / 100^0	99.6^0
K-N	422 / 157^0	160.8^0
L-O	220 / 168^0	170.4^0
M-P	218 / 177^0	180^0

The induced voltages given in Table 2-3 is shown with a vector diagram for a better understanding of induced voltage phase shifting. When the search coil is moved one cooling fin where the mechanical angle corresponds to 9.6^0 the induced voltage of the search coil also shifts approximately same amount. Also, if the search coil is moved 90^0 the induced voltage shifts 87^0.

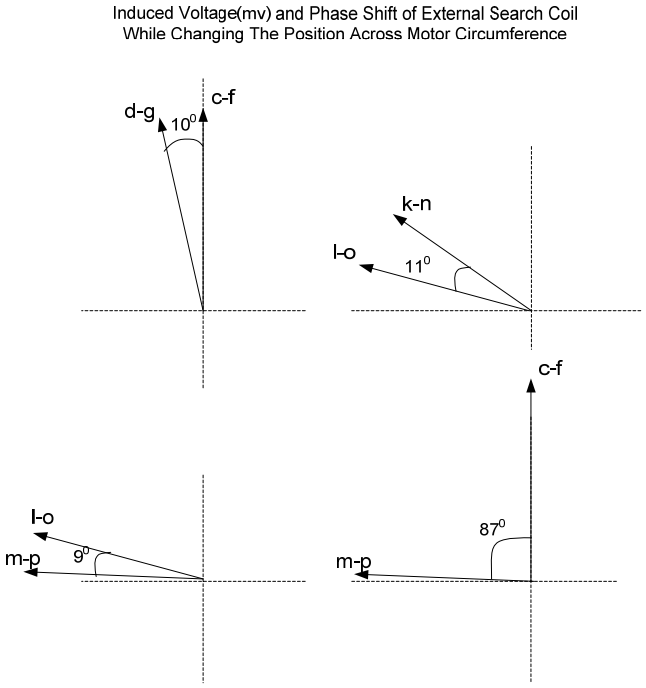

Fig. 2-24 Vector representation for induced voltage for various positions

2.5 Conclusion for Search Coil Experiments

In this chapter, the finite element analyses on different search coil types are applied. Simulations showed that the external search coil may link peak flux densities between 0.1 T – 0.45 T. The U-shaped laminated core search coil has the best performance among other types of search coils. U-shaped search coil is found to have induced the largest voltage with a maximum flux of 0.0675 mWb. It has lower reluctance because it touches the frame of the machine whereas other search coils utilizes the cooling fins. Some experiments are performed also with different search coil types. Experiment results are consistent with the simulations.

Also, the effect of the position of the search coil is investigated. The search coil is placed on different positions on axial and radial direction then the induced voltages are presented. The axial direction experiments showed that the external search coil induces largest voltage when the search coil lays over stator core and windings.

For radial positioning, the induced external search coil voltage is compared with respect to internal search coil voltage and the phase shift and the magnitude are presented. The experiment results show that the phase of the induced search coil voltage shifts as the position of the search coil is shifted. This is an expected result; because when a three phase balanced excitation is applied to the machine rotating air gap flux will be generated. Thus, when the search coil is moved, the magnitude of the induced voltage does not change but the phase of the induced voltage shifts. Since, the machine used in experiments is a two pole machine, the shift angle of induced search coil voltage nearly identical with the mechanical displacement angle. Also, the magnitude of the induced search coil voltage stays nearly constant for all positions that search coil can fit properly. Thus, the experiments showed that the search coil can be placed over all positions along the circumference of the machine. The displacement of the search coil can be modelled simply by using a phase shift term.

The simulations and the experiments showed that a measurable voltage can be induced from the flux that fringes out of the machine frame. Using this induced voltage, a model that can estimate the machine flux and rotor speed may be constructed. In the next chapters these methods will be investigated.

2.6 Hardware

In this section, the hardware that is used for the experiments will be explained. There is a need for an inverter drive that is capable of measuring motor electrical signals and induced search coil voltages. The drive is also capable of measuring rotor speed accurately with an incremental encoder.

The drive is designed not only for the experiments used in this study, but also for a general purpose induction motor drive. The drive can be utilized as a general purpose field oriented control drive by using its, two phase current, two phase voltage and DC link voltage measurements. Moreover, the 1000 pulse/rev. encoder delivers rotor position data for a direct torque control algorithm. The braking resistor enables the drive to operate as a four quadrant drive.

The block diagram of the motor control hardware is given in Fig. 2-25.

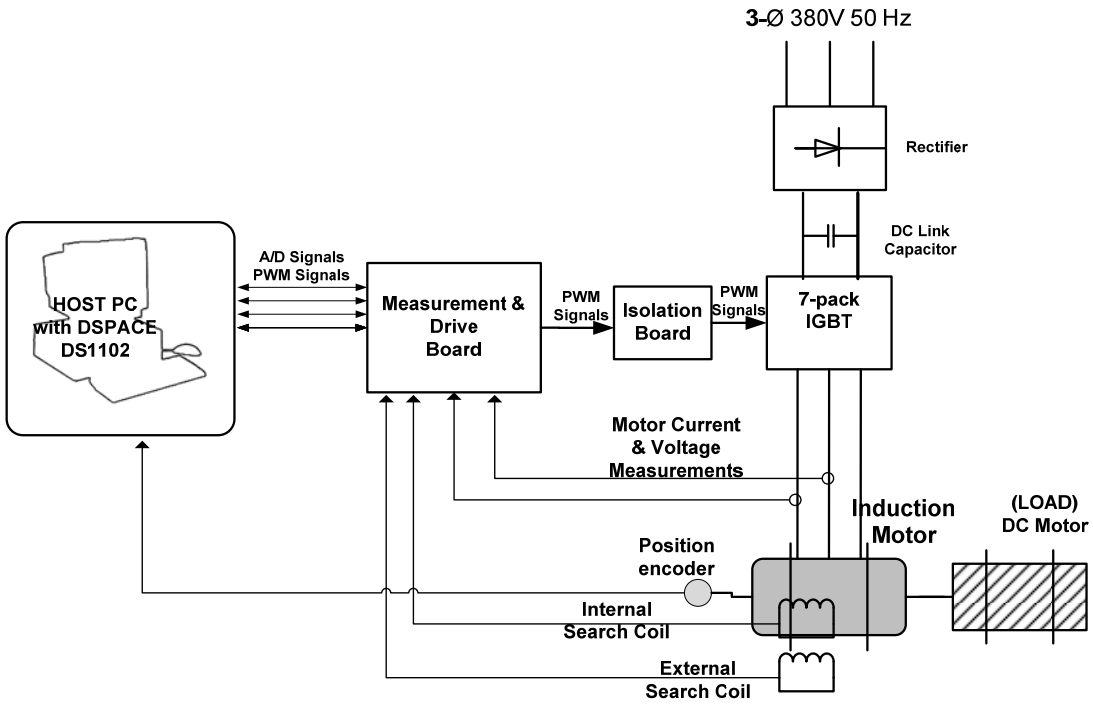

Fig. 2-25 Block diagram of the hardware

The main controller is a DSPACE DS1102 digital signal processing card which is mounted on a PC via PCI slots. The controller has four built-in ADC and six precise pwm generators and two incremental encoder inputs. A circuit board is designed to interface the DSP card to power stage and electrical measurement card. The circuit board consists of two PCB cards. Measurement & drive circuit and isolation & power control circuit. The hardware and PCB card can be seen from Fig. 2-26.

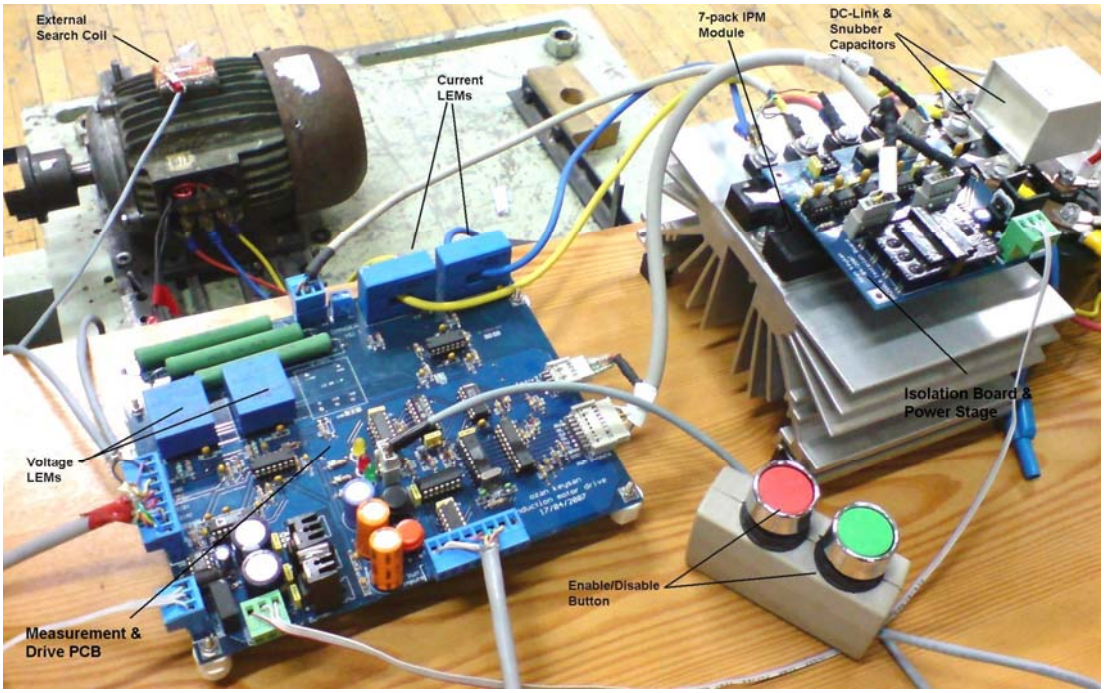

Fig. 2-26 The photo of motor drive hardware

2.6.1 Measurement – Drive Circuit

This circuit board measures the analog signals and transmits the pwm signals to isolation board. Also, the pwm signals may be enabled or disabled by a button, and a fault signal disable the system automatically. The PCB layout of the card is available in Appendix E.

The measurement part consists of two current transducers, two voltage transducers and two instrumentation amplifiers. Current transducers (LEM LA 55P) measure the two phase currents. Voltage transducers (LEM LV 25P) measure the phase voltages of the induction machine. The induced search coil voltages are measured via a dual channel low current instrumentation differential amplifier (AD8273). The amplifier both isolates the search coils from the circuitry and draws negligible current from the search coils.

The block diagram of analog signal measurements is given in Fig. 2-27.

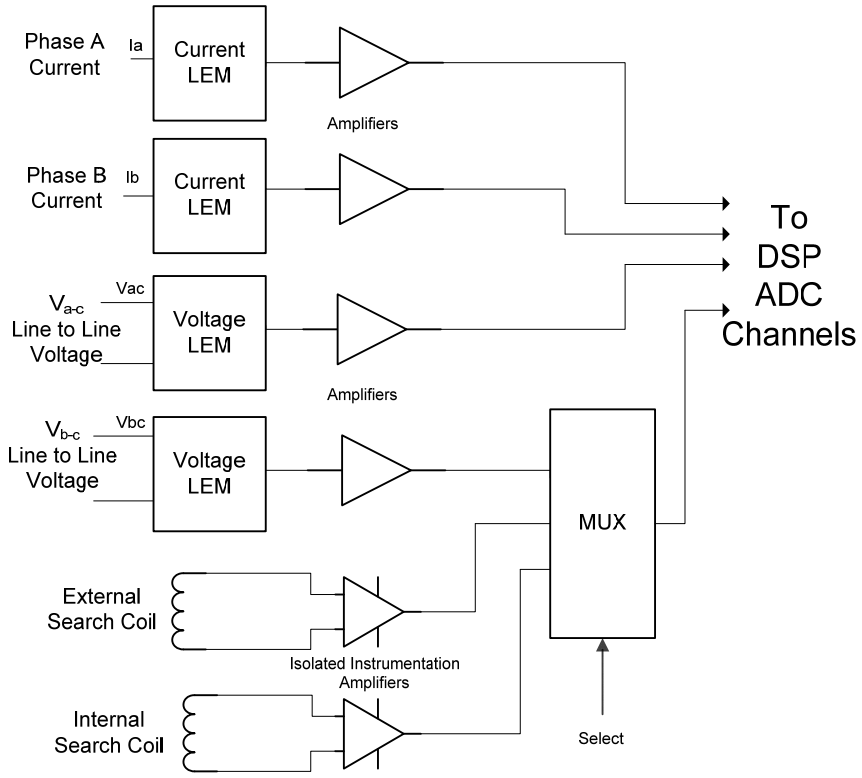

Fig. 2-27 Block diagram of analog measurements

The pwm signals send from the DSP card are not symmetrical and without dead time. In order to obtain symmetrical pwm signals XOR gates are used and the dead time is generated with IXDP631. IXDP631 is a very accurate death time

generator with an oscillator crystal. A 2.5 μsec dead time is generated with an 8MHz oscillator.

The IPM used in the hardware generates fault signals if one of the following cases occurs.

- Short circuit of upper and lower IGBT's
- Over temperature
- Over current
- Low control voltage

If one of the listed faults occurs; the pwm signals are disabled automatically. Also buttons for manual enable and disable of the system is available. And, in order to avoid high dc link capacitor voltage when the machine is operating as generator a brake signal is included. Excessive charge of DC link capacitor may be discharged over a braking resistor. The block diagram of the digital part of the system is given in Fig. 2-28.

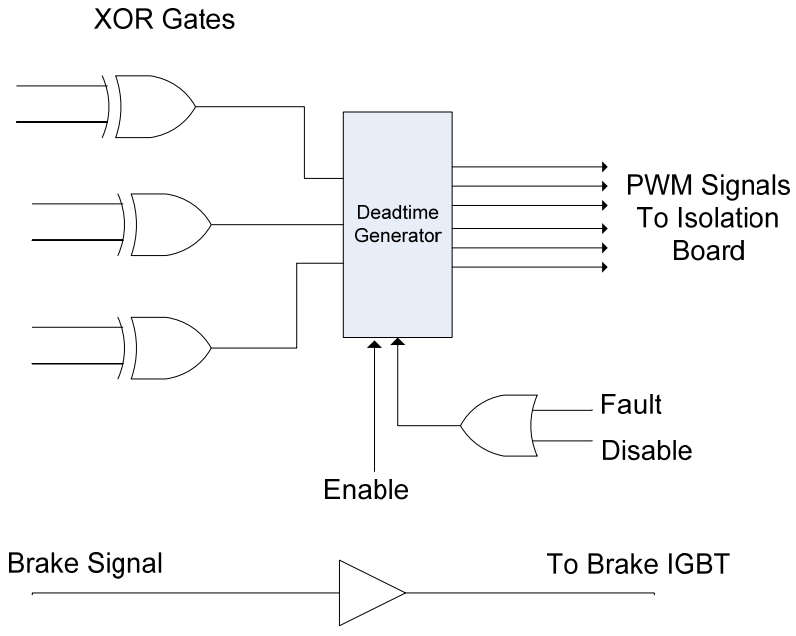

Fig. 2-28 Block diagram of pwm signals and dead time generator

2.6.2 Isolation Board – Power Stage

In order to isolate power stage from the control stage an isolation board is designed. Isolation board consists of four isolated DC supplies and seven optocouplers. The PCB layout of the isolation board is given in Appendix E.

The power stage consists of a 3-phase uncontrolled rectifier, DC link capacitor, snubber capacitor and the seven pack IGBT Module is used. The block diagram of the power stage is given in Fig. 2-29.

IGBT module is Mitsubishi IPM25RLA120 with the following specifications:

- 1200V, 25A (available up to 75 A with same packaging)
- Monolithic gate drive and protection logic
- Detection, protection and status indication circuits for over current, short circuit, over temperature and under voltage.

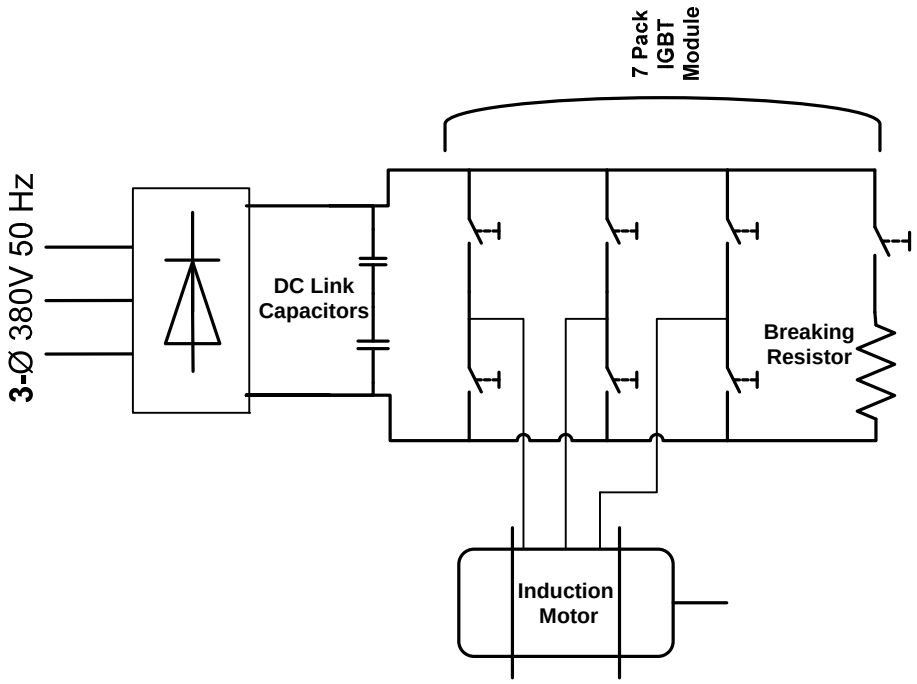

Fig. 2-29 Block diagram of power stage

2.6.3 Speed Measurement & Load

In order to measure rotor speed and measurement an incremental encoder is used. The encoder is OMRON E6C2-CWZ6C 1000pulse/revolution incremental encoder. Since, the DSPACE 1102 has an internal incremental encoder input; the position of the rotor can be measured accurately using built-in functions of the DSP controller Built-in function can also count number of pulses to measure the rotor position or can measure the elapsed time between encoder pulses to measure the speed of the machine.

To load the induction machine a 9 kW DC motor is used which is directly coupled to induction motor. The DC motor is torque controlled with the Mentor II DC motor controller (with specifications given in Appendix C) to load the induction machine.

2.6.4 Software

To control the hardware, the DSP card can be programmed with C programming language. The control algorithm is based on the software used in [40] with some modifications. The software produced pwm signals based on space vector pulse width modulation techniques. The software has a sampling ratio of 6.67 kHz which is same with the frequency of pwm signals.

There is a built-in module for the incremental encoder. Using this module, the position and the speed of the method can be measured accurately. This signal is used for comparison of the speed and position data estimated from search coils.

The software has a data capture toolbox which is called TRACE. It is used to capture and visualizations of the variables used in the software. The captured signals can be exported to MATLAB environment for a more detailed analysis. A sample, screenshot is given in Fig. 2-30. In that capture, measured phase voltages, phase currents, internal search coil voltage, external search coil voltage and the rotor position measured from incremental encoder is given.

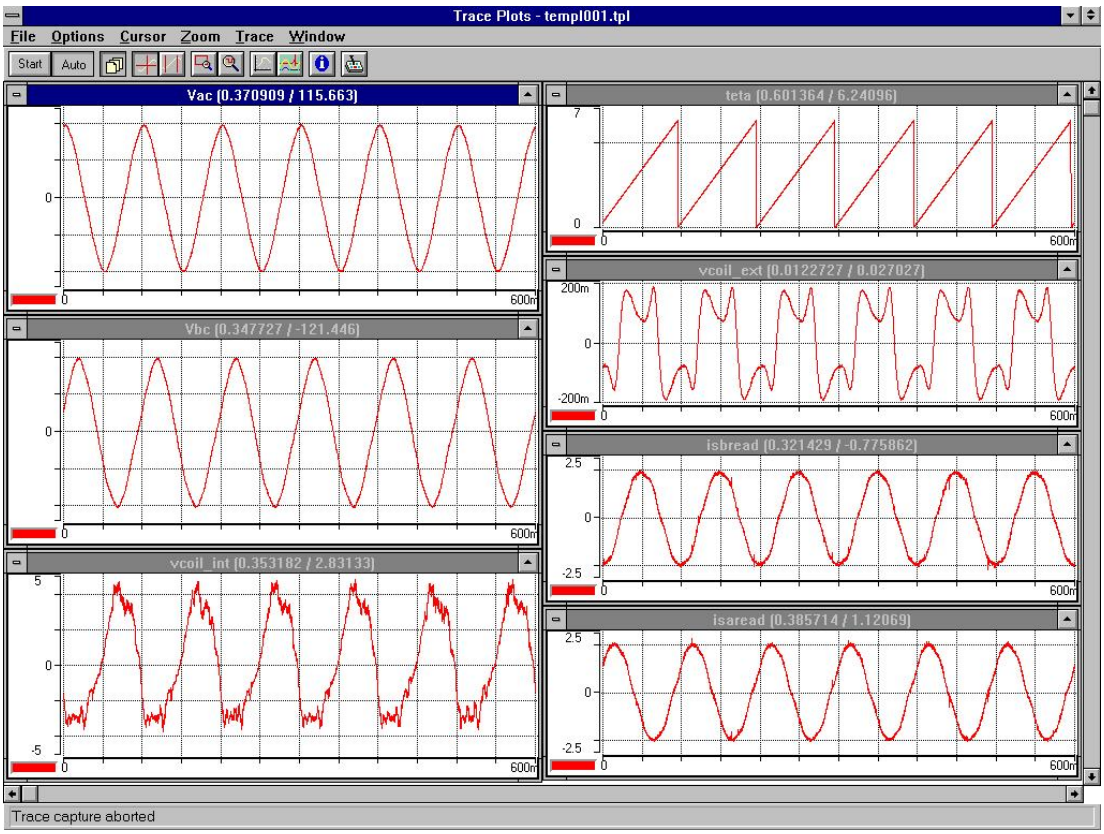

Fig. 2-30 Screenshot of built-in data capture software of DS1102 (TRACE)

2.6.5 Evaluation of Hardware

For the experiments that will be performed in this study, hardware was designed. The hardware is not designed for only this study but as a general purpose induction machine inverter drive. The designed hardware is capable of driving the motor by field orientation techniques utilizing its phase current, phase voltage and DC link voltage measurements. With some small modifications hardware can be applied to many other studies.

CHAPTER 3

EXTERNAL SEARCH COIL FOR DETECTION OF ROTOR SPEED AND ROTOR SLOT NUMBER

3.1 Introduction

In the first chapter, a literature survey was presented. In the literature, there are several methods which utilize rotor slot saliencies for rotor speed estimation. Most common method is detecting rotor slot harmonics by measuring the line currents for a voltage controlled inverter. The line currents can be measured by injecting a high frequency carrier signal to the fundamental excitation or without high frequency signal injection. For both methods, the most studied method is the spectral analysis method. In this method, the captured line current data is analyzed via spectral analysis techniques in frequency domain. Due to large data acquisition periods and computation time this methods either work offline or have low transient performance [32]. To estimated rotor speed, first irrelevant harmonics are eliminated, then the frequency of the rotor slot harmonics can be obtained as described briefly in 1.3.3.

In this chapter, the rotor speed will be estimated using the spectral analysis techniques. Measuring fringing flux using an external search coil for rotor speed estimation is a new method in literature.

It is proposed in the previous chapter to place a search coil outside of the machine frame can induce measurable voltage utilizing fringing mutual flux. The fringing flux across the machine is directly related with its source; the air gap flux. Thus, the harmonics of the air gap flux which induces voltage on stator coils also appear similarly in the fringing flux. Thus, using a spectrum analysis method on the induced voltage of the external search coil the rotor speed may be extracted in the same manner as in equation (1-27).

The aim of this chapter is to analyze if the already mentioned rotor slot harmonics exists in the induced search coil voltage. The analysis will be performed offline in MATLAB environment using the captured data. The details of the experimental procedure are available in 3.4

3.2 Introduction to Rotor Slot Harmonics

It is stated in Chapter 1 that, air gap flux contains some harmonics. These harmonics can result from stator winding, machine design, mechanical faults, permeance variations caused by stator-rotor slots. The slot harmonics is used for rotor speed estimation in literature with many methods. In this section, elaborate explanation of rotor slot harmonics will be presented which were briefly explained in section 1.3.3 and 1.3.4.

In Fig. 3-1, the MMF distribution of an induction machine is given. Due to the stator slots, the MMF in the air-gap has a stepped waveform as shown in figure. The harmonics owing to stator structure induce voltages of the same frequency as the power supply in the stator windings since their influences to the rotor windings or bars are reduced by distributed stator windings, skewed slot, etc. [4]. For the calculations in this section, only the fundamental component of the MMF distribution will be taken into account. Thus, the air-gap flux will be assumed sinusoidal and the harmonics due to spatial distribution of stator windings will be neglected.

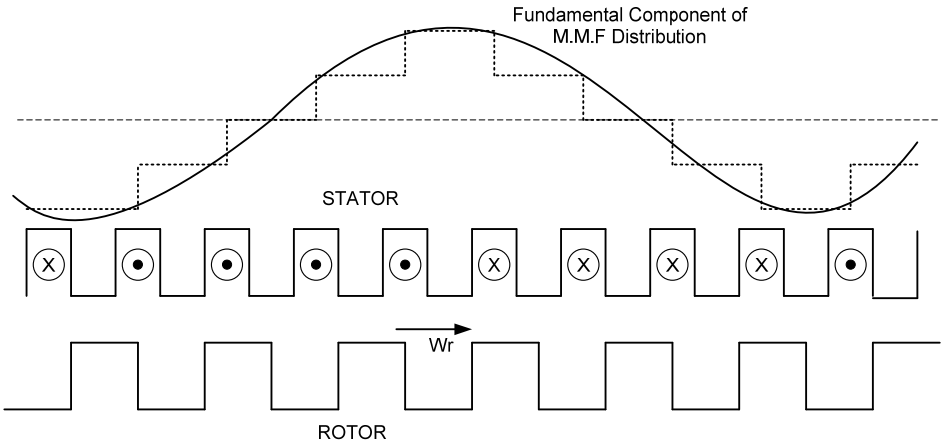

Fig. 3-1 MMF distribution in an induction machine

Thus, the stator side of the machine is assumed to be without space undulations as show in Fig. 3-2. Thus the permeance of the air gap will vary only due to rotor slot openings. Fig. 3-2 displays variations of air gap permeance with θ. If a stationary position on the stator is considered, this figure may be viewed as the time variation of permeance with respect to this stationary reference.

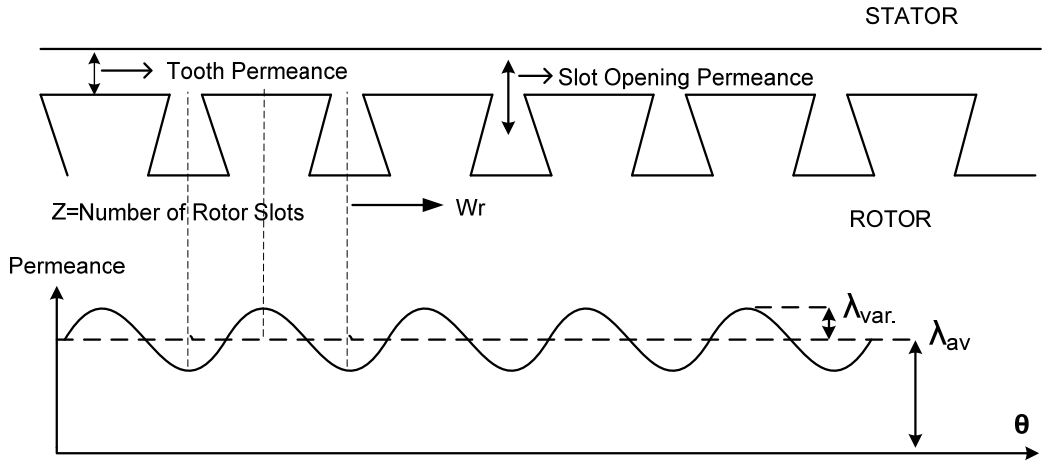

Fig. 3-2 The rotor slot openings and permeance variation (stator slots neglected)

The permeance variation can be expressed as;

$$\lambda(\theta,t) = \lambda_{av.} + \lambda_{var}.\cos\left[\frac{\mathrm{Z}}{\mathrm{P}}(w_r t - \theta)\right] \quad (3\text{-}1)$$

where, $\lambda_{av.}$ is the average magnitude of permeance, λ_{var} magnitude of permeance fluctuations, w_r angular rotor velocity, Z number of rotor slots, P number of pole pairs, θ angular position.

As mentioned the magneto motive force produced by stator windings is assumed to be sinusoidal and can be expressed as [38];

$$\mathcal{F}(\theta,t) = \mathcal{F}_1.\cos(w_s t - \theta) \quad (3\text{-}2)$$

F_1 is the magnitude of fundamental component of MMF, w_s is the fundamental frequency of the power supply. Thus, the corresponding flux is equal to;

$$\phi(\theta,t) = \mathcal{F}(\theta,t).\lambda(\theta,t) \quad (3\text{-}3)$$

$$\phi(\theta,t) = \mathcal{F}_1.\cos(w_s t - \theta).\{\lambda_{av.} + \lambda_{var}.\cos\left[\frac{\mathrm{Z}}{\mathrm{P}}(w_r t - \theta)\right]\}$$

Referring to [4] and section 1.3.3 the induced voltage a search coil wound around a stator tooth can be expressed as;

$$v_c(t) = -N.\frac{d\emptyset}{dt} \quad (3\text{-}4)$$

Taking the derivative of the flux given by equation (3-3); the induced voltage can be expressed basically[4];

$$v_c(t) = -\mathrm{K}_1\sin(w_s t - \theta_n) \quad (3\text{-}5)$$

$$-\mathrm{K}_\mathrm{f}\sin\left[\left(\frac{\mathrm{Z}}{\mathrm{P}}w_r + w_s\right)t - \left(\frac{\mathrm{Z}}{\mathrm{P}} + 1\right)\theta_n\right]$$

$$-\mathrm{K}_\mathrm{r}\,sin\left[\left(\frac{\mathrm{Z}}{\mathrm{P}}w_r - w_s\right)t - (\frac{\mathrm{Z}}{\mathrm{P}} - 1)\theta_n\right]$$

K_1, K_f, K_r gives the magnitudes of three components respectively, θ_n is the angular position of search coil. There are three components in equation (3-5). First component is the fundamental component of the induced voltage. The other two components describe the rotor slot side band harmonics (components at frequencies; $(Z/P).w_r+w_s$ and $(Z/P).w_r–w_s$). The induced voltage waveform is visualized in Fig. 3-3 [4].

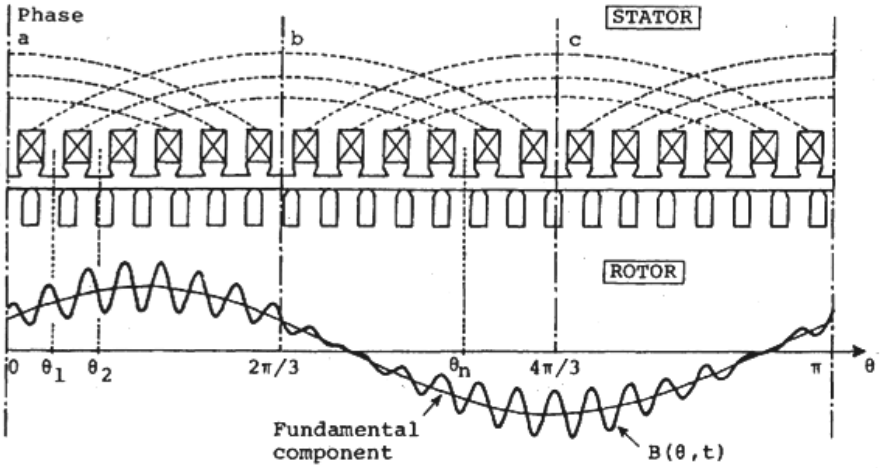

Fig. 3-3 Air-gap structure and flux distribution of induction motor [4]

As seen from the equations and figure, the induced voltage on the search coil will be modulated with a term directly related with rotor frequency (w_r). This can also be verified using the induced search coil voltages. In Fig. 3-4, the experimentally captured internal search coil voltage is given when the motor #2 is operating at rated voltage and frequency (50 Hz, $220V_{l\text{-}n}$). Similar results for the external search coil will be presented in following sections. It can be observed from the figure that the waveform is similar to what the theory predicts.

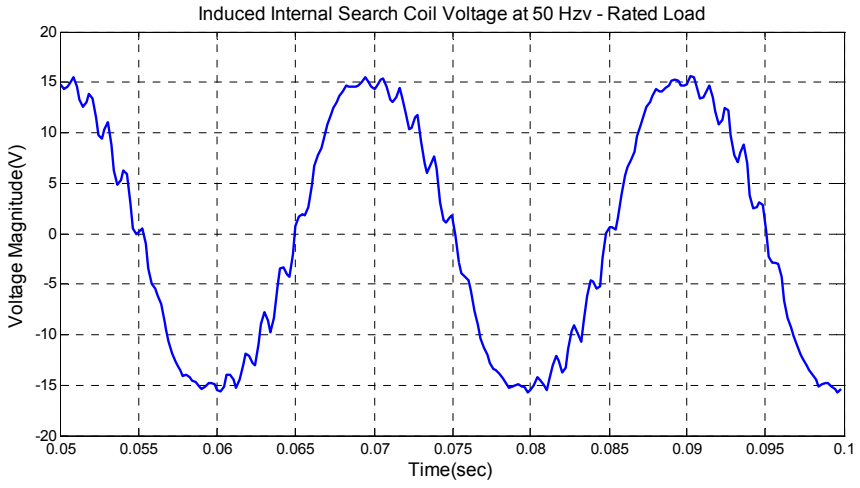

Fig. 3-4 Induced internal search coil voltage at 50 Hz – rated load

To conclude, in this section rotor slot harmonics will be investigated in the external search coil voltage. The equations derived and experimental results show that, the induced search coil voltage will include rotor slot harmonic components besides the fundamental component. Rotor slot harmonics has two sideband components;

- Rotor Slot Harmonic Lower Sideband: $(Z/P).w_r - w_s$
- Rotor Slot Harmonic Upper Sideband: $(Z/P).w_r + w_s$

If the frequency of these rotor slot harmonics can be obtained, rotor speed (w_r) can be extracted [4]. In the following section, methods to extract frequency of these rotor slot harmonics will be investigated.

3.3 Analysis Techniques for Search Coil Captured Data

As mentioned in Chapter 1, the rotor slot harmonics can be measured utilizing phase current measurement, zero sequence voltage measurement, etc. After the measurements are taken, the captured data should be analyzed. Spectral analysis techniques are the most common methods [33]. There are also another techniques like, phase locked loops or demodulation which will be studied in the following chapters. In this chapter, spectral estimation techniques will be investigated.

3.3.1 The Spectrum Analysis Methods

In order to obtain spatial information of rotor slots from search coil captured data, some kind of spectrum analysis may be applied. However, Fast Fourier Transform (FFT) is the most commonly used method in literature to analyse the obtained data [32], there are many studies that compare different spectrum analysis methods.

The selection is mainly dependent on the application and signal characteristics. Habetler and Hurst presented valuable results in [33], which compares interpolated FFT, Blackman-Tukey method, Steglitz-McBride method and multiple signal classifier method and parameter estimation methods. Habetler and Hurst in [33] mentioned that, DSP techniques can effectively extract saliency harmonics from the stator current, but they require long sampling times, particularly at low speeds. They

suggested parametric spectrum estimation techniques which can offer improved peak-extraction particularly for short data periods. They showed that these methods may present more accurate results than classical FFT method in calculating rotor slot harmonics especially when short data sets are available.

There are other studies that focus the optimization of spectral analysis techniques rather than improvement of rotor slot harmonic search algorithms. In [48], other spectrum estimation techniques are compared like; multiple signal classification method, Welch Method and Chirp-Z Transform especially for periodic non stationary signals. Also, in [21], Chirp-Z transform is compared with classical FFT method. To compare these two methods it is useful to mention some basic definitions. Assume an FFT algorithm that takes N samples with a sampling frequency of $f_{sampling}$. This gives a spectrum of base resolution over the frequency range which is given in equation (3-6).

$$f_{resolution} = \frac{f_{sampling}}{N} \qquad (3\text{-}6)$$

$$f_{range} = \left(0, \frac{f_{sampling}}{2}\right)$$

Therefore to improve spectral resolution a wide sampling time window (large number of sampled points), with fixed sampling frequency is required [21]. But, neither current signal nor induced search coil voltage can be considered stationary in a long time window because of supply frequency and load conditions may vary during data acquisition period. Therefore, in both [21] and [33] the main problem is considered as; to obtain a good spectral resolution with a short sampling time window. In [48], the Chirp-Z transform is used to improve resolution for a fixed and limited frequency window. Chirp-Z transform provides spectrum analysis on a restricted frequency search window. Restricted frequency search window is suitable for rotor speed detection once the number of rotor slots is known. The disadvantage of the Chirp-Z transform is it needs longer processing time than FFT analysis. But this increased processing time may still be advantageous compared to the data acquisition period for the modern digital signal processing cards. The resolution of the chirp-Z transform can be expressed as [21];

$$f_{resolution} = \frac{f_{window}}{N} \quad (3\text{-}7)$$

Where f_{window} is the frequency window interval that Chirp-Z transform (CZT) covers and N is the number of samples. Thus, frequency window can be narrowed to improve resolution in a specified frequency range or to reduce the number of samples.

In [21], some experiment results were presented to compare FFT and Chirp-Z transform (CZT) for rotor slot harmonics frequency detection. Fortunately, the DSP card used in [21] is same with the one used in this study, which is a DSPACE DS1102 floating-point controller with specifications given in Appendix C. In [21], the frequency window (f_w) is selected as 70 Hz, sampling frequency as 2 kHz. CZT is calculated for 1024 data points and FFT for 8192 data points. The experiment results are presented in Table 3-1.

Table 3-1 Comparison between the features of CZT and FFT applied to rotor slot harmonic frequency detection [21]

Spectral Estimation Technique	Resolution f_{res} (Hz)	Sampling time window (s)	Processing time (s)	Total time required (s)
FFT	0.244	4.096	0.060	4.156
CZT	0.068	0.512	0.470	1.452

As seen from experiment results of [21], the CZT gives better spectral resolution. Moreover, shorter sampling time window helps to decrease errors. One disadvantage of the CZT is processing time required by the method is much longer compared to FFT. But still, total required time is shorter than the FFT method.

The CZT can estimate the speed in 1.5 seconds, where FFT in 4 seconds. Thus, both methods can not be considered as online rotor speed estimators.

On the other side, there are also many studies which aim to decrease the acquisition and computation time for FFT. One practical method for decreasing computation time for FFT is taking number of samples in a power of two (2^n) generally the number of samples are chosen as 1024 or 2048 points.

In [32], other factors affecting the dynamic performance of FFT algorithm is investigated, improvements suggested. It is recommended to use a real value based on split-radix algorithm which minimises the number of multiplications and additions. Also in [32], it is proposed that; Hanning window gives the best performance on low dB signals.

In rotor speed estimation algorithm proposed in [32], N points are taken from stator current with a sample frequency of $f_{samp.}$ Then the data is analyzed with FFT method and searched for rotor slot harmonics. Then, at each cycle the oldest m samples are discarded from the record buffer, and then refilled with m new data. This reduces the speed update time to m/f_{res}.

The experiment results are also presented in [32]. The experiments are performed with i860 vector processor, f_{samp}=1 kHz, N=4096, T_{aq}=4sec, m=40, T_s=100ms. In other words, all data (N) is captured at 4 sec, then the speed information is updated at each 100ms. The computation times for each step for N=2048 and N=4096 is given in Table 3-2.

Table 3-2 Computation times for speed detection for various data samples [32]

Data Samples(N)	Hanning Window (msec)	FFT (msec)	Search Algorithm (msec)	Total (msec)
4096	2.5	39.5	8.2	50.2
2048	1.3	11.3	4.2	16.8

As seen from Table 3-2, total speed estimation time is reduced enormously compared with the results of Table 3-1. This is achieved by renewing a small partition of captured data set at each cycle with the oldest ones. But this improvement does increase the dynamic performance of the method that effectively. The experiment results performed in [32] are presented in Fig. 3-5. First graph shows the estimated and actual motor speed in a fast transient. Second graph shows the same response for a slower rate transient.

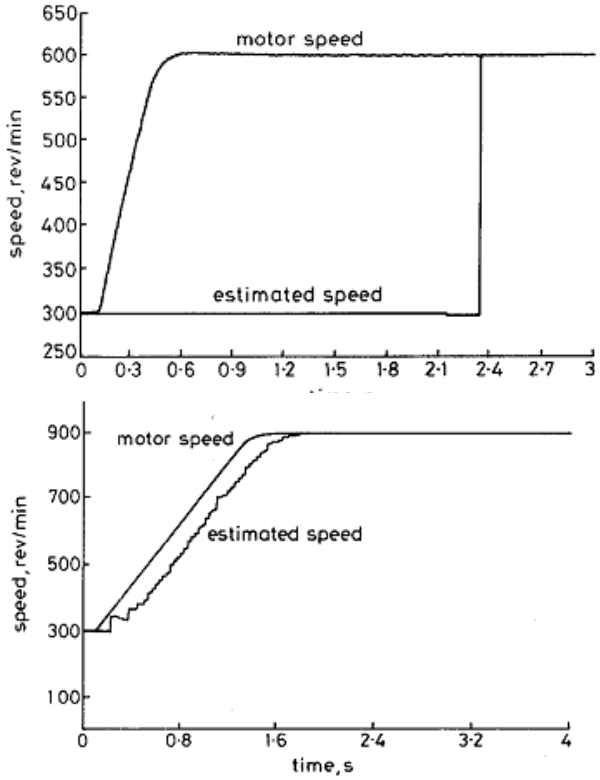

Fig. 3-5 Actual and estimated speed for fast and slower rate transients [32]

As seen from experiment results, if the transient rate is high, the estimation process stalls. Then estimates the speed correctly after a totally new data set is captured which corresponds to a period about 2 seconds. For slower rate transients, the estimation process does not stall but has an estimation lag about 200 msec. Thus, this method is suitable for large motors that does not have high dynamic responses or motors running at steady state conditions. [32]

Different spectral analysis methods are explained in this section. This thesis does not aim to improve spectral analysis methods and dynamic performance of speed estimators. In this chapter, it is aimed to investigate the existence of rotor slot harmonics in the induced search coil voltage. A better spectral estimation may be used for better performance but, FFT seems to be simplest and most practical method for the purpose. FFT is a reliable and fast algorithm which can be easily implemented with MATLAB blocks.

In this chapter of the study, experiments are performed with induction motors driven with a sinusoidal 3-phase supply, and the search coil induced voltage will be captured with a digital oscilloscope with specifications given in Appendix C. Then, the motor will be driven by the inverter described in 2.6 and search coil voltage will be captured by the same hardware. Then the captured data is analyzed in MATLAB to investigate the rotor slot harmonics in the external search coil and rotor speed estimated from this data will be compared with the actual rotor speed.

The purpose can be restated as identifying whether the induced voltage in the external search coil contains same information as the air gap flux and whether this voltage can be used to detect the motor speed or/and number of rotor slots.

In the following section, the method for rotor speed estimation will be explained and the experiment results will be presented.

3.3.2 An Algorithm for Rotor Speed Detection with External Search Coil

In order to obtain the speed information from the induced search coil voltage data, the following steps will be followed. First, data samples necessary for spectral analysis will be captured. Then, a spectral estimation method is applied to the captured data, and a search algorithm is performed over the results of spectrum analysis.

The search algorithm consists of the following parts; identifying fundamental supply frequency, filtering the harmonics of supply frequency, searching and verifying the rotor slot harmonics in the filtered data. Finally calculating and refreshing the speed data using the number of rotor slots.

The block diagram of the proposed search algorithm is given in Fig. 3-6. Details of the each will be explained.

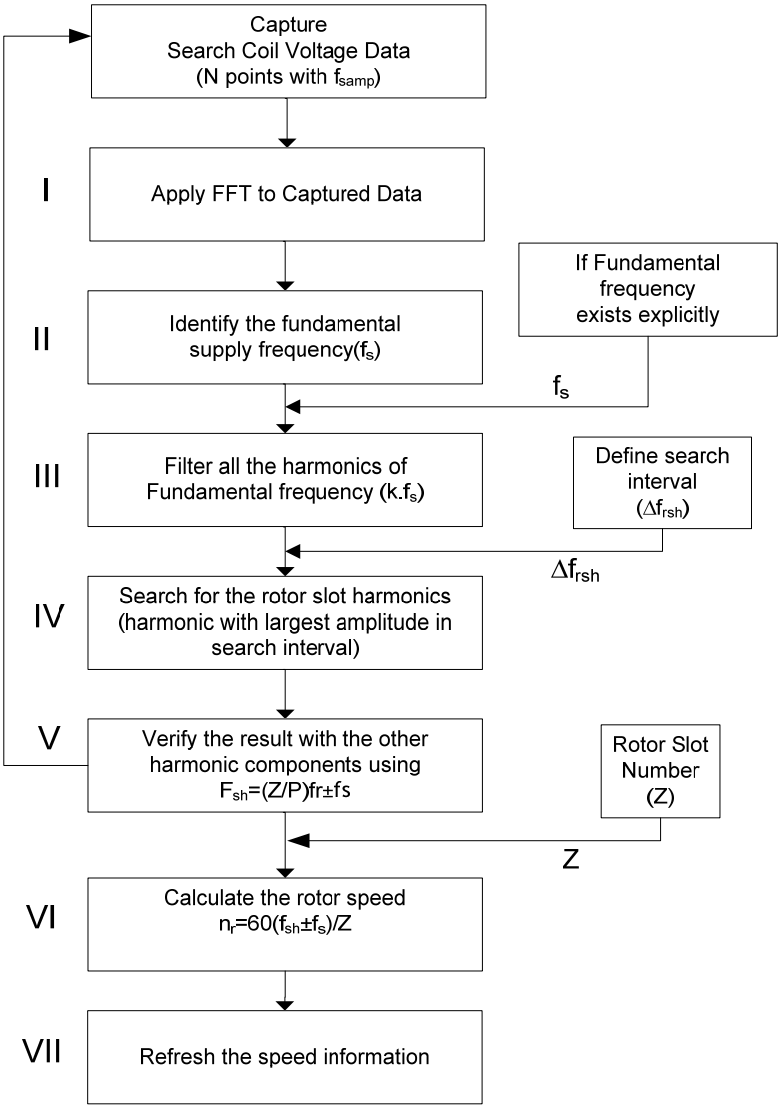

Fig. 3-6 Block diagram of rotor speed detection algorithm

I) Apply Spectral Analysis: As mentioned in previous section, Fast Fourier Transform will be used for spectral analysis for easy implementation. FFT will be applied using built-in function blocks in MATLAB. Captured data will be analyzed offline in MATLAB environment.

II) Identify Fundamental Supply Frequency: In order to filter, the fundamental excitation component, and harmonics of fundamental excitation; the supply voltage frequency should be identified. Fundamental supply frequency can be easily

detected using the component with the largest amplitude in the spectrum analyzed data. On the other side, in most cases the fundamental supply frequency can be determined explicitly such as in V/f control or indirect field oriented control. For such a case, this step may be omitted.

III) Filter Harmonics of Fundamental Frequency: The harmonics of the fundamental component should be removed to obtain rotor slot harmonics. The multiples of fundamental supply frequency ($k.f_s$, k=1,2,3...) are detected in spectrum analysis and discarded in this block.

IV) Search for Rotor Slot Harmonics: After the removal of supply frequency harmonics the rotor slot harmonics can be searched over the spectral data. But a narrower search interval for the algorithm can be defined that will decrease the computation time and increase the stability of the system. Search interval should contain all the speed range that motor can run. For example; a search interval between synchronous speed (s=0) and the speed that maximum torque is generated (s_{max}) is a reasonable interval that will work for many applications at steady-state conditions. The slip at the maximum torque generation can be calculated from machine parameters. But, if these parameters are not available s_{max} can be assumed between 0.3 - 0.4 with a safety factor. The search interval for rotor slot harmonics (Δf_{rsh}) used in the algorithm is given in terms of slip(s) and applied stator frequency (f_s) in equation (3-8).

$$\Delta f_{rsh} = [f_s(1 - s_{max}) , \quad f_s] \qquad (3\text{-}8)$$

The search interval should contain the over synchronous speeds (s<0) if the machine runs as a generator. Moreover, search interval is drastically reduced if the rotor mechanical time constant is available. By this way, previous speed information and rotor mechanical time constant is used to estimate the next maximum and minimum speed that is possible. Also, these method increases method stability by eliminating unreasonable speed fluctuations considering rotor inertia.

V) Verification of Rotor Slot Harmonics: In the filtered data within search interval, first the harmonic with the largest amplitude is detected. Then it is checked whether it is a rotor slot harmonic or not by searching other harmonic couples using equation (1-23). If the rotor slot harmonics are not verified with its side band frequencies, the speed information is not refreshed and the search algorithm is restarted with a new set of data. If the detected harmonic is verified to be a rotor slot harmonic data then the frequency of rotor slot harmonic is send to next block to calculate the rotor speed.

VI) Rotor Speed Calculation: If the rotor slot harmonics are detected and verified, the rotor speed may be calculated. It will be useful to reemphasize the equations explained in section 1.3.3. The frequency of rotor slot harmonics (f_{rsh}) is given in using equation (3-9).

$$f_{rsh} = \frac{Z}{P} f_r \pm f_s \quad (3\text{-}9)$$

Where, Z is the number of rotor slots, P is the number of pole pairs and f_r and f_s is the rotor and stator electrical frequencies respectively. From equation (3-9), f_r can be extracted as;

$$f_r = \frac{P}{Z}(f_{rsh} \pm f_s) \quad (3\text{-}10)$$

In an induction motor the rotor speed in revolution per-minute (rpm) is given in equation (3-11).

$$N_r = \frac{60\, f_r}{P} \quad (3\text{-}11)$$

Using equation (3-10) and (3-11) the rotor speed in revolutions per minute (Nr) can be expressed as in equation (3-12) [4], [14].

$$Nr = \frac{60}{Z}(f_{rsh} \pm f_s) \quad (3\text{-}12)$$

Obtaining rotor slot side band harmonics, the rotor speed can be calculated. But, notice that, the number of rotor slots should be known for this process. The number of rotor slot data may be obtained from the manufacturer's data. If it is not

available as for most cases, the number of rotor slots may be estimated with an initialization algorithm. This method will be explained in section 3.7.

VII) Refresh the Speed Information: After the speed is calculated successfully using equation (3-12), the speed information is updated and the algorithm starts from the beginning for each data set.

3.4 Rotor Slot Harmonics Verification Experiments

In this part, the described algorithm will be realized and the results of the experiments will be evaluated with the external search coil.

The experiments are performed on two induction motors. The first induction motor is a 1.1 kW 6-pole wye-connected induction motor. The motor has 36 stator and 26 rotor slots. The second motor is 2.2 kW 2-pole wye-connected induction machine. Second motor has 24 stator and 18 rotor slots. Both machine frames is made of cast iron. The parameters and lamination drawings of the induction motor are given in Appendix A.

The induction motors coupled to a DC motor with a DC drive which is used for mechanical loading. In the first part of experiments, a three phase sinusoidal AC supply is used at rated frequency and voltage (50 Hz, 380 $V_{l\text{-}l}$). The sinusoidal supply is utilized in order to eliminate the harmonics that would result from an inverter. Once the rotor slot harmonics is obtained similar experiments are performed with the inverter drive system to verify the operation under noisy operation of the inverter. The estimated speed is compared with the speed measurement of a 1000 pulse/rev. incremental encoder.

The experiments are performed using the search coil described and selected in section 2.3. The search coil used is U-core search coil (type #1) with 120 coil turns.

The experiment data is captured with an oscilloscope in this part. The sampling frequency is 2 kHz and number of captured data points is 2000 which gives a FFT resolution of 1 Hz. The captured data is transferred to computer and analyzed offline with MATLAB. The list of equipments used in experiments and their specifications are given in Appendix C.

3.4.1 The Experiment Results

First, rated stator voltage ($380V_{l\text{-}l}$, 50 Hz) is applied to induction motor and induction motor is loaded to run at 718 rpm, and FFT analysis of the induced external search coil voltage is shown in Fig. 3-7. When the motor is running at 718 rpm, (35.8 Hz electrically) it generates rotor slots harmonics at 310 Hz referring to equation (3-9). And the rotor slot harmonics are modulated with the fundamental applied stator frequency resulting in harmonics at; 310±50 Hz sideband frequencies. As seen from Fig. 3-7, the rotor slot harmonics are dominant at 260Hz & 360 Hz, which are the fundamental sideband harmonics. Also, third sideband harmonics can be seen at 160Hz, 460Hz (310±150Hz). Also the odd and even harmonics of the supply frequency (3^{rd}, 4^{th}, 5^{th}, 6^{th}, 7^{th}) are distinctive.

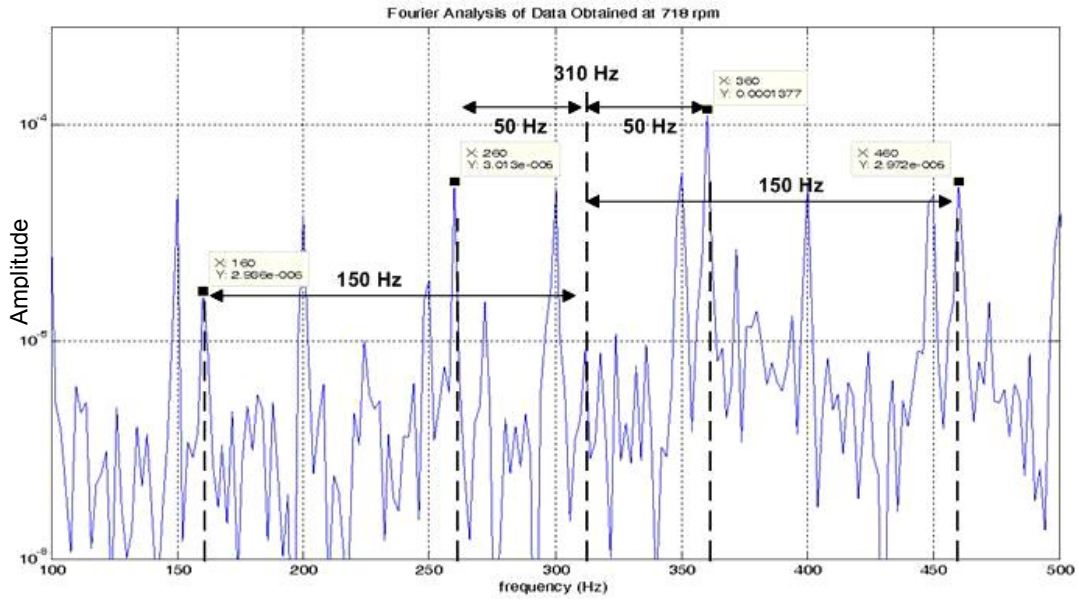

Fig. 3-7 FFT analysis of the induced search coil voltage when the motor #1 is running at 718 rpm with 50 Hz stator frequency

It is stated that the number of rotor slots for the relevant motor is 26. Using equation (1-23), it can be shown that 260 Hz, 360 Hz are first sidebands of rotor slot harmonics and the 160, 460 Hz are the third sidebands. The actual speed of the motor

is measured as 718 rpm from the coupled encoder. The estimated speed of the motor using equation (3-12) is 716 rpm. Thus the method gives an error less than 0.3%.

Another experiment is performed at 907 rpm (rotor electrical speed 45.4 Hz). FFT analysis is applied to data obtained from the induced external search coil voltage. As seen from Fig. 3-8 the rotor slot harmonic sidebands are dominant at 342 Hz and 442 Hz. Also, the third sideband harmonics are apparent at 242 Hz and 542 Hz. This states that rotor slot harmonics appear at: 392±k.50 Hz.

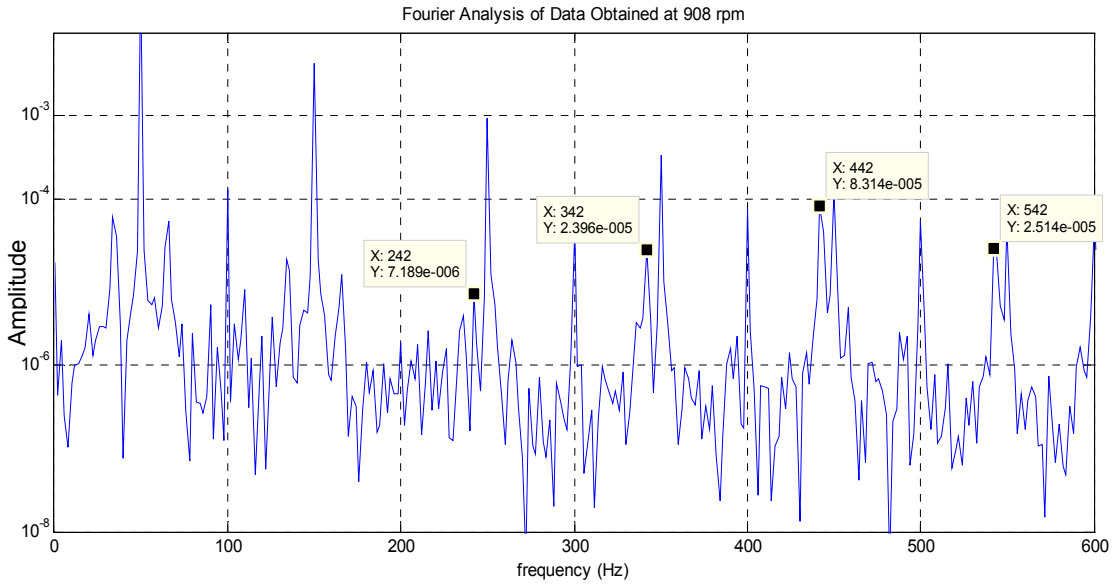

Fig. 3-8 FFT analysis of external search coil voltage when the motor #1 is running at 907 rpm with 50 Hz stator frequency

In this experiment the estimated speed from the rotor slot harmonics is 904.6 rpm. This gives an estimation error of 0.3%.

Similar experiments are performed from no load to full load at rated stator frequency for both motor #1 and motor #2. The experiment results for both motors and the estimation errors are presented in Table 3-3.

Table 3-3 Measured and estimated rotor speed data using external search coil voltage

MOTOR TYPE	Measured Speed (RPM)	Estimated Speed (RPM)	Absolute Error (RPM)	Estimation Error (%)
MOTOR #1	718	716.1	1.9	0.28
	792.7	794	1.3	0.16
	868.3	867.7	0.6	0.07
	906.7	904.6	2.1	0.23
	946	948.5	2.5	0.26
	978.3	976.1	2.2	0.22
MOTOR #2	2286.5	2286.7	0.2	0.01
	2454	2456.7	2.7	0.11
	2603.7	2600	3.7	0.14
	2811.6	2813.3	1.7	0.06
	2975.7	2980	4.3	0.14

The estimated speed percentage error is smaller than 0.3% for steps performed. The experiments proved that the rotor speed can be predicted very accurately using the external search coil. The experiment results also confirm the relation between accuracy of the method and the number of rotor slots. The motor #1 has 26 rotor slots where the motor #2 has 18 slots. As seen from Table 3-3, the speed estimation performed on motor #2 has larger absolute speed error values compared to those of motor #1. Thus there is a direct relation between accuracy of the method and the number of rotor slots.

3.5 Inverter Driven Machine Experiments

Similar experiments are also performed while the test motor is driven with the inverter described in 2.6. For PWM generation space vector pulse width modulation (SVPWM) method is used in the inverter. The motor is driven at constant stator voltage to frequency ratio at 20 Hz and 40 Hz at rated load

In Fig. 3-9 FFT analysis of the induced voltage from search coil type #1 is given while the supply frequency is 40 Hz and machine is running at 686.2 rpm. In Fig. 3-10 FFT analysis of the induced voltage on the same search coil is given while the supply frequency is 20 Hz and the machine is running at 236 rpm.

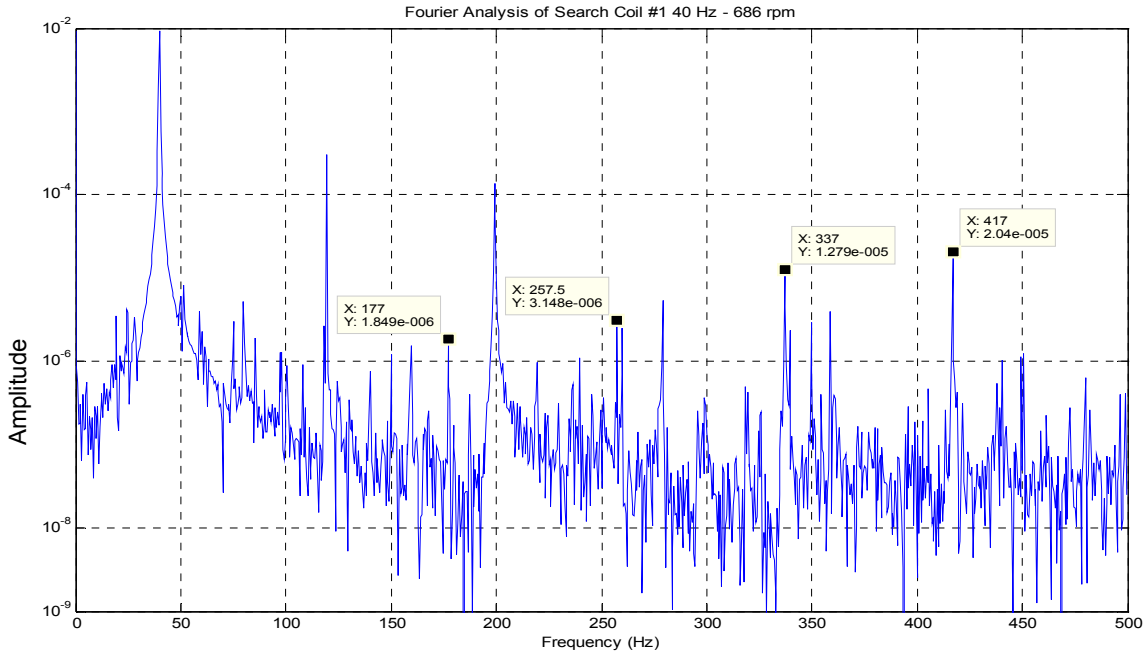

Fig. 3-9 FFT analysis of search coil voltage data at 686.2 rpm with f_s=40Hz

The predicted speed using the same algorithm with previous section are found to be 685.4 rpm and 236.5 rpm respectively where the speed encoder measures the rotor speed as 686.2 rpm and 236 rpm respectively.

Other experiment results and the estimated and measured rotor speeds are presented in Table 3-4.

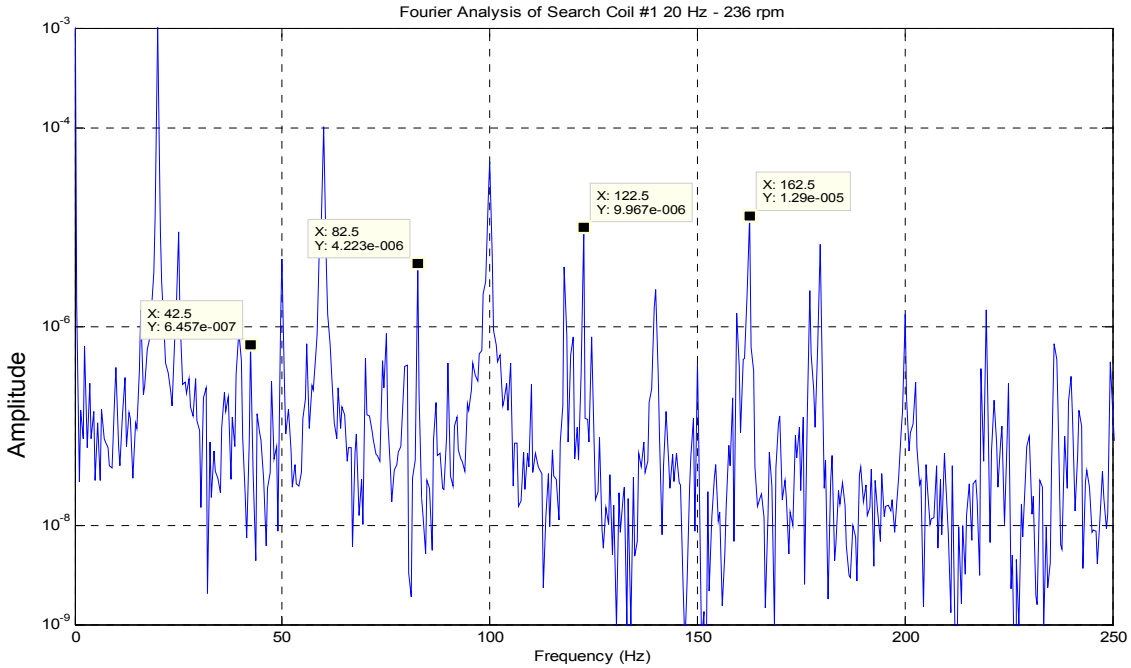

Fig. 3-10 FFT analysis of search coil voltage data at 236 rpm with f_s=20Hz

Table 3-4 Measured and estimated rotor speed with external search coil voltage for inverter driven motor

Applied Stator Frequency (Hz)	Measured Rotor Speed (RPM)	Estimated Rotor Speed (RPM)	Absolute Speed Error (RPM)
20	236	236.5	0.5
20	309.9	311.5	1.6
40	686.2	685.4	0.8
40	741.6	743.1	1.5
50	811.2	810	1.2
50	910.4	909.2	1.2
50	950.3	950.8	0.5

The experiment results showed that, the rotor slot harmonics are also observable in the induced external search coil voltage for inverter driven case. Thus, the harmonics of inverter does not disturb the rotor speed prediction algorithm.

3.6 Evaluation of Rotor Speed Estimation Method with Spectral Analysis Techniques

In this part, the method for rotor speed estimation using spectral estimation techniques will be evaluated in two points; accuracy of the method and the case where rotor slot harmonics coincide with the applied stator voltage harmonics.

3.6.1 Accuracy of Method

The accuracy of rotor speed estimation using rotor slot harmonics with spectral analysis techniques mainly depends on two factors; the frequency of measured slot harmonics and the resolution of the spectral analysis technique. From equation (3-6) it can be seen that the spectrum analysis method has a resolution frequency inversely proportional with the sampling period. In the inverter driven experiments, constant sampling frequency of 6.67 kHz is used. Thus, for a constant sampling frequency the spectral estimation method has better accuracy if the data sampling period is increased. This is the main trade off between accuracy and better transient response in speed estimation algorithms using rotor slot harmonics [33]. Although, our system estimates rotor speed offline, if the method is applied as an online estimator, the trade off between accuracy and better transient response can be an advantage for adaptive speed estimation algorithms by using varying sampling periods. In dynamic conditions shorter sampling periods may be used to acquire a better refresh rate. And in steady state conditions sampling period may be increased to get a better speed tuning.

In order to find the accuracy of rotor speed estimation algorithm that utilizes rotor slot harmonics the following equation may be used. Suppose that data is acquired with f_{res}, where f_{res} is the resolution of spectral analysis method. The average error of the harmonics can be assumed as $f_{res}/2$ [32].

Thus, the error on rotor speed (Hz) can be expressed using the previously explained equation (3-9) as;

$$\epsilon(f_r) = \frac{P}{Z}[\epsilon(f_{rsh}) + \epsilon(f_s)] = \frac{P}{Z}\left[\frac{f_{res}}{2} + \frac{f_{res}}{2}\right] \quad (3\text{-}13)$$

$$= \frac{P}{Z} f_{res}$$

Where $\varepsilon(f_{rsh})$ and $\varepsilon(f_s)$ is the average error in rotor slot harmonics and the fundamental supply frequency which is both equal to $f_{res}/2$.

Considering a classical encoder with N pulse/revolution that takes measurement over a period $T = 1/f_{res}$ the average speed error of the encoder in RPM is [32];

$$\epsilon(_{encoder})_{rpm} = \frac{60}{N} \cdot \frac{f_{res}}{2} \quad (3\text{-}14)$$

Using equation (3-13) error of the method in RPM becomes;

$$\epsilon(f_r)_{rpm} = \frac{60}{Z} f_{res} \quad (3\text{-}15)$$

Combining equation (3-14) and (3-20), it can easily shown that [32];

$$N = \frac{Z}{2} \quad (3\text{-}16)$$

The equation shows the average error of FFT spectral estimate using fundamental slot harmonics is equal to an encoder with Z/2 pulses per revolution. However, this is the case where the fundamental supply frequency is obtained with spectral analysis techniques. But for most cases, there is no need to estimate the applied fundamental frequency; it is already available as an output of the control algorithm. If the applied fundamental supply frequency is explicitly available where its error is then equals to zero. Equation (3-13) transforms to;

$$\epsilon(f_r) = \frac{P}{Z}[\epsilon(f_{sh}) + 0] = \frac{P}{Z} \cdot \frac{f_{res}}{2} \quad (3\text{-}17)$$

Assuming a spectral analysis of with resolution f_{res} equals to 1 Hz and using motor #1 with 26 rotor slots equation (3-17) gives an accuracy of ±1.2 rpm.

Following similar steps with equations (3-14) to (3-16). It can be shown that, the accuracy of the algorithm for this case is equal to;

$$N=Z \quad (3\text{-}18)$$

In other words, the accuracy of the method is equivalent to an encoder with pulse number which is equal to number of rotor slots of induction machine. However, this accuracy is low compared to a general type of encoder. But, this method would be promising as a speed estimation method. In the following chapters, some methods will be proposed to increase the accuracy of the rotor speed estimation.

3.6.2 Coincidence of Rotor Slot Harmonics with Supply Harmonics

It is necessary to state one weak point of speed estimation method using rotor slot harmonics with spectral analysis techniques. If the frequency of rotor slot harmonics is very near to harmonics of applied stator voltage, the determination of the rotor speed would be harder. Or if the rotor slot harmonics clash with harmonics of supply frequency rotor speed cannot be evaluated for that value.

It is of interest to find out, how much difference between the supply frequency and rotor slot harmonics which coincides with that is enough to identify and separate supply frequency from the rotor slot harmonics. The formula for the rotor slot harmonics to coincide with one of the supply harmonics can be obtained using equation (3-9). Define the rotor speed to be equal to a harmonic of the supply frequency.

$$\frac{f_r.Z}{P} = k.f_s \quad (3\text{-}19)$$

$$k=1,2,3\ldots$$

Transforming electrical rotor speed to mechanical rotor speed in revolution per-minute (N_r).

$$N_r = \frac{k.f_s.60}{Z} \quad (3\text{-}20)$$

Using equation (3-20) and the motor parameters used in the experiment, for the supply frequency is 50 Hz, the critical rotor speeds that rotor slot harmonics coincide with fundamental line harmonics for motor #1 are shown in Table 3-5. The error band is calculated for the accuracy conditions expressed with (3-17); which is

measured as ±1.2 rpm previously. By adding a safety margin, the error band assumed to be 2 rpm.

Table 3-5 The rotor speed intervals that supply frequency and rotor slot harmonic clash problems at 50 Hz stator frequency

Critical Rotor Speed Range (RPM)	Rotor Slot Harmonic Frequency (Hz)	Ratio of Rotor Harmonics to 50 Hz	Slip
921 - 925	400	8	0.077
806 – 810	350	7	0.192
690 - 694	300	6	0.308

When the motor runs at the given rotor speed bands, the algorithm can not update speed data and uses previous speed information until a new speed data is estimated. For a constant FFT frequency resolution, the chance of coincidence of rotor slot harmonics with line harmonics increases as the stator fundamental frequency is decreased. Thus, in order to reduce overlapping of rotor slot harmonics and line harmonics, the resolution of FFT should be increased for lower speeds. Another method is to use a machine with higher number of rotor slots that will increase accuracy of the method.

3.7 Method for Detection the Number of Rotor Slots

As explained in the previous section; the rotor slot harmonics can be obtained from the search coils placed on the frame of the motor. The frequency of rotor slot harmonics are directly related with the number of rotor slots of the machine, so in order to predict the rotor speed; the number of rotor slots should be known.

The number of rotor slots can be acquired from the manufacturer's data, but it may not be accessible for all manufacturer products. When the number of rotor slots is not available, a method to estimate the number of rotor slots needs to be used.

In literature, some methods are proposed for rotor slot number estimation. The most basic method is to use a speed sensor for calibration of number of rotor slots as stated in [16]. In this method, the rotor speed is measured with speed sensor and the

number of rotor slots is selected for estimation algorithm to give correct speed information. But this is not a preferred way because it disturbs invasive property of the system also the coupling of speed sensor is either impossible or expensive.

Another method for determining the number of rotor slots is running the motor at no-load and assuming the machine runs at synchronous speed than calibrating the number of rotor slots using this speed information [32]. But, this assumption may lead to an error in number of rotor slots and this will obviously leads to an error in speed measurements. Since, even a small possibility of incorrect rotor slot number estimation leads to false speed measurement all the time, it is proposed in [32] that best method is to use a human eye to calibrate the algorithm or to use the manufacturer's data.

In [35] valuable contributions are made for detecting the number of slots. Current measuring, vibration sensing, and axial flux measurement techniques are applied in [35] and it is proposed that current measuring is to be best suitable method for number of rotor slots detection. In this section, a new method will be proposed to determine the number of rotor slots using external search coil induced voltage. In section 1.3.3, it is stated that every machine has some forms of rotor slot saliency, and it is used for speed estimation in previous section. Also, other types of saliencies exist in the induced search coil voltage even in a healthy machine [5]. The saliency of the rotor itself will introduce a harmonic independent from number of rotor slots. This harmonic is only related with the speed of the rotor and appears at;

$$f_{saliency} = f_s \pm k.\frac{f_r}{P} \qquad (3\text{-}21)$$

where f_s is supply frequency, k is the harmonic order, f_r rotor electrical speed and P is the number of pole pairs. It may seem that these harmonics would be more suitable for prediction of rotor speed because they are independent of number of rotor slots. But, it should be noted that the frequencies of these harmonics are much lower than the frequency of rotor slot harmonics. Thus, in order to make successful spectral analysis, data acquisition will take much longer compared to rotor slot harmonics referring to equation (3-7). On the other side, these saliency harmonics

can be used for estimation of number of rotor slots. The number of slots can be calibrated using rotor saliency harmonics and rotor slot harmonics simultaneously.

The block diagram of the proposed method is given in Fig. 3-11. Note that this algorithm should be run once at the commissioning of the motor. Once the number of rotor slots is estimated the rotor speed algorithm will use this information to obtain rotor speed. The algorithm is similar to rotor slot harmonics speed detection algorithm with FFT method. First, FFT is applied over the captured signal of induced external search coil voltage. Then the applied fundamental frequency is defined. After filtering the higher harmonics of fundamental stator frequency, the algorithm searches for two harmonics of interest; the rotor slot harmonics and the rotor saliency harmonics.

Rotor speed frequency (f_r) is extracted for lower side harmonics from rotor slot harmonics as given in equation (3-9) and also from equation (3-21);

$$f_r = \frac{P}{Z}(f_{rsh} + f_s) \qquad (3\text{-}22)$$

$$f_r = \frac{P.(f_s - f_{saliency})}{k}$$

Using these two equations, f_r can be eliminated and number of rotor slots (Z) can be expressed as;

$$Z = \frac{(f_{rsh} + f_s)}{(f_s - f_{saliency})} \qquad (3\text{-}23)$$

As seen from equation (3-23) once the rotor slot harmonics frequency(f_{rsh}), saliency harmonics frequency($f_{saliency}$) and stator fundamental frequency(f_s) is known the number of rotor slots can be measured. Note that, equation (3-23) is based on the first order (k=1) lower side band harmonics and upper side band harmonics are used for verification of the number of rotor slots.

Searching for rotor slot harmonics is explained in a detailed manner in section 3.3.2. Detecting rotor saliency harmonics algorithm is similar to that algorithm. First, harmonic component with largest magnitude is detected near to applied stator frequency in spectrum data. Then, that component is checked to be a rotor saliency harmonic by using upper side band harmonic using equation (3-21). Then the number of rotor slots is calculated using equation (3-23). Finally the number of rotor

slots is cross checked from the idea that number of rotor slots must be an integer. If the real number calculated using equation (3-23) has a decimal of range 0.1 - 0.9, this may indicate a possible error and the algorithm recalculates the number of rotor slots with a new set of data. If the decimal place is smaller than 0.1 or larger than 0.9, the number of rotor slots prediction is assumed to be successful the algorithm gives the nearest integer number as the number of rotor slot number and the estimation process ends.

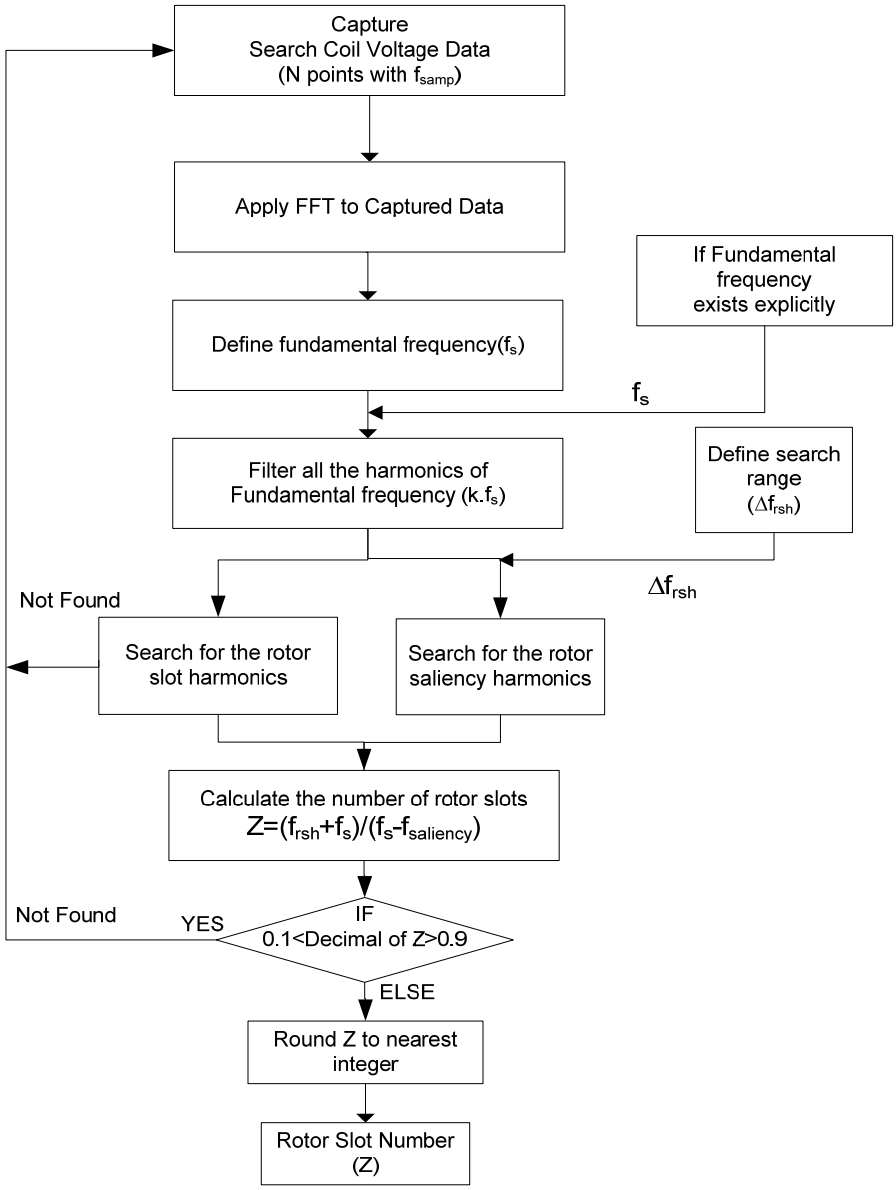

Fig. 3-11 Block diagram of number of rotor slots estimation algorithm

3.7.1 Experiments for Detection of Number of Rotor Slots

Various experiments are performed to test the method and the proposed algorithm. The induced external search coil voltage is captured for estimation of number of rotor slots. Motor #1 and motor #2 are driven with inverter at various load conditions. But it is stated in [30] that the rotor saliency harmonics are directly related with load. So at rated load, the saliency harmonics would be larger in magnitude, making the operation of the algorithm more stable. This is proved by experiment results that will be presented.

For rotor speed detection algorithm described in previous section a FFT which has a resolution of 1 Hz is used. Since, dynamic performance of number of rotor slot estimation does not have priority, it is better to make a FFT analysis with better resolution. Thus, a FFT analysis with 0.1 Hz will be used which is satisfied by taking longer data sets up to ten seconds. Referring to equation (3-6), this is satisfied by taking around 65536 (2^{16}) number of samples.

The experiments are performed for three different applied stator frequencies; 20 Hz, 40 Hz and 50 Hz.

Fig. 3-12 shows the data obtained from the external search coil at a rotor speed of 916 rpm while the machine #1 is driven with 50 Hz. Fig. 3-13, shows the data obtained at a rotor speed of 811 rpm.

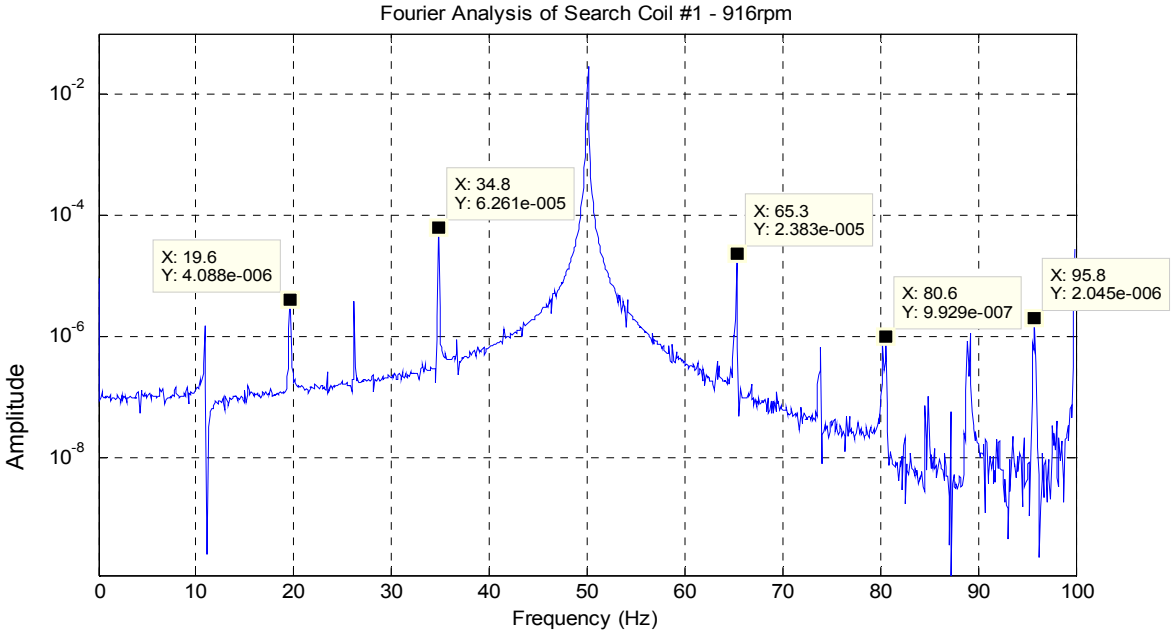

Fig. 3-12 FFT analysis of search coil voltage data at 916 rpm with f_s=50Hz

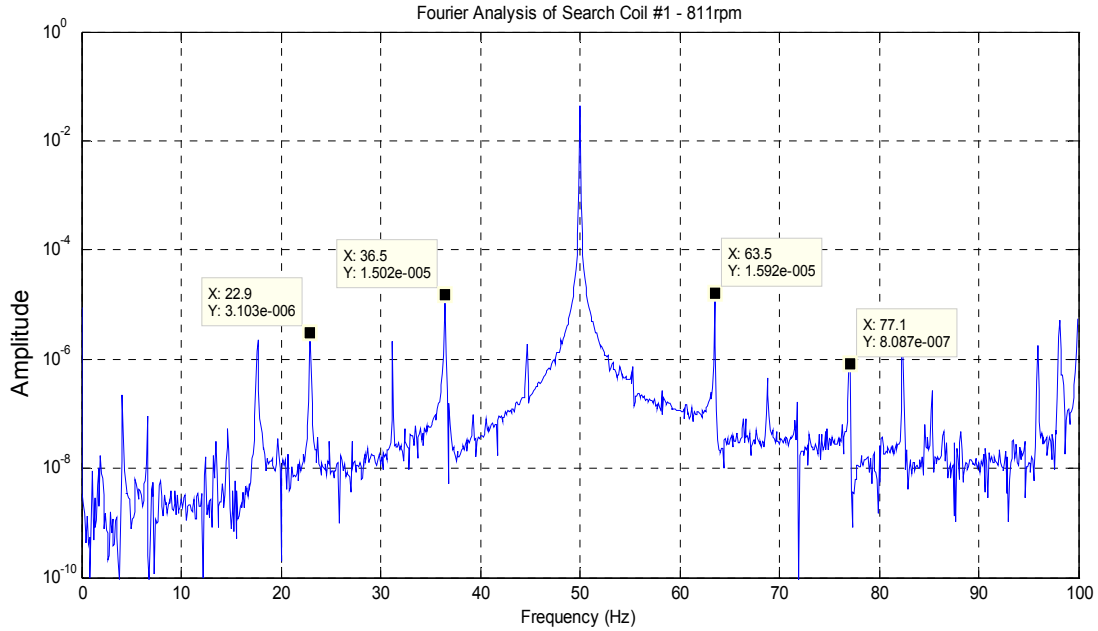

Fig. 3-13 FFT analysis of search voltage data at 811 rpm with f_s=50Hz

Then the motor is driven at 20 Hz and 40 Hz at rated flux. In Fig. 3-14, FFT analysis of the induced voltage on the same search coil is given while the supply frequency is 20 Hz and the machine #1 is running at 236 rpm. In Fig. 3-15, FFT analysis of the induced voltage from external search coil is given while the supply frequency is 40 Hz and machine is running at 686 rpm.

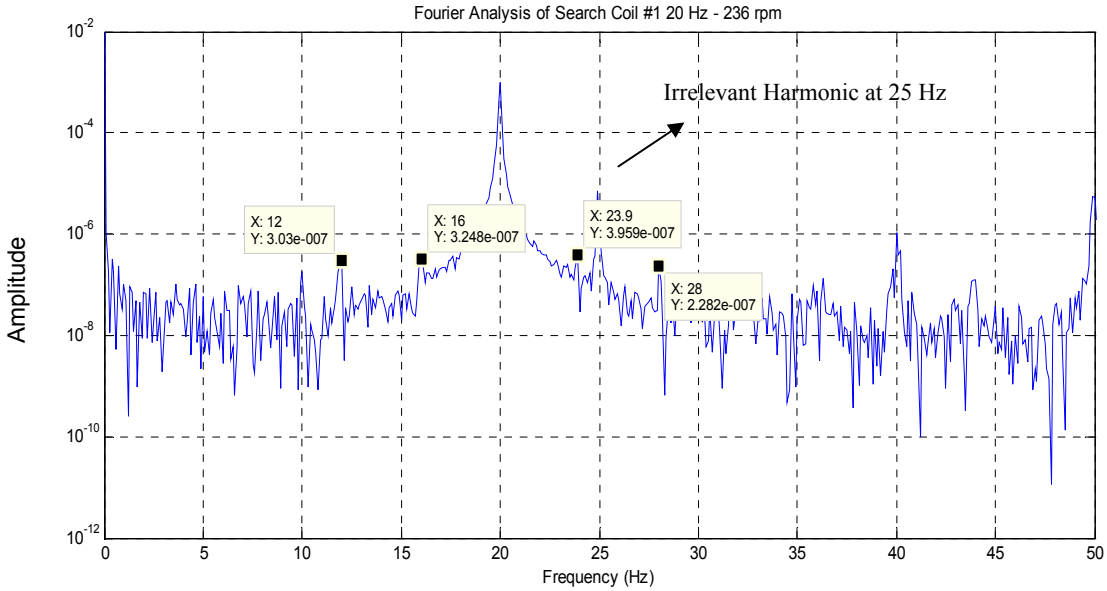

Fig. 3-14 FFT analysis of search coil voltage data at 236 rpm with f_s=20Hz

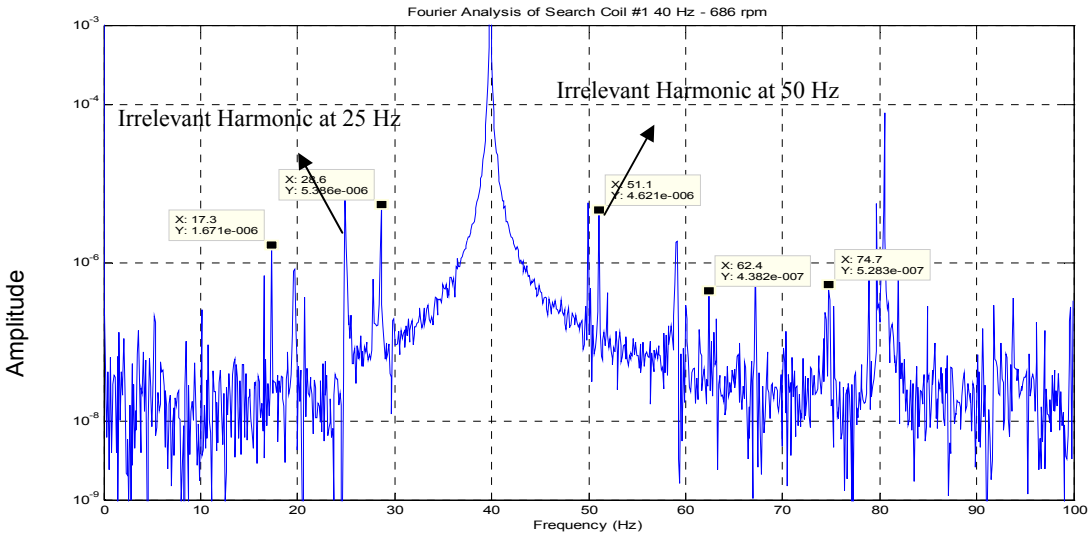

Fig. 3-15 FFT analysis of search coil voltage data at 686 rpm with f_s=40Hz

Experiment results showed that upper and lower side band rotor saliency harmonics are observable in the induced external search coil voltage. It can be seen that behind the first order (k=1) rotor saliency harmonics also second order (k=2) saliency harmonics are also observable as mentioned in equation (3-21). There also some parasitic harmonic components at 25 Hz and 50 Hz probably caused by the line frequency (50 Hz). They may be confused with the rotor saliency harmonics. This will be discussed in the next section.

3.7.2 Evaluation of the Proposed Method

As mentioned, after the detection of the rotor saliency harmonics. The lower side harmonics frequency is measured and verified with the upper side rotor saliency harmonics. If the selected harmonic is a parasitic component such as harmonics detected at 25 Hz and 50 Hz; then the verification process fails then it is understood by the algorithm that this component is not a rotor saliency harmonics. Then, the algorithm sets a no result flag and the algorithm restarts with a new set data.

Another verification made after calculating the ratio of rotor slot harmonic frequency to rotor saliency harmonics frequency, if the decimal part of the ratio is greater than 0.1 or smaller than 0.9 then again no result flag is set and the algorithm starts with a new data set. If not, then the ratio is rounded to nearest integer and the number of rotor slots is estimated.

The rotor slot number estimation algorithm is examined at different stator frequencies with varying slip values. As mentioned, if the algorithm cannot estimate the number of rotor slots, it runs again and average number of these iterations for a successful rotor slot number estimation is given in Fig. 3-16.

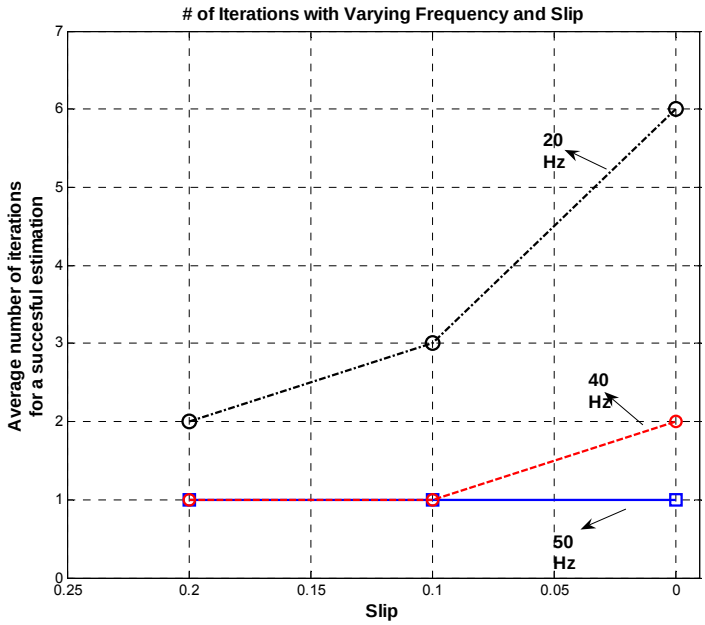

Fig. 3-16 Average number of iterations with varying frequency and slip

The graphs show that the number of iterations increases with the decreasing slip and stator frequency. Decreasing the frequency and slip worsens the performance of the system as seen from the figure. This is caused by two reasons; first, at lower frequencies the rotor slot harmonics are confused with parasitic harmonic components at 25 Hz and 50 Hz, and the process is repeated till the detected harmonics are verified with its side band harmonics. Another reason is that, magnitude of saliency harmonics in the search coil voltage decrease with the decrease of rotor currents as claimed in [30] which increases the estimation period at low loads. Thus, for quickest and most accurate estimation of number of rotor slots; the calibration should be performed at rated stator frequency (50 Hz) and at or near rated load.

The number of rotor slots estimation results at rated stator frequency with motor #1 and motor #2 is presented in Table 3-6.

Table 3-6 Estimated rotor slot numbers for motor#1 and motor#2 at 50 Hz

Slip	$Z_{estimated}$ (Motor #1) Z_{actual} =26	$Z_{estimated}$ (Motor #2) Z_{actual} =18
0.2	25.97 → 26	18.02 → 18
0.15	25.92 → 26	17.94 → 18
0.1	26.08 → 26	18.04 → 18
0.05	26.09 →26	18.10 → 18

The results presented shows that, for all slip values, the number of rotor slots is predicted correctly for both motors. But it is stated that, the algorithm estimates the number of rotor slots in rated load easier. Thus, it is better to run the algorithm at rated load and rated frequency.

3.8 Major Harmonics in the Search Coils

The FFT analysis of the induced search coil voltage in experiments performed with the inverter at 20 Hz and 40 Hz is given already. The major harmonics in the induced external search coil voltage, excluding harmonics of supply frequency are given in Table 3-7. As seen from the table, similar harmonics occur at 20 Hz and 40 Hz. But at lower frequencies some higher order harmonics are not observable. Notice that, all the harmonics observed can be expressed using equations (1-23) and (1-28).

Table 3-7 Major harmonics in external search coil voltage for and inverter driven machine

Rotor Saliency Harmonics				Rotor Slot Harmonics		
Harmonic	20 Hz	40 Hz		Harmonic	20 Hz	40Hz
$f_s \pm f_r$	X	X		$Z/P.f_r \pm f_s$	X	X
$f_s \pm 2.f_r$		X		$Z/P.f_r \pm 3.f_s$	X	X
$f_s \pm 3.f_r$		X		$Z/P.f_r \pm 5.f_s$		X

3.9 Conclusion

In this chapter, the rotor slot harmonics in the air gap and fundamentals of rotor speed estimation method using spectral estimation techniques are explained. In literature, the rotor slot harmonics are obtained usually from phase currents or voltages. In this study, the rotor slot harmonics are measured using the external search coil selected in chapter 2. The aim of this chapter is to investigate the possibility of using an external search coil placed on the machine frame for identifying rotor slot harmonics.

It is known that, after capturing the search coil voltage on the external search coil, some kind of spectral analysis techniques should be applied to detect the frequencies of rotor slot harmonics. Different spectral estimation techniques are investigated in literature. By using specific spectral analysis techniques the performance of the method can be improved. But, there still exist a very important drawback of the method; large data acquisition periods (orders of seconds) worsen the transient of the performance. In [32, 21, 48], valuable studies performed to improve the dynamic performance of the proposed method. But it is still very hard to consider this method as a fast online speed estimator with estimation periods up to four seconds. As mentioned, in this study the dynamic performance of the method has not been improved but implemented to external search coil. Thus, an algorithm commonly used in literature is utilized to test the presence of rotor slot harmonics. A new method that will increase the dynamic performance will be proposed in Chapter 5.

In order to validate the method for external search coil; tests are performed on two motors and developed algorithm is applied. First, experiments are performed with a balanced 3-phase sinusoidal voltage supply and captured data is analyzed in MATLAB environment. Once the rotor slot harmonics are verified from these tests, the similar experiments are performed on the machines while it is driven with the inverter defined in 2.6 with varying stator frequencies. The experiments showed that, rotor slot harmonics are observable for both sinusoidal supply and inverter driven cases. The experiments also showed that, the rotor speed can be estimated with an accuracy of ± 1.2 rpm using an FFT resolution of 1 Hz with motor #1. And also it is

proved that the machines with higher number of rotor slot numbers have a better accuracy which is verified by theoretical equations.

One drawback of the method comes across when the frequency of rotor slot harmonics clashes with the higher harmonics of fundamental stator frequency. In that case, the rotor speed may not be refreshed. But, it was showed that this occurs in a narrow speed range so it is not a big disadvantage. An important advantage of the method is; its independency from machine electrical parameters such as, stator rotor resistance.

On the other side, the algorithm needs the number of rotor slots information and number of pole pairs in order to estimate the rotor speed. These parameters are time invariant, thus the speed measurement is reliable. But, the number of rotor slots may not be available from the manufacturer data. In these situations, the number of rotor slots should also be predicted. Methods in literature are either use an extra speed sensor for calibration [16] or other methods that do not require a speed sensor are not accurate enough. A new method is proposed to estimate the number of rotor slots. In this method, rotor saliency harmonics are utilized that occur near to applied stator voltage harmonics [35]. The algorithm should run once during commissioning, and then the predicted rotor slot number will be used in speed estimation algorithm. In the experiments made with both motors, it is shown that the algorithm estimates number of rotor slots accurately. The algorithm is tested at various load and stator frequency conditions. They all estimated the rotor speed correctly. But at low frequency and low load conditions number of iterations for algorithm increases due to decreased magnitude of saliency harmonics and parasitic harmonics of line frequency. Thus, it is a wise approach to run the number of rotor slots estimation algorithm at rated stator frequency (50 Hz) and load conditions.

To conclude, it is shown that estimation of rotor speed is possible using an external search coil placed on frame of the machine. In this section, the both algorithms are tested at offline conditions on the captured search coil data. The spectral analysis methods give accurate estimation of rotor speeds and this accuracy is directly related with the number of rotor slots per pole. The online rotor speed estimation using spectral analysis techniques is realized in literature for steady state

conditions or with low transient rate conditions. The online implementation of these methods with good transient characteristics is difficult due to time consuming properties of spectral analysis techniques (complex computations, long data periods up to order of seconds). In the next chapters, different methods will be investigated that promises online estimation of rotor speed and position.

CHAPTER 4

TIME DOMAIN SEARCH COIL VOLTAGE ANALYSIS

4.1 Introduction

In this chapter, time domain analysis of induced voltage at search coil will be explained. It is stated in Chapter 3 that rotor speed estimation is possible from the spectrum analysis of induced external search coil voltage. However, the main disadvantage of spectrum analysis is the estimation lag (up to four seconds) because of long data acquisition period and spectral analysis computation time. Due to these disadvantages, a new method will be proposed in this chapter that can provide online estimation of air gap flux position.

Instead of analysing the harmonics of the induced search coil voltage, the fundamental component part may be investigated. If there is a relation between machine air gap flux and the induced voltage on search coil, flux position can be estimated using the search coil in real time.

In this method, the zero crossings of the induced search coil voltage will be detected. Then, based on the model proposed between search coil and air gap flux, information about the air gap flux will be extracted.

In order to build a model between machine flux and the induced voltage on the external search coil, following procedure is followed. First, using an internal search coil that spans one pole-pitch, the relation between internal search coil induced voltage and machine flux is investigated. Once, this model is built similar experiments are performed for external search coil voltage. Then, the machine flux will be represented using the induced voltages on both search coils.

4.2 Internal Search Coil Experiments

In order to verify, the operation of external search coil, the air gap flux should be measured. To measure the air gap flux, the simplest method is to use an internal search coil. Since internal coil spans one-pole pitch, its induced voltage should be directly proportional with the air gap flux of the machine. To verify this, some experiments are performed at various load conditions, supply frequency and supply voltage.

4.2.1 Internal Search Coil Experiment Conditions

The internal search coil is wound on the stator slots of the 2.2 kW 2-pole induction machine. The machine parameters are available in Appendix A. The internal search coil has 10 turns and spans one pole pitch of a two pole induction machine. The picture of the internal search coil has already given in Fig. 2-22 in chapter 2. Also, the effect of positioning of external search coil has also discussed in Chapter 2. In time domain experiments of this chapter, the placement of internal and external search coils will be as shown in Fig. 4-1.

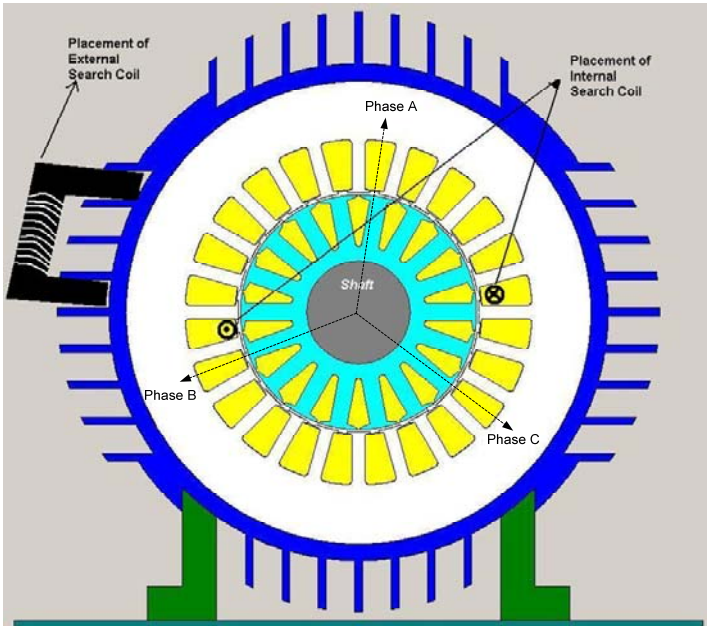

Fig. 4-1 Position of internal and external search coils, as seen from motor shaft

4.2.2 Experimental Procedure

In the experiments, internal and external induced search coil voltages are captured by using a digital oscilloscope, the data is captured without any filter. The oscilloscope has been used with a sampling frequency of 5 kHz and with 2000 captured data. The technical specifications of experimental equipments are available in Appendix C.

Once the signal is captured, it is processed offline in MATLAB. This process also includes digital filtering of the captured data when necessary. The digital filters are low pass filters that are designed with MATLAB Filter Design & Analysis Toolbox. They are used for extracting the fundamental component from the induced search coil voltage.

The induction motor is driven with the inverter drive described in section 2.6 using space vector pulse width modulation (SVPWM) method. The induction machine is loaded with a directly coupled DC motor as explained in 2.6.3.

In the experiments, the 2.2 kW 2-pole induction machine is used. The machine has a frame made of cast iron. The machine equivalent circuit parameters are as follows;

$r_s = 2.65\ \Omega$	(Stator resistance)
$r_r' = 3.06\ \Omega$	(Referred rotor resistance)
$L_{ls} = 13.14$ mH	(Stator Leakage Inductance
$L_{lr} = 13.14$ mH	(Rotor Leakage Inductance)
$L_m = 384.27$ mH	(Mutual Inductance)

4.2.3 Varying Applied Stator Voltage

In order to verify that the induced internal search coil voltage is proportional with the machine air gap flux; the applied stator voltage is varied and the induced internal search coil is captured for each case.

The stator voltage is the sum of magnetizing voltage and serial impedance voltage drop as shown in (4-1).

$$\overrightarrow{Vs} = (Rs + jX_{ls}).\overrightarrow{Is} + \vec{E}_a \qquad (4\text{-}1)$$

The per phase equivalent circuit of the induction motor is given in Fig. 4-2.

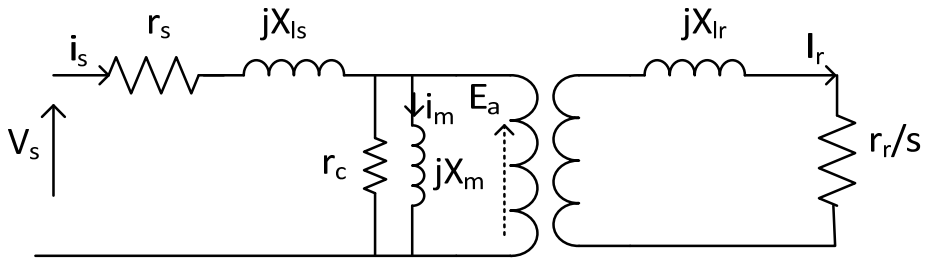

Fig. 4-2 Induction motor per phase equivalent circuit

Using equation (4-1) the magnetizing voltage (E_a) can be easily calculated. It is expected that the induced internal search coil voltage is directly proportional with the magnetizing voltage. Equation (4-2) is a well-known equation that defines the induced voltage in a closed loop placed in a changing magnetic flux.

$$e = -N.\frac{d\Phi}{dt} \qquad (4\text{-}2)$$

Where, e is the induced voltage, N is the number of turns and Φ is the flux that links the coil. Assuming that the amplitude of flux is proportional with the magnetizing voltage and defining Φ as;

$$\Phi = A.\sin(wt) \qquad (4\text{-}3)$$

where w is frequency and A is the amplitude.

The induced voltage in the search coil becomes;

$$e = -N.w.A.\sin(wt) \qquad (4\text{-}4)$$

where N=10 (the number of turns of internal search coil). Thus, it can be concluded from equation (4-4) that the induced voltage on the search coil is directly proportional with the magnetizing voltage (E_a).

Fig. 4-3 gives the experiment results where the internal search coil voltage is recorded as the magnetizing voltage calculated using the applied stator voltage and equivalent circuit of the machine. The linear increase in the induced voltage verifies equation (4-4).

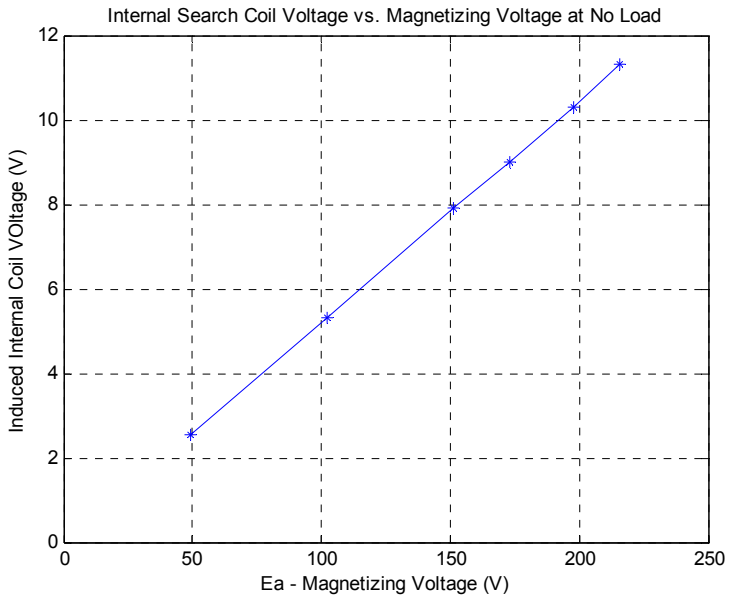

Fig. 4-3 Internal search coil voltage at varying phase voltage

The flux at the rated voltage at no load can be calculated from equation (4-2). Reemphasizing, the applied frequency is 50 Hz, number of turns of the coil is 10, the rms value of the flux becomes; 3.6mWb/pole.

4.2.4 Varying Frequency

In order to verify the operation of internal search coil with varying frequencies, frequencies from 5 Hz to 100 Hz are applied to the machine. The machine is supplied with a three phase sinusoidal voltage supply in order to prevent inverter harmonics.

The experiment results at varying frequencies are given in Fig. 4-4. For frequencies less than 50 Hz constant flux operation mode is applied. For frequencies above 50 Hz, flux weakening operation is applied in order to avoid of higher values of phase voltage in other words, the applied voltage is kept constant at rated value.

It can be seen from equation (4-4) that the induced voltage of the search coil is also proportional with the applied voltage frequency.

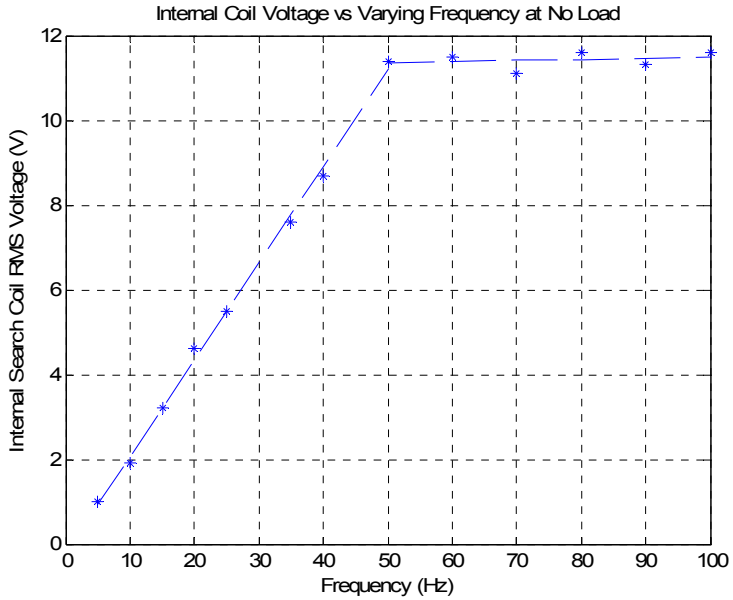

Fig. 4-4 Internal search coil voltage at varying frequency at no load

Between 5Hz and 50 Hz the induced voltage of internal search coil increases linearly that implies the search coil is suitable for measuring the air gap flux. For frequencies higher than 50 Hz, the search coil voltage nearly remains constant which also implies the search coil voltage is appropriate. For these frequencies, the frequency is linearly increased where the air flux is linearly decreased, thus as can be seen from equation (4-4). The experiment results showed that, the internal search coil voltage is consistent with equation (4-4) implying search coil can be used as a flux observer.

4.2.5 Varying Load Conditions

In this part, the induced internal search coil voltage is measured at varying loads at different frequencies. The induced search coil voltage may change due to saturation of stator core or armature reaction as the load conditions is varied. To test this, induction machine is loaded to its rated power and half of rated power and induced internal search coil voltage is measured for each case. The applied stator voltage is adjusted to compensate the voltage drop at stator resistance such that the machine operates at rated flux conditions for each step till 50 Hz stator frequency.

For frequencies higher than 50 Hz the applied stator voltage is kept constant at 220 $V_{l\text{-}n}$, thus flux weakening operation is applied. In the flux weakening region (for frequencies higher than 50 Hz), the applied stator voltage is kept constant at rated value. The experiment conditions, applied stator voltages and currents are given in Appendix D. The experiment result is given in Fig. 4-5.

The experiment results showed that the induced internal search coil voltage does not change with the varying load conditions. Hence, the search coil voltage measures the air gap flux properly independent of machine load conditions.

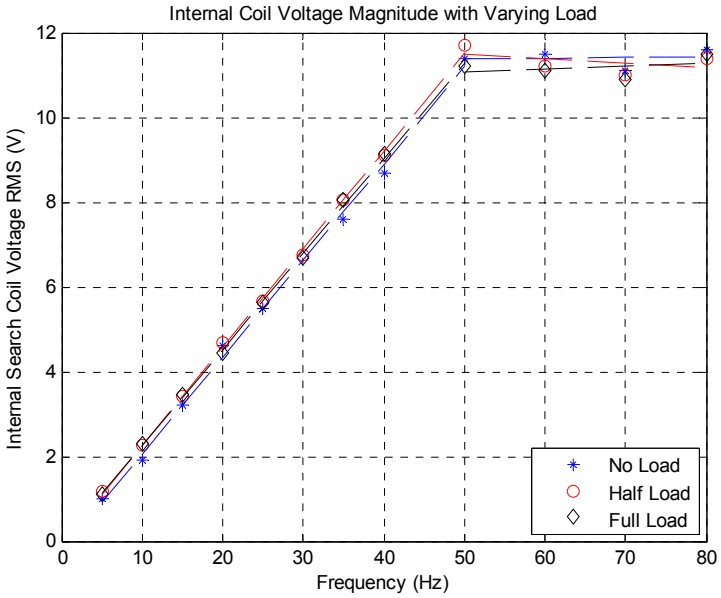

Fig. 4-5 Internal search coil voltage with varying load conditions

4.3 Modelling of Internal Search Coil

Induced internal search coil voltage should be modelled properly in order to obtain a reliable flux observer. This flux observer should be independent of stator phase voltage, excitation frequency and load conditions. Also, the model should cover various positions of the search coil. In Fig. 4-6, the ideal placement of search

coil, where the magnetic axis of the search coil coincides with the magnetic axis of Phase A is shown. Also, the actual positioning is shown where there is a placement angle (δ) magnetic axis of search coil and Phase A.

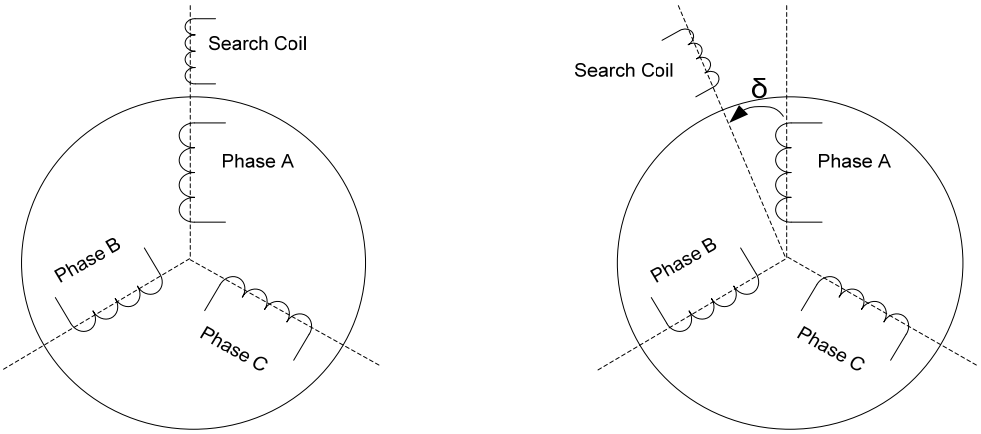

Fig. 4-6 Search coil placement with/without placement angle between Phase A

Two methods of internal search modelling shall be considered; phase to coil mutual inductance model and turns ratio modelling. To introduce these methods briefly; phase to coil mutual inductance model is based on the mutual inductance measurement between search coil and each stator phase as shown in Fig. 4-7. Details of the method will be explained in the following part.

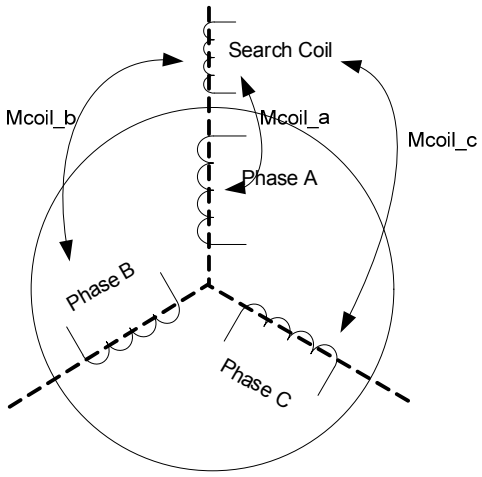

Fig. 4-7 Mutual inductances between search coil and stator phases ideal case

The other method uses resultant flux vector instead of mutual inductances. In this model, the resultant flux vector and magnetizing voltage is calculated using the electrical measurements and machine equivalent circuit and compared with the induced search coil voltage. The phasor diagram of the main variables in the machine and the induced search coil voltage for ideal case is represented in Fig. 4-8. For non ideal positioning of the search coil, the induced search coil voltage phasor shifts δ (position offset) degree from the magnetizing voltage. If the induced search coil voltage can be modelled, then using δ, the position of air gap flux can be estimated.

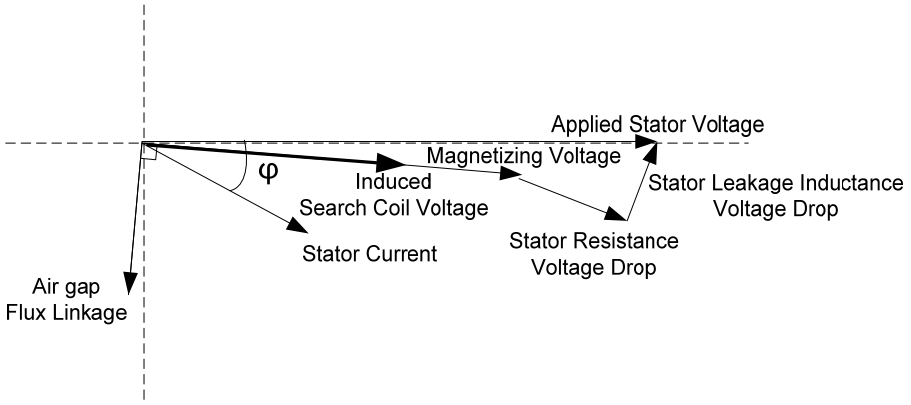

Fig. 4-8 Phasor diagram representation of search coil voltage (ideal case)

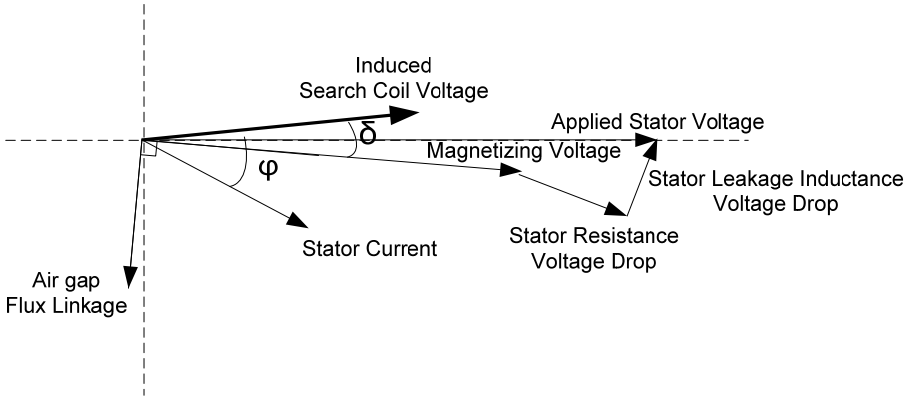

Fig. 4-9 Phasor diagram representation of search coil voltage (actual case)

4.3.1 Phase to Coil Mutual Inductance Model

In this model, mutual inductances between each stator phase and search coil are measured and the total induced voltage on the search coil is modelled using these measurements. To acquire phase to coil mutual inductances single phase excitation is applied on each phase of the machine and the induced voltage on the search coil is measured. From the single phase excitation data and the machine parameters, mutual inductance between stator windings and the internal search coil can be measured. Considering single phase excitation of the stator (for phase A), the induced voltage on the search coil can be expressed as [38];

$$V_{coil} = r_{coil}.I_{coil} + L_{coil}\frac{dI_{coil}}{dt} + \mathrm{M}_{a\_coil}.\frac{dI_a}{dt} \quad (4\text{-}5)$$

Where, r_{coil}, L_{coil} is the resistance and inductance of search coil respectively and M_{a_coil} is the mutual inductance between stator phase A and search coil. Since no current is drawn from search coil, the search coil current is taken to be zero, thus first two terms may be neglected. Then the induced voltage on the search coil becomes directly related with the derivative of the flux linking the search coil. Also, the induced voltage can be expressed in terms of the mutual inductances between machine stator phases and the search coil as expressed in equation (4-6) and (4-8) [38].

$$V_{coil} = N.\frac{d\Phi}{dt} = \mathrm{M}_{a\_coil}.\frac{dI_a}{dt} \quad (4\text{-}6)$$

The same equation for three phase balanced stator phases where the magnetic axis of phase A coincides with the magnetic axis of search coil can be expressed as;

$$V_{coil} = \begin{bmatrix}\mathrm{M}_{a\_coil} & M_{b\_coil} & M_{c\_coil}\end{bmatrix}.\begin{bmatrix}1 & 0 & 0\\ 0 & \cos(-2\pi/3) & 0\\ 0 & 0 & \cos(2\pi/3)\end{bmatrix}.\frac{\mathrm{d}}{\mathrm{dt}}\begin{bmatrix}\mathrm{i_a}\\ \mathrm{i_b}\\ \mathrm{i_c}\end{bmatrix} \quad (4\text{-}7)$$

But, if there exist a placement angle (δ) which describes the angle between search coil magnetic axis and stator phase A magnetic axis then equation (4-7) transforms to;

$$V_{coil} = \left[\mathrm{M}_{a\_coil}\ M_{b\_coil}\ M_{c\_coil}\right].\begin{bmatrix}\cos\delta & 0 & 0\\ 0 & \cos(\delta-2\pi/3) & 0\\ 0 & 0 & \cos(\delta+2\pi/3)\end{bmatrix}.\frac{\mathrm{d}}{\mathrm{dt}}\begin{bmatrix}\mathrm{i_a}\\ \mathrm{i_b}\\ \mathrm{i_c}\end{bmatrix} \qquad (4\text{-}8)$$

The single phase excitation values for each of the stator phases and the induced voltages for each single phase excitation case is given in Table 4-1. In the given tables phase voltages and phase currents RMS values are given, phase differences are given in degree and calculated with respect to the terminal voltage of the each excited stator phase. Also, the angle of placement between magnetic axis of stator phases and the magnetic axis of the search coil and the calculated mutual inductances between stator phases and internal search coil using the given excitations are given in the same table. The experiment results of induced search coil voltages for different applied stator voltage values are available in Appendix D.

Table 4-1 Induced internal search coil voltages for single phase excitation and calculated inductances

Single Phase Excitation For Each Phase	Phase Voltage(V)	Phase Current (A)	Magnetizing Voltage- Ea (V)	Magnetizing Current (A)
	30 /0^0	3.1 /-60^0	26.7 /1^0	0.22 /-89^0
Measured Data	Phase A	Phase B	Phase C	
Induced Search Coil Voltage (mV)	1060 / +4^0	29 /-180^0	256 /-177^0	
δ -Phase Angles between coil and stator Phases (degree)	22^0	-98^0	142^0	
Mutual Inductances between search coil and stator phases	16.54 mH	3.01 mH	4.7 mH	

At a first glance it may be seen that, Phase A induces largest voltage on the search coil where Phase B induces a very small value. This situation can be assessed from the placement of internal search coil as seen from Fig. 4-1. The magnetic axis of the internal search coil is nearly orthogonal with the magnetic axis of stator Phase B.

Using equation (4-8) and the inductance values obtained from single phase excitation experiments which are presented in Table 4-1, the induced search coil voltage can be calculated for other operation points. The calculated search coil

voltage will be compared in two situations; the no load test and locked rotor test. The locked rotor and no load motor measurement values are given in Table 4-2. In this table, measured and estimated search coil voltages are compared in Table 4-2.

Table 4-2 Measured and estimated internal search coil voltage for single phase excitation experiments

	Phase A Voltage (V)	Phase A Current (A)	Measured Coil Voltage (V)	Estimated Coil Voltage (V)
Locked Rotor	48 V $/0^0$	4.8 A $/-53^0$	2.1 V / $+136^0$	1.83 V $/+131^0$
No Load	220 V $/0^0$	2.01 A $/-53^0$	11.5 V / $+145^0$	10.4 V $/+131^0$

In this section, the mutual inductances between each stator phase and the search coil is used to model the induced search coil voltage. The measured and the estimated search coil voltages are compared. This model has some insufficiency in modelling the induced search coil voltage; especially the phase of the induced voltage. This may be caused from inaccurate inductance measurements errors or from saturation of the saturation core at single phase excitation. Thus, this method will be improved in the next section.

4.3.2 Turns Ratio Modelling

Another model for the induced voltage on the search coil is to use the equivalent circuit of the induction motor instead of mutual inductances between each stator phase and the search coil. The equivalent circuit of the motor is given on Fig. 4-2 and the machine parameters used in experiments are available in Appendix A.

In order to build a model between induction motor and the search coil, it is better to clarify the equivalent circuit parameters. Stator resistance (r_s) is related with the stator coil wiring, and cannot be changed by inserting a search coil. Stator leakage flux (L_{ls}) is a term related with stator flux that does not link the rotor side. For internal search coil leakage inductance between stator and search coil this value can be assumed as equal to stator leakage inductance because, the internal coil is directly wound on stator slots. Since there is no current drawn from search coil the

resistance and the inductance of the search coil can be neglected as shown in Fig. 4-10.

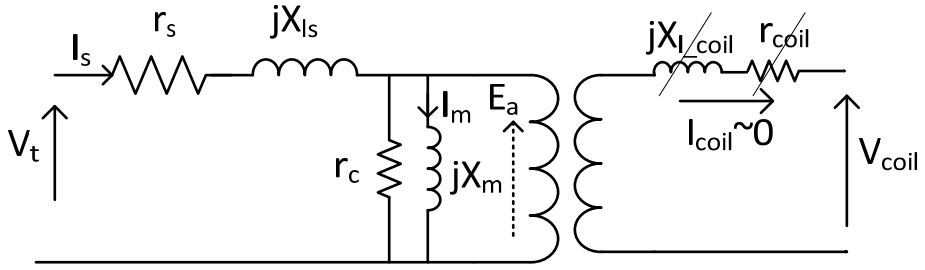

Fig. 4-10 Equivalent circuit between stator phases and search coil

Neglecting search coil resistance and inductances the measured search coil voltage should be directly related with the magnetizing voltage E_a. Following experiments are performed at various frequencies with rated flux while the induction machine is running at no load.

Table 4-3 Measured internal search coil voltage at various frequencies

Freq (Hz)	Vt- Phase A Voltage (V)	Is - Phase A Current (A)	Magnetizing Voltage (V)	Measured Coil Voltage (Normalized wrt Phase A)	Ea /Vcoil
10	$38 / 0^0$	$1.4 / -78^0$	$36.2 / 5.3^0$	$1.9 / 9^0$	19.05
25	$108 / 0^0$	$1.7 / -78^0$	$103.7 / 1.9^0$	$5.5 / 2^0$	18.85
50	$220 / 0^0$	$1.9 / -78^0$	$211 / 0.9^0$	$11.4 /0^0$	18.51
70	$218 / 0^0$	$1.2 / -78^0$	$210.5 / 0.5^0$	$11.3 /1^0$	18.63

Using experiment results performed at various frequencies, the ratio of magnetizing voltage and the induced search coil is nearly constant. As an average values turn's ratio is selected as; N=18.6.

Thus, this value can be used as the turn ratio (N) of the model.

$$\vec{E}_a = \overrightarrow{Vs} - \left(Rs + jX_{leakage\_stator\_coil}\right).\vec{Is} \quad (4\text{-}9)$$

$$\vec{E}_a = N.\vec{V}coil \quad (4\text{-}10)$$

where E_a defines the magnetizing voltage of the stator phases. The estimated magnetizing voltages using the equation (4-10) is calculated as given in Table 4-4.

Table 4-4 Measured and estimated magnetizing voltage using turns ratio model (N=18.6)

Freq. (Hz)	Measured Magnetizing Voltage - Ea (V)	Measured Coil Voltage (V)	Estimated Magnetizing Voltage (V)	Magnitude Percent Error
10	$36.2 / 5.3^0$	$1.9 / 9^0$	$35.3 / 9^0$	2.5 %
25	$103.7 / 1.9^0$	$5.5 / 2^0$	$102.3 / 2^0$	1.1 %
50	$211 / 0.9^0$	$11.4 /0^0$	$212 / 0^0$	0.5 %
70	$210.5 / 0.5^0$	$11.3 /1^0$	$210.2 /1^0$	0.2 %

As seen from table, the model is very successful to estimate the magnetizing voltage. The estimated and the measured magnetizing voltage perfectly match, but at lower frequencies, the phase difference between model and the measured value increases up to 4 degrees. The performance comparison between actual air gap flux position and the position calculated from induced search coil voltage will be given in the following sections.

4.4 External Search Coil Experiments

In the previous section experiments are performed using the internal search coil. In this chapter similar experiments are performed with the external search coil and its characteristic with varying flux, frequency and load conditions will be investigated.

The external search coil voltage induces voltage utilizing the fringing flux of the machine frame. The external coil is placed between cooling fins of the machine. Since, the fringing flux is a very small part of the total flux, the induced voltage on the external search coil is much smaller than the internal coil voltage. And the

external coil voltage is dependent on the back core and frame characteristics. For the experiments of this section a machine frame made of cast iron will be used.

In time domain analysis experiments, search coil type #1 is used which is selected as the most suitable one in chapter 2. Search coil core is a laminated U-shaped core made of cold rolled steel. Search coil has 120 turns. The search coil is shown in Fig. 4-11. The external coil may be placed over some places between cooling fins. The search coil is placed between cooling fins of the machine as shown in Fig. 2-19.The effect of different positions of search coil has already discussed in Chapter 2.

Fig. 4-11 External search coil used in time domain experiments

4.4.1 Varying Air Gap Flux

In this part induced voltage on the external search coil will be investigated for different air gap flux values. The aim of these experiments is to obtain the characteristics of the induced external search coil voltage with varying air gap flux.

Firstly, the induced external search coil voltage is measured under different phase voltages. The phase voltage frequency is 50 Hz and applied at no load. The experiment results are given in Fig. 4-12.

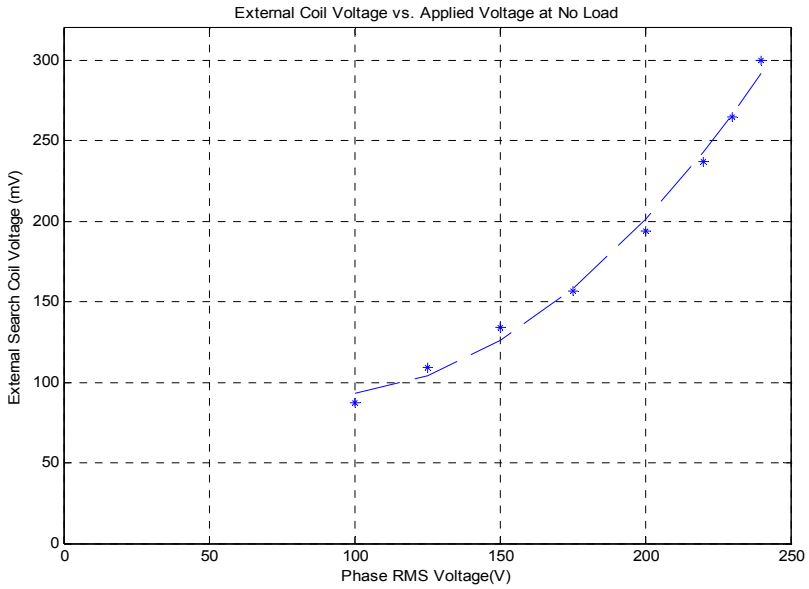

Fig. 4-12 External search coil voltage at varying phase voltage at no load at 50 Hz

As seen from Fig. 4-12, the induced voltage on the external search coil displays a different variation with phase voltage as compared to the internal coil because of the non-linear relation between air gap flux and the external coil induced voltage. The induced external search coil voltage characteristic mainly depends on the properties of the stator core and the frame of the machine. As, the flux density in the machine is increased, the stator core and the frame tends to saturate, thus the outside of the machine becomes a more preferable path. Thus, more flux fringes out of the motor frame, inducing larger voltage on the external search coil. A detailed model of this phenomenon will be explained later.

In previous section, similar experiments with internal search coil are performed and the experiments showed that the internal search coil can be used as a consistent air gap flux observer. As a consistent flux observer, we desire the induced voltage is linearly proportional with the magnetizing voltage and also linearly proportional with the applied frequency referring to equation (4-4). Thus, the flux values in the X-axis are calculated using the internal search coil voltage. The experiments are performed for two frequencies; 25Hz and 50 Hz. The flux is changed by changing applied stator voltage at constant load and constant frequency. The flux values are varied from 50%

of rated flux to 120% of rated flux. The rated flux using the internal search coil can be calculated as in equation (4-11).

The induced internal search coil voltage is measured at rated operation point (50 Hz, 220V) as 11.3 V (RMS). Using equation (4-11) which gives the flux value generated by a sinusoidal voltage, the peak value of rated air gap flux can be approximately calculated as; 5.04 mWb/pole.

$$\Phi p = \frac{Vinternal\_coil}{\sqrt{2}.\pi.f.N} = \frac{11.3}{\sqrt{2}.\pi.50.10} = 5.04\frac{mWb}{pole} \qquad (4\text{-}11)$$

In this experiment, frequency held constant at 50 Hz and 25 Hz, while varying the applied voltage, the experiment results are given in Fig. 4-13, Table 4-5 and Table 4-6.

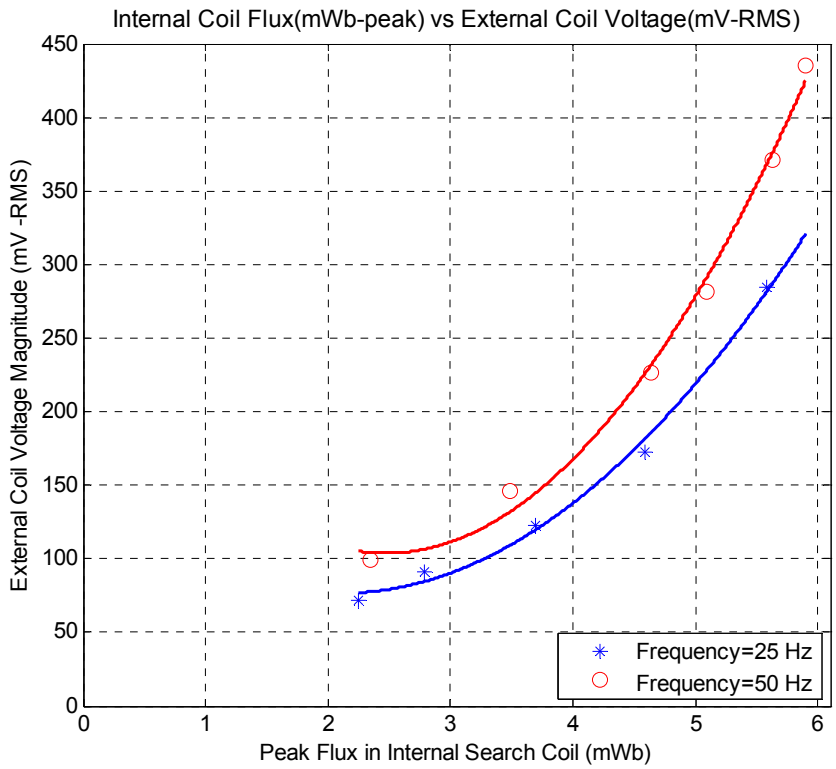

Fig. 4-13 Induced external coil voltage with varying flux

Table 4-5 Measured external coil voltage with varying stator voltage at 50 Hz

Terminal Voltage(V)	Phase B Current(A)	Internal Coil Voltage (V)	External Coil Voltage (mV)
100	0.6	5.2	99
150	0.94	7.7	148
200	1.48	10.3	227
220	1.85	11.3	279
242	2.43	12.5	371
255	2.9	13.1	438

Table 4-6 Measured external coil voltage with varying stator voltage at 25 Hz

Terminal Voltage(V)	Phase B Current(A)	Internal Coil Voltage (V)	External Coil Voltage (mV)
50	0.6	2.5	75
60	0.7	3.1	91
80	1.0	4.1	125
100	1.4	5.1	174
120	2.24	6.2	287

In these experiments, it can be seen that the external search coil voltage does not increase linearly with linearly increasing air gap flux. Induced voltage increases exponentially when the rated flux operation point is exceeded. This implies that as the flux density of the machine increases more flux fringe over the frame of the machine linking the external search coil. The reason for increase of fringing flux is probably, the saturation of stator core and frame. As the air gap flux rises, the stator core approaches to the point of saturation and the reluctance of the flux path increases. As a result, the frame and the outside of the machine preferable way for flux. More flux fringes from the frame induces larger voltage on the external search coil.

This non-linear behaviour with varying flux conditions may not be a serious problem if the machine operates at rated flux which is the case in field oriented drive systems. But if the machine operates at above rated frequencies by flux weakening, the induced voltage will decrease rapidly. This will be discussed in following sections.

Table 4-7 External search coil voltage ratio at 50 Hz to induced voltage at 25 Hz (Expected voltage ratio is 2)

Flux (mWb)	$V_{induced}(50Hz)/V_{induced}(25Hz)$
3	1.24
4.8	1.26
5.5	1.3

Another point that should be emphasized is the non-linearity as the frequency is changed for the same air gap flux conditions. If the flux is constant, the induced voltage at 25Hz should be halved compared with 50 Hz referring to equation (4-4), which is applicable for internal search coil. But as the frequency is doubled, the induced voltage on the external search coil does not increase proportionally with the frequency. As mentioned in 4.2.4, this is a result of eddy current that flows on the frame of the induction machine. With the increasing frequency, the amount of the eddy current increases, decreasing the induced voltage on the external search coil.

To make a comparison, the ratio of the induced voltage at 50 Hz and 25 Hz for the same flux value is given in Table 4-7. At ideal conditions, the ratio should be equal to two.

4.4.2 Varying Frequency

In order to identify the operation of external search coil under varying frequencies, different frequencies are applied to the stator windings of the machine. It is verified that the internal search coil voltage increases linearly with the applied frequency that can be proved from equation (4-4). The experiment results at varying frequencies are given in Fig. 4-14. For frequencies that is smaller than 50 Hz constant air gap flux operation is satisfied. For frequencies above 50 Hz, the phase voltage is held constant at 220 V and the flux weakening method is applied. It can be seen from experiment results that, the induced external search coil voltage does not increase linearly with the frequency.

Fringing flux that induces voltage on the external search coil decreases as the frequency is increased. This phenomenon may be attributed to the eddy currents that occur in the machine frame. Eddy currents are closed loops of induced current

circulating in planes perpendicular to the magnetic flux [39]. In order to reduce eddy currents, laminated cores are used in stator and rotor cores. But, the frame of the machine frames is not laminated and as a result; more eddy currents will be generated in the frame. Eddy currents increases with the frequency. As the frequency is increased larger eddy currents generated opposing the magnetic field. Thus, the induced voltage on the external search coil will be decreased.

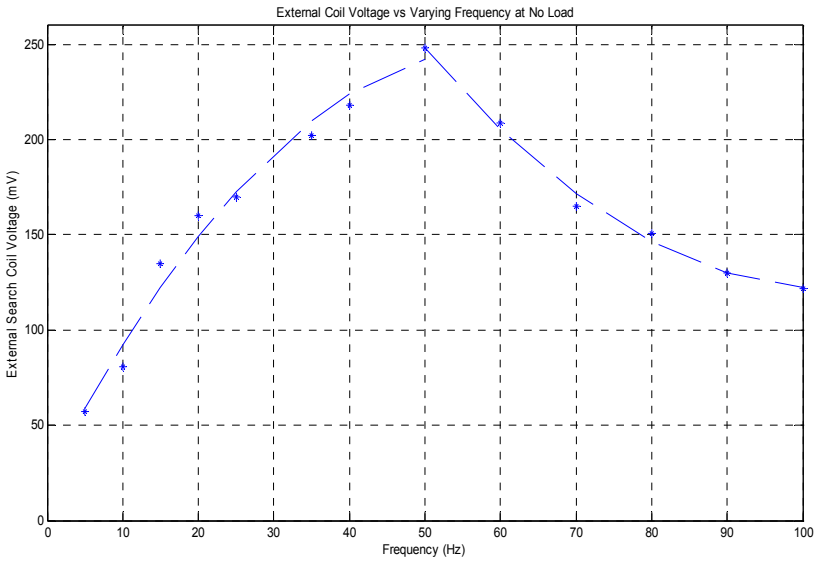

Fig. 4-14 External search coil voltage at varying frequency at no load

As seen from Fig. 4-14, between 5-50 Hz where the machine flux is kept constant, the induced search coil voltage increases nonlinearly due to eddy currents. After 50 Hz where flux weakening method is applied, the induced search coil voltage is affected both from eddy currents and from the decreasing machine flux. Thus, the induced external search coil voltage is decreased for frequencies larger than 50 Hz.

4.4.3 Varying Load Conditions

In this part, the relation between the magnitude of induced external search coil voltage and machine loading conditions will be investigated. In section 4.2.5 this

relation is investigated and it is shown that, internal search coil voltage does not vary with machine loading conditions.

The induction motor #2 (same motor used in internal coil experiments) is used for experiments; the machine is loaded to half of rated load and rated load. The voltage drop on the serial stator branch is compensated as the load is increased in order to satisfy the rated flux operation for frequencies lower than 50 Hz. For higher frequencies, the applied stator voltage is kept constant at 220V and flux weakening method is used.

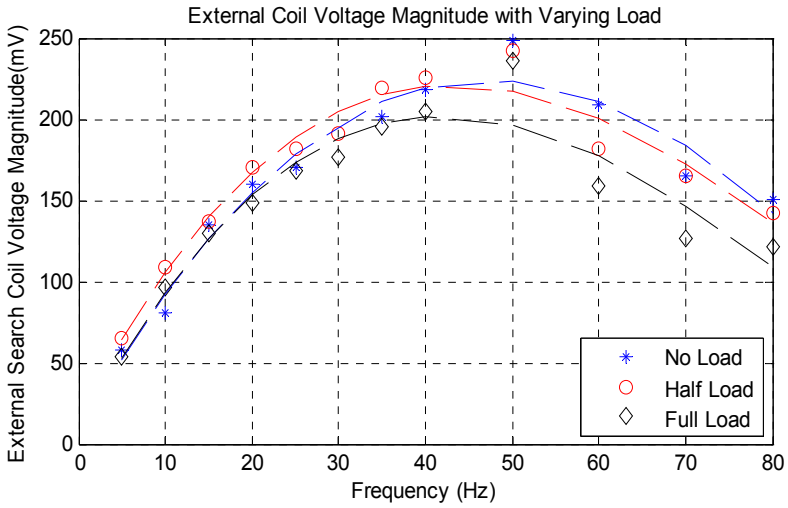

Fig. 4-15 External search coil voltage with varying load conditions

The experiment results are given in Fig. 4-15. The magnitude of induced external search coil voltage varies as the load changes thus, the results differ from internal search coil experiments. The magnitude of the induced external search coil voltage decreases as the stator phase current increases. Moreover, this reduction is also dependent with the applied stator frequency. As the frequency increases, the difference between the magnitudes of induced voltage at no load and full load increase. Thus, this non-linearity should be included in the external search coil model.

4.5 Variation of External Coil Voltage Waveform with Load and Frequency

As stated in previous sections, the internal and external search coil has a displacement angle (δ) with respect to the magnetic axis of Phase A. The calculated displacement angles for internal and external search coils are given in Table 4-1 and Table 4-11. Because of this positioning disparity, the internal and external search coil voltages will have a phase difference between each other. This is verified with test results. More over, the external search coil voltage magnitude and phase difference changes as the load and frequency is changed. In the following figures, the magnitude variation and phase shifting of external search coil voltage with respect to internal search coil voltage will be presented.

In order to understand the characteristics of the induced voltage on the search coil, the voltage waveform of both the internal and external search coils are recorded. Internal and external search coil types are the same with used in section 4.2 and 4.4. The data is captured using a digital oscilloscope and graphs are plotted in MATLAB environment. The waveforms are captured at three different applied stator frequencies; 10 Hz, 50 Hz and 80 Hz. The stator voltage is applied with a synchronous generator in order to decrease any harmonics that can be produced from the source side. For each frequency, experiments are performed at motor #2 running at no load, half load and full load.

The low frequency experiments are performed with a stator voltage frequency of 10 Hz, the terminal voltage is adjusted for rated flux operation. The experiment results are given in Fig. 4-16 and Table 4-8.

In the figure, both external and internal search coil voltages are plotted. The more sinusoidal signal shown with green colour is the internal coil voltage. The right axis of the figure indicates the magnitude of the internal search coil. The signal that contains more harmonics with blue colour is the external search coil voltage. The left axis of the figure shows, the magnitude of the external search coil.

In Table 4-8, RMS values of phase A voltage is given. Also, RMS values of fundamental components of induced search coil voltage are given. The phase differences of internal and external search coil are calculated according to the phase

A terminal voltage. And the variation of the phase angle difference between internal and external search coil voltages is presented.

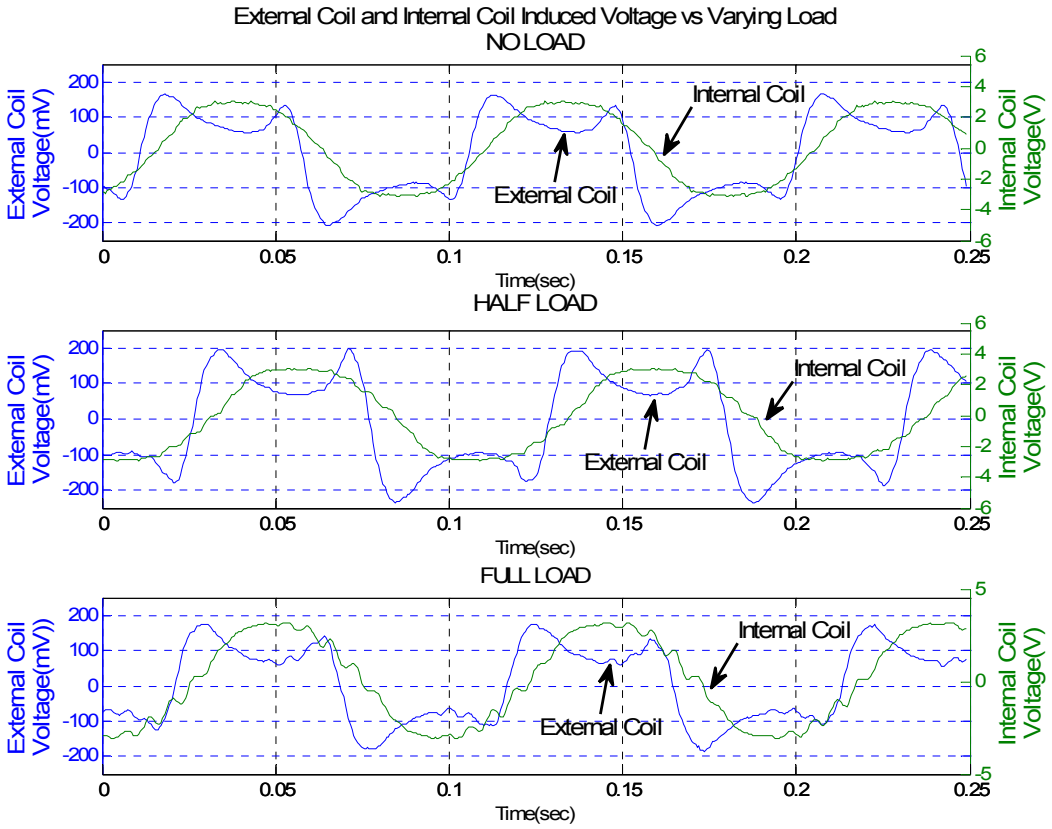

Fig. 4-16 Induced search coil voltages at 10 Hz, No Load – Half Load – Full Load

Table 4-8 Phase difference between internal and external coil voltages at 10Hz

	Freq. (Hz)	Terminal Voltage (V)	Internal Coil Voltage (V)	External Coil Voltage (mV)	Phase Difference between Internal and External Coil Voltages (degree)
No Load	10	$38 / 0^0$	$1.9 / -88^0$	$81 / -66^0$	12^0
Half Load	10	$47 / 0^0$	$2.3 / -94^0$	$109 / -70^0$	24^0
Full Load	10	$57 / 0^0$	$2.3 / -88^0$	$96 / -57^0$	31^0

From experiment results, it can be observed that, the phase angle difference between internal and external search coil voltage increases as the load is increased.

Thus, this non-linearity should be included in the model for external search coil. Also, notice that as the load increases, the rotor slot harmonics becomes more observable in both internal and external search coil voltage which is consistent with [14].

The similar experiment performed at rated stator frequency; 50 Hz. The terminal voltage is adjusted for rated flux operation. Experiment conditions are same with the experiments performed at 10 Hz. Experiment results are presented in Fig. 4-17 and Table 4-9.

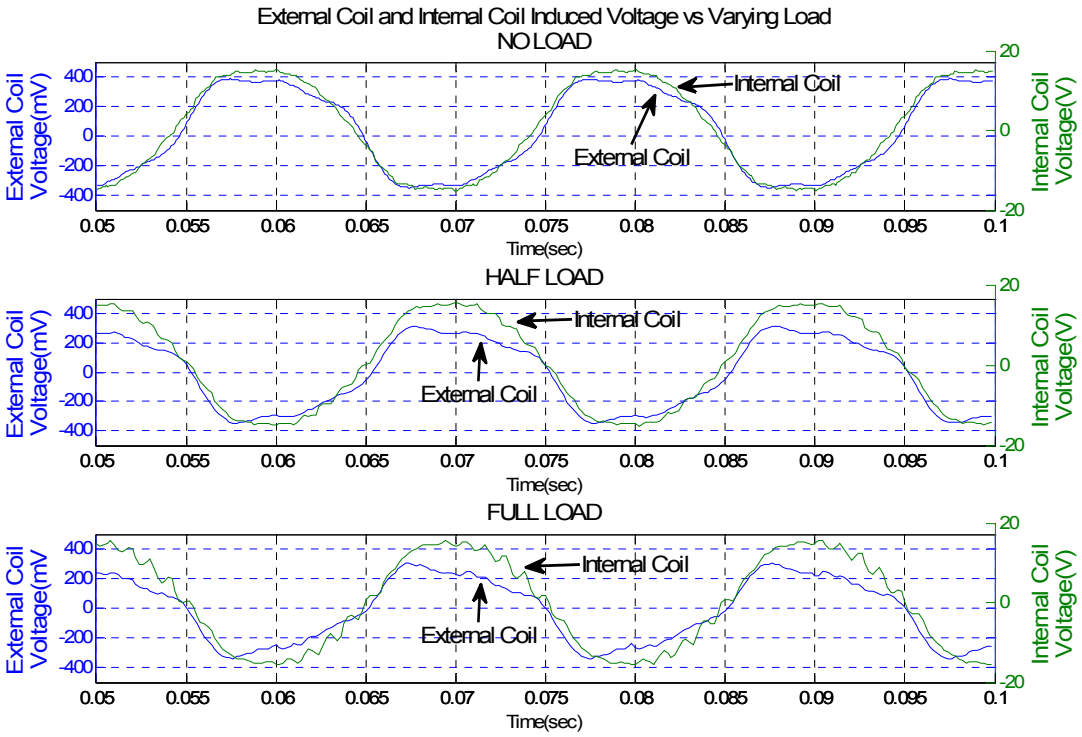

Fig. 4-17 Induced search coil voltages at 50 Hz, No Load – Half Load – Full Load

Table 4-9 Phase difference between internal and external coil voltages at 50Hz

	Freq. (Hz)	Terminal Voltage (V)	Internal Coil Voltage (V)	External Coil Voltage (mV)	Phase Difference between Internal and External Coil Voltages (degree)
No Load	50	$220 / 0^0$	$11.4 / -98^0$	$248 / -100^0$	-2^0
Half Load	50	$220 / 0^0$	$11.7 / -97^0$	$226 / -96^0$	1^0
Full Load	50	$222 / 0^0$	$11.2 / -97^0$	$236 / -92^0$	5^0

Although, the physical placement of internal and external search coils are same with the those in experiment performed at 10 Hz, the external search coil voltage shifts as the frequency is changed. This change with frequency will be discussed in the following section.

Another experiment is performed at 80 Hz applied stator voltage frequency; the terminal voltage is kept constant at rated value resulting flux weakening operation. The other experiment conditions are same with previous ones. The experiment results are given in Fig. 4-18 and Table 4-10.

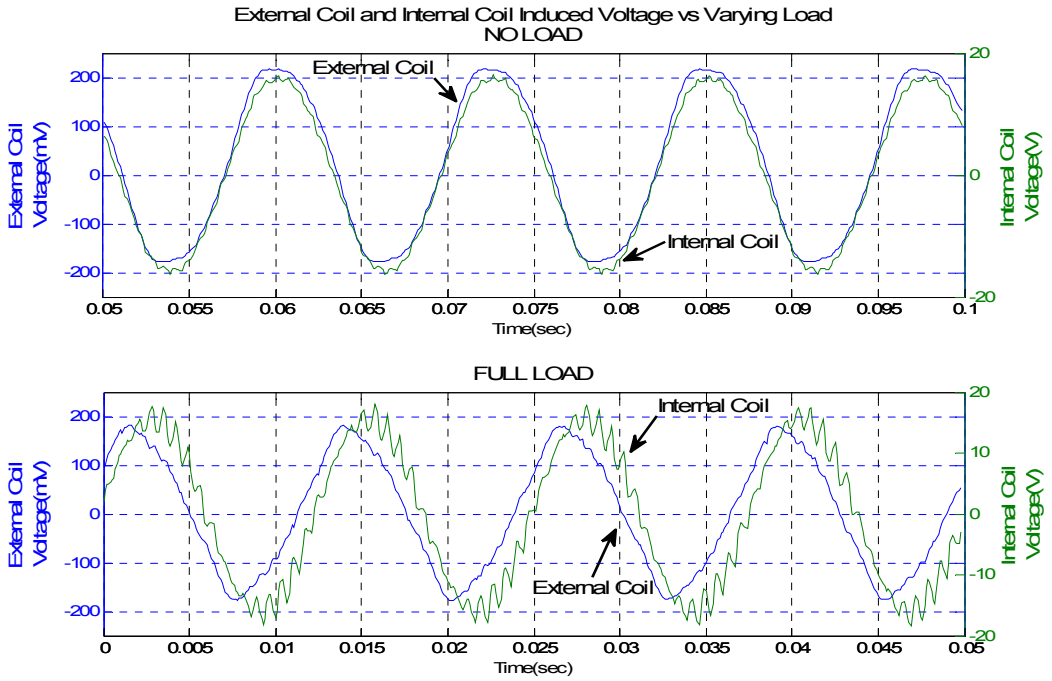

Fig. 4-18 Induced search coil voltages at 80 Hz, No Load– Full Load

Table 4-10 Phase difference between internal and external coil voltages at 80Hz

	Freq. (Hz)	Terminal Voltage (V)	Internal Coil Voltage (V)	External Coil Voltage (mV)	Phase Difference between Internal and External Coil Voltages (degree)
No Load	80	$224 / 0^0$	$11.6 / -98^0$	$151 / -98^0$	0^0
Half Load	80	$224 / 0^0$	$11.4 / -99^0$	$142 / -84^0$	15^0
Full Load	80	$225 / 0^0$	$11.5 / -99^0$	$121 / -68^0$	31^0

Similar phase shifting of external search coil voltage also exists in the 80 Hz stator frequency experiments.

For a better understanding of variation of internal and external search coil voltage magnitudes and phase angle variations, the many graphs are presented in Appendix D with the experimental data. The experiment results for no load, half load and full load conditions are given in Fig. D-3, Fig. D-4 and Fig. D-5.

On the basis of experiment results, the internal search coil voltage is not distorted considerably with the changing frequency or load. The most significant distortion for internal search coil is due to the rotor slot harmonics that increase in magnitude with the increasing rotor currents.

On the other side, the external search coil voltage has more nonlinearity compared to internal search coil voltage. In the previous chapter, the non-linear properties of the external search coil voltage is examined at three different conditions; varying air gap flux, varying stator frequency, varying load conditions. From these experiments the nonlinearities of the induced external search coil can be classified as,

- **Induced voltage magnitude variation:** As mentioned in previous section, the induced external search coil voltage does not increase proportionally with the increasing frequency. Also machine load conditions affect the induced external search coil voltage magnitude more than the internal search coil voltage magnitude.
- **Phase angle variation:** From the experiments performed in this section, the phase of the induced external search coil voltage varies with changing frequency and load conditions. This phase difference may be resulted from the eddy currents in the

machine frame. In next section, a model will be tried to build that can estimate these phase angle variations.

- **Harmonic content of induced voltage:** As the frequency is decreased distortion on the external coil voltage increases with the decreasing frequency. This can be verified from Fig. 4-16. Especially, the 3^{rd} and 5^{th} harmonics of the applied stator frequency exists dominantly in the external search coil voltage at low frequencies. This phenomenon will be investigated in section 4.7. The rotor slot harmonics are also observable from the external coil induced voltage as expected and discussed in Chapter 3.

In the next chapter, different models will be proposed to estimate the externals search coil voltage.

4.6 Modelling of External Search Coil

As discussed previously, if the air gap flux predicted using the measurement from the search coil voltage, it may be possible to estimate the rotor position. In section 4.3, a model is proposed using the induced internal search coil voltage. Similar methods will be followed for the external search coil. The model for external search coil voltage should include all non-linear characteristics of the induced external search coil voltage which are discussed with experiment results in previous section. Once the search coil voltage is modelled, the magnetizing voltage and the air gap flux position can be reconstructed using the model parameters obtained.

It should be highlighted again that, for modelling, the experiment results with cast iron frame machine #2 and the U-core search coil are used. The experiment results showed that the induced voltage on the external search coil is harder to model compared with internal search coil due to non-linear properties of external search coil with frequency and flux. To overcome this non-linear properties a varying turn's ratio model will be proposed instead of a constant turn's ratio model. And in order to model the load dependency of the induced external search coil voltage a term related with the phase currents will be proposed. The model should also include the effect of placement angle (δ) which is the angle between the magnetic axis of search coil and

magnetic axis of stator Phase A as given in Fig. 4-6. Also, a method for self calibration of the model parameters by the drive itself will be proposed.

4.6.1 Phase to Coil Mutual Inductance Model

This model is the same as the proposed in 4.3.1 as the internal search coil. Again, the mutual inductance between a stator phase and search coil is measured by applying a single phase voltage to each stator phase sequentially. The excitation is applied at line frequency; 50 Hz. To remind again, this model assumes that the magnetic circuit is linear and the principle of superposition is valid.

Once, the mutual inductance between stator phases and search coil (M_{a_coil}, M_{b_coil}, M_{c_coil}) is measured; the search coil voltage is given with the expression (4-7) and (4-8). The applied voltage and measured voltage for each stator phase in given in Table 4-11. Also, utilizing internal search coil measurements, air gap flux and magnetizing voltage can be measured. Phase difference of magnetizing current and magnetizing voltage is measured with respect to applied terminal voltage of each phase. At each step of experiment, only one phase of the stator is excited and the fundamental component of the induced external search coil voltage is measured for each stator phase excitation and results are presented in Table 4-11. Single phase excitation data is available for other flux values in Appendix D.

Also, the angle of placement between magnetic axis of stator phases and the magnetic axis of the search coil and the calculated mutual inductances between stator phases and are calculated using equation (4-8). In this formula, δ defines the angle between search coil magnetic axis and stator phase A magnetic axis.

Table 4-11 Induced external search coil voltages for single phase excitation and calculated inductances

Single Phase Excitation For Each Phase	Phase Voltage(V)	Phase Current (A)	Magnetizing Voltage- Ea (V)	Magnetizing Current (A)
	30 /0^0	3.1 /-60^0	26.7 /1^0	0.22 /-89^0
Measured Data	Phase A	Phase B	Phase C	
Induced Search Coil Voltage (mV)	63 / +5^0	20 /-163^0	15.4 /-159^0	
δ - Displacement Angle (Phase Angles between coil and stator Phases) (degree)	11^0	-109^0	131^0	
Mutual Inductances between search coil and stator phases	0.93 mH	0.88 mH	0.34 mH	

Using equation (4-8) and the inductance values obtained in Table 4-11, the induced external search coil voltage can be expressed as a sum of the induced voltages from each phase. The calculated search coil voltage will be compared in two situations; the no load test and locked rotor test. The experiment conditions, measured search coil voltage and the estimated search coil voltage values are given in Table 4-12.

Table 4-12 Measured and estimated external search coil voltage for single phase excitation experiments

	Phase A Voltage (V)	Phase A Current (V)	Measured Coil Voltage (mV)	Estimated Coil Voltage (mV)
Locked Rotor	48 V /0^0	4.8 A /-53^0	99 mV / +26^0	112 mV / +19^0
No Load	220 V /0^0	2.01 A /-53^0	262 mV / -43^0	630 mV /+19^0

In table, estimation results for two conditions are given. The estimation results showed that, this model does not give reasonable predictions. The mutual inductance between stator phases and external search coil is calculated at single phase excitation and does not provide the information for the non-linear behaviour of the search coil for different flux and frequency values. Thus, we can conclude that, the assumption of linear magnetic circuit and superposition is not valid. Thus, a new model will be proposed in following sections.

4.6.2 Turns Ratio Modelling

In this part, the induced voltage on the external coil will be modelled using a turn's ratio term. This model is the same as the proposed in 4.3.2 as with the internal search. Since the external search coil has a non-linear relation with frequency, we expect to achieve a varying turn's ratio with frequency. In this model, the equivalent circuit of the motor and search coil is given on Fig. 4-19 will be used with the motor#2 parameters which are available in Appendix A.

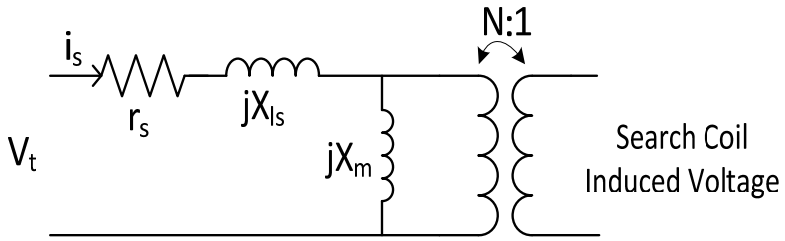

Fig. 4-19 Search coil model equivalent circuit (Classical transformer model)

Experiments performed at no load, and the induced external search coil voltage is recorded for various frequencies. For frequencies lower than 50Hz constant flux operation is applied and for higher frequencies the applied stator voltage is kept at rated value (220 $V_{l\text{-}n}$), thus decreasing the flux in the machine. Experimental data is presented in Appendix Table D-1.

The turns ratio for each frequency is calculated by taking the ratio of magnetizing voltage to the fundamental induced search coil voltage magnitude, using equations (4-9) and (4-10). The calculated values for turn's ratio are given in Fig. 4-20.

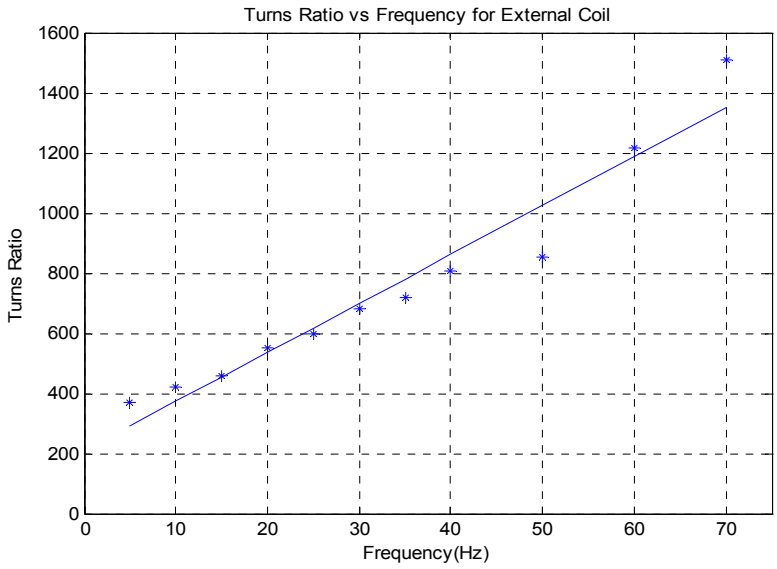

Fig. 4-20 Estimated turn ratios at various stator frequencies

For external search coil, the turn ratio is not constant, because the amount of flux linking the external search coil changes as the frequency is changed. Since the turns ratio is calculated only considering the fundamental component magnitude of the induced search coil voltage. The reconstructed signal based on these parameters using equations (4-9) and (4-10), will perfectly match with the fundamental magnitude of external search coil voltage. Since, the non-linearity in the phase angle variation is not considered in this model, the phase estimation of this model is not satisfactory. The model matches the phase difference for frequencies higher than 50 Hz.

The measured external search coil voltage and the predicted signal based on the given turns ratios are compared in Fig. 4-21. The first graph shows the comparison of the fundamental component magnitude of the search coil voltage and the second figure shows the phase difference comparison.

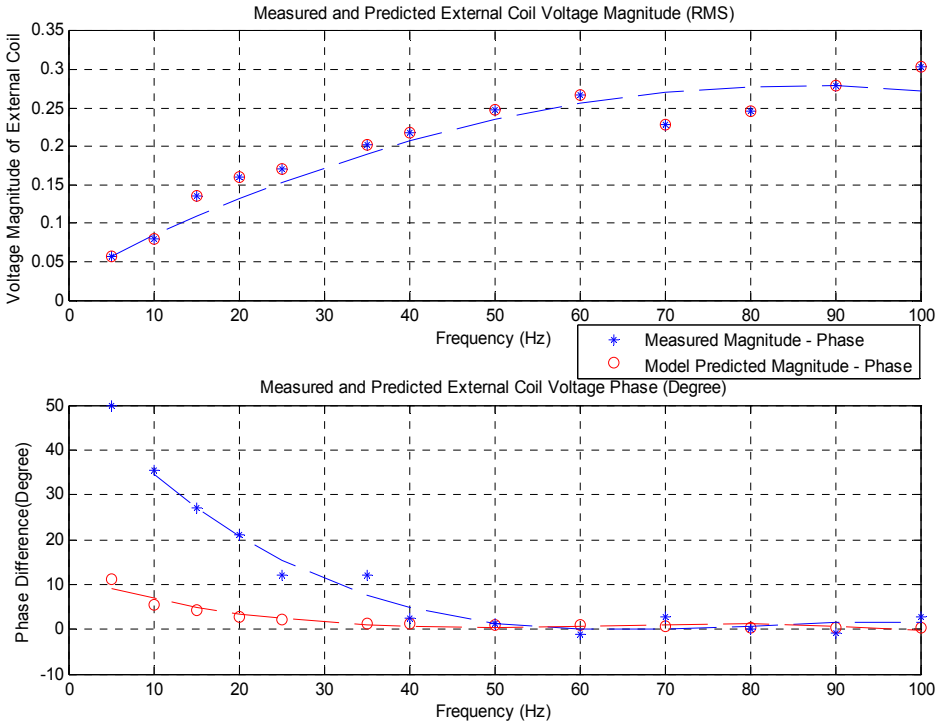

Fig. 4-21 Experimental and model estimated data using turns ratio data for external search coil

The experiment results show that the proposed method is not adequate for modelling the search coil voltage. The model should include the non-linearity of the fringing flux of the machine, and the effect of eddy currents. To achieve this, a model with both non-linear turn ratio and the non-linear equivalent circuit parameters will be utilized. On the other side, this method may make the modelling of machine flux harder and less robust. The proposed method will be introduced in the next section.

4.6.3 Estimation of Magnetizing Voltage with Turns Ratio and Leakage Inductance

In the previous section, the external search coil is modelled based on a varying turn's ratio. But the proposed model is insufficient to estimate the phase angle variations of the induced external search coil voltage.

The experiments showed that, the phase difference of the external search coil voltage varies as the load conditions change. Thus, the external search coil voltage affected both from the mutual flux and leakage flux component of the machine. In this section, another component that is related with the leakage inductance term will be included into the model. The equivalent circuit of the model is given in Fig. 4-22.

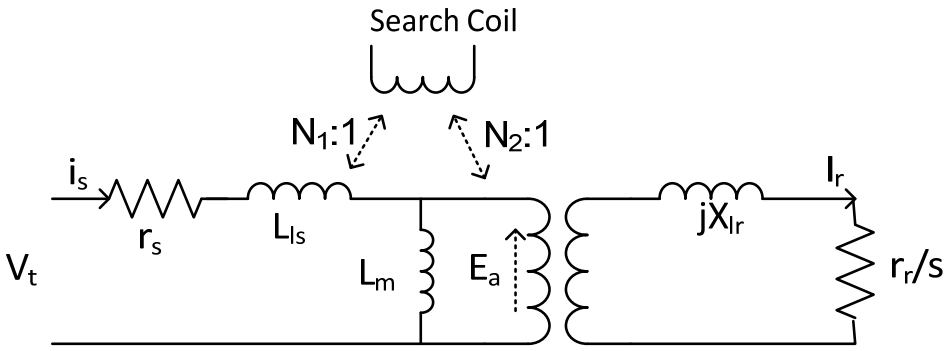

Fig. 4-22 Search coil equivalent circuit using motor parameters

In this equivalent circuit, the motor parameters (r_s, L_{ls}, L_m) are used. The external coil voltage can be modelled by using the voltage on leakage inductance term, and the magnetizing voltage. The term related with leakage term (N_1) aims to model the phase and magnitude variation of external search coil voltage with load.

The induced voltage on the external search coil can be expressed as a sum of these two components;

$$\vec{V}_{search\_coil} = \vec{V}_{lekage\ branch} + \vec{V}_{mutual\ branch} \quad (4\text{-}12)$$

$$\vec{V}_{search\_coil} = \frac{\vec{V}_{Lls}}{N_1} + \frac{\vec{V}_m}{N_2} \quad (4\text{-}13)$$

N_1: Turns ratio between leakage branch and the search coil.

N_2: Turns ratio between magnetizing branch and the search coil.

Where;

$$\vec{V}_{Lls} = X_{ls}.\vec{I_s} = j.w.L_{ls}.\vec{I_s} \quad (4\text{-}14)$$

$$\overrightarrow{V_m} = X_{lm}.\overrightarrow{I_m} = j.w.L_m.\overrightarrow{I_m} = \overrightarrow{V_t} - (r_s + j.w.L_{ls}).\vec{I_s} \quad (4\text{-}15)$$

Thus, search coil voltage is equal to;

$$\vec{V}_{search\_coil} = \frac{j.w.L_{ls}.\vec{I_s}}{N_1} + \frac{\overrightarrow{V_t} - (r_s + j.w.L_{ls}).\vec{I_s}}{N_2} \quad (4\text{-}16)$$

Where; w supply frequency, r_s stator resistance, L_{ls} stator leakage inductance, I_s motor phase current, V_t motor terminal voltage.

Equation (4-16) is used to estimate the induced external search coil voltage at different frequencies. The turn's ratios N_1 and N_2 are the variables that will be estimated terms of the equation where all the other terms are obtained from machine equivalent circuit of motor #2.

The model equation and the experiment results are analyzed and N_1 and N_2 values are estimated at different frequencies at no load. The parameters estimated at no load are held constant for other loading experiments. The parameters are estimated at no load because, a method that estimates parameter automatically can be proposed by this way. This method can run an initialization algorithm that sweeps all the frequencies at no load. And if the parameters estimated at no load are valid for other load conditions, the machine flux can be estimated for all operation conditions based on these parameters estimated at no load.

The parameters are (N_1, N_2) estimated with many experiment results performed at different frequencies (10, 25, 50, 70 Hz) at no load since the magnetic properties of the motor frame changes with the frequency as mentioned in 4.4.2. The experiment results performed at different frequency and load conditions are given in Table 4-13.

The N_1 and N_2 terms will be estimated using the MATLAB Parameter Estimation Toolbox. This toolbox is a very practical way of estimating the parameters of a model (N_1,N_2). The toolbox needs the experiment results of the estimated system with input data given to the system and the output data taken from the system. An appropriate model should be defined for the system with the parameters that will be tuned and the tuning range for each parameter. Once these

prerequisites are satisfied, the MATLAB Parameter Estimation Toolbox optimizes the tuned parameters (N_1, N_2) for best match. For this process, basic optimization algorithms are used with a cost function proportional with the square of difference between measured and estimated data set. After optimization is converged, the parameters (N_1, N_2) are found for the proposed model.

Then the estimated values at no load are applied to the experimental results at half load and full load. The estimation results and the fundamental magnitude and phase angle errors are given in Table 4-13.

Once the search coil is modelled using equation (4-16), the magnetizing voltage V_m, thus the position of air gap flux can be expressed using the induced external search coil voltage and the phase current as given in equation (4-18).

$$\vec{V}_{search\_coil} = \frac{j.w.L_{ls}.\vec{I_s}}{N_1} + \frac{\overrightarrow{V_m}}{N_2} \quad (4\text{-}17)$$

$$\overrightarrow{V_m} = N_2.\left(\vec{V}_{search\_coil} - \frac{j.w.L_{ls}.\vec{I_s}}{N_1}\right) \quad (4\text{-}18)$$

As seen from equation (4-18) the magnetizing voltage V_m can be obtained once the search coil voltage and phase current is measured. Once V_m with true phase angle is obtained, the position of the air gap flux and the rotor position can be obtained which is vital for field oriented drives. Another point that should be stated is, the air gap flux position measured from induced external search coil is independent of stator resistance (r_s) and rotor resistance (r_r') which is a great advantage.

Table 4-13 Estimated model parameter values, estimated and measured external search coil voltage for the proposed model

		Search Coil Voltage(mV) and Phase Difference w.r.t. Phase Voltage					
Freq. (Hz)	Load	Experimental	Estimation	N1	N2	Magnitude Error (%)	Phase Angle Error (degree - electrical)
10	No Load	81 / -66^0	84 / -67^0	198	463	3.7	1^0
	Half Load	109 / -70^0	98 / -65^0			10	5^0
	Full Load	96 / -57^0	104 / -61^0			8.3	4^0
25	No Load	170 / -89^0	169 / -89.3^0	184.5	690	0.6	0.3^0
	Half Load	182 / -86^0	172 / -85.5^0			5.4	0.5^0
	Full Load	168 / -78^0	178 / -78^0			6.0	0^0
50	No Load	248 / -100^0	169 / -99.6	339	999	23	0.6^0
	Half Load	226 / -96^0	172 / -97^0			15	1^0
	Full Load	236 / -92^0	178 / -91.6^0			16	0.4^0
70	No Load	167 / -97^0	142 / -95^0	325	1725	15	2^0
	Half Load	165 / -85^0	141 / -88^0			14.5	3^0
	Full Load	127 / -77^0	166 / -76^0			23	1^0

As seen from Table 4-13, the induced external search coil voltage can be estimated very accurately. The phase error is less 2 degree for most cases. But at lower frequencies the estimation errors increases up to 4-5 degrees, because the decrease in the fundamental component magnitude of the induced search coil voltage makes it harder to make an accurate estimation. For frequencies lower than 10 Hz, the induced external search coil voltage to noise ratio becomes smaller so that it is harder to detect zero crossing of the search coil voltage.

But the aim of this section is to obtain the magnetizing voltage (V_m) in order to calculate the rotor position. This can be achieved by using the equation (4-10). Using search coil voltage, N_1 and N_2, the magnetizing voltage may be reconstructed. In Table 4-14, the estimated magnetizing voltage using the proposed model is compared with the measured magnetizing voltage using the internal search coil.

The internal search coil voltage changes linearly with frequency and flux. For that reason, the magnetizing voltage is calculated using the internal search coil voltage and used as a reference signal.

Table 4-14 Estimated and measured magnetizing voltage values for different frequency and load conditions

		Magnetizing Voltage Magnitude and Phase Difference Estimation Using External Search Coil Voltage			
Freq. (Hz)	Load	Magnetizing Voltage (V)	Estimated Magnetizing Voltage (V)	Magnitude Error (%)	Phase Angle Error (degree - electrical)
10	No Load	$36.2/\ 5.3^0$	$35/\ 2.6^0$	3.4	2.7^0
	Half Load	$41/\ 4.8^0$	$37.7/\ 1.2^0$	7.9	3.6^0
	Full Load	$43.3/\ 1.8^0$	$46.7/\ -0.6^0$	7.1	2.4^0
25	No Load	$104/\ 2.1^0$	$96/\ 2.5^0$	0.8	0.4^0
	Half Load	$103/\ 0.9^0$	$107/\ 1.5^0$	3.9	0.6^0
	Full Load	$101/\ -1.7^0$	$106/\ -0.8^0$	5.3	0.9^0
50	No Load	$211/\ 1.0^0$	$178/\ 0.3^0$	16	0.7^0
	Half Load	$215/\ -0.6^0$	$241/\ -0.5^0$	12	0.1^0
	Full Load	$199\ /\ -3.3^0$	$217/\ -2.7^0$	9	0.6^0
70	No Load	$210/\ 0.2^0$	$185/\ 1.4^0$	12	1.6^0
	Half Load	$207/\ -1.9^0$	$240/\ -3.2^0$	16	1.3^0
	Full Load	$198\ /-4.2^0$	$226/\ -\ 6.6^0$	14	2.4^0

The phase angle estimation accuracy is better compared to magnitude estimation. The phase angle estimation error is less than 1 degree for rated frequency which is a reasonable estimation. But for low and high frequencies the estimation error increases up to 3.6 degrees which can be problem for accurate control of the machine.

In conclusion; it is found that by measuring coil voltage and phase current, the magnetizing voltage can be estimated. The magnitude and phase angle errors are small and it can be argued that; the rotor position can be predicted in this manner.

But the proposed method will have some difficulties. These are;

- The need for measuring model parameters for different machines at different frequencies. In other words, an initialization algorithm should be run during commissioning that will sweep various frequencies to estimate the parameters, which is not an easy task.
- Poor position update performance. Since, the model is based on the zero crossing points of the induced search coil voltage; we can get single flux position data at each stator voltage cycle. For example this period is 100 msec at 10 Hz stator frequency. The computation times are about tens of μsec so it can be neglected.

To overcome some of difficulties observed in this section; it is aimed to investigate the harmonic content of the search coil voltage.

4.7 Estimation of Induced External Search Coil Voltage Harmonics

The experiments performed in the previous section showed that, the external search coil voltage includes more supply harmonics than the internal search coil. Especially, as the frequency is decreased, the magnitudes of the 3^{rd} and 5^{th} stator voltage harmonics become comparable with the fundamental component. In this section, the 3^{rd} and 5^{th} stator voltage harmonics will be investigated for two purposes; if these harmonics can be included in the model proposed in previous section then better estimation results may be achieved. Or even better, if these harmonics are found to be invariant to frequency or load conditions, a new method using only these harmonics can be proposed. Moreover, the frequencies of these harmonics are higher than the fundamental component; this will make a better refresh rate compared to model proposed in previous section.

Experiments are performed to analyze the magnitude and phase of 3^{rd} and 5^{th} harmonics similar to those performed for fundamental component. The experiments cover the variation of harmonics with frequency, flux and load conditions.

4.7.1 Search Coil Voltage Harmonics with Varying Frequency

In this section, the distortion of the external search coil voltage with frequency will be investigated. The harmonic content of the induced voltage increases as the frequency is decreased as it can be seen from Fig. 4-16, Fig. 4-17 and Fig. 4-18.

In order to model the harmonic content of the search coil, induced voltages are expressed as sum of fundamental component and harmonics. Since the phase angle information is also needed beside the magnitude information, the spectral estimation techniques like Fast Fourier Transform are not used in this section. The estimation is realized using MATLAB Parameter Estimation Toolbox. In the toolbox, the search coil voltage is expressed as a sum of fundamental component and two harmonics components. The approximation includes the fundamental component, 3^{rd} and 5^{th}

harmonics. Higher harmonics and rotor slot harmonics are neglected. The equation used for estimation is given in (4-19).

$$V_{coil} = K_1.\sin(w.t+\Phi_1) + K_2.\sin(3.w.t+\Phi_2) + K_3.\sin(5.w.t+\Phi_3) \quad (4\text{-}19)$$

Then, the model parameters, K_1, K_2, K_3 are changed by the Parameter Estimation Toolbox to find best fit to the measured data using least squares method. After the optimum point is reached, estimation process ends. Then the modelled and measured data is plotted in order to validate the estimation. The relevant figures are given in Fig. 4-23, Fig. 4-24 and Fig. 4-25 for 10 Hz, 50 Hz, 70 Hz stator frequencies respectively.

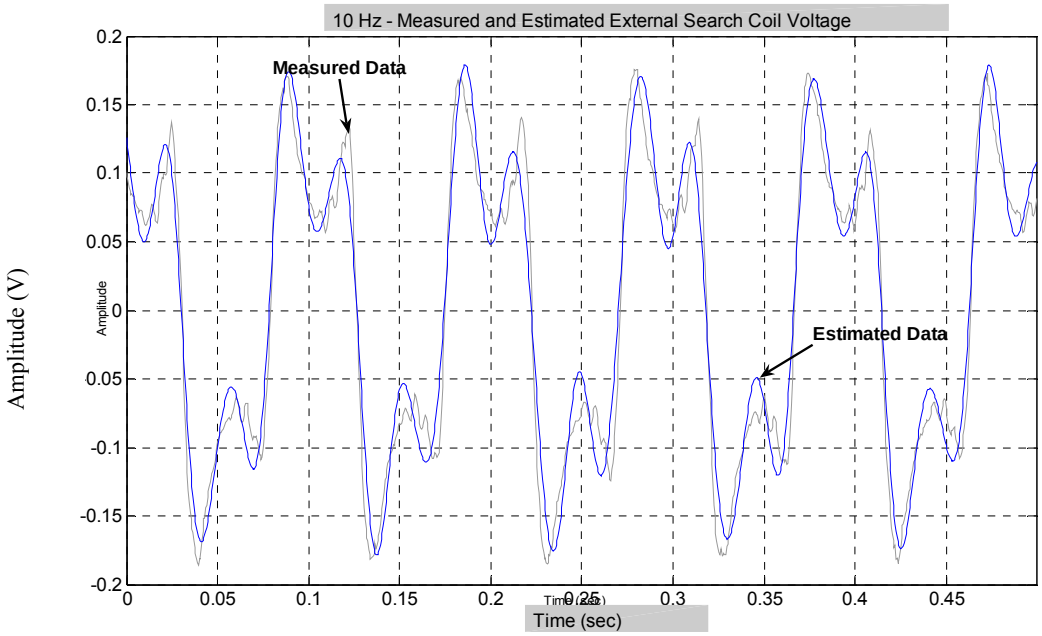

Fig. 4-23 Measured and estimated data at 10 Hz stator frequency

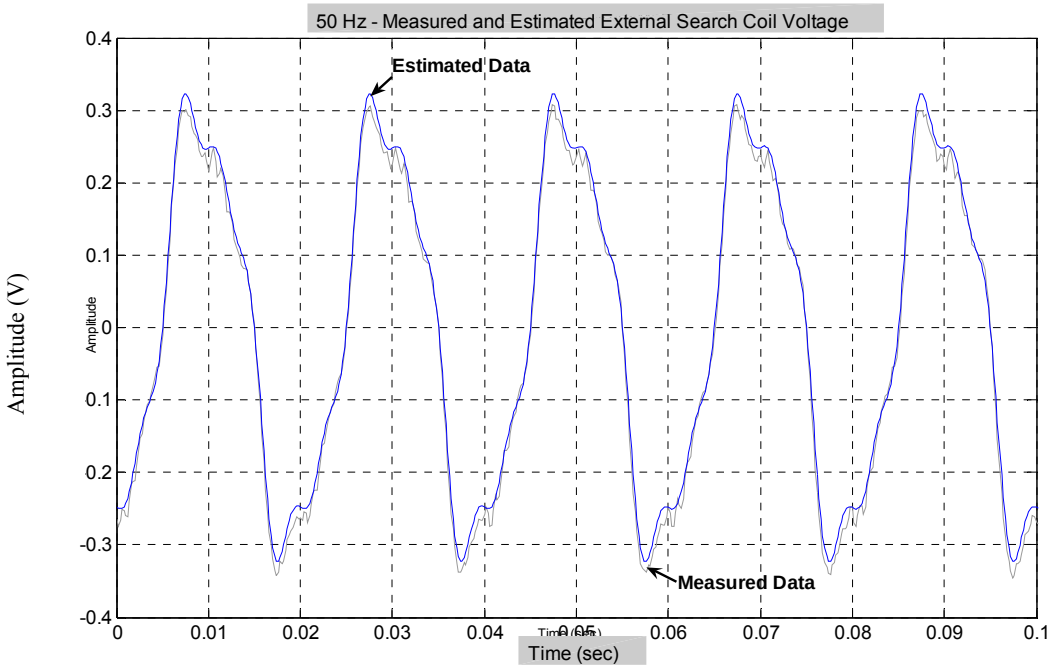

Fig. 4-24 Measured and estimated data at 50 Hz stator frequency

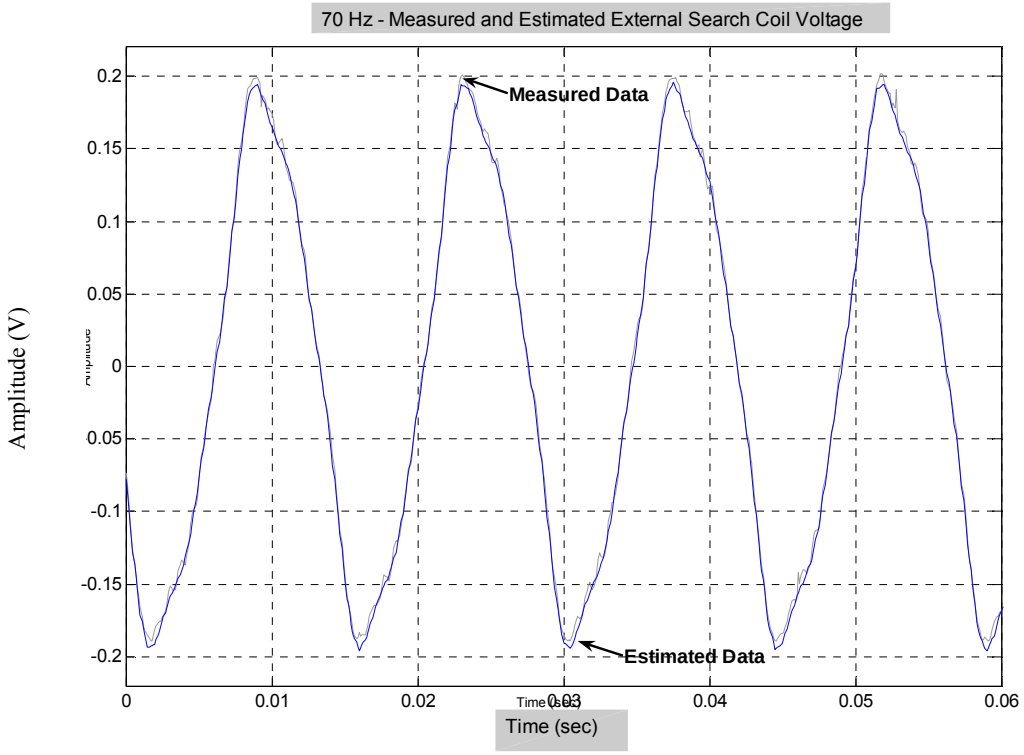

Fig. 4-25 Measured and estimated data at 70 Hz stator frequency

As it can be validated from figures, estimation matches the measured data perfectly. The estimation results give the magnitude and phase difference of the 3rd and 5th harmonics of the external search coil voltage. The graph of this data is presented in Fig. 4-30 and the experimental data is available at Appendix D, Table D-4 and Table D-5. The experiments results showed that the ratio of the magnitude of 3rd and 5th harmonic components to the magnitude of fundamental component decreases with increasing frequency.

The idea of obtaining constant magnitude harmonics insensitive to frequency variation fails. Thus, the model that will predict the magnitude of these harmonics should be non-linear similar to the fundamental component. In the following section, magnitude variation of these harmonics will be investigated with different flux conditions.

4.7.2 Search Coil Voltage Harmonics with Varying Flux

In order to observe the relation between machine air gap flux and search coil voltage, various waveforms of the external search coil are captured for different air gap flux value. In order to change the flux, the terminal voltage is varied while the load and frequency is kept constant. The experiments are performed at 25 Hz and 50 Hz. The captured data for varying terminal voltages are given in Fig. 4-26 and Fig. 4-28. The experiment data are available in Table 4-15 and Table 4-16. Lastly, the spectrum analysis of the captured data is performed and the graphs are given in Fig. 4-27 and Fig. 4-29.

Table 4-15 Internal and external coil voltages with varying flux at 25 Hz

Terminal Voltage (V)	Phase B Current (A)	Peak Flux/pole (mWb)	Internal Coil Voltage (V)	External Coil Voltage (mV)
50	$0.6 / -73^0$	2.2	$2.5 / -97^0$	$75 / -84^0$
80	$1.0 / -81^0$	3.6	$4.1 / -97^0$	$125 / -88^0$
100	$1.4 / -81^0$	4.5	$5.1 / -95^0$	$174 / -91^0$
120	$2.24 / -81^0$	5.5	$6.2 / -98^0$	$287 / -89^0$

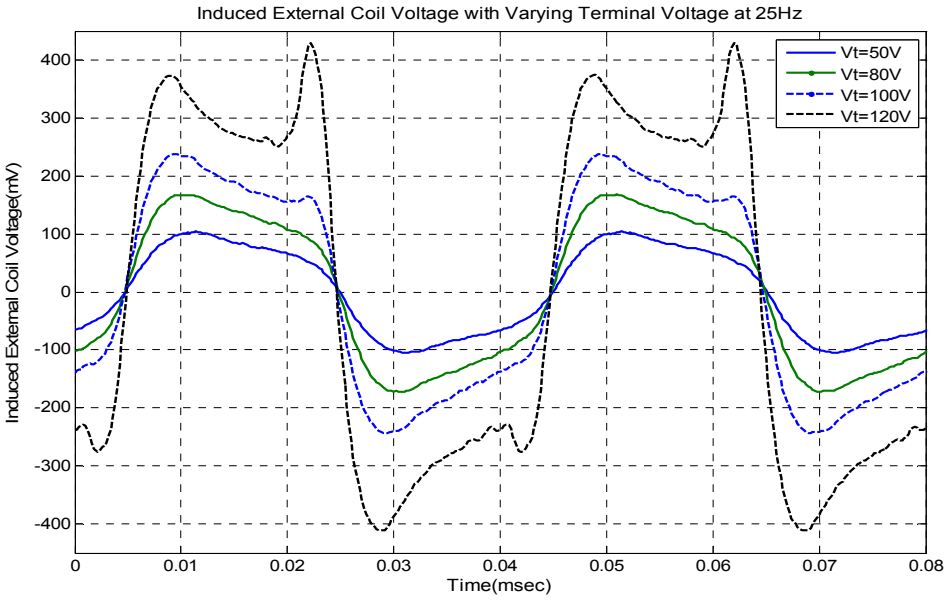

Fig. 4-26 External search coil voltage with varying flux at 25 Hz

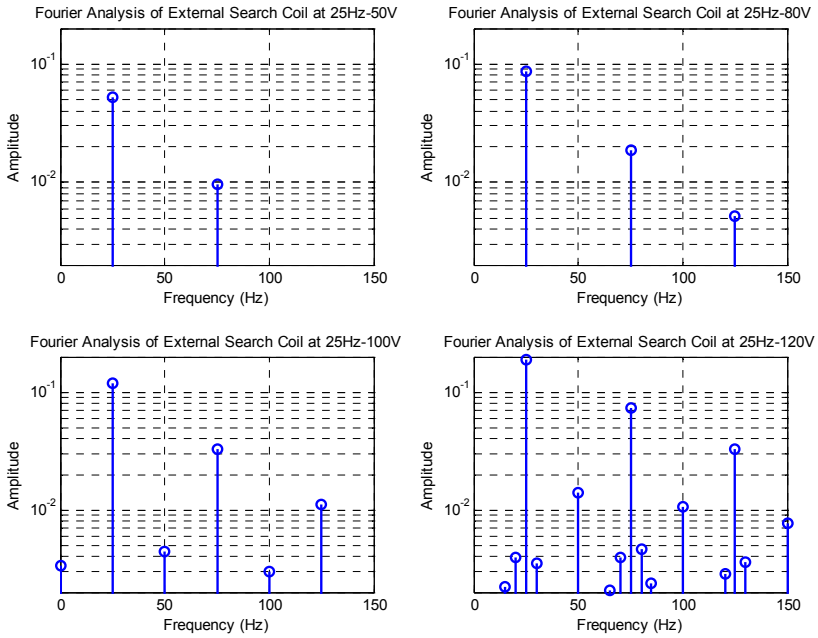

Fig. 4-27 FFT analysis of external search coil voltage with different terminal voltages at 25 Hz

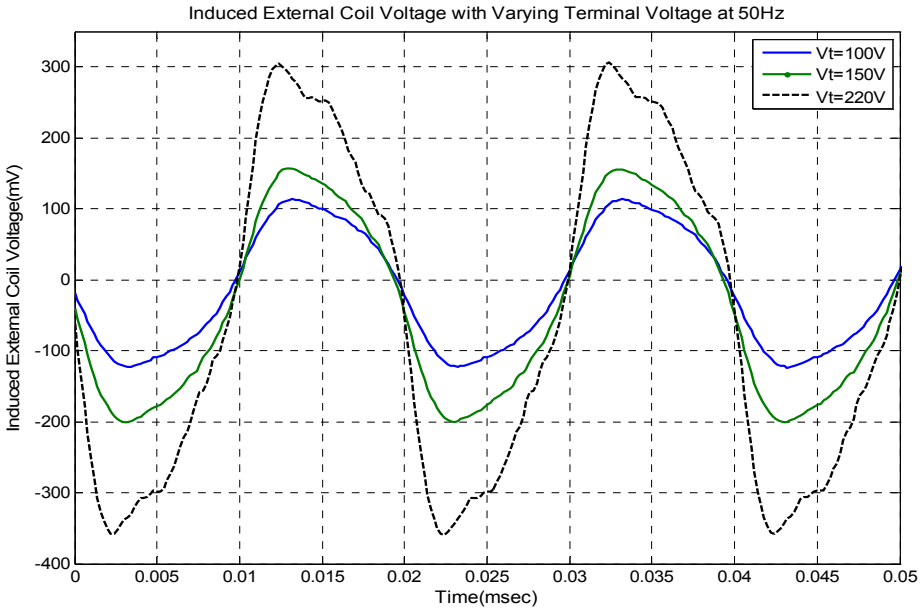

Fig. 4-28 External search coil voltage with varying flux at 50 Hz

Table 4-16 Internal and external coil voltages with varying flux at 50 Hz

Terminal Voltage (V)	Phase B Current (A)	Peak Flux/pole (mWb)	Internal Coil Voltage (V)	External Coil Voltage (mV)
100	0.6 / -690	2.4	5.2 / -980	99 / -940
150	0.94 / -770	3.5	7.7 / -990	148 / -990
220	1.85 / -810	5.1	11.3 / -970	279 / -1060

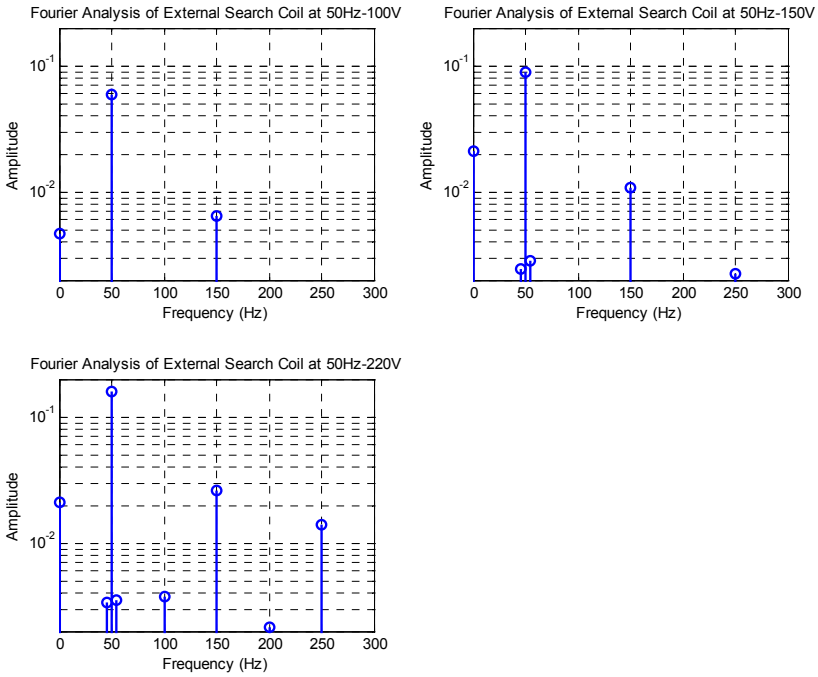

Fig. 4-29 FFT analysis of external search coil voltage with different terminal voltages at 50 Hz

The experiments results showed that the magnitude of 3rd and 5th harmonic components increases as the air gap flux increases. This result will be discussed in section 4.7.4.

4.7.3 Search Coil Voltage Harmonics with Varying Load

In this section magnitude and phase angle variations of the 3rd harmonic of the induced search coil voltage is investigated and compared with the magnitude and phase difference of the fundamental component at no load, half load and full load.

In Fig. 4-30, there are four graphs represented. These are;

I- Fundamental component magnitude variation with load

II-3rd harmonic magnitude variation with load

III- Fundamental component phase angle variation with load

IV- 3rd harmonic component phase angle variation with load

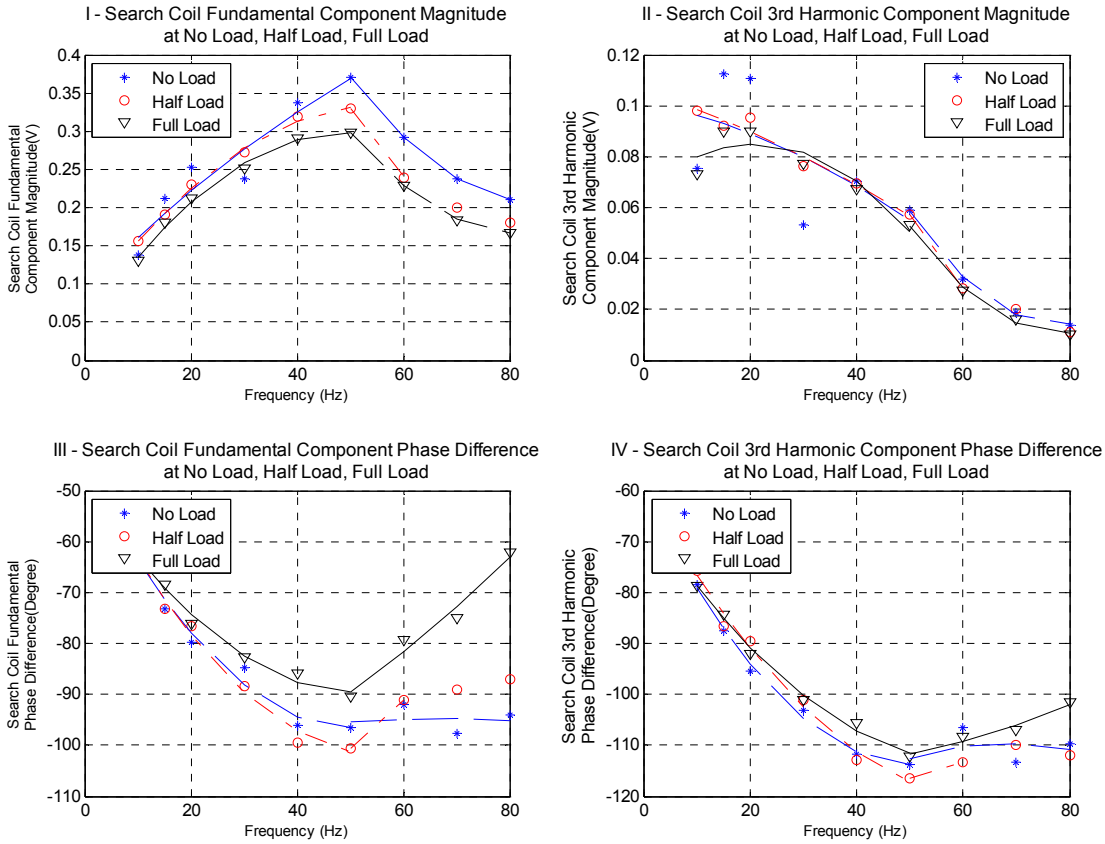

Fig. 4-30 Estimated data for fundamental and 3rd harmonic component

From Fig. 4-30, it is clear that the 3rd harmonic component magnitude is nearly constant with different load conditions. Phase difference variation with load is also smaller than the variation of the fundamental component. Also note that, the magnitude of the 3rd component decreases as the applied frequency is increased as mentioned in section 4.7.1.

4.7.4 Conclusion for Search Coil Voltage Harmonics

In this section, magnitude and phase variation of 3rd and 5th harmonics in the external search coil voltage is investigated. It is thought that, if the characteristics of the 3rd harmonic component with load, frequency and flux is known, and then it can be a better way to obtain the flux position of the machine. Similar to fundamental component once the magnetizing voltage is modelled using the induced search coil

voltage harmonics, the flux position may be obtained utilizing the equations (4-6) and (4-11). But, as a first step, the characteristic of the induced search coil voltage harmonics should be investigated. To achieve this, experiments are performed with varying frequency, load and flux conditions. From the experiment following results can be obtained with each experiment step.

- **Frequency Variation:** It can be concluded from Fig. 4-30 that, the magnitude of the 3rd harmonic component increases as the frequency is decreased. But the phase angle variation with frequency is still present. Thus, making these harmonics unsuitable for air gap flux estimation.

- **Flux Variation:** In Fig. 4-26 and Fig. 4-28 it may be seen that the magnitudes of the 3rd and 5th harmonics increase as the flux in the machine is increased. The experiments are performed at 25 Hz and 50 Hz and give similar results. A spectral analysis for all waveforms obtained is given in Fig. 4-27 and Fig. 4-29. Especially, when the flux is increased just above the rated value, the harmonics in the induced search coil voltage increases drastically. This increase can be easily observed from the peak points of the induced voltage waveform.

- **Load Variation:** Different from fundamental component, the 3rd harmonic magnitude does not change with different load conditions. It can be seen from Fig. 4-30 that the phase angle varies with load but is much smaller than the phase variation of the fundamental component with load.

As seen from experiment results, the harmonic content of the induced external search coil voltage increases as the applied frequency is decreased. Also, the magnitude of harmonic contents increases when the machine flux is increased. In order to model the induced external search coil voltage, the magnitudes of the harmonic contents are investigated with changing frequency, flux and load conditions. Using these experiment results, induced search coil voltage can be estimated more accurately including the 3rd and 5th harmonics.

There are two main advantages of 3rd and 5th harmonics compared to fundamental component. The magnitudes of these harmonics are nearly insensitive to load variations differing from the fundamental component. Thus, the modelling of these harmonics may be easier. But, the magnitude and phase difference non-

linearity of the 3rd and 5th components with varying flux and frequency are still exist. Another advantage may be the higher frequency of these harmonics satisfies to obtain zero crossing data at shorter periods which increases the accuracy of the method.

Thus, these 3rd and 5th harmonic components may also be directly used for machine flux estimation. This thesis does not cover this method, but the experiments results in this study may supply valuable information for future studies. But, the load insensitivity of the harmonics measured in this section inspired, the idea of using harmonics for rotor position estimation as described in next chapter.

4.8 Evaluation of Search Coil Models

In this chapter, many experiments results with internal and external search coils are presented. And some models are proposed and evaluated to model magnetizing voltage and air gap flux.

Based on the experiment results, it can be proposed that; the induced internal search coil voltage has almost a linear relation at a given frequency with the machine air gap flux; this makes the internal search coil a reliable flux observer. Since the magnitude of internal coil voltage is directly related with the air gap flux, the induced voltage can be modelled only with single turn's ratio term. And the turn's ratio is constant for all frequencies and flux conditions making the flux observation from the internal search coil straight forward and easy. But the placement of the internal search coil is not easy because of invasive techniques or modification of motor design procedure. Thus makes the internal search coil method impractical but a reliable method for determining air gap flux position.

The external search coil has advantages of easy mounting and low cost. But modelling of induced external coil voltage is harder than the internal coil due to non-linear characteristic of the external search coil voltage. Experiments showed that, the fringing flux outside of the machine has a varying characteristic with the air gap flux, applied stator frequency and load conditions. To conclude, referring to experimental results presented in 4.4 and Appendix D; the characteristic of external search coil can be summarized as;

- **Flux Variation:** The experiment results are presented in 4.4.1. These results show that, the induced voltage magnitude on the external search coil increases exponentially with the machine air gap flux. As, the flux density in the air gap is increased, the stator core and the frame tends to saturate, thus the outside of the machine frame becomes a more preferable path. Thus, more flux fringes out of the motor frame, inducing larger voltage on the external search coil. To estimate the air gap flux position properly a non-linear model between induced search coil voltage and air gap flux should be established.
- **Applied Frequency Variation:** As the applied stator frequency is increased the magnitude of the induced external search coil voltage also increases. But the ratio between the voltage magnitude and frequency is not linear, differing from the internal search coil characteristic as can be seen from Fig. 4-14. Also the phase of the induced voltage varies as the frequency is changed. This makes the modelling of the external search coil harder. Also, the lower frequency limit for external search coil is determined as 5 Hz. For frequency lower than 5 Hz, noise to signal ratio becomes larger and it is difficult to obtain reliable measurements**.**
- **Load Variation:** As the machine is loaded the induced voltage magnitude on the external search coil is slightly decreased as shown in Fig. 4-15. But the phase angle variation of the induced external search coil voltage increases as the load is increased as shown in Fig. D-6.

Due to these nonlinearities, the model for internal search coil should be modified. Firstly, instead of using a model with constant turn's ratio, a model is used with varying turn's ratio term in section 4.6.2. But the model is still insufficient to estimate the phase difference variations of the external search coil voltage.

Thus, a new model is proposed in 4.6.3. In this model, the phase difference variation is modelled with a term related with phase currents and leakage inductance. The phase difference variation of the search coil voltage with load and frequency is modelled with a term related with leakage inductance branch and phase currents. The experiment results presented in Table 4-14, showed that with this model; the position of the air gap flux can be estimated. The proposed method in 4.6.3 is independent of

rotor and stator resistances making the external search coil method insensitive to resistance variations.

Once the model parameters are determined, the estimation algorithm detects the zero crossings of the induced search coil voltage. Based on these zero crossings and the proposed model, we can obtain single flux position data at each cycle of stator frequency. In equation (4-16) the method for estimation of magnetizing voltage from search coil is explained. Similarly, equations (4-6) and (4-11) can be utilized to estimate the position of air gap flux.

But the proposed method has two major difficulties;

Firstly, an initialization algorithm is needed to determine the model parameters (N_1, N_2) for different machines. The initialization process will run once during commissioning to determine the parameters. But, an optimization algorithm should be designed that will evaluate for different model parameters and to select the best pair that gives reasonable outcome for all load and frequency conditions. This process may be even harder than the main algorithm.

Secondly, single estimation per each induced voltage period is not accurate enough. This means a 100 msec period at 10 Hz stator frequency excluding the computation period which is not a satisfactory performance. This means, once the algorithm completes estimation, the rotor speed new position will be far from the actual position.

To overcome this difficulty some interpolation techniques may be applied or harmonics with higher frequencies should be used.

In section 4.7, the 3^{rd} and 5^{th} harmonics of the external search coil voltage is investigated whether or not they vary with frequency, load and flux conditions. Also, higher frequency harmonics means shorter rotor position update period. Because, for the same time interval; the 3^{rd} harmonics will have three times more number of zero crossings compared to those of fundamental component. Similar experiments are performed to those performed for the fundamental component. Experiment results showed that the magnitude of these harmonics does not change with load conditions. But, the phase differences of the harmonics vary with frequency and load conditions.

Thus, in modelling of these harmonics same difficulties arise as the difficulties in fundamental component so this method is also inadequate.

Another disadvantage of method for both fundamental and harmonics component occur at dynamic conditions. In this chapter, the steady state induction machine equivalent circuit is used. Thus, the model should be improved for dynamic conditions.

To conclude, the proposed model using the fundamental or 3rd harmonic components of the external search coil voltage is not a very reliable method due to following reasons;

- Nonlinear characteristics of the induced external search coil voltage
- Difficulty in defining model parameters for other machines
- Long update period for flux position estimation
- Model valid for only steady state conditions

However, the flux position estimation method is found to be insufficient, the experiments performed in this chapter may provide valuable information on the behaviour of induced voltage of external search coil, placed on the machine frame. More over, the higher harmonics of the external search coil investigated in this chapter gave inspiration of analyzing higher order rotor slot harmonics in real time which will be discussed in the next chapter.

CHAPTER 5

POSITION & SPEED ESTIMATION BY DEMODULATING THE SEARCH COIL VOLTAGE

5.1 Introduction

In chapter 3, the rotor slot harmonics are analyzed using spectral analysis methods like Fast Fourier Transform (FFT). It is proved in chapter 3 that, using FFT method rotor speed can be estimated accurately using the induced search coil voltage. The biggest advantage of FFT method is easy detection of rotor slot harmonics among many other harmonics of supply frequency.

On the other side, the proposed methods in chapter 3 have an important drawback; they need large data acquisition periods necessary for the spectral analysis techniques. For a successful spectral analysis up to ten cycles of fundamental stator frequency is needed which means about one second lag at 10 Hz excluding the computation time. Thus, these methods cannot be considered as online speed estimation methods due to time lag resulted by data acquisition and computation period.

A new method that can reduce the estimation time will be proposed in this chapter. Instead of applying spectral analysis on the search coil voltage, rotor slot harmonics will be analyzed in time domain. Analysis in time domain decreases computation, data acquisition time and provides online estimation of rotor speed. Moreover, if the rotor slot harmonic voltage signals can be isolated from other components of induced search coil voltage in time domain, instantaneous rotor position can be estimated.

It is realised that air gap flux is nothing but a signal modulated with rotor slot harmonic frequency.

In order to obtain this rotor slot harmonics, demodulation techniques will be applied on the induced search coil voltage. Then, the demodulated signal will be filtered to isolate the desired rotor slot harmonics. It is necessary to emphasize that; this operation can be performed in real time. In other words, instantaneous rotor position will be achieved as the data points are captured at each sampling period without data acquisition period.

Obtaining rotor position and rotor speed online without using position encoder is very useful for field operation of induction machines.

5.2 Estimation of Rotor Speed and Position from Rotor Slot Harmonics in Time Domain

In section 3.2, the theory of the rotor slot harmonics has already been explained. Similar harmonics will be utilized in this section. But, they will be analyzed in time domain.

It is proved in chapter 3 that induced external search coil voltage contains rotor slot harmonics. The rotor slot harmonics have two side band frequency components.

- Rotor Slot Harmonic Lower Sideband Frequency: $\mathbf{(Z/P).f_r - f_s}$
- Rotor Slot Harmonic Upper Sideband Frequency: $\mathbf{(Z/P).f_r + f_s}$

Refer to Fig. 5-1, to visualize these rotor slot harmonics. In Fig. 5-1-a, the induced voltage on the internal search coil is given at rated operation conditions for motor #2 is given. The voltage fluctuation on the fundamental component is due to rotor slot permeance variation as explained in section 3.2.

In Fig. 5-1- b, the fundamental component is removed and rotor slot harmonics is isolated. In Fig. 5-1- b, the upper side band lower side band rotor slot harmonics is given. The obtained waveform is a typical amplitude modulated data. Thus, it can be concluded that rotor slot harmonics are modulated signals with fundamental stator frequency. The details of amplitude modulation will be presented in section 5.4.

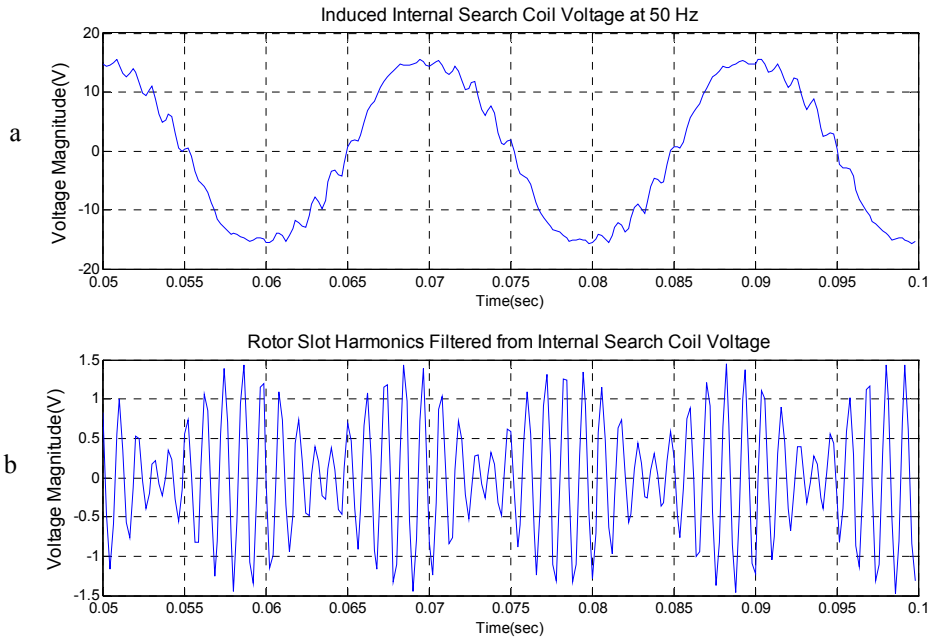

Fig. 5-1 Induced internal search coil voltage and rotor slot harmonics at 50 Hz

5.3 Higher Order Rotor Slot Harmonics

One of the reasons for using spectral analysis techniques in chapter 3 is to distinguish easily rotor slot harmonics from the applied stator frequency harmonics. Spectral analysis methods still seem to be best method for detection of the rotor slot harmonics if the rotor slot harmonics are mixed with the other harmonics.

If higher order rotor slot harmonics also exist, they are often located far from the applied stator voltage harmonics in the spectrum line. It would be easier to detect the rotor slot harmonics. The existence of the higher order rotor slot harmonics are introduced in Chapter 1, in the generalized harmonics equation given by [26]. Equation (5-1) is found to be a very useful equation in speed estimation and fault detection algorithms in many studies.

$$f_h = \left[(k.Z \pm n_d).\frac{(1-s)}{P} \pm v\right].f_s \qquad (5\text{-}1)$$

Where, f_h defines the harmonics in the machine flux, k is positive integer, Z number of rotor slots, n_d order of eccentricity, s slip, P number of pole pairs, v stator

harmonics of the power supply driving the motor (v=1, 3, 5...), f_s applied fundamental stator frequency.

In a healthy machine, the order of eccentricity is zero (n_d=0). Putting n_d=0 in equation (5-1) with first order power supply harmonics (v=1), the equation becomes;

$$f_h = \left[(k.Z).\frac{(1-s)}{P} \pm 1\right].f_s \quad (5\text{-}2)$$

$$f_h = \mathrm{k}.\left(\frac{Z}{P}\right).f_r \pm f_s \quad (5\text{-}3)$$

$$k = 1, 2, 3 \ldots$$

In these equations, f_r is the rotor frequency; (1-s).f_s, k is the harmonic order number. Equation (5-3) is the major equation that implies, not only the rotor slot harmonics with harmonics order one(k=1) exist but also higher order rotor slot harmonics (k=2,3,...) exist in the air gap flux. By spectral analysis techniques proposed in chapter 3, rotor slot harmonics with only first order harmonics (k=1) have been investigated.

In this chapter, the rotor slot harmonics with higher harmonic order will be investigated. Higher order rotor slot harmonic frequencies are located far away from the line harmonics in the spectrum line as shown in Fig. 5-2 and Fig. 5-3. Thus, this provides us to distinguish them easily with the proposed method.

Since the fundamental rotor slot harmonics are observable in the search coil voltage, higher order rotor slot harmonics should also be detectable. In Fig. 5-2 the spectral analysis of the induced voltage from internal search coil is shown. The FFT is applied to induced search coil voltage data when the motor #2 is running at rated load with a stator frequency of 40 Hz. Fig. 5-3 gives the spectral analysis of external search coil voltage with the same conditions.

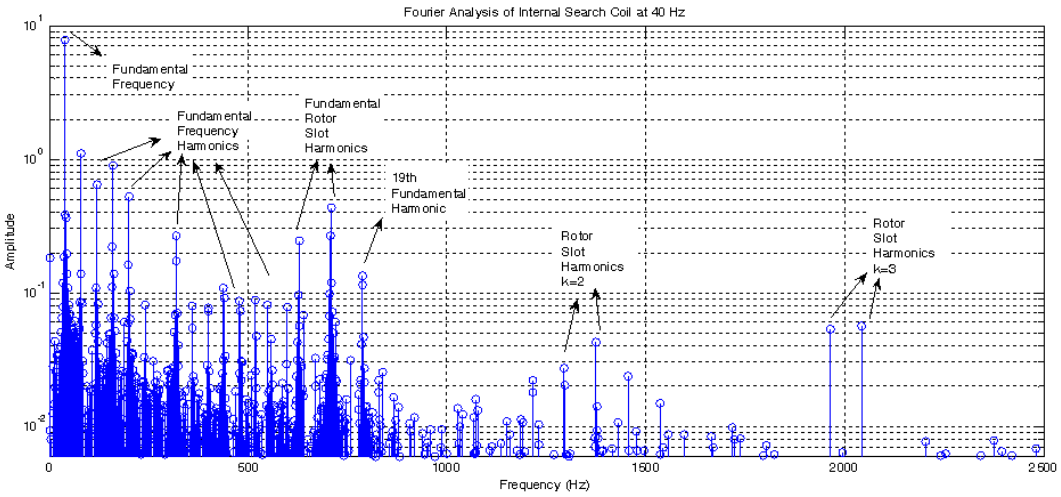

Fig. 5-2 FFT analysis of internal search coil at 40 Hz at rated load

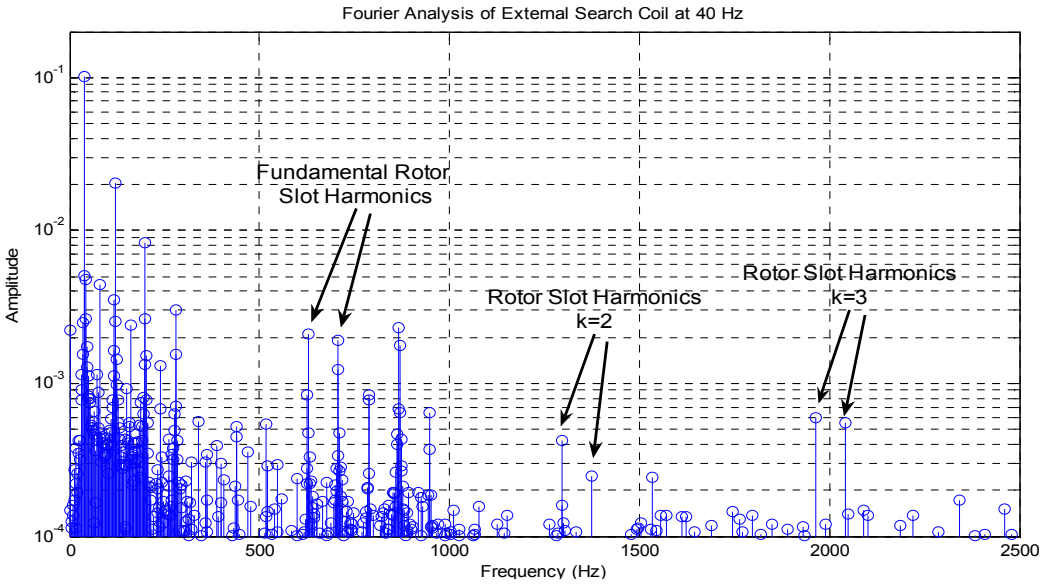

Fig. 5-3 FFT analysis of external search coil at 40 Hz at rated load

From Fig. 5-2 and Fig. 5-3, it can be observed that as well as the fundamental component of rotor slot harmonics, higher order (k=2, 3) rotor slot harmonics are also observable in the captured internal voltage. Notice that, the fundamental rotor slot harmonic is in a part of spectrum where many other harmonics exist as

discussed. On the other hand, 2nd and 3rd harmonic of the rotor slot harmonic appear to be in a region of the spectrum where other harmonics are not significant. This observation indicates that it may be a wise approach to utilize these components in rotor speed and position estimation process.

The second (k=2) and third (k=3) rotor slot harmonics are smaller in magnitude than the fundamental rotor slot harmonic. But they are still observable. The harmonics of the induced search coil voltage are investigated at various frequencies. The magnitude of higher order rotor slot harmonics are compared with the magnitude of fundamental rotor slot harmonics. The results are tabulated in Table 5-1. In table, the percentage ratios of the 2nd and 3rd order rotor slot harmonics with respect to the fundamental rotor slot harmonics are given.

The results presented in Table 5-1, shows that the magnitude of 3rd order rotor slot harmonic is larger than the magnitude of 2nd order rotor slot harmonic. Also, the 3rd order rotor slot harmonic is advantageous because of its higher frequency. Its higher frequency prevents rotor slot harmonics sideband components to mix with supply harmonics. Higher frequency also offers the possibility of higher accuracy if the zero crossings can be detected in time domain.

Thus, in this chapter, the 3rd order rotor slot harmonic will be used for rotor speed and position estimation.

Also, notice that generally the ratio of the 3rd order rotor slot harmonic magnitude ratio to the fundamental rotor slot harmonic magnitude is larger in external search coil compared to internal search coil.

Table 5-1 Magnitude comparison of higher order rotor slot harmonics with fundamental rotor slot harmonic

	Internal Search Coil		External Search Coil	
	Percentage ratio of higher order harmonics to fundamental rotor slot harmonic (%)		Percentage ratio of higher order harmonics to fundamental rotor slot harmonic (%)	
Frequency	k=2	k=3	k=2	k=3
20	9	13	11.1	16.4
40	10.3	14.4	9.6	16.7
50	10.8	15.4	7.8	10.6

5.4 Search Coil Voltage as a Modulated Signal

In this section, demodulation process of search coil voltage will be investigated. Before continuing on the induced search coil voltage analysis, it will be very helpful to give brief information about amplitude modulation.

Amplitude modulation is widely used in communication and signal processing area. Amplitude modulation is basically the multiplication of two signals. Generally, the signal with lower frequency is called modulating signal and the signal with higher frequency is called the carrier frequency [41].

Consider two signals;

$$f_m(t) = \mathrm{A}.\cos(w_m t) \tag{5-4}$$

$$f_c(t) = \mathrm{B}.\cos(w_c t)$$

The amplitude modulation is achieved by multiplying modulating signal and the carrier frequency.

$$f_{AM}(t) = f_m(t)\ x\ f_c(t) = A.cos(w_m t)\ x\ B.cos(w_c t) \tag{5-5}$$

$$f_{AM}(t) = \frac{A.B}{2}[cos((w_c - w_m)t) + cos((w_c + w_m)t)]$$

The resultant modulated signal consists of two frequency components; w_c - w_m (lower side band), w_c + w_m (upper side band).

Comparing equations (5-5) and (5-3) similarities between an amplitude modulated signal and the rotor slot harmonics can be easily noticed. From these equations and figures it can be easily concluded that rotor slot harmonic components are modulated signals.

For this modulated signal; carrier signal frequency is equal to rotor slot permeance variation frequency, modulating signal frequency is equal to fundamental component of air gap flux as shown in Fig. 5-5.

The representation of the rotor slot sideband harmonics of the induced voltage of a search coil in frequency domain is given in Fig. 5-4. It can be seen from figure that, the rotor slot harmonic sideband frequencies are apart from each other twice the applied stator frequency.

The modulated signal should be demodulated to obtain the desired rotor slot frequencies (rotor permeance variation frequency).

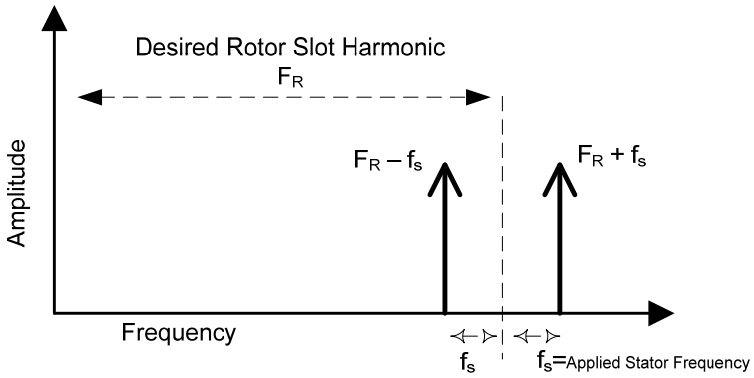

Fig. 5-4 Rotor slot sideband harmonics of the search coil in frequency domain

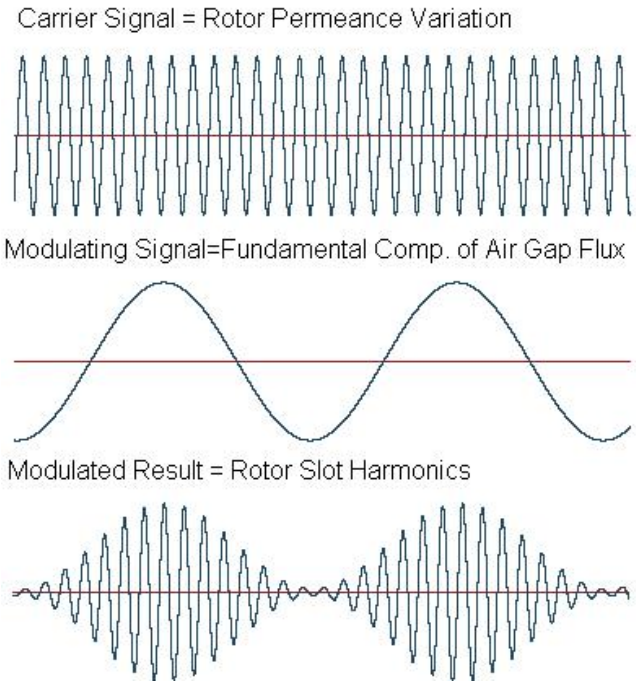

Fig. 5-5 Rotor slot harmonics as a modulated signal

5.4.1 Demodulation Process

To obtain the original signal from the modulated result, some demodulation techniques should be applied. For an amplitude modulated signal; the demodulation process can be realized using the carrier signal. Actually demodulation for a modulated signal is same process with modulation. In other words, modulated signal should be multiplied again with the carrier signal for demodulation [41].

It is shown in the previous section that high rotor slot harmonic frequencies are modulated signals with applied stator frequency. In frequency domain this means two side band frequencies as given in (5-6).

$$f_{rsh} = kf_R \pm f_s \quad (5\text{-}6)$$

where; f_{rsh}: rotor slot side band harmonics frequency, f_R: rotor slot permeance variation frequency(number of rotor slots per pole multiplied with rotor frequency), f_s: applied fundamental stator frequency.

To obtain rotor slot harmonics, the demodulation technique defined should be applied to induced rotor slot harmonic. For demodulation, the applied stator frequency will be used. If the rotor slot harmonics is demodulated with fundamental supply frequency (f_s), the desired rotor slot harmonic is obtained and the two components that $2f_s$ apart from the rotor slot harmonics is obtained. The modulation process is given in equations (5-7) to (5-13).

$$f_{demod}(t) = f_{rsh}(t)\ x\ f_s(t) \quad (5\text{-}7)$$

$$f_{rsh}(t) = A.\sin\big((k.2\pi f_R - 2\pi f_s)t\big) + A.sin\big((k.2\pi f_R + 2\pi f_s)t\big) \quad (5\text{-}8)$$

$$f_s(t) = \cos(2\pi f_s t)$$

$$f_{demod}(t) = A.cos(2\pi f_s t).[\sin\big((k.2\pi f_R - 2\pi f_s)t\big) + sin\big((k.2\pi f_R + 2\pi f_s)t\big)] \quad (5\text{-}9)$$

$$f_{demod}(t) = A.cos(2\pi f_s t)[\sin(\mathrm{k}.2\pi f_R t).cos(2\pi f_s t) - \cos(\mathrm{k}.2\pi f_R t).sin(2\pi f_s t)] \quad (5\text{-}10)$$

$$+A.cos(2\pi f_s t)[sin(\mathrm{k}.2\pi f_R t).cos(2\pi f_s t) + cos(\mathrm{k}2\pi f_R t).sin(2\pi f_s t)]$$

$$f_{demod}(t) = 2A.\cos^2(2\pi f_s t).\sin(k2\pi f_R t) \quad (5\text{-}11)$$

$$\cos^2(2\pi f_s t) = \frac{1+\cos(2.2\pi f_s.t)}{2} \quad (5\text{-}12)$$

$$f_{demod}(t) = A.\sin(2\pi f_R t) + A.\cos(2.2\pi f_s t)\sin(k.2\pi f_R t) \quad (5\text{-}13)$$

$$f_{demod}(t) = A.\sin(k.2\pi f_R t) + \frac{A}{2}.[\sin((k.2\pi f_R - 2.2\pi f_s)t) + \sin((k.2\pi f_R + 2.2\pi f_s)t)]$$

Equation (5-13) shows the demodulated signal. First part of the equation gives the signal that is directly related with the rotor speed where the second part is the modulated signal of rotor speed harmonics with the double stator frequency ($2.f_s$).

It is necessary to note that, for the calculations rest of this study, the discrete signals will be used since the search coil voltage is sampled with an ADC with a sampling frequency of f_{samp}. In equation (5-14), the discrete form of equation (5-13) is presented.

$$f_{demod}[n] = A.\sin[k.2\pi f_R.n] + \frac{A}{2}.\{\sin[(k.2\pi f_R - 2.2\pi f_s).n] + \sin[(k.2\pi f_R + 2.2\pi f_s).n]\} \quad (5\text{-}14)$$

5.5 The Proposed Method for Obtaining Rotor Slot Harmonics Magnitude Time Variation

In chapter 3, spectral analysis methods are utilized to calculate the rotor speed as given in equation (3-12). In frequency domain where spectral analysis techniques are utilized, the rotor permeance variation frequency can be easily obtained by an addition/subtraction operation of rotor slot harmonics with applied stator frequency as seen from equation (5-6). However, without spectral estimation methods where the data is available in time domain; the frequencies of the rotor slot harmonics cannot be obtained easily. Thus, demodulation techniques are introduced to extract rotor slot harmonics.

In this section, a method will be proposed to obtain rotor slot harmonics without using spectral analysis techniques. The modulation process that is described with in previous section is visualized in frequency domain with Fig. 5-6.

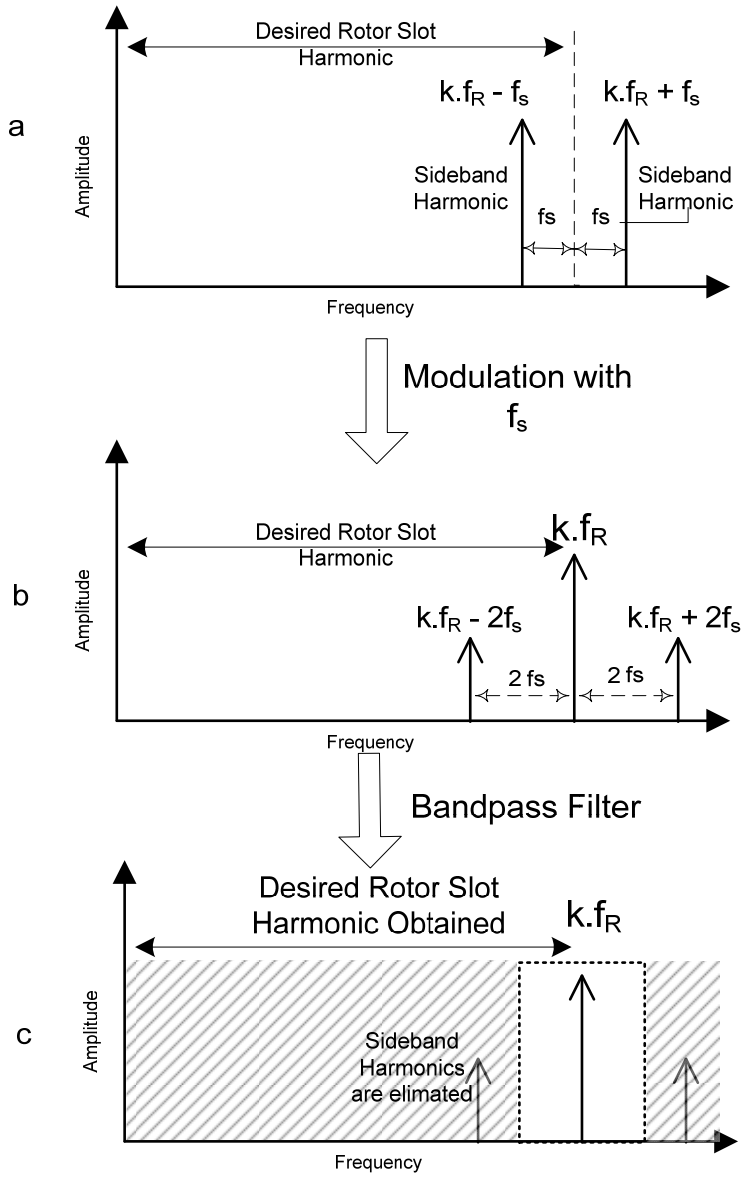

Fig. 5-6 Modulation and filtering process of search coil data

As seen from the Fig. 5-6, a larger component at the desired rotor slot frequency is obtained and two side band components are generated that are apart twice fundamental supply frequency from rotor slot frequency.

The data acquisition method for obtaining rotor slot harmonics is summarized in Fig. 5-7. First, induced search coil voltage is amplified with an isolated instrumentation amplifier. Amplifier is a dual-channel, low noise, audio differential amplifier (AD8273) with a gain of 20 as given in Appendix C. Then this signal is converted to a digital signal with sampling frequency of f_{samp} using the built-in ADC of DSP controller board (DS1102). The digitalized search coil voltage is divided with the amplification ratio to obtain real search coil voltage magnitude. Then using the fundamental stator frequency an a sinusoidal signal with stator frequency (f_s) is generated for demodulation of the data. Then the demodulated signal is filtered with a band-pass filter to eliminate sideband harmonics. After filtering, the signal is obtained which is suitable for rotor position estimation.

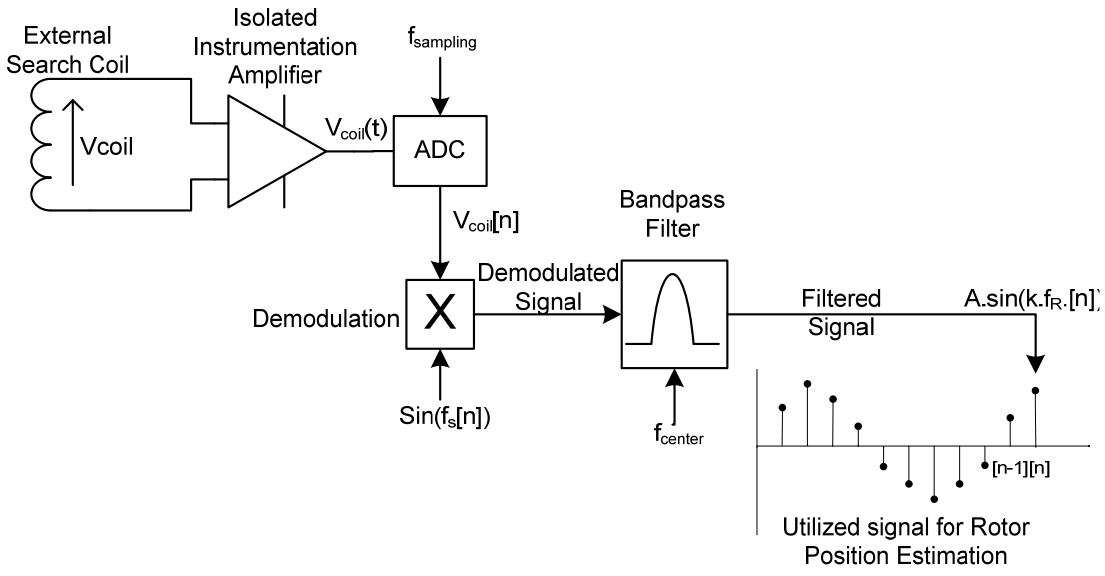

Fig. 5-7 Analog to Digital Conversion and demodulation process of search coil voltage

As given in Fig. 5-6 and Fig. 5-7, the demodulated signal should be filtered to obtain the desired rotor slot harmonic. The filter should eliminate the side-band frequencies. For this purpose a band-pass filter will be used. The specifications of the band-pass filter may be identified as follows. The magnitude response of a typical band-pass filter is given in Fig. 5-8.

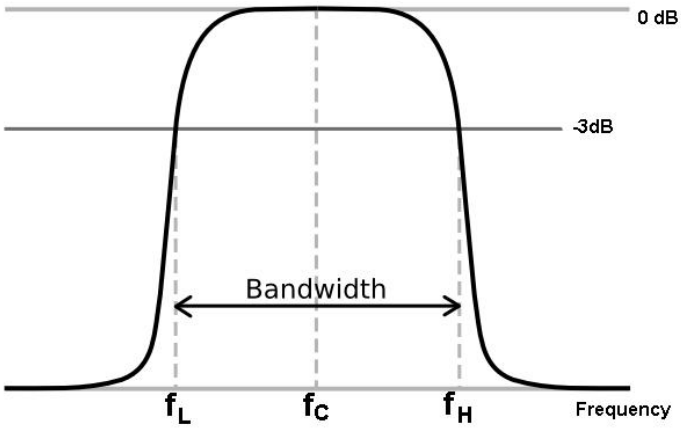

Fig. 5-8 Band-pass filter magnitude transfer function vs. frequency

In figure, f_L,f_H is the lower and higher cut-off frequencies respectively and f_c is the center frequency of the filter. For proper operation of the method, the band-pass filter should pick the main rotor slot harmonics and reject the side band frequencies. Thus it should be designed as;

- The bandwidth of the filter must include the frequency of desired rotor slot harmonics. Or better, the center frequency of the filter should be equal to desired rotor slot harmonic frequency ($\mathbf{f_c = k.f_R}$).
- The bandwidth of the filter should be narrower than the distance between sideband harmonics which is four times the applied fundamental frequency (**Band-width < 4.f_s**).

In this study, MATLAB Filter Design & Analysis Tool is used for filter design. Filter Design & Analysis Tool is a useful toolbox that enables to design various filters by defining filter specifications like, bandwidth, corner frequencies, etc. And

the designed filter constants can be exported to various software environments. User interface of the toolbox is given in Fig. 5-9.

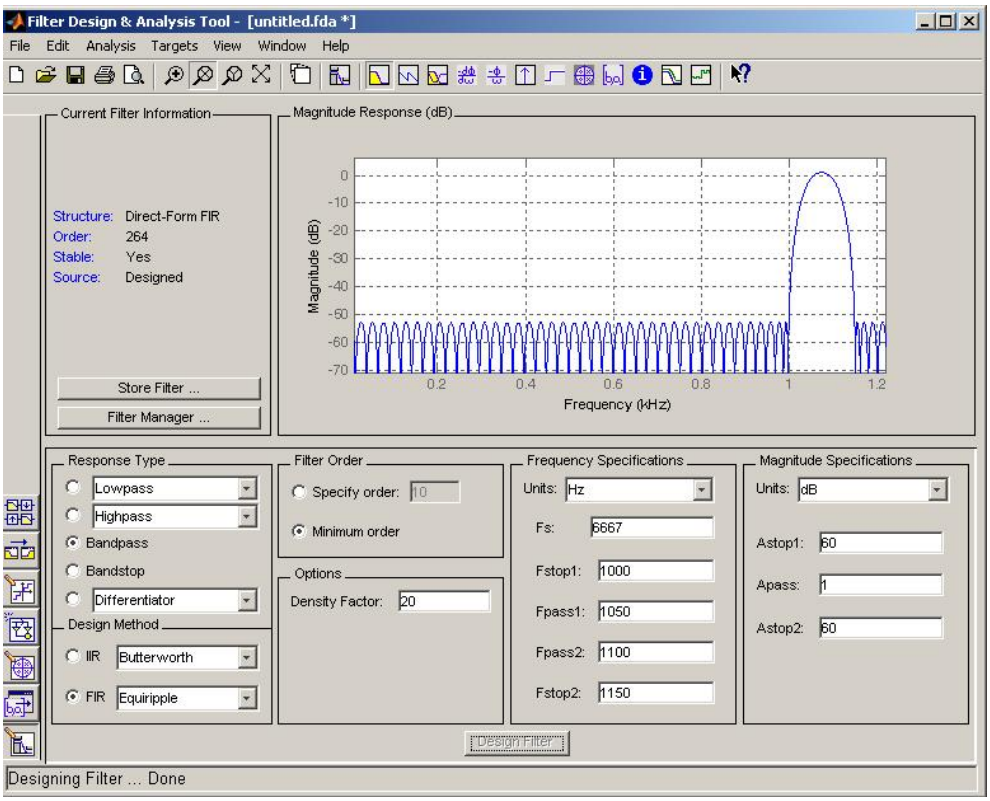

Fig. 5-9 Screenshot of MATLAB Filter Design & Analysis Tool user interface

The filter is a one-dimensional digital filter and has the following specifications;

- Band pass
- Finite Impulse Response
- Design Method: Equiripple

Designed filter constants is exported to programming environment using MATLAB Filter Design Toolbox. The fundamentals of a FIR filter and filter constants of a band-pass filter with center frequency of 1150 Hz and 200 Hz bandwidth is given in Appendix F.

5.5.1 Prediction of Rotor Position

Once the harmonics directly related with rotor permeance variation is obtained, rotor position may be predicted using the waveform of this harmonic. Referring to Fig. 3-2, the relation between rotor permeance variation and movement of rotor slot can be realised. Note that, once cycle of permeance variation harmonic corresponds to one rotor slot passed over the stator slots. Thus, the obtained data can be used as a rotational encoder. Each zero crossings of the filtered signal correspond to small displacements of rotor. This displacement angle can be represented as $\Delta\theta$ which is equal to;

$$\Delta\theta = \frac{2.\pi}{k.Z} \quad (5\text{-}15)$$

Thus, the position of the rotor can be calculated by counting the zero crossings of the signal as given in equation (5-16) where n represents the number of zero crossings of the filtered data.

$$\theta_r = \frac{2.\pi.n}{k.Z} \quad (5\text{-}16)$$

It is already mentioned that, the captured data will be a discrete signal with a sampling frequency of f_{samp} as given in Fig. 5-10. Thus the actual zero crossing instants will not be available, instead we can detect from negative signed data to positive signed data. In this study, first positive signed data after the set of negative signed data at each cycle are used as zero crossing points. Accuracy of position estimation can be improved by some basic interpolation techniques that will calculate the zero crossing instants more accurately.

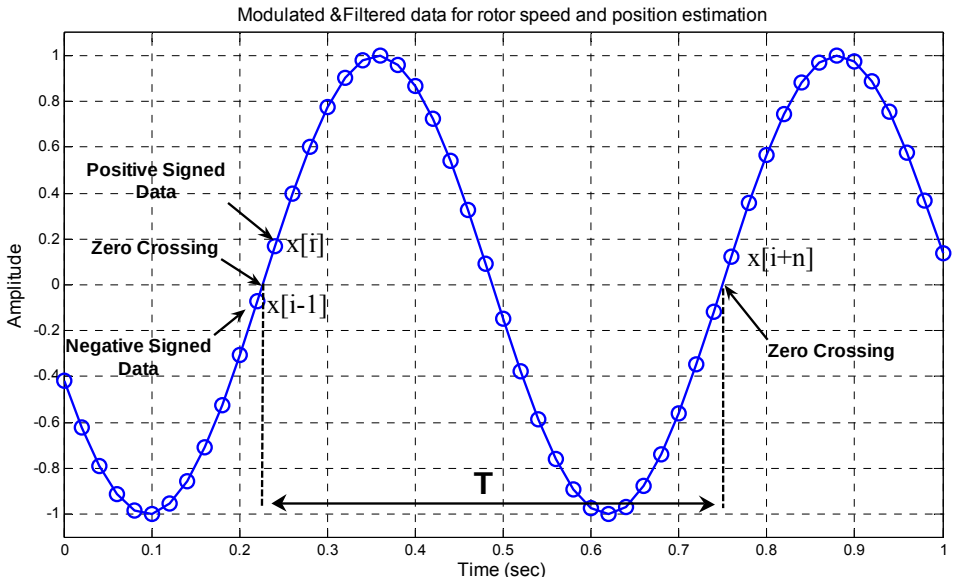

Fig. 5-10 Filtered data for rotor speed and position estimation

5.5.2 Estimation of Rotor Speed

After the rotor position is obtained, rotor speed can be calculated easily. Knowing the frequency of rotor permeance variation harmonic the rotor electrical frequency can be expressed as in equation (5-17).

$$f_r = \frac{f_R}{k.\left(\frac{Z}{P}\right)} \qquad (5\text{-}17)$$

where, k: harmonic order, Z:number of rotor slots, P: number of pole pairs, f_r: rotor electrical frequency.

To determine the frequency of rotor permeance variation harmonic, one period of the signal can be measured by elapsing the time between | x[i+n] – x[i] | as shown in Fig. 5-10. Let the period of this signal is T seconds as shown in Fig. 5-10, then the equation (5-17) can be represented in RPM as follows; which is a similar equation with (1-27).

$$Rotor\ Speed_{(RPM)} = \frac{60}{T.k.Z} \qquad (5\text{-}18)$$

5.5.3 The Algorithm

Obtaining rotor position and rotor speed without a rotational encoder is important especially for field oriented control techniques. In this study, we focus mainly on rotor position estimation using the external search coil. In this section the method described in previous section will be implemented as an algorithm.

The block diagram of the proposed algorithm is given in Fig. 5-11. Firstly, the real time search coil induced voltage data is modulated with a sinusoidal signal with fundamental supply frequency.

Then, the modulated data is band pass filtered. Thus, the filtered data only contains the rotor slot harmonics. After that, zero crossings of the filtered signal is chosen as reference signal and utilizing rotor slot number, rotor position is updated on each of the zero crossings. The five blocks of the proposed method can be explained as;

I) Demodulation: This is the basic step of the proposed method. The method is explained elaborately in 5.4.1. Demodulation is multiplying the search coil data with a unity sinusoidal signal with frequency equal to applied fundamental stator frequency. Notice that, this demodulation is performed with sampled search coil voltage as given in equation (5-14) and does not require a data acquisition period. Demodulation can be performed continuously as the new search coil voltage data is captured. By this demodulation the desired rotor slot harmonic (rotor permeance variation frequency) is obtained. Also, this process generates two sideband frequencies each apart from rotor slot harmonic twice the applied fundamental frequency as shown in Fig. 5-6 - b.

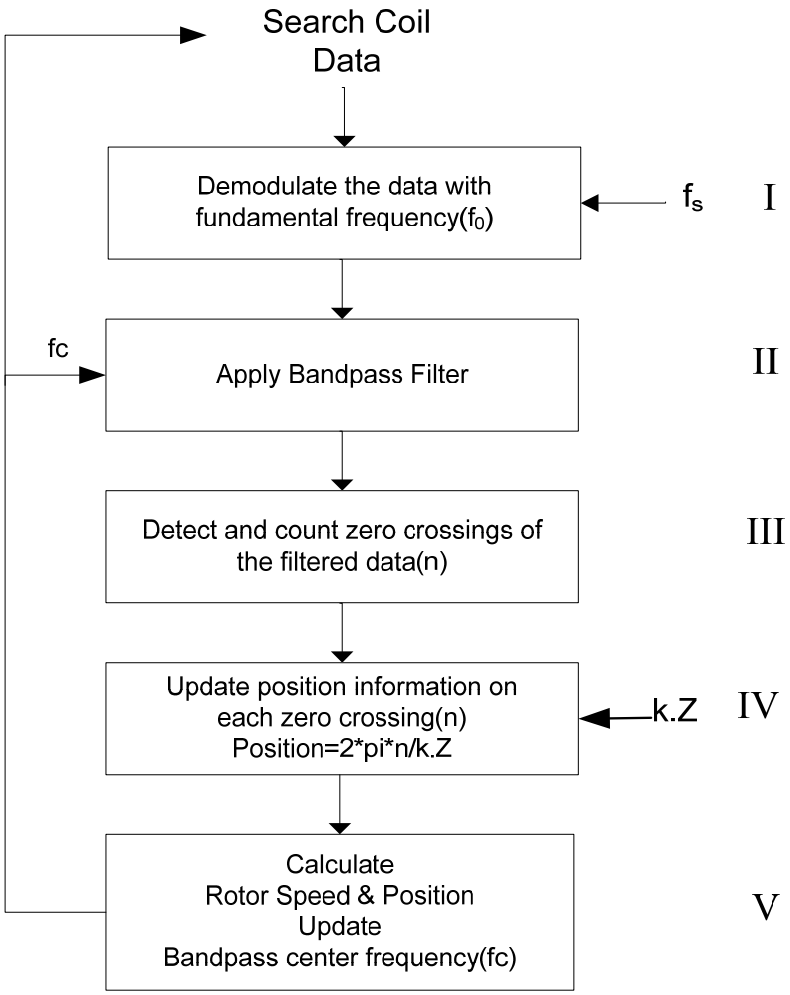

Fig. 5-11 Block diagram for rotor speed & position detection algorithm

II) Band-pass Filtering: In order to obtain desired rotor slot harmonic component, the sideband frequencies should be eliminated. For this purpose, a band-pass filter will be used with the specifications defined in previous section.

One of the biggest difficulties for filtering the signal is to redesign the filter with new center frequency as the rotor speed changes. Notice that, the filter does not need to be redesigned if the speed fluctuations lay in the bandwidth of the filter. But if the variation of rotor speed is larger than the bandwidth of the filter, then the center frequency of the filter should be adjusted to respond the new rotor speed.

In one cycle of the algorithm which generally takes not more than 200 μsec, it is unusual for rotor speed to change more than the bandwidth of the filter due to rotational inertia of the machine and load. Using the motor parameters given in Appendix A, the motor time constant can be calculated as 68msec which is much more longer than the software cycle. Thus, it is possible for algorithm to adapt new rotor speed. This study does not cover the design of this varying corner frequency band pass filter. The experiments performed at steady state rotor speeds using a filter designed for that rotor speed.

III) Detection of zero crossings: Once the rotor slot harmonic is filtered out from other components, the resultant signal is directly related with the rotor position as explained in 5.5.1. Each crossing of signal from negative signed cycle to positive signed cycle will be counted. This can be implemented on software with a simple logic loop as shown in Fig. 5-12.

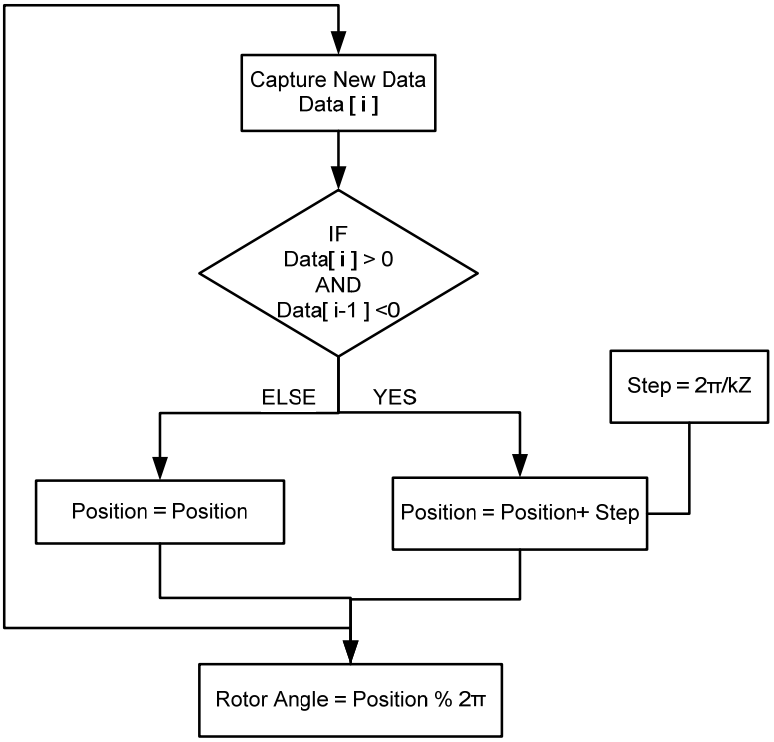

Fig. 5-12 Block diagram of zero crossing detection algorithm

In the block diagram, each new data is compared with the previous data. If the new data is positive where the previous data is negative, that means a zero crossing occurs.

IV) Position Estimation: At each zero crossing, the position data is updated with the step angle defined by equation (5-16). For this, knowledge of rotor slot numbers and relevant harmonic order (k) is needed. The number of rotor slots can be used from manufacturer data or using the method introduced in 3.7. The third rotor slot harmonic will be used in the method (k=3). Finally, rotor angle is output as the remainder of total position by 2π as shown in Fig. 5-12. Since, the rotor position is measured similar to an incremental encoder, first a reference position should be selected. This is generally achieved by applying a DC excitation to stator phases, and then the rotor aligns itself to the resultant excitation direction. This position can be assumed as initial position, and each position update is added to this value and the actual rotor position is calculated. Then, the rotor position is reset when the position reaches a full cycle ($2.\ \pi$).

V) Speed Estimation: In previous step, the rotor position has been calculated. The rotor speed can be calculated by measuring the period of one cycle of rotor slot harmonics signal, as shown in equation (5-18).

5.6 Verification of the Method

In order to verify the method, experiments are performed with the hardware explained in chapter 2. The experiments are performed with the motor #2. The induction motor is driven at constant flux operation at various speeds. To compare the estimated rotor position with the actual one a 1000 pulse/rev. incremental encoder mounted on the shaft of test motor is used. The encoder specifications are available in Appendix C.

One cycle of the algorithm holds 150 μsec. Notice that, this period includes all software codes necessary for SVPWM V/f control or field oriented control. The necessary time for the algorithm would be much smaller. For our hardware setup, the

captured internal and external search coil voltages have a sampling frequency of 6.67 kHz. The internal and external search coil voltages are captured and analyzed offline in MATLAB environment for a better understanding of method performance.

5.6.1 Internal Search Coil Experiments

First, internal search coil induced data is analyzed. The first experiment is performed with motor #2 when the machine is driven at 20 Hz and rotating at 1181 rpm at no load. The captured data is analyzed by applying fast Fourier transform. Note that, FFT method is not necessary for the proposed method but it is a very useful tool to visualize the operation of modulation and filtering processes. The spectral analysis results are given in Fig. 5-13.

In Fig. 5-13-a, FFT analysis of the captured search coil voltage is given. Applied stator frequency harmonics and rotor slot harmonics are visible in the graph. The rotor slot harmonic with third harmonic order (k=3) is labelled in figure.

Fig. 5-13-b, the search coil data is demodulated with supply frequency (f_0=20Hz). Thus, the desired rotor slot harmonic is obtained as seen from the figure; also sidebands $2.f_0$ apart from the rotor slot harmonic are present are shown in graph. Since the rotor slot harmonics are far from the supply frequency harmonics in the modulation process no crossovers are detected between them. So it is not necessary to pre-filter the supply harmonics before demodulation. Thus, only one filtering process is necessary, decreasing the complexity of the method.

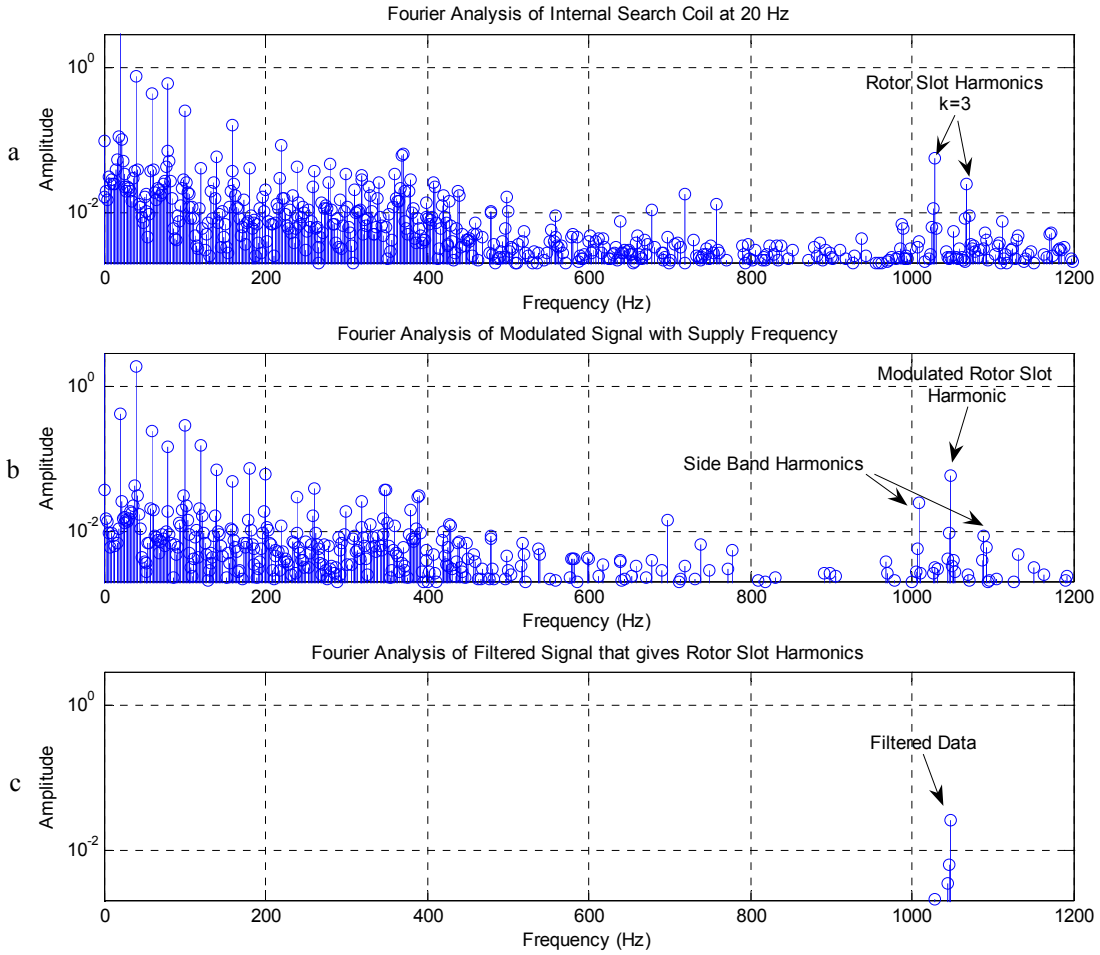

Fig. 5-13 FFT analysis of internal search coil voltage, modulated and filtered signal at 20 Hz stator frequency at no load

Fig. 5-13-c, the band pass filter is applied to the search coil data and the rotor slot harmonic is isolated which will be used for position estimation. As mentioned, this study does not focus on the design of the band-pass filter.

It is mentioned that, the spectral analyses of the steps are just given to visualize the operation of method. The actual data processed is processed in time domain and graphs related are presented in Fig. 5-14.

First graph shows the induced internal search coil voltage. Second graph shows the modulated and filtered rotor slot harmonics data. Using this data, the zero crossings are counted as described before. And the estimated position is updated on each of the zero crossing using equation (5-16).

In the third graph, estimated rotor position data and the actual rotor position data measured using the incremental encoder is plotted on the same figure. Since, both of them match perfectly, they seem to be a single line.

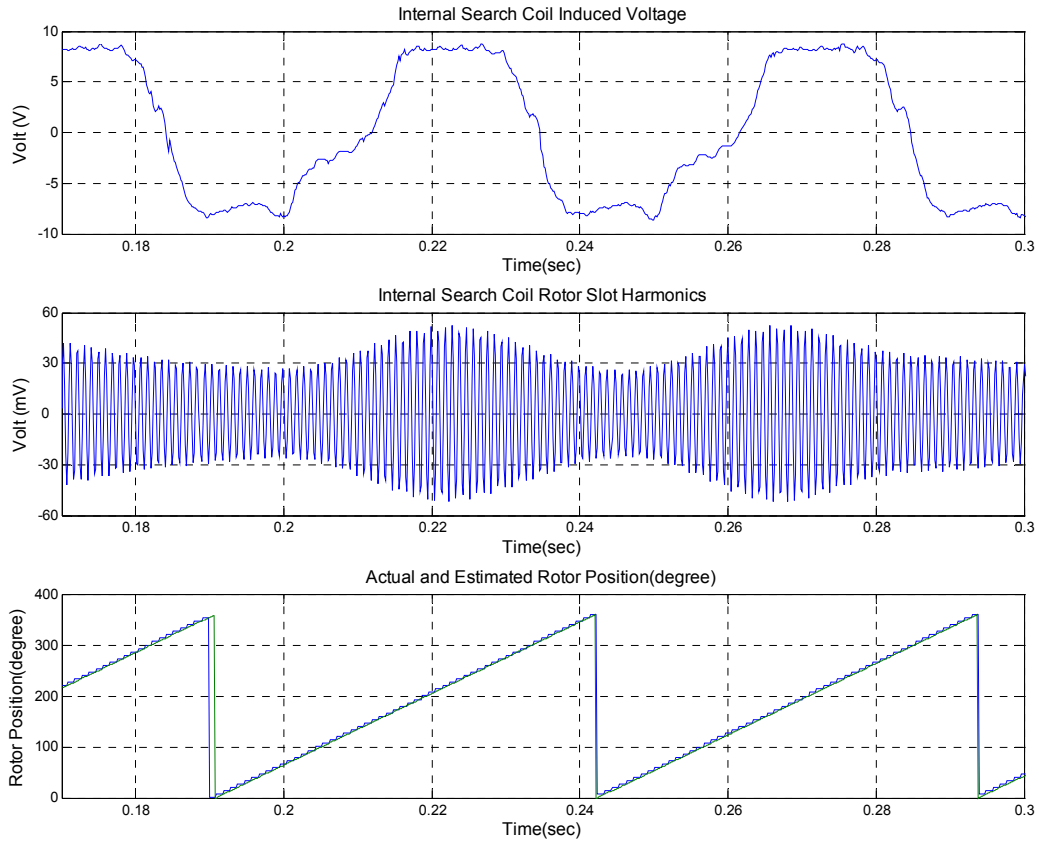

Fig. 5-14 Time domain representation of the method for internal search coil at 20 Hz at no load

The detailed view of rotor slot harmonics, estimated and actual rotor position is given in Fig. 5-15 and Fig. 5-16.

In Fig. 5-16, a sample point where zero crossing occurs and program updates the rotor position is shown on the graph. The rotor position kept constant until next zero crossing instant.

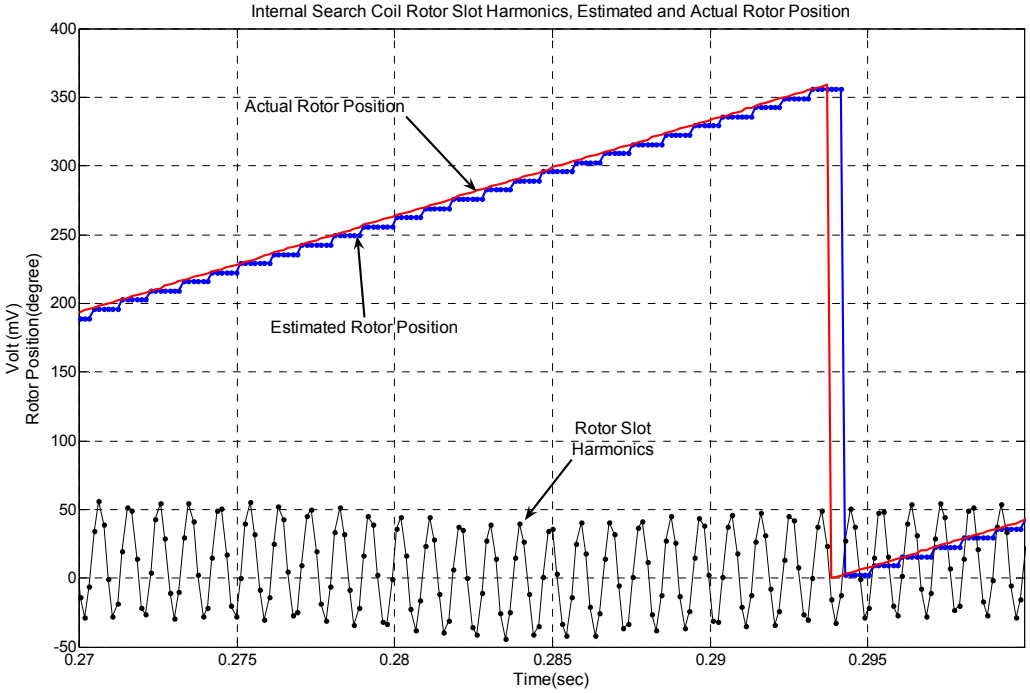

Fig. 5-15 Rotor slot harmonics, actual and estimated position data for internal search coil at 20 Hz

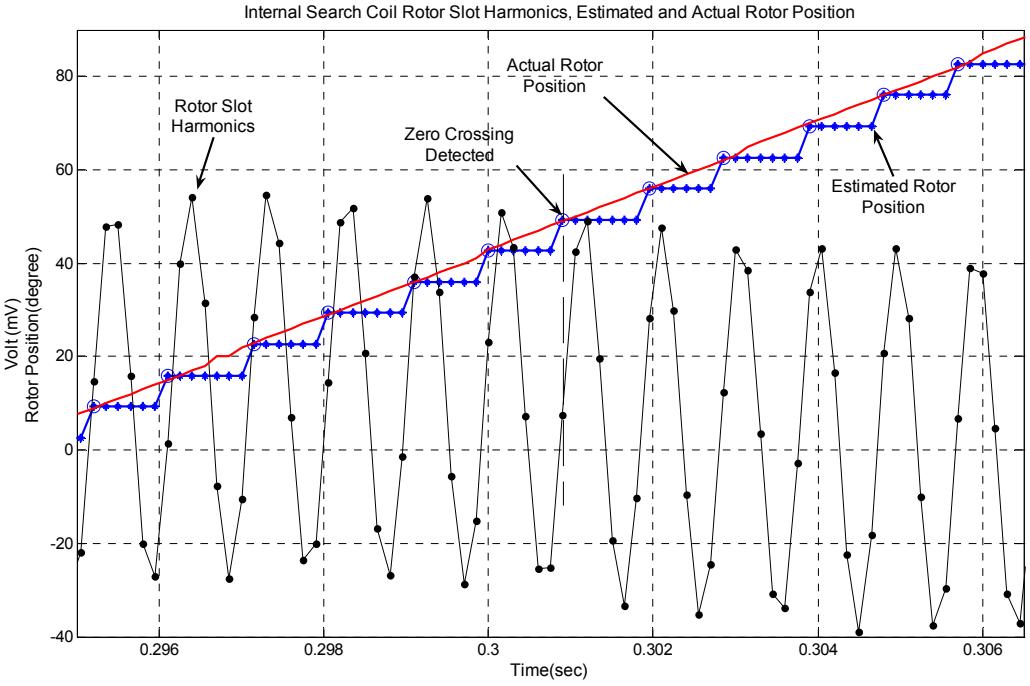

Fig. 5-16 Detailed view of rotor slot harmonics, actual and estimated position data for internal search coil at 20 Hz

Then the algorithm is tested when motor #2 is driven at 50 Hz stator frequency at rated voltage and load and the machine is running at 2817 rpm. The experiment results are given in Fig. 5-17 and Fig. 5-18.

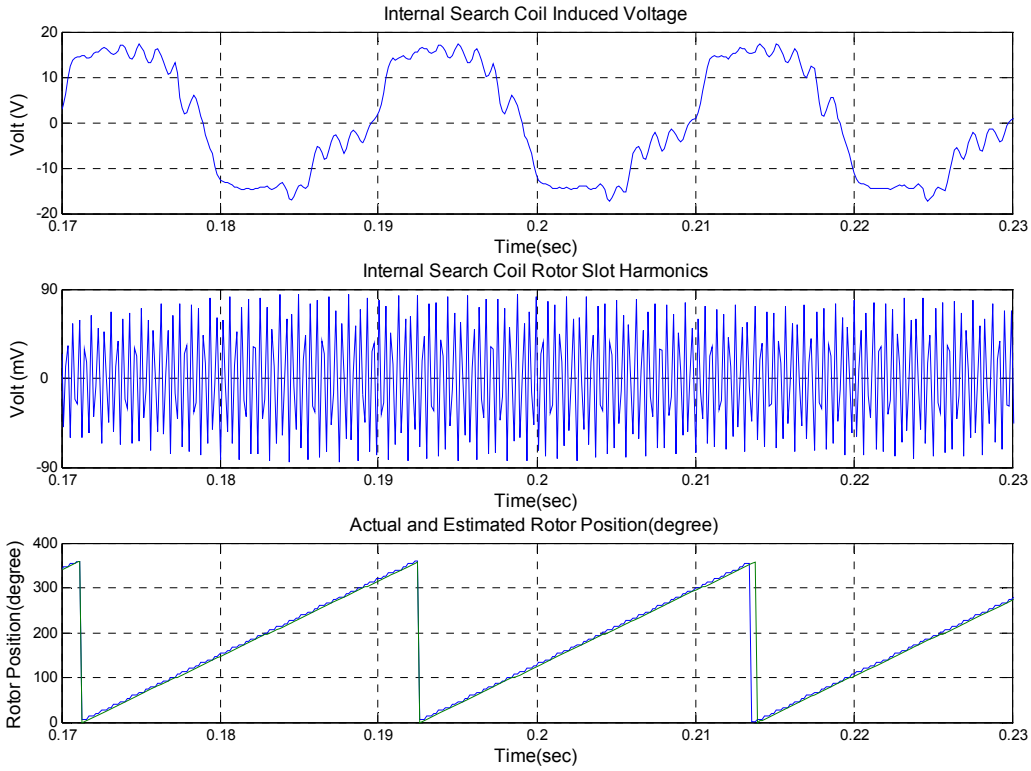

Fig. 5-17 Time domain representation of the method for internal search coil at 50Hz rated load

In Fig. 5-18, a sample point where zero crossing occurs and program updates the rotor position is shown on the graph. Also it can be noticed from the graph that, as the applied stator frequency increases, the number of samples for one cycle of rotor slot harmonic decreases. This would be a problem if the frequency of the rotor slot harmonics is larger than the half of the sampling frequency. This issue will be discussed in the following section.

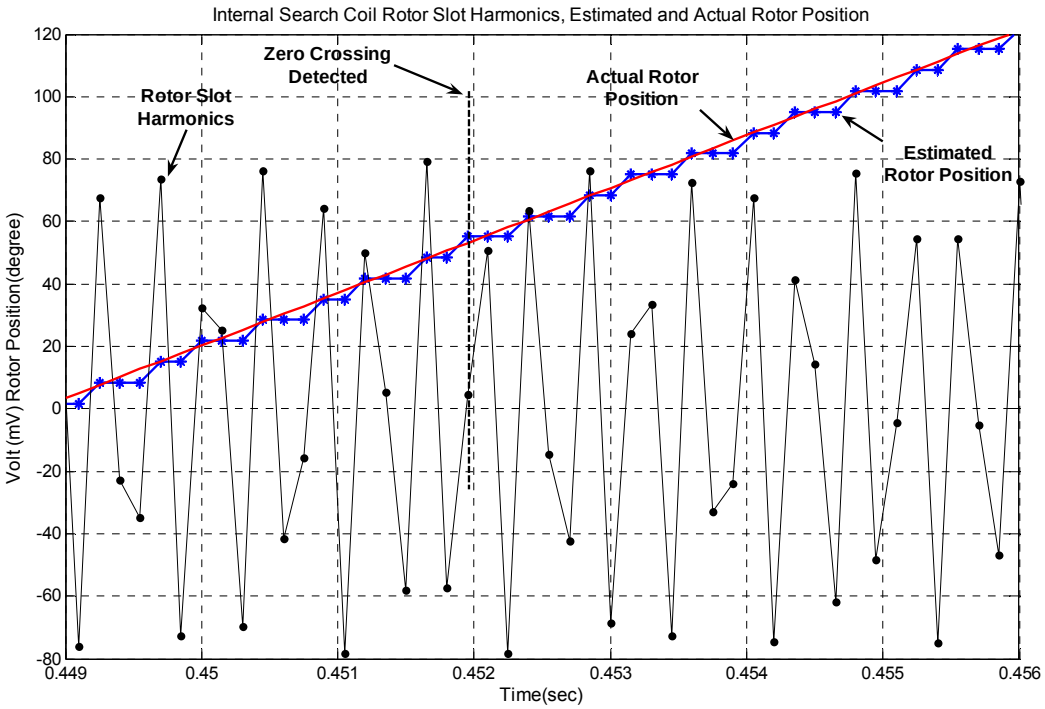

Fig. 5-18 Detailed view of rotor slot harmonics, actual and estimated position data for internal search coil at 50 Hz rated load

5.6.2 External Search Coil Experiments

In chapter 3 it is discussed that, the harmonics that exist in the air gap also exist in the fringing flux of the machine. Thus, to verify the proposed method is applicable to external search coil, similar experiments are performed with the external search coil.

In Fig. 5-19, the experiment results are performed with motor #2 which is driven at 20 Hz stator frequency, at no load with 1165 rpm rotor speed.

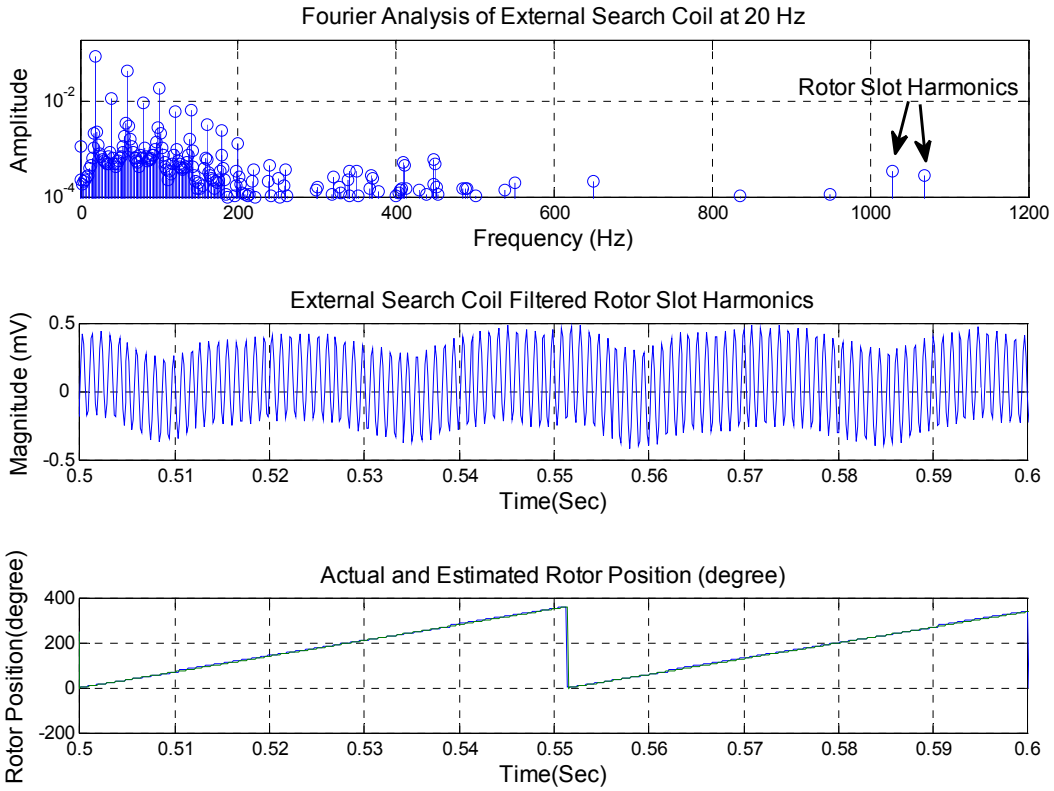

Fig. 5-19 External search coil harmonics, actual and estimated rotor position for external search coil at 20 Hz no load

First graph shows the spectral analysis of the external search coil. In the graph, the third order rotor slot harmonics is shown. The second graph is obtained after demodulating and filtering the external search coil voltage. In the third graph the actual rotor position and the estimated rotor positions are presented. For a better comparison of actual and estimated rotor positions a more detailed view is given in Fig. 5-20.

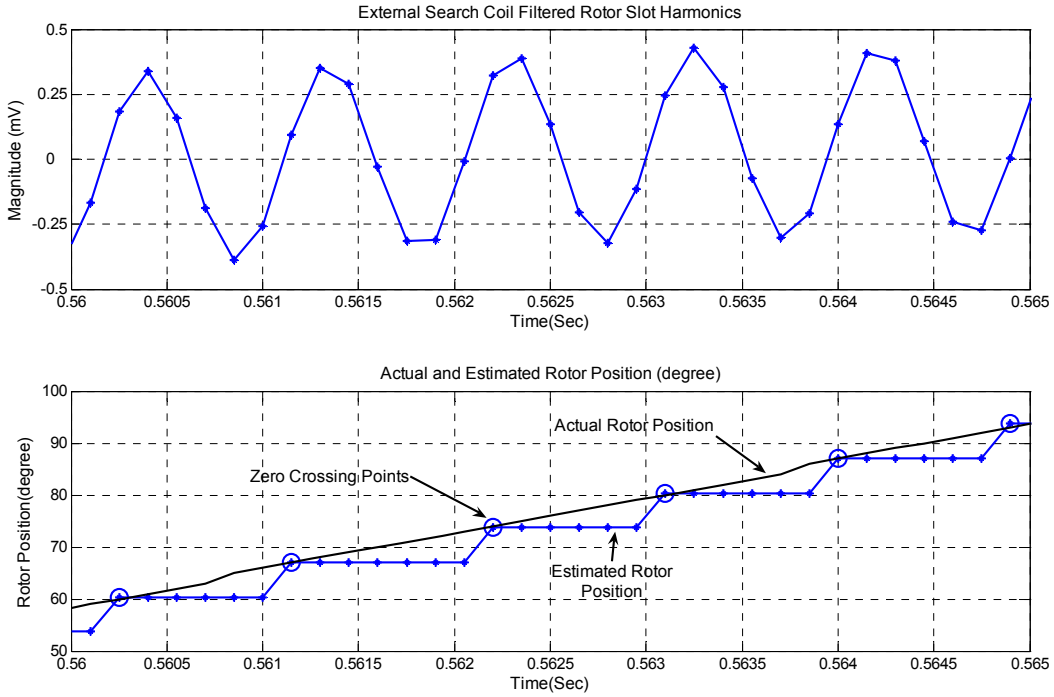

Fig. 5-20 Detailed view of rotor slot harmonics, actual and estimated position data for external search coil at 20 Hz no load

From Fig. 5-20, it may be seen the rotor position can be estimated accurately at 20 Hz stator frequency with the external search coil. Notice that, the estimation is successfully performed at no load. Other methods that use spectral estimation techniques generally fail at low load conditions because rotor slot harmonics can be confused with applied stator voltage harmonics. However, the higher order rotor slot harmonics used in this method exist in a spectrum where no other distinctive harmonics present. Thus, the method is applicable at all load conditions.

In Fig. 5-21, the experiment results are performed with motor #2 is driven with 40 Hz stator frequency at rated load while the machine is running at 2225 rpm.

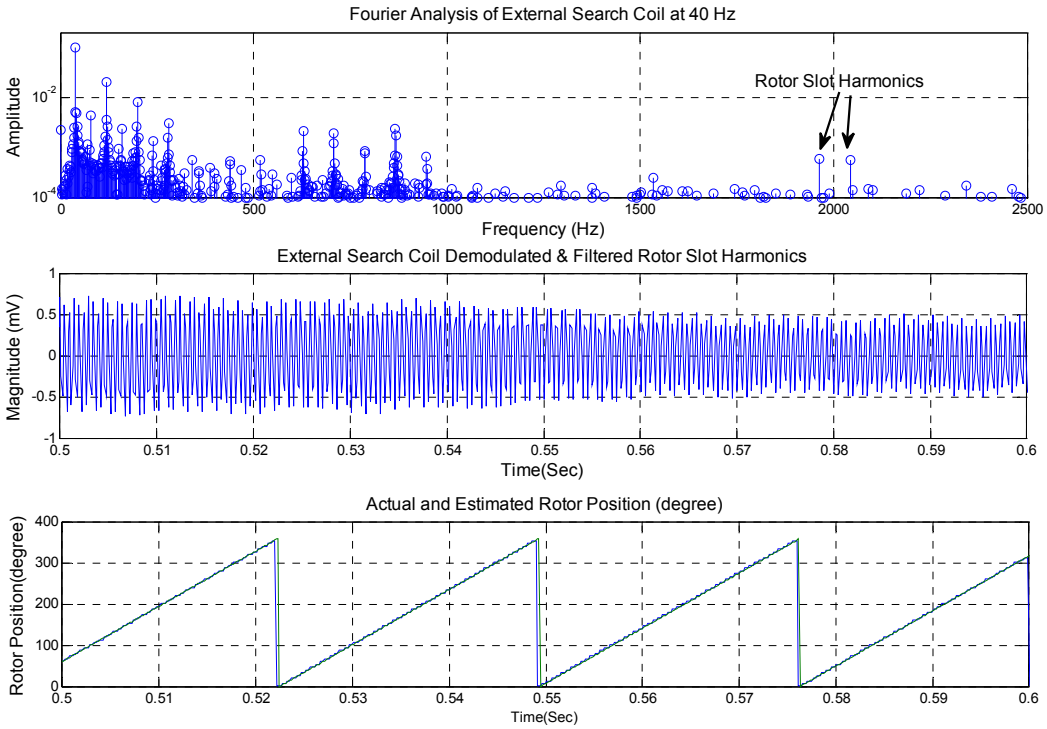

Fig. 5-21 Rotor slot harmonics, actual and estimated position data for external search coil at 40 Hz rated load

The experiment results shows that the rotor position can be estimated correctly with 40 Hz stator frequency at rated load. In Fig. 5-22, detailed views of the graphs are presented.

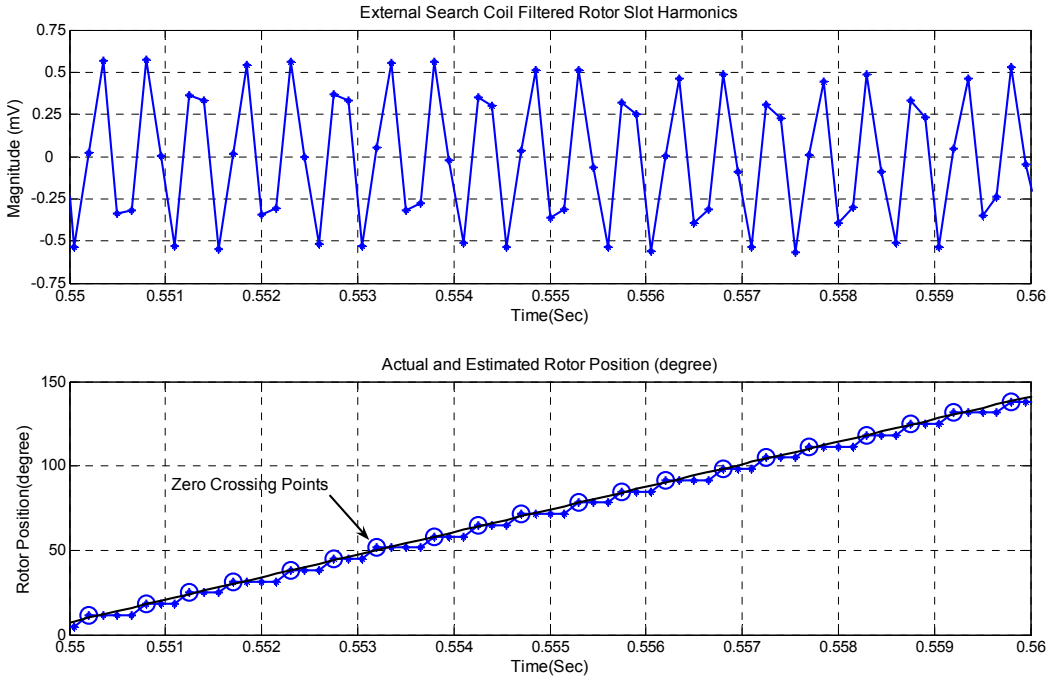

Fig. 5-22 Detailed view of rotor slot harmonics, actual and estimated position data for external search coil at 40 Hz rated load

The experiments in this section showed that, the proposed method works well both with internal and external search coil. In the following section 5.7, performance comparison of the proposed method for different load conditions and different rotor speeds and the limitations of the method will be investigated. In section 5.8, some improvements are suggested to overcome these limitations.

5.7 Limitations of the Method

The estimation results of the proposed method for a few operation points have already been presented. In this section, limitations of the proposed method will be investigated for different load conditions, applied stator frequency range and direction of rotation. In Chapter 4, the fundamental components of internal and external search coil induced voltages for different load conditions and applied stator frequencies were investigated. In this part, similar experiments will be performed for induced voltages for 3rd order rotor slot harmonics. The performance of method with different load conditions is investigated. The variables affecting the upper and lower

stator frequency limits for the method are discussed. Also other factors affecting the performance of the method such as, sampling ratio, A/D conversion accuracy and environmental noise harmonics will be studied.

5.7.1 Load Conditions

As discussed in previous sections one disadvantage of the rotor slot harmonics speed measurement techniques using stator voltages or currents is the magnitude change of the desired harmonics as the load varies as stated in [14] . It could be harder for these techniques to estimate rotor speed in light or no load conditions for two main reasons; the decrease of the rotor slot harmonics magnitude make it harder to detect these harmonics. Moreover, as load decreases the rotor slip decreases, thus making rotor slot harmonics occur very near to harmonics of applied stator voltage as stated in chapter 3. Then, the rotor slot harmonics would be confused with these supply harmonics. As a result, with methods that use spectral analysis, the estimation of rotor speed will be harder as the load decreases.

Experiments are performed on motor #2 at no load, half load and full load in order to measure the variation of the magnitude of the rotor slot harmonics induced in internal and external search coils. The results of the experiments are presented in Fig. 5-23, Fig. 5-24, Fig. 5-25 and Fig. 5-26.

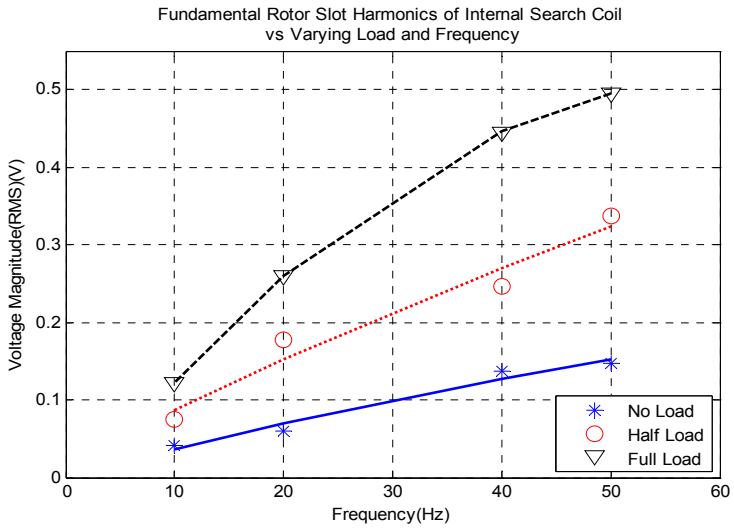

Fig. 5-23 Magnitude of fundamental rotor slot harmonic (k=1) of internal search coil voltage

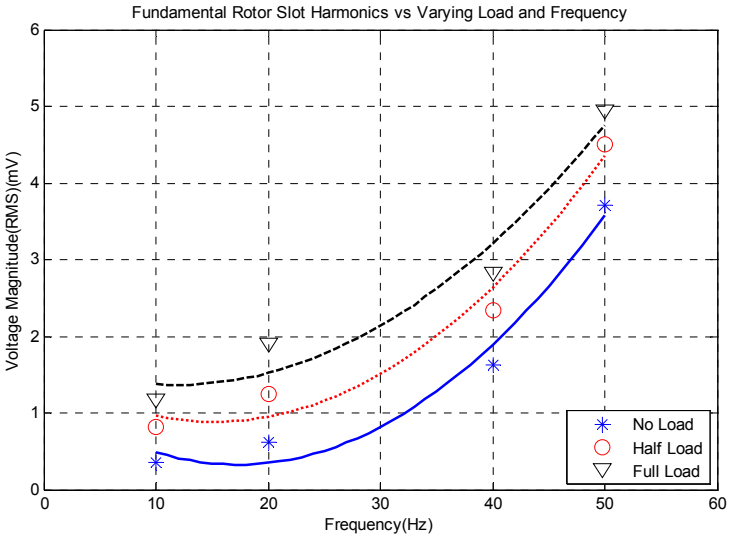

Fig. 5-24 Magnitude of fundamental rotor slot harmonic (k=1) of external search coil voltage

In Fig. 5-23 the magnitudes of the fundamental rotor slot harmonics of the internal search coil are given. This figure verifies the fundamental rotor slot harmonics decreases as the load is decreased. Reduction in magnitude is nearly 70%

from full load to no load for internal search coil. For external search coil the magnitude reduction is not so much but still present.

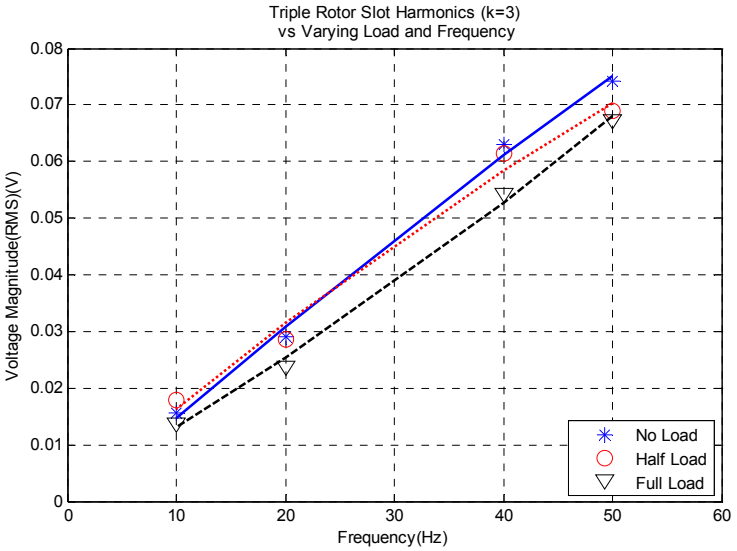

Fig. 5-25 Magnitude of rotor slot harmonic with harmonic order three (k=3) of internal search coil voltage

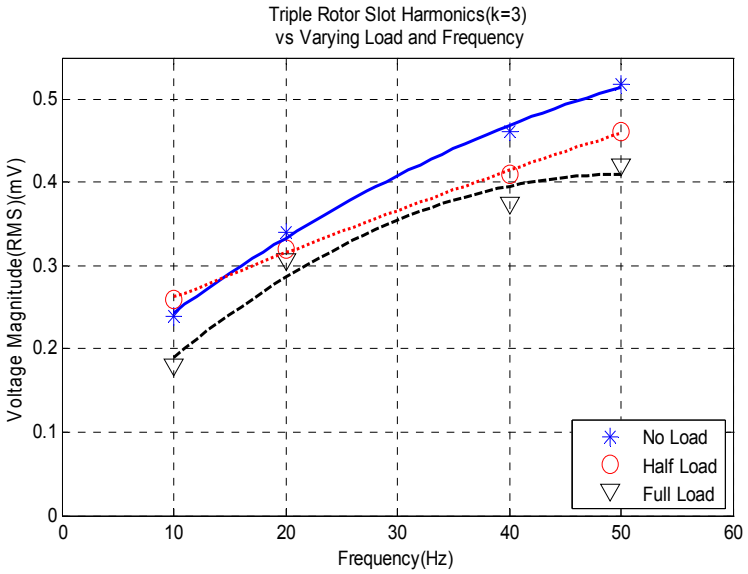

Fig. 5-26 Magnitude of rotor slot harmonic with harmonic order three (k=3) of external search coil voltage

Referring to Fig. 5-24 and Fig. 5-25, it can be observed that the third order rotor slot harmonics which are used for the proposed method, the magnitude is nearly insensitive to load variations. This property makes them suitable for all load conditions including no load and light load conditions. Furthermore, since these rotor slot harmonics are far from the fundamental supply frequency harmonics, they do not interfere with them at light load. Thus, the proposed model can be used for all load conditions.

5.7.2 High Rotor Speeds

For stator frequencies higher than the rated frequency, generally flux weakening operation is applied for induction machines to prevent applying over rated voltage to machine. In 4.2.5 it is shown that the external search coil induced voltage reduces drastically for the flux weakening conditions. Thus, the induced voltage on the external search coil due to rotor slot harmonics will reduce also. But, this decrease does not affect the performance of the method if the rotor slot harmonics are still in the measurable range.

As the supply frequency of the machine is increased the frequency of the utilized rotor slot harmonics also increases as given in equation (5-3). The proposed method uses rotor slot harmonics in time domain. Thus, in order to measure the rotor slot harmonics properly the sampling frequency should be at least twice the frequency of rotor slot harmonics. It should be remembered that this ratio is the theoretical limit for the rotor slot harmonic voltage frequency that can be measured.

At zero slip the frequency of the rotor slot harmonics has the largest value. In zero slip, rotor frequency is equal to stator frequency. Using equation (5-3) for this condition, equation becomes;

$$f_h = \left(k.\frac{Z}{P} \pm 1\right).f_s \qquad (5\text{-}19)$$

The upper side band rotor slot harmonic has the higher frequency and limits the operation of the method. So only the upper side band rotor slot harmonic is considered for the rest of calculations. And the rotor slot harmonic with harmonic

order three (k=3) is utilized in the proposed method. Putting these values and the necessary condition about the sampling frequency, the equation becomes;

$$2\left(3.\frac{Z}{P}+1\right).f_s < f_{sampling} \quad (5\text{-}20)$$

$$f_s < \frac{f_{sampling}}{2\left(3.\frac{Z}{P}+1\right)} \quad (5\text{-}21)$$

Thus, the upper speed limit of the proposed method is determined by equation (5-21). It is stated that the used hardware has a sampling period of 150 μsec, giving a sampling frequency of 6.67 kHz. For the motor #1 and motor #2 used in the experiments the upper stator frequency limits are 123 Hz and 60 Hz respectively. Equation (5-21) implies that the machines with larger number of rotor slots per pole pair has a lower upper frequency limit for the proposed limit. Thus, the second motor which has 18 rotor slots per pole is limited to 60 Hz fundamental stator frequency. Thus combining the results obtained in 3.6.1, as the number of rotor slots per pole increases the accuracy of position and speed estimation increases but on the other side, upper frequency limit of the method decreases.

The upper operation frequency limit can be improved by increasing the sampling frequency.

5.7.3 Low Rotor Speeds

At lower stator frequencies the frequencies of the rotor slot harmonics also decreases. Thus, the A/D conversion system may take more samples for a period of rotor slot harmonics. But, the magnitude of the rotor slot harmonics decrease with the decreasing supply frequency like all components of the induced voltage as given in equation (4-4). Thus, the observation of induced voltage on search coils would be harder with the decreasing frequency and excitation voltage. Some experiments are performed to show the magnitude of the induced rotor slot harmonics with various stator frequency and load conditions. In the experiments the magnitudes of the fundamental rotor slot harmonics and the rotor slot harmonics with harmonic order three is measured. The results of the experiments are given from Fig. 5-23 to Fig. 5-26.

As seen from the experiment results, both the fundamental and triple harmonics of rotor slot harmonics decays to zero as the fundamental supply frequency decreases also. The decrease in the induced voltage of the search coils may be compensated with an amplifier with higher gain and accuracy. This can be somehow applicable to internal search coil but different problems arise for the external search coil.

The spectral analysis of the induced search coil voltages are given in Fig. 5-27 for 5 Hz applied stator frequency at half load.

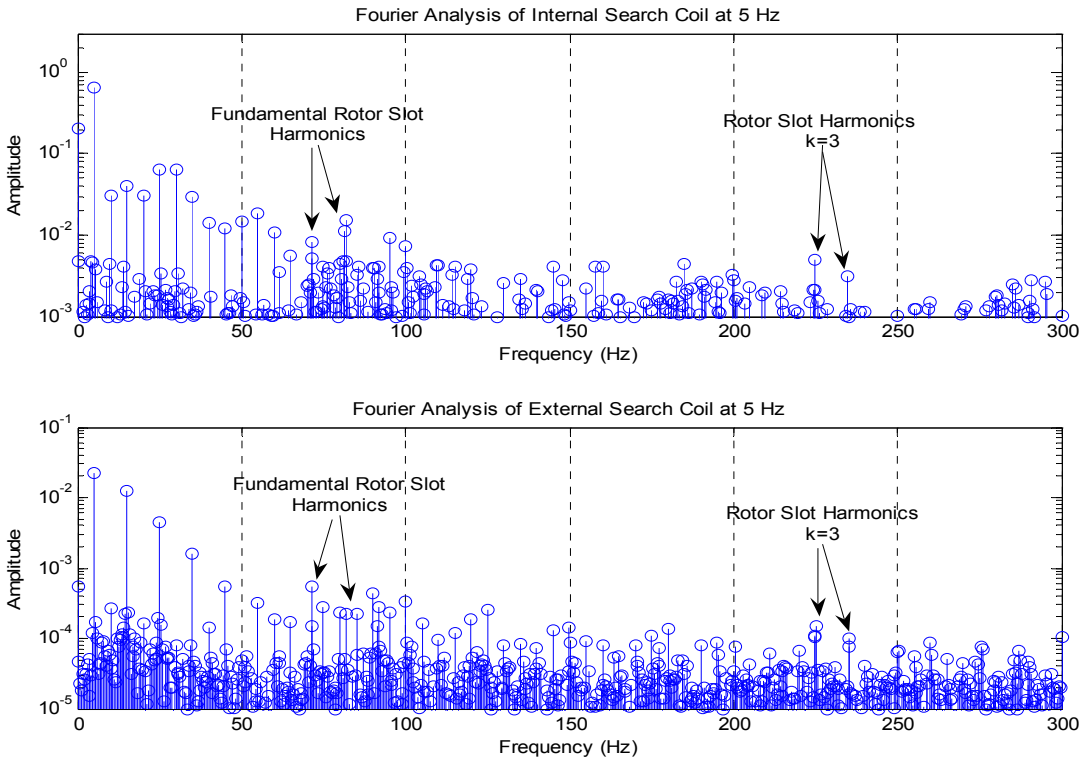

Fig. 5-27 Internal and external search coil harmonics at 5 Hz half load

Notice that, the external search coil rotor slot harmonics exists in a spectrum range with many parasitic harmonics resulting from the placement of external search coil. These parasitic harmonics may result from the inverter harmonics, or other electromagnetic noises exist in the environment. Moreover, increasing the number of turns of the coil or using a higher amplification ratio does not solve the problem since. Because, this will increase the parasitic components as well as the rotor slot harmonics.

These parasitic harmonics would result in false position estimations and proposed method will be unstable. Such a condition when the machine supply frequency is 5Hz at half load, the external coil estimation results are given in Fig. 5-28 and Fig. 5-29.

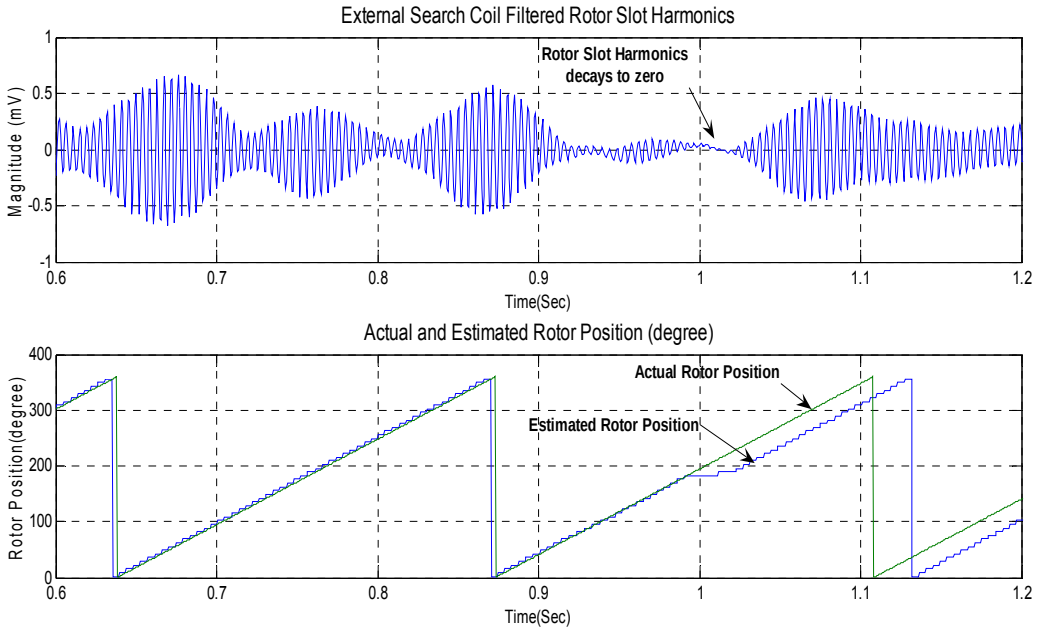

Fig. 5-28 Rotor slot harmonics of external search coil, actual and estimated rotor position at 5 Hz half load

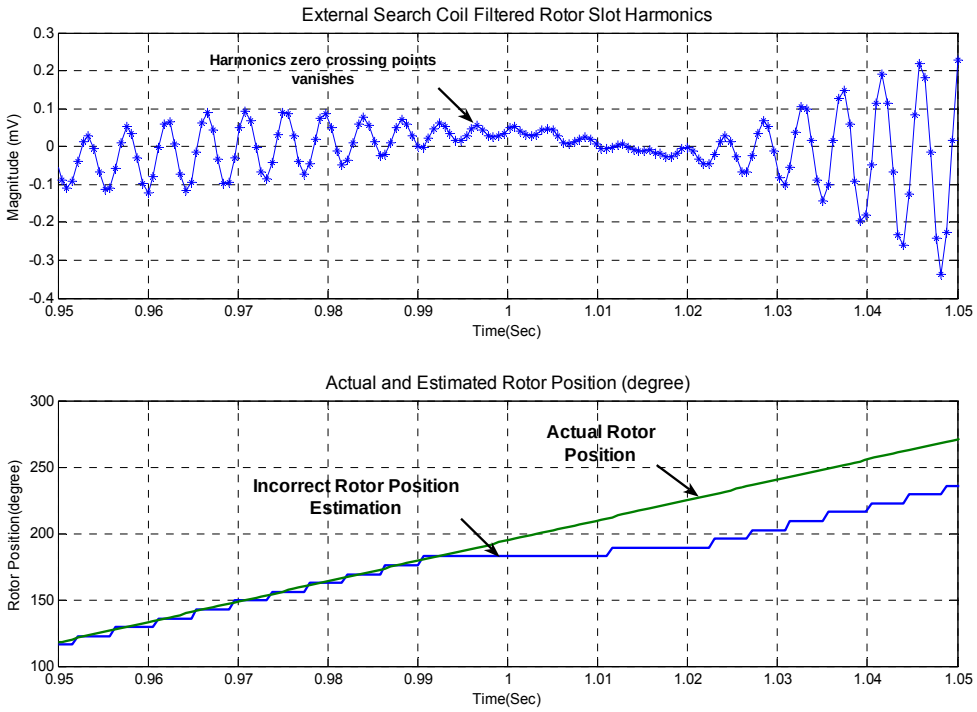

Fig. 5-29 Incorrect rotor position estimation with external search coil at 5 Hz half load

Since, the parasitic components are comparable with the rotor slot harmonics, in the demodulation process, the parasitic components interfere with the rotor slot harmonics. As a result, the filtered data has a fluctuating waveform, and decays to zero at some instants. At these instants, the algorithm cannot detect the zero crossing of the signal and the position algorithm halts till next detectable zero crossing. This halting period results in a incorrect rotor position estimation as given in Fig. 5-29.

5.7.4 Direction of Rotation

Since the rotor slot harmonics data is observed from a single search coil induced voltage the direction of rotation cannot be estimated based on only search coil induced voltage data. In order to obtain the direction of rotation either the phase voltages or currents should be utilized. Phase voltages and phase currents are measured and available for most modern drives. But if the motor is driven without measuring any motor electrical parameters than multiple search coils placed on

different positions may be used. In section 2.4.2, where the effects of placements of search coils are investigated, it is shown that there would be a phase difference between the induced search coil voltages. Depending on this phase difference between search coils the direction of rotation can be estimated. However, this study does not cover the solution to this problem.

5.8 Improvements on the Method

In previous section, the limitations of the method have been mentioned. These are; frequency of rotor slot harmonics exceed the sampling frequency at higher speed, difficulty in extracting desired rotor slot harmonics from other noisy components at lower speeds. In this section, some improvements will be proposed to overcome these issues and also some modifications are proposed to increase the accuracy of the method.

5.8.1 Using Different Harmonic Order Rotor Slot Harmonics

In section 5.3, higher order rotor slot harmonics were introduced. In that section, magnitude comparison of second and third order rotor slot harmonics is presented in Table 5-1. And the third order rotor slot harmonic is selected as most suitable one due to its larger magnitude and higher frequency than the second order harmonic. On the other side, it may be wise to add an exception for high stator frequencies.

It is mentioned in 5.7.2, rotor position estimation algorithm halts at high stator frequencies where the frequency of rotor slot harmonics exceed the sampling frequency. Instead of using third order harmonic, using the second order rotor slot harmonic will increase the upper frequency limit for the algorithm.

For the experiment conditions given in section 5.7.2, the upper operation limit for motor #2 is 60 Hz when utilizing the third order rotor slot harmonic. When the second order rotor slot harmonic is utilized this limit increases to 90 Hz as given in Table 5-2.

Table 5-2 Upper limit of stator frequency for motor #2 for rotor slot harmonic order k=2, k=3

Rotor Slot Harmonic Order	Upper Limit of Stator Frequency for Motor #2
k=3	60 Hz
k=2	90 Hz

Similar method may be applied at low stator frequencies to increase the accuracy of the method. At lower stator frequencies, instead of third order rotor slot harmonic, higher order (i.e. k=4, 5, 6,...) rotor slot harmonics may be used. But, it is necessary to mention that, the induced voltage in search coil at lower frequencies decreases. Thus, main problem at low stator frequencies is isolating rotor slot harmonic components from irrelevant noisy components. Using higher order rotor slot harmonics will give even smaller magnitudes. The experiment result presented in Fig. 5-30 supports this proposition. In Fig. 5-30, the spectral analysis of the external search coil with a 5 Hz stator applied frequency is given. The higher order rotor slot harmonics (k=3, 4, 5, 6) are shown on the figure. There are no significant harmonics that has a larger magnitude than the third order rotor slot harmonic. Thus, the usage of higher order rotor slot harmonics at low frequencies is infeasible for same results discussed in 5.7.3.

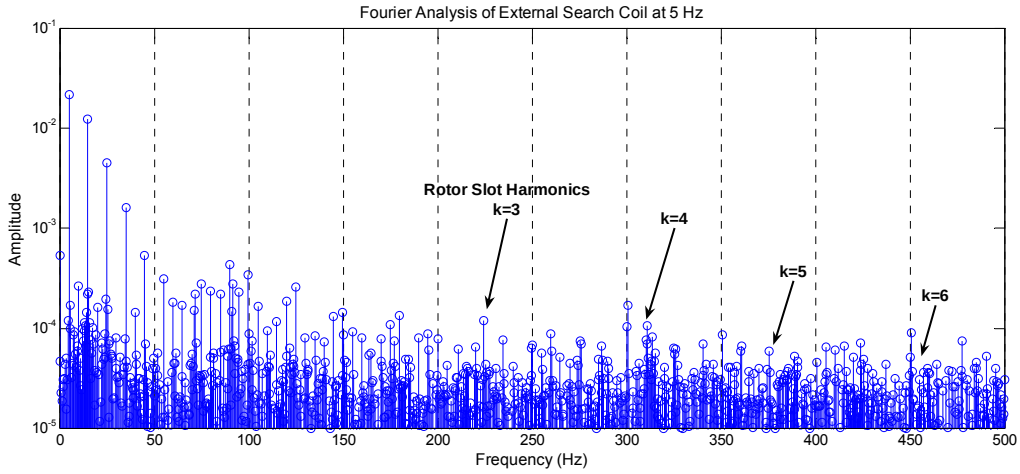

Fig. 5-30 Higher order harmonics (k=3, 4, 5, 6) of external search coil at 5 Hz

In conclusion, for higher applied stator frequencies, second order (k=2) rotor slot harmonics may be used instead of third order (k=3) rotor slot harmonic to increase the upper operation limit. But at low speed, due to low voltage of rotor slot harmonics, higher order (k=4, 5, 6) harmonics can not be utilized.

5.8.2 Peak Detection Instead of Zero Crossing Detection

For the algorithm proposed, an algorithm based on the detection of zero crossing is used. In this method, after the rotor slot harmonics is obtained, the zero crossings are detected and counted. But, the algorithm fails at low stator frequencies as discussed in 5.7.3. And a case for zero crossing detection algorithm fails has already presented in Fig. 5-29. For the case given in Fig. 5-29, rotor slot harmonics peaks are still barely detectable. So, a small algorithm change may improve the performance of the system enormously. The algorithm will be based on the peak detection, and at each peak, the position information will be refreshed. The block diagram of peak detection algorithm for rotor position estimation is given in Fig. 5-31. The block diagram is very similar with the one explained in Fig. 5-12. There is only a modification in the IF-ELSE stage.

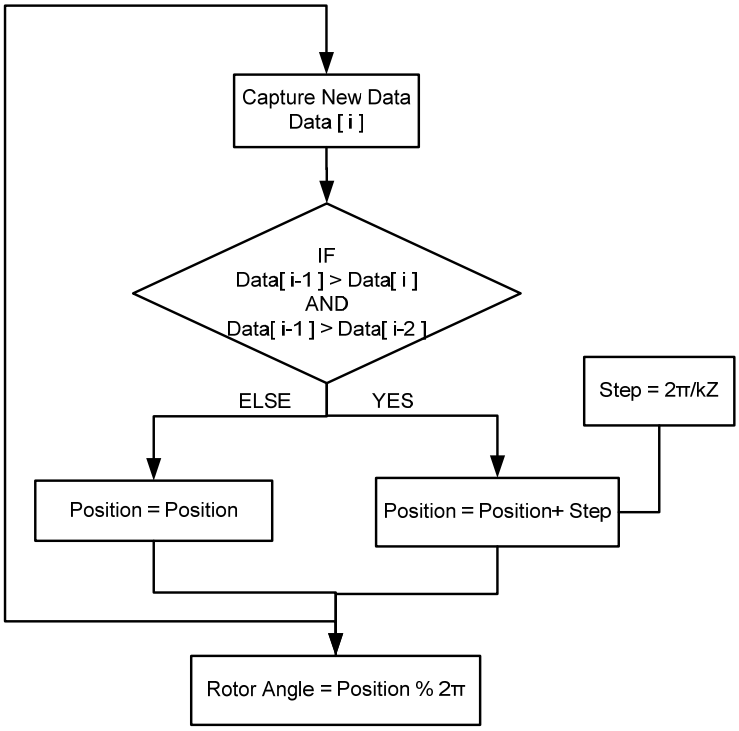

Fig. 5-31 Block diagram of peak detection algorithm

The modified estimation results are given in Fig. 5-32. Comparing these results with the results given in Fig. 5-29, it can be observed that, peak detection algorithm works properly at 5 Hz. But due to demodulation problems discussed in 5.7.3, the magnitude variation of the induced search coil voltage still exists. Although, the performance of the peak detection algorithm is better than the zero cross detection algorithm, the algorithm may estimate the rotor position with an offset error of 6 degrees. This error may lead to some cumulative estimation error.

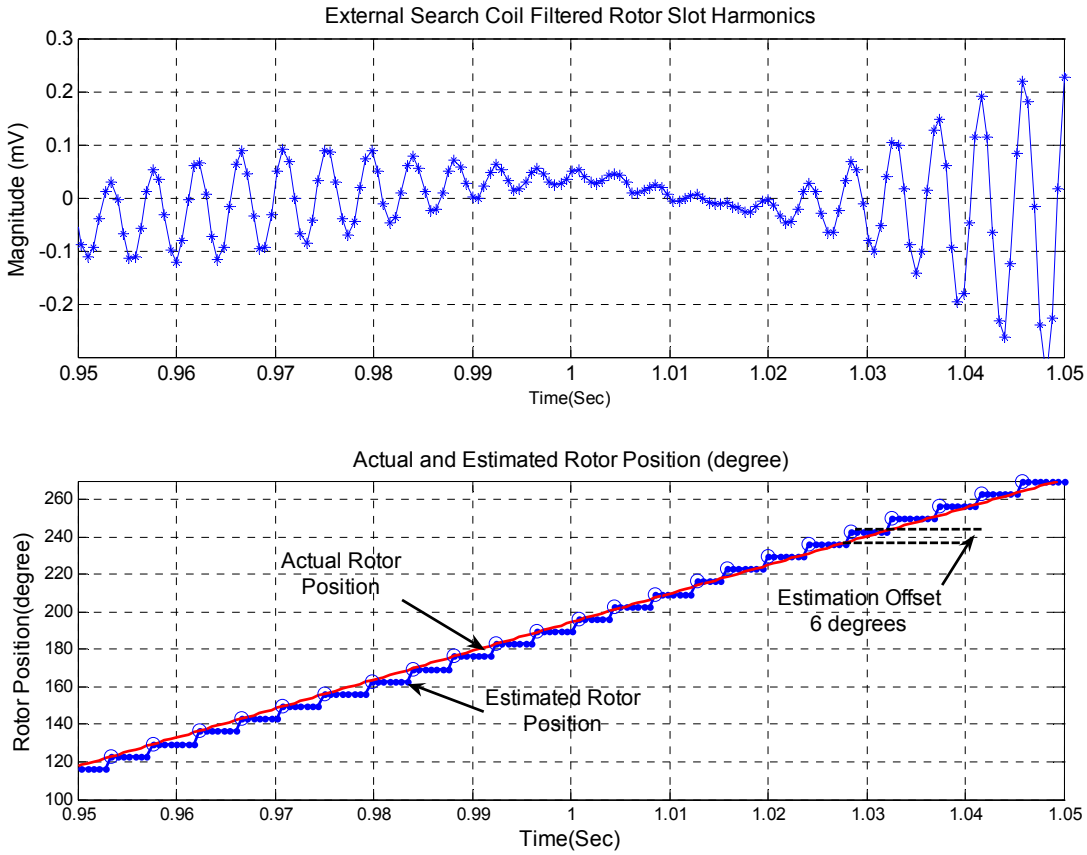

Fig. 5-32 Rotor position estimation with external search coil using peak detection algorithm at 5 Hz half load

5.8.3 Using Instantaneous Speed Data for Position Estimation

In section 5.7.3, it is discussed that the rotor position estimation algorithm halts when zero crossings of the rotor slot harmonics cannot be detected. In previous section, a method that will detect peaks instead of zero crossing is proposed. In this section, the instantaneous rotor speed information is utilized when the rotor position data is unavailable. The rotor mechanical time constants of electrical machines is large enough compared to position estimation cycle periods. For example, the rotor mechanical time constant for motor #2 is 68msec, where the software cycle takes 150 μsec. Note that, the rotor mechanical time constant is much longer than the control program cycle (nearly 500 times longer). It is therefore possible to predict the next position using the speed information available in the previous step.

For a small time interval compared to rotor mechanical time constant, the rotor position displacement angle(Δθ) can be expressed as;

$$\Delta\theta = w_r.\Delta t \qquad (5\text{-}22)$$

Where, w_r is the rotor mechanical speed in rad/sec, Δt is the elapsed time in sec. Using this information, rotor position can be interpolated during the intervals where rotor slot harmonic zero crossing cannot be detected. The block diagram of the proposed algorithm is presented in Fig. 5-33.

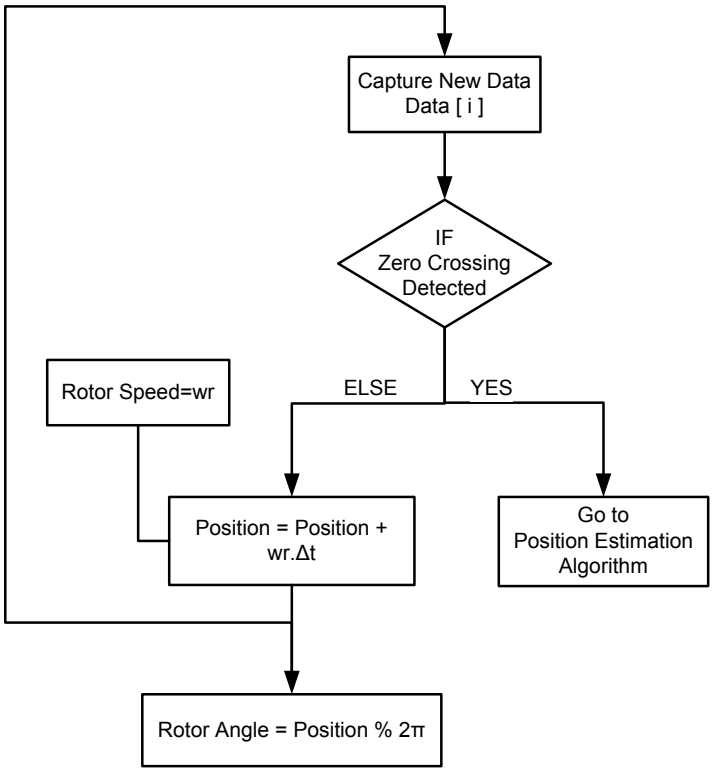

Fig. 5-33 Block diagram of rotor position algorithm with speed information

The position estimation results using speed information is given in Fig. 5-34. The estimation is performed with zero crossing detection algorithm when the zero crossing of the rotor slot harmonics is detectable. If the algorithm can not detect the

zero crossings of the rotor slot harmonics, then it estimates the rotor position based on the previously calculated rotor speed information as given in Fig. 5-33. The experimental results shows that, rotor speed data can be used for position estimation within small intervals compared to rotor mechanical time constant give precise estimation results.

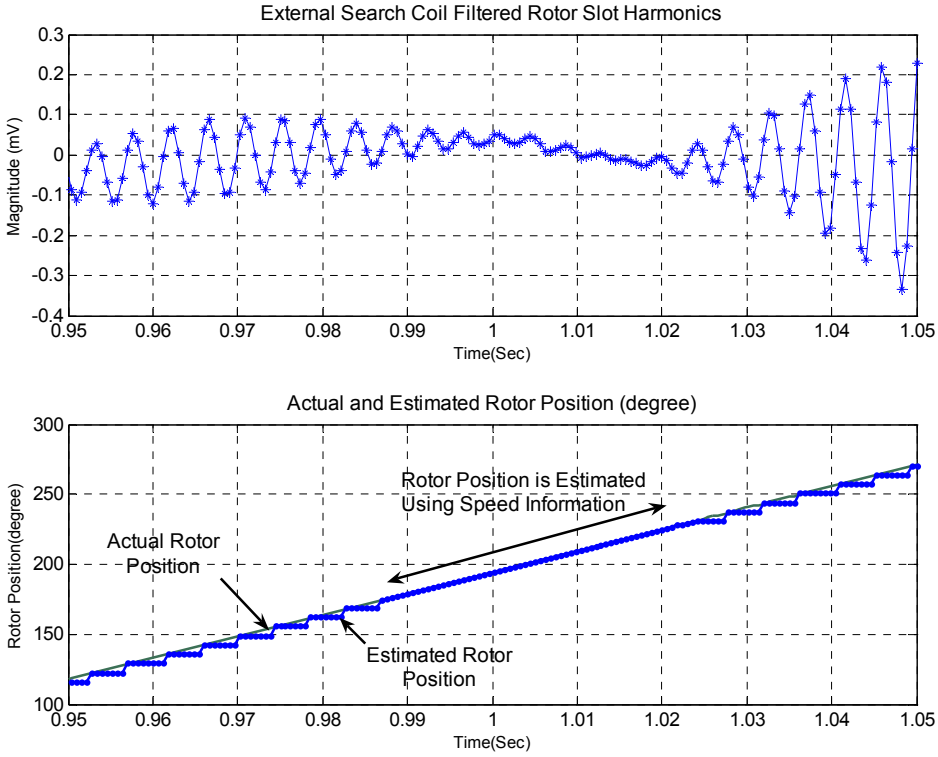

Fig. 5-34 Rotor position estimation using speed information with external search coil at 5 Hz half load

5.8.4 Accuracy Improvement with Interpolation

In the rotor position estimation method presented in 5.5.3, a very simple algorithm is utilized. In this method, rotor position is updated at each zero crossing of rotor slot harmonics data. And the rotor position data is kept constant until a new zero crossing is detected. This method results a stepped rotor position estimation with a step magnitude defined in equation (5-15). Resolution of the method can be improved, some means of interpolation. To achieve this, the number of program cycles between zero crossings is counted. Then, the rotor position data is updated at

each program cycle, with a much smaller step size. This step size is found by dividing the displacement angle presented by (5-15) by the number of cycles counted. This is given with equation (5-23).

$$\Delta\theta = \frac{\frac{2.\pi}{k.Z}}{\#\ \text{of Computation Cycles between zero crossings}} \qquad (5\text{-}23)$$

The block diagram of the method is presented in Fig. 5-35.

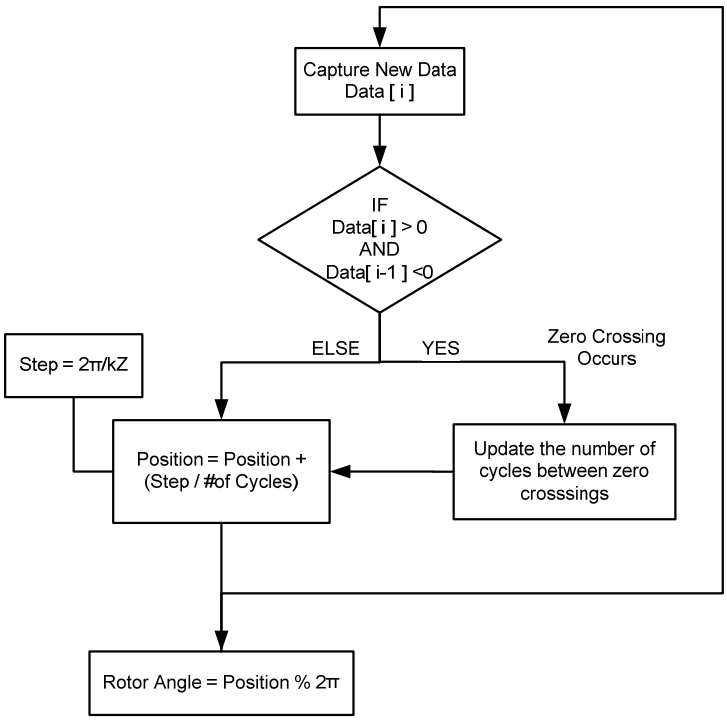

Fig. 5-35 Block diagram of zero crossing detection algorithm with interpolation

The interpolation method is applied to the same data presented in Fig. 5-20. The rotor position results with interpolation are given in Fig. 5-36. As seen from the graph, the rotor position is estimated accurately not only at zero crossing instants but also at other cycles that zero crossing not occurs. With this small modification, we achieved accurate rotor position estimation at every program cycle (150 μsec).

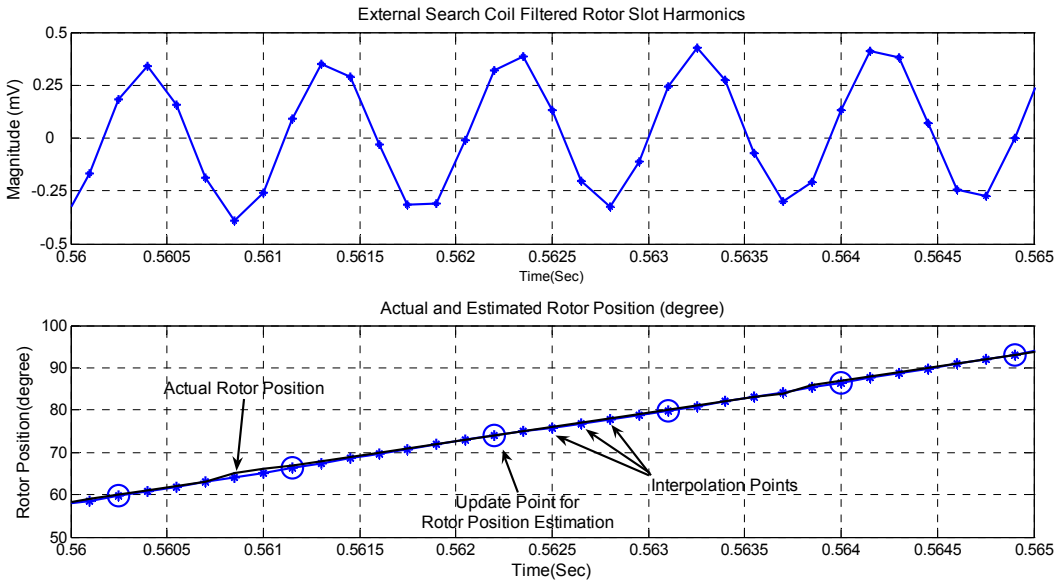

Fig. 5-36 External search coil harmonics, actual and estimated rotor position with interpolation method (detailed view) – 20 Hz

5.9 Conclusion

To conclude, in this chapter a new method for rotor position estimation is proposed. This method utilizes higher order rotor slot harmonics in time domain. This method is advantageous as compared to spectral estimation methods because, it does not require a data acquisition period and spectral estimation calculations. By this way, the rotor position can be calculated instantaneously as the search coil voltage data is captured at each program cycle (150 μsec). This is achieved by using third order rotor slot harmonics which exist in a spectrum band where no other distinctive harmonics present.

To summarize the method, first captured search coil data is modulated with the applied stator frequency. This modulation produces a rotor slot harmonic directly related with rotor speed and number of rotor slots. Assuming number of rotor is known or estimated using the method proposed in section 3.7, the rotor position and speed can be estimated. But the modulated signal also contains side band frequencies, so these components should be filtered out. For this purpose, a band-pass filter is used. The corner frequency of the band-pass filter should be equal to

desired rotor slot harmonics frequency and has a narrow bandwidth enough to eliminate side band frequencies. Largest drawback of the method is to update the filter characteristics as the rotor speed changes. Solution to problem is not covered in this study. But, it is possible to use a varying corner frequency band-pass filter that can adapt to new rotor speeds. In this study, filters designed using MATLAB Filter Design& Analysis Tool is used for each experiment condition when the motor is running at steady-state.

The experiments proved that higher rotor slot harmonics are observable in both internal and external search coils. Using the proposed method, rotor position is estimated and compared with the actual rotor position obtained from the incremental encoder. The experiment results with various applied stator frequencies. Also, the sensitivity of the method to load conditions is tested with various stator frequencies. The experiment results showed that, the magnitude of the higher order rotor slot harmonic does not change as much as the fundamental rotor slot harmonic. Moreover, since the frequency range of these harmonics is much higher than line harmonics, they are not confused with line harmonics at light load conditions. This makes the method applicable for all load conditions.

In addition to this, experiments are performed to measure the frequency range of the proposed method. At higher stator frequencies, the frequency of the rotor slot harmonics also increases. If the frequency of the desired rotor slot harmonics becomes larger than the half of the sampling frequency, the algorithm is unable to estimate the rotor position. The upper limit for applied stator frequency is defined by equation (5-21). According to the equation, the higher number of rotor slots per pole means lower stator frequency limits. For motor #2 the upper frequency range is 60 Hz, where for motor #1 this increases up to 120 Hz. To increase the operating limits of the method, the sampling frequency can be increased. Also a new method to increase the operating limits is proposed. In this method, instead of third order rotor slot harmonic (k=3), the second order rotor slot harmonic (k=2) may be used. By this way, the operation limit for motor #2 is increased from 60 Hz to 90 Hz applied stator frequency. This method would be very useful for motors that have a high rotor slot number per pole.

Different problem arises when the applied stator frequency is decreased. As the stator frequency and voltage is decreased, the induced voltage on the search coils also decreases as expected. Since the external search coil placed on the machine frame, the induced voltage includes more parasitic components. If the magnitude of higher order rotor slot harmonics becomes comparable with these parasitic components, the modulation and filtering step will interfere with these components. This will fail the rotor speed estimation at low stator frequencies. Such a case with a stator frequency of 5 Hz is presented in Fig. 5-29.

To overcome this three methods are proposed. First, instead of zero crossing detection a peak detection algorithm is proposed. Compared to detection of zero crossing instants, detection of peaks in the rotor slot harmonics is easier. As a result, the accuracy of the method is increased at low speed conditions. Secondly, it is proposed that instantaneous rotor speed information can be utilized at cases where zero crossing or peak detection algorithms fail. This idea is based on the fact that, rotor speed cannot change much on small time intervals due to motor and load inertia. The experiment results showed that, with this method rotor position can be estimated accurately down to 5Hz applied stator frequencies.

Finally, an improvement on the rotor position estimation is proposed with a basic interpolation technique. In this method, the rotor position is updated at each cycle of program cycle (150 μsec). Thus, the interpolation prevents the stepped waveform of the estimated rotor position data and gives more accurate rotor position with a higher refresh rate.

As conclusion, the experiments performed in this section proved that the proposed method can be used with both internal and external search coils. And the method performance is nearly invariant with the machine load conditions. Also, refresh rate of the rotor speed estimation with this method is much higher than the spectral estimation techniques described in chapter 3. If, a varying corner frequency band pass filter will be designed the method can be implemented as rotor position observer.

CHAPTER 6

CONCLUSIONS

6.1 Brief Summary of the Study

In this thesis, rotor position and speed estimation of induction motors using an external search coil was studied. Using an external search coil for rotor and speed estimation has some advantages over speed sensors. These advantages are; low cost of search coil compared to speed sensors, no modification is needed. In literature, there are some speed and position estimation methods such as, using specially designed rotor cages, or superimposing a high frequency carrier signal on the fundamental excitation. These methods also need some modification of the machine or the inverter.

Using an external search coil or an antenna that links the fringing flux is investigated in a few studies. And most of them focussed on the detection of faults in the machine. In this study, we have widened the usage of external search coil for rotor speed and position estimation. The purpose is to measure search coil voltage and relate this to air gap flux of the machine. In this manner, zero crossing of the air gap flux may be identified and this information may be used to determine rotor flux position for vector control.

Firstly, the type and position of the search coil is selected. Experiment results presented in Table 2-1 and simulations showed that U-shaped search coil induces largest voltage. For axial placement, anywhere in the range of machine core is acceptable. Radial placement of the search coil does not have any importance as expected. Position variation on radial direction only introduces a phase difference angle consistent with the mechanical displacement angle. For air gap flux measurement, a search coil is placed on the stator slots (internal search coil). It is

proved with experiments that the induced internal search coil voltage measures the air gap flux correctly. The data obtained from the internal search coil is used to verify the accuracy of the estimation performed with external search coil. Then, external search coil is examined with varying frequency, flux and load conditions. The following results are obtained from the external search coil experiments;

- The external search coil voltage exponentially increases as the air gap flux increases and the machine core saturates.
- The ratio between induced voltage magnitude and frequency at same flux condition decreases if the frequency is increased. But the relationship is nonlinear and the induced voltage exponentially converges to a lower value than one would expect from a linearly increasing relationship.
- The magnitude of the induced voltage decreases if the machine load is increased. But a nonlinear relationship is observed in the characteristic as the load is increased, the induced external search coil voltage magnitude decreases.

Therefore it is clear that the external search coil is not as good a flux observer as an internal search coil. It is obvious that a more complex approach is needed if it is desired to obtain information on the air gap flux position from its induced voltage. Before attempting to predict the air gap flux from the search coil voltage further experiments are performed to investigate whether the rotor speed can be identified from the measured external coil voltage. In this manner it is desired to increase familiarity with the available information.

To verify the harmonic content of the external search coil voltage some well known rotor speed estimation method is applied FFT spectral analysis technique. The experiments proved that the rotor speed can be estimated using the external search coil voltage. The experiment results showed that using the rotor slot harmonics rotor speed may be estimated with an accuracy of ± 1.2 rpm. The accuracy of the method can be further increased with;

- A machine with higher number of rotor slots per pole
- A higher resolution FFT by taking longer data samples.

But, using spectral estimation techniques have some drawbacks. These are;

- Long data acquisition and computation period worsens the transient performance of the method
- Difficulty in detecting the rotor slot harmonics among many other harmonics
- Probability of rotor slot harmonics coincidence with line harmonics
- The number of rotor slots should be known for speed estimation

The biggest disadvantage of the method is the first one and prevents usage of the method as an online speed estimator with good transient response.

It is understood that knowledge of number of rotor slots is needed for speed estimation. A new method is proposed for predicting the rotor slot number automatically using the ratio of rotor slot harmonics to saliency harmonics identified via FFT analysis of the external search coil voltage. This approach is tested for 2 motors and it is found that the rotor slot number of both motors is calculated correctly by the algorithm. It is also observed that this approach works under all load conditions and while driving the motor at different frequencies (tests are done at 20, 40 and 50 Hz)

Then, it is aimed to build a model between induced search coil voltage and the air gap flux. By this way, the spectral estimation techniques are eliminated and estimation is performed in time domain. In this method zero crossing of the induced external search coil voltage is detected and hence the air gap flux position and magnitude is estimated using this data.

To model the nonlinear characteristic of the external search coil voltage some models are proposed such as, using coil to stator phase mutual inductance and using standard induction motor equivalent circuit. Experiments are performed between 10-70 Hz at no load, half load and full load. The machine is driven at constant flux conditions for frequencies lower than rated frequency. For higher frequencies flux weakening method is applied. These experiment results showed that the varying turn's ratio equivalent circuit gives good results. The equation for estimating the air gap flux with this model is given in equation (4-18). As can be seen from the equation, model parameters (N_1, N_2) can be estimated only using the machine measurable parameters such as leakage inductance. The experiment results

performed at no load are used for parameter estimation of the model. Then estimated parameters are applied to the half load and full load experiment results and air gap flux estimations are obtained and compared with the internal search coil predictions at the same conditions. This comparison showed that, using external search coil air gap flux position angle can be estimated with an error less than 5 degrees. This phase angle estimation error decreases as the applied frequency increases. For example the angle estimation error is less than 1 degree for rated stator frequency (50 Hz) as seen from Table 4-14. The magnitude estimation has lower performance. The magnitude estimation error is around %20 for rated frequencies and decreases to 8% for 10 Hz applied stator frequency. These results show that the induced external search coil voltage may be used as an air gap flux observer. But the method has serious disadvantages on implementation. These are;

- Long flux position update period especially at low applied stator frequencies
- Low position and magnitude accuracy due to nonlinear characteristics fo the induced external search coil voltage
- Difficulty in defining model parameters and need for self tuning test, for each stator frequency to determine these parameters.

For this reason a better approach is sought and the probability of using 3^{rd} and 5^{th} coil voltage harmonics for better modelling of coil voltage or estimation of air gap flux position is investigated. By identifying these harmonics in the measured external coil voltage the air gap flux predictions are made but with constants determined via measurements. Taking these harmonics into account it is observed that a more accurate estimation can be performed as seen from Fig. 4-23 to Fig. 4-25. The magnitudes and phase angles of the harmonics are estimated with MATLAB Parameter Estimation Toolbox. A model may be also proposed for voltage harmonics similar to fundamental component. But, the search coil voltage harmonics has similar characteristics with the fundamental component. Using 3^{rd} and 5^{th} harmonics for the estimation has greater difficulties such as nonlinear induced voltage characteristics and estimation of model parameters for other machines. There is no easy way to find out the variation of the relationship between the external search coil 3^{rd} and 5^{th}

harmonics magnitudes and the air gap flux. Thus, a model to estimate the air gap flux using the 3rd and 5th harmonics is not covered in this study.

Finally, the rotor position is estimated in time domain using the higher order rotor slot harmonics. Higher order rotor slot harmonics exist in a spectrum band where no other distinctive harmonics present. Thus, they can be detected easily by some means of digital filtering without using complex spectral analysis techniques. Advantages of this method can be listed as;

- Analysis in time domain permits position update at each rotor slot harmonic cycle
- Higher frequency of these harmonics ensures better accuracy
- Elimination of spectral analysis satisfies much less computation periods
- Magnitudes of higher order rotor slot harmonics is nearly insensitive to load

Largest drawback on online implementation of the method would be to design a filter with varying corner frequency that can adapt to new rotor speeds.

The proposed method estimates the rotor position with a high refresh rate and high accuracy. As can be seen from the experiment results given in section 5.6.2, the rotor position estimation is accurate enough that the estimated rotor position is inseparable from the actual rotor position obtained from the incremental encoder. Also the estimation accuracy is not affected from the load conditions.

Then, the limits of the proposed method are investigated in section 5.7. The utilized higher order rotor slot harmonics has high frequency. Thus, the upper frequency limit of the method is determined by the sampling frequency. The frequency of the third order rotor slot harmonics should be lower than the sampling frequency. The sampling frequency may be increased to overcome this issue. Or an alternative method is to use the second order rotor slot harmonic instead of the third one. The experiment results given in 5.7.2 showed that for motor #2 the upper stator frequency limit can be increased from 60 Hz to 90 Hz by using the second order rotor slot harmonics instead of the third order harmonic.

Different problems arise as the applied stator frequency is decreased; the magnitude of the search coil voltage becomes smaller and signal to noise ratio decreases. Incorrect estimation results performed at 5 Hz stator frequency is given in

Fig. 5-29. It can be observed that in some instants position tracking is lost. To overcome this incorrect estimation; firstly, a method that will detect the peaks of the rotor slot harmonics is proposed. Peak detection algorithm gives better results compared to zero detection algorithm and the results are presented in Fig. 5-32. Another method is to use rotor speed information when rotor position data in unavailable. Since the rotor mechanical time constant is much longer than the program cycle, this method gives accurate results if detection algorithm recovers on short periods compared to rotor mechanical time constant. The experiment result presented in Fig. 5-34.

Also, a basic interpolation technique implemented to increase the accuracy. By this interpolation approach rotor position data can be updated at each program cycle (150 μsec) with a negligible position estimation error. Note that, the performance of the system may be even increased by using a higher sampling frequency or a machine with higher number of rotor slots per pole.

Using interpolation techniques and other methods the rotor position is successfully estimated down to 5 Hz stator frequency for steady state conditions. The lower limit of the system can be improved by software or hardware modifications.

Comparing the techniques covered in this thesis, the method using higher order rotor slot harmonics in time domain is advantageous among others. The rotor position obtained by this technique is independent of motor electrical parameters and load conditions. It also has the best accuracy and has the shortest update period.

To sum up, using an external search coil to estimate the position of machine flux or the rotor position is proposed. Several experiments are performed and the relationship between machine operating conditions and the induced search coil voltage is investigated. Although, the method introduces a signal cable, the installation of the proposed sensor does not need any modification to the system. And the installation is much easier than to install a classical speed sensor or position encoder. Obviously, a search coil wound on a core will be much cheaper than a speed sensor. The signal cable drawback can be eliminated by an inverter packed together with the sensor and drive circuitry placed on the motor body thus providing more compact solution and eliminating the signal cable.

6.2 Suggestions & Future Work

The purpose of this is to study is to validate the proposed methods using an external search coil. Thus, all the methods proposed are applied offline with captured data. The practical implementation of the proposed methods is essential. The following suggestions maybe applied to future studies to improve the proposed methods;

- **Online Implementation of the methods:** Since this thesis is focussed on the verification of the rotor speed and position estimation methods using external search coil, nearly all estimations are made at offline conditions at steady state. A study that can implement the methods online is very essential to assess the usefulness of the proposed rotor position prediction method.

- **Determination of higher order rotor slot harmonics from phase currents:** If the higher order rotors slot harmonics in the air gap induce measurable rotor harmonic current components in the stator windings, the proposed method can be even implemented without the usage of an external search coil. This will, sure increase the robustness of the method and the value of the study.

- **Improvement on search coil:** Limited numbers of search coils are tested in this thesis. If some improvements on the search coil shape or position can be done, that gives better signal to noise ratio, and then the lower operation limit of the search coil can be reduced further from 5 Hz.

REFERENCES

[1] Vas, P. , " Sensorless Vector And Direct Torque Control " , Oxford University Press, 1998.

[2] Negrea M.D "Electromagnetic flux monitoring for detecting faults in electrical machines", Helsinki University of Technology, Doctoral Dissertation 2006

[3] J. Holtz "Sensorless Speed and Position Control of Induction Motors" IECON, 2001

[4] Ishida M., Iwata K. "A New Slip Frequency Detector of an Induction Motor Utilizing Rotor Slot Harmonics", IEEE Transactions on Industry Applications Vol.IA-20, No.3, May-June 1984, pp. 575-582

[5] Ferrah A., Bradley J., Asher G. M., "Application of the FFT to the Speed Measurement of Inverter Fed Induction Motors", IEEE, 1992

[6] Asher G. M, Bradley K. J. "Sensorless Position Detection for Vector-Controlled Induction Motor Drives Using an Asymmetric Outer-Section Cage", IEEE, 1996

[7] Jansen P.L, Lorenz R.D. "Transducerless Position and Velocity Estimation in Induction and Salient AC Machines", IEEE transactions on industry applications, vol. 31, no. 2, 1995

[8] Consoli A., Testa A. "A New Zero-Frequency Flux-Position Detection Approach for Direct-Field-Oriented-Control Drives", IEEE, 1999

[9] Degner M. W, Lorenz R. D. "Position Estimation in Induction Machines Utilizing Rotor Bar Slot Harmonics and Carrier Frequency Signal Injection", IEEE, 2000

[10] Briz F, Degner M. W. , Lorenz R. D. "Comparison of Carrier Signal Voltage and Current Injection for the Estimation of Flux Angle or Rotor Position", IEEE, 1998

[11] Vaclavek, P. & Blaha, P., "An Induction Machine Speed Estimation Based On Rotor Slot Harmonics Analysis", Daaam, 2006

[12] Nandi S. "Slot Permeance Effects on Rotor Slot Harmonics in Induction Machines", IEEE, 2003

[13] Asher G. M, Sumner M, "Sensorless Position Detection for Symmetric Cage Induction Motor under Loaded Conditions", IEEE, 2000

[14] Moreria J.C., Lipo T.A.,"Modelling of Saturated AC Machines Including Air Gap Flux Harmonic Components", IEEE Trans. Industry Applications, Vol.28, no.2. Mar./April.1992, pp. 343-349

[15] Aime. M, Degner M.W, Tice. N. H., Lorenz. R.D., "Measuring the Location of Saliencies in AC Machines", IEEE, 1998

[16] Briz F., Degner M. W., Lorenz R.D. "Comparison of saliency-based sensorless control techniques for AC machines", IEEE, 2003

[17] Degner M.W., Lorenz R.D. "Using Multiple Saliencies for the Estimation of Flux, Position and Velocity in AC Machines", IEEE vol.34, pp.1097-1104, 1999

[18] Holtz J., "Sensorless Position Control of Induction Motors – an Emerging Technology", IEEE transactions on industrial electronics, 1998

[19] Consoli A., Scarcella G., "A new Zero-Frequency Flux-Position Detection Approach for Direct Field Oriented Control Drives", IEEE transactions on industry applications, vol. 36, no.3, 2000

[20] Mathew J. Corley, Lorenz R.D., "Rotor Position and Velocity Estimation for a Salient-Pole Permanent Magnet Synchronous Machine at Standstill and High Speeds", IEEE transactions on industry applications, vol. 34, no.4, 1998

[21] M. Aiello, A. Cataliotti, S. Nuccio, "An Induction Motor Speed Measurement Based On Current Harmonic Analysis With Chirp-Z Transform", IEEE Instrumentation and Measurement Technology Con. , 2001, pp.578-582

[22] Kaikkaa M.Y., Boucherma M. "Analytical Analysis of Rotor Slot Harmonics in the Line Current of Squirrel Cage Induction Motors", Journal of Electrical Engineering, Vol.7, 2006

[23] Guldemir H., Bradley K. J. "An Improved Method to the Prediction of Line Current Spectrum in Induction Machines", Journal of Electrical Engineering, 2003

[24] Brudny J. F., Roger. D. "Induction Machine Speed Sensor Based on Stator Current Measurement", Power Electronics and Variable Speed Drives, 1996

[25] Vaclavek P., Blaha P. "An Induction Machine Speed Estimation Based on Rotor Slot Harmonics Analysis", DAAM Symposium, 2006

[26] Nandi S., Shebab A. "Detection of Rotor Slot and Other Eccentricity Related Harmonics in a Three Phase Induction Motor with Different Rotor Cages", IEEE Energy Conversion, Vol.16, No.3, 2001

[27] Nandi S., Toliyat H. A. "Selection Criteria of Induction Machines for Speed Sensorless Drive Applications", IEEE Industry Applications Vol.39 No.3, 2003

[28] A. Yazidi, D. Thailly, H. Henao, R. Romary, G.A. Capolino, J. F. Brudny "Detection of Stator-circuit in Induction Machines Using an External Leakage Flux Sensor", IEEE International Conference on Industrial Technology, 2004

[29] Voitto K. "Condition Monitoring of Squirrel Cage Motors by Axial Magnetic Flux Measurements", University of Oulu, 2003

[30] Negrea M.D., "Electromagnetic Flux Monitoring for Detecting Faults in Electrical Machines", Helsinki University of Technology, Doctoral Dissertation, 2006

[31] Hwang D.H., Chang J. H., Lee J. H. "A Method for Dynamic Simulation and Detection of Air-gap Eccentricity in Induction Motors by Measuring Flux Density", IEEE, 2006

[32] R. Blasco-Gimenez, G. M. Asher, M.Sumner, K.J. Bradley," Performance of FFT-Rotor Slot Harmonic Speed Detector for Sensorless Induction Motor Drives", IEEE Proc.-Elkctr. Power Appl., Vol. 143/3, May 1996, pp. 258-268

[33] Hurst K. D., Habetler T.G." A Comparison of Spectrum Estimation Techniques for Sensorless Speed Detection in Induction Machines", IEEE Industry Applications, Vol.33 No.4, 1997

[34] M. Ishida, K. Hayashi, Ueda M. "A Speed Detection Method of Squirrel-Cage Induction Motor Utilizing Rotor Slot-Harmonics in the Air Gap and its Application to Slip-Frequency Control" Trans. IEEE Japan, Vol.99B, 1979

[35] R. Supangat, N. Ertugrul, W. L. Soong, D. A. Gray, C. Hansen and J. Grieger, "Estimation of the Number of Rotor Slots and Rotor Speed in Induction Motors Using Current, Flux, or Vibration Signature Analysis", Proceedings of the 2006 Australasian Universities Power Engineering Conference

[36] Gimenez B.R "High Performance Sensorless Control of Induction Motor Drives", University of Nottingham, Doctorate Thesis, 1995

[37] Schroedl M., "Sensorless Control of Induction Motors at Low Speed and Standstill", ICEM' 92, pp. 863-867, 1992

[38] Guru B. S., Hızıroğlu H.R. "Electric Machinery and Transformers", Oxford University Press, 2001

[39] http://www.ndt-ed.org , last accessed on December 2008

[40] Acar Akın, "Implementation of a Vector Controlled Induction Motor Drive", M.S. Thesis, 2004

[41] Oppenheim Alan V., Willsky Alan S., Young Ian T. "Signals and Systems", Prentice Hall, 1983, pp. 448-473

[42] Say M.G. "The Performance and Design of Alternating Current Machines", Pitman Paperbacks, 1970, pp. 222-224.

[43] Hwang D., Lee, K. Lee. J., Kang D., Choi K. "Analysis of a Three Phase Induction Motor under Eccentricity Condition", 2005, IEEE

[44] Liou S., Wang W. " Indirect Rotor Position Sensing for Switched Reluctance Motor using Search Coil", 1996, IEEE

[45] Voitto Kokko, "Condition Monitoring of Squirrel-Cage Motors by Axial Magnetic Flux Measurements", University of Oulu, 2003

[46] D. Belkhayat, R. Romary, M. E. Adnani, R.Corton, J. F. Brudny, "Fault Diagnosis in Induction Motors Using Radial Magnetic Field Measurement with an Antenna", Measurement Science and Technology, 2003

[47] T. Assaf, H. Henao, G. A. Capolino, "Simplified Axial Flux Spectrum Method to Detect Incipient Stator Inter-Turn Short-Circuits in Induction Machine", IEEE, 2004

[48] M. Aiello, A. Cataliotti, S. Nuccio, "A Comparison of Spectrum Estimation Techniques for Periodic Not Stationary Signals", IEEE Instrumentation and Measurement Technology Conference, Budapest, 2001, p.p 1130-1134

[49] N. Bianchi, **"**Electrical machine analysis using finite elements" Talor&Francis, 2005, p.269

[50] Bose B. K , "Modern Power Electronics and AC Drives", Prentice Hall, 2001

[51] Novotny D.W., T. A. Lipo, "Vector Control and Dynamics of AC Drives", Oxford University Press, 1998

[52] http://en.wikipedia.org/wiki/Finite_impulse_response, last accessed on: December 2008

APPENDIX A

MANUFACTURER DATA OF TEST MOTORS

Table A-1 Manufacturer data and equivalent circuit parameters for motors used in experiments

	Motor #1 NM 90L - 6	Motor #2 NM90L – 2
Output power (kW)	1.1 kW	2.2 kW
Nominal current (A)	3.1	4.8
Nominal speed (rpm)	907	2839
Power factor	0.77	0.89
Efficiency (%)	70	79
Number of poles	6	2
Nominal moment (Nm)	11.6	7.4
Breakdown torque (Tbd/Tr)	1.9	2.9
Stator Resistance (r_s)	6.52 Ω	2.65 Ω
Referred Rotor Resistance (r_r')	7.67 Ω	3.07 Ω
Mutual Inductance (L_m)	338.5 mH	384.27 mH
Stator Leakage Inductance (L_{ls})	29.75 mH	14 mH
Rotor Leakage Inductance (L_r)	29.75 mH	14 mH

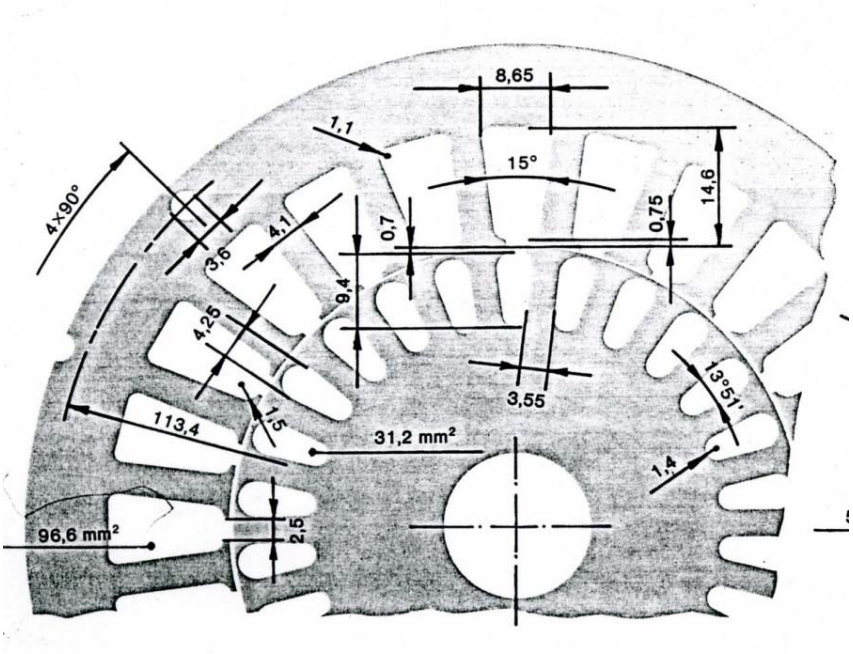

Fig. A-1 Lamination of Motor #1

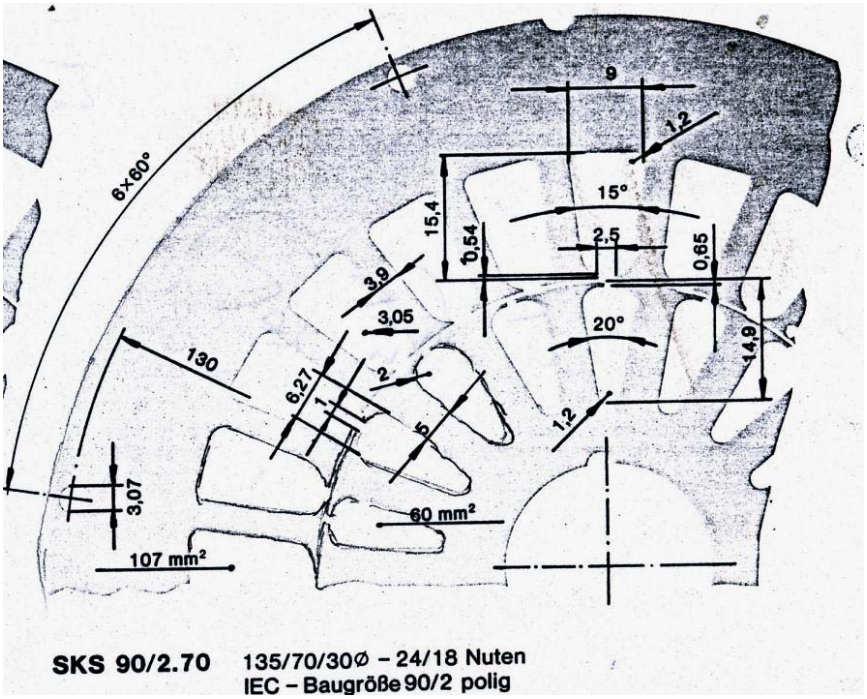

Fig. A-2 Lamination of Motor #2

APPENDIX B

MATERIAL MAGNETIC PROPERTIES

Based on the given material magnetic properties for finite element analysis in [49]:

Magnetic Behaviors of Some Massive Magnetic Materials

Flux Density	Forged Steel and Melted Steel		Gray Cast Iron and Tempered Steel		Iron Steel		Nickel	
B (T)	H (A/m)	μ_r	H (A/m)	μ_r	H (A/m)	μ_r	H (A/m)	μ_r
0.1	70	1140	200	400	25	3200	215	372
0.2	90	1780	450	355	50	3200	420	380
0.3	100	2400	800	300	85	2820	1020	235
0.4	120	2660	1300	246	115	2780	2660	120
0.5	140	2860	2000	200	160	2500	8000	50
0.6	170	2820	2800	171	200	2400	24000	20
0.7	220	2500	4000	140	250	2240	88000	6.4
0.8	270	2370	5500	117	310	2060		
0.9	320	2260	8000	90	380	1900		
1.0	400	2000	11000	73	490	1630		
1.1	500	1750	15000	58	640	1380		
1.2	620	1550	20000	48	850	1130		
1.3	850	1230	—	—	1480	705		
1.4	1200	930	—	—	2800	400		
1.5	2000	600	—	—	5000	240		
1.6	3500	365	—	—	9300	138		
1.7	6000	226	—	—	17000	80		
1.8	10000	144	—	—	29000	50		
1.9	16000	95						
2.0	25000	64						

Flux Density	Normal Iron Thickness 0,5 mm c_p = 3,6 W/kg		Silicon Iron Thickness 0,5 mm c_p = 2,5 W/kg		Silicon Iron Thickness 0,35 mm c_p = 1,1 W/kg		Grain-Oriented Thickness 0,35 mm c_p = 0,6 W/kg	
B (T)	H (A/m)	μ_r	H (A/m)	μ_r	H (A/m)	μ_r	H (A/m)	μ_r
0.8	230	2770	120	5305	140	4545	40	15920
0.9	330	2170	160	4475	200	3580	80	8950
1.0	470	1695	240	3315	290	2745	140	5685
1.1	630	1390	340	2575	430	2035	230	3805
1.2	800	1195	510	1870	680	1405	320	2985
1.3	1050	985	780	1325	1150	900	460	2250
1.4	1350	825	1320	845	1960	568	630	1770
1.5	1750	680	2360	505	3240	370	840	1420
1.6	3500	365	3720	340	5430	235	1110	1145
1.7	6200	220	5670	240	7160	190	1560	865
1.8	9000	160	8450	170	9000	160	2060	695

APPENDIX C

EXPERIMENTAL EQUIPMENT SPECIFICATIONS

Incremental Encoder: OMRON - E6C2CWZ6C Rotary Incremental Encoder, 1000 pulse/revolution

Digital Oscilloscope: Agilent 54624A MegaZoom, 100 MHz, 200MSa/s

Differential Probe: Agilent N2772A, 600 V, 20 Mhz

Current Probe: HP-1146 A, 0-70A RMS, 0-100 kHZ, 10/100 mV/A

Current Transducer: LEM LA-55-P, 50A, AC/DC

Voltage Transducer: LEM LV-25-P, 0-500V, AC/DC

Isolation Amplifiers: AD8273, Dual-Channel, Low noise, Audio differential amplifier

DSP Controller Board: dSPACE DS1102, Floating point controller, 40 Mhz, 4 ADC Channels, 16 Digital I/O, Incremental Encoder Interface

DC Motor: Awdsleys, 220V, 45A, 12 hp, 1600A

DC Motor Drive: Control Techniques Mentor II, 30 kW

APPENDIX D

EXPERIMENTAL WAVEFORMS & DATA OBTAINED

In this section, the experimental data will be presented. These experiments include, no load, half load, full load tests for machines using internal and external search coil at various stator frequencies.

Table D-1 Measured internal and external search coil voltage with motor #2 at various frequencies at no load

Frequency (Hz)	Terminal Voltage (V)	Stator Current (A)	Internal Coil Voltage (V)	External Coil Voltage (mV)
5	$22 \angle 0^0$	$1.7 \angle -65^0$	$1 \angle -42^0$	$57 \angle -51^0$
10	$38 \angle 0^0$	$1.4 \angle -78^0$	$1.9 \angle -88^0$	$81 \angle -66^0$
15	$64 \angle 0^0$	$1.9 \angle -81^0$	$3.2 \angle -94^0$	$135 \angle -74^0$
20	$92 \angle 0^0$	$1.8 \angle -80^0$	$4.6 \angle -96^0$	$160 \angle -80^0$
25	$108 \angle 0^0$	$1.7 \angle -80^0$	$5.5 \angle -96^0$	$170 \angle -89^0$
35	$149 \angle 0^0$	$1.7 \angle -78^0$	$7.6 \angle -95^0$	$202 \angle -89^0$
40	$170 \angle 0^0$	$1.8 \angle -78^0$	$8.7 \angle -98^0$	$214 \angle -99^0$
50	$220 \angle 0^0$	$1.9 \angle -81^0$	$11.4 \angle -98^0$	$248 \angle -100^0$
60	$225 \angle 0^0$	$1.6 \angle -77^0$	$11.5 \angle -97^0$	$209 \angle -99^0$
70	$218 \angle 0^0$	$1.2 \angle -72$	$11.1 \angle -97^0$	$165 \angle -97^0$
80	$224 \angle 0^0$	$1.1 \angle -80^0$	$11.6 \angle -98^0$	$151 \angle -98^0$

Table D-2 Measured internal and external search coil voltage with motor #2 at various frequencies at half load

Frequency (Hz)	Terminal Voltage (V)	Stator Current (A)	Internal Coil Voltage (V)	External Coil Voltage (mV)
5	$27 \angle 0^0$	$2.5 \angle -41^0$	$1.2 \angle -84^0$	$65 \angle -55^0$
10	$47 \angle 0^0$	$2.55 \angle -47^0$	$2.3 \angle -94^0$	$109 \angle -70^0$
15	$70 \angle 0^0$	$2.5 \angle -47^0$	$3.4 \angle -94^0$	$137 \angle -76^0$
20	$95 \angle 0^0$	$2.6 \angle -49^0$	$4.7 \angle -97^0$	$170 \angle -83^0$
25	$111 \angle 0^0$	$2.5 \angle -51^0$	$5.7 \angle -97^0$	$182 \angle -86^0$
30	$130 \angle 0^0$	$2.4 \angle -51^0$	$6.8 \angle -95^0$	$191 \angle -88^0$
35	$159 \angle 0^0$	$2.5 \angle -53^0$	$8.1 \angle -95^0$	$219 \angle -94^0$
40	$177 \angle 0^0$	$2.34 \angle -58^0$	$9.1 \angle -95^0$	$226 \angle -96^0$
50	$229 \angle 0^0$	$2.7 \angle -50^0$	$11.7 \angle -97^0$	$226 \angle -96^0$
60	$220 \angle 0^0$	$2.3 \angle -43^0$	$11.2 \angle -96^0$	$182 \angle -90^0$
70	$218 \angle 0^0$	$1.9 \angle -34$	$11 \angle -98^0$	$165 \angle -85^0$
80	$224 \angle 0^0$	$2.1 \angle -33^0$	$11.4 \angle -99^0$	$142 \angle -84^0$

Table D-3 Measured internal and external search coil voltage with motor #2 at various frequencies at full load

Frequency (Hz)	Terminal Voltage (V)	Stator Current (A)	Internal Coil Voltage (V)	External Coil Voltage (mV)
5	$30 / 0^0$	$3.9 / -21^0$	$1.1 / -84^0$	$54 / -52^0$
10	$57 / 0^0$	$4.94 / -24^0$	$2.3 / -88^0$	$96 / -57^0$
15	$76 / 0^0$	$4.67 / -28^0$	$3.5 / -93^0$	$130 / -72^0$
20	$97 / 0^0$	$4.67 / -29^0$	$4.4 / -94^0$	$148 / -76^0$
25	$117 / 0^0$	$4.8 / -29^0$	$5.6 / -96^0$	$168 / -78^0$
30	$138 / 0^0$	$4.7 / -29^0$	$6.7 / -96^0$	$177 / -79^0$
35	$165 / 0^0$	$4.8 / -31^0$	$8.0 / -96^0$	$195 / -85^0$
40	$184 / 0^0$	$4.8 / -31^0$	$9.1 / -97^0$	$205 / -87^0$
50	$220 / 0^0$	$4.8 / -31^0$	$11.2 / -97^0$	$236 / -92^0$
60	$219 / 0^0$	$3.94 / -30^0$	$11.1 / -99^0$	$159 / -84^0$
70	$215 / 0^0$	$3.4 / -27^0$	$10.1 / -99^0$	$127 / -77^0$
80	$225 / 0^0$	$3.5 / -27^0$	$11.5 / -99^0$	$121 / -68^0$

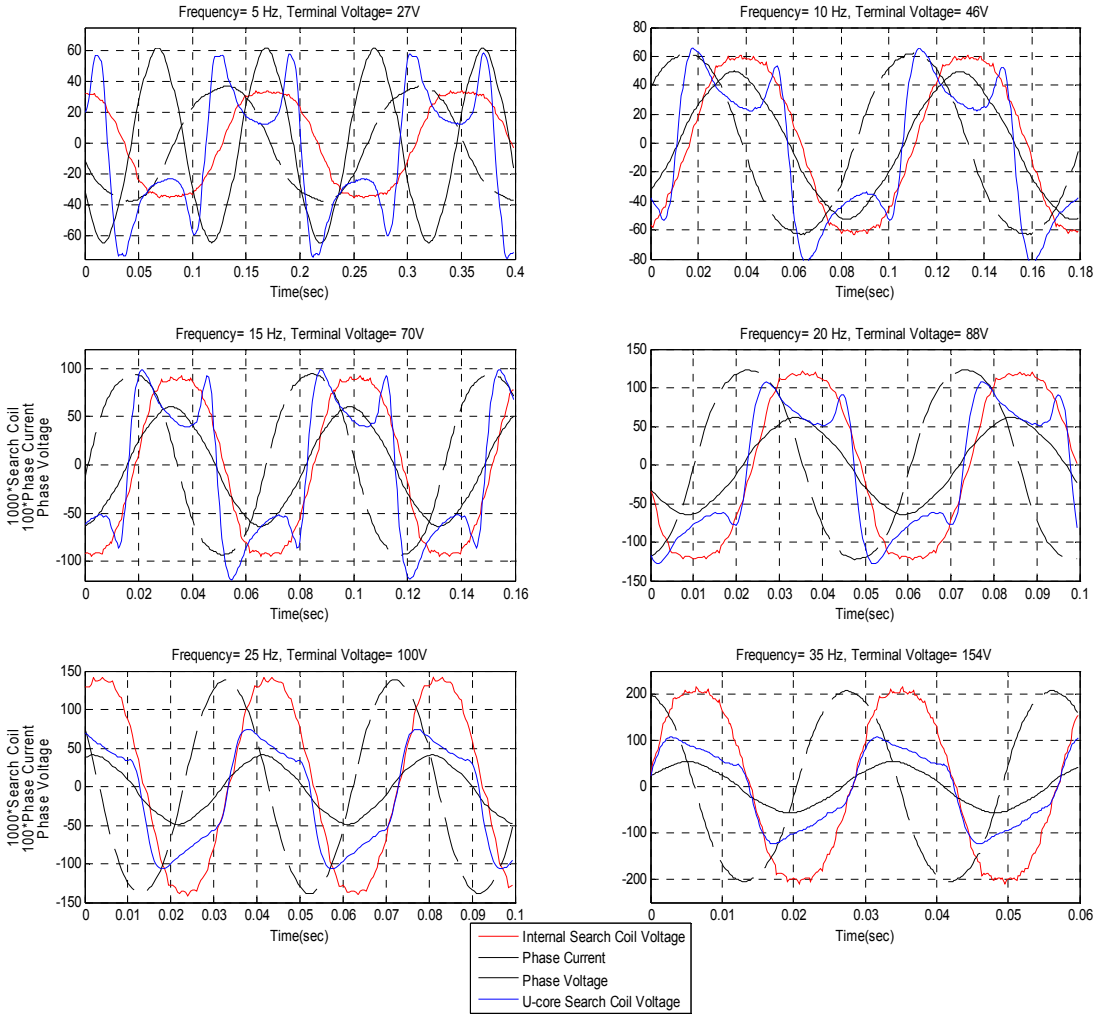

Fig. D-1 Waveforms of internal and external search coil with various stator frequencies (5 - 35 Hz) at no load

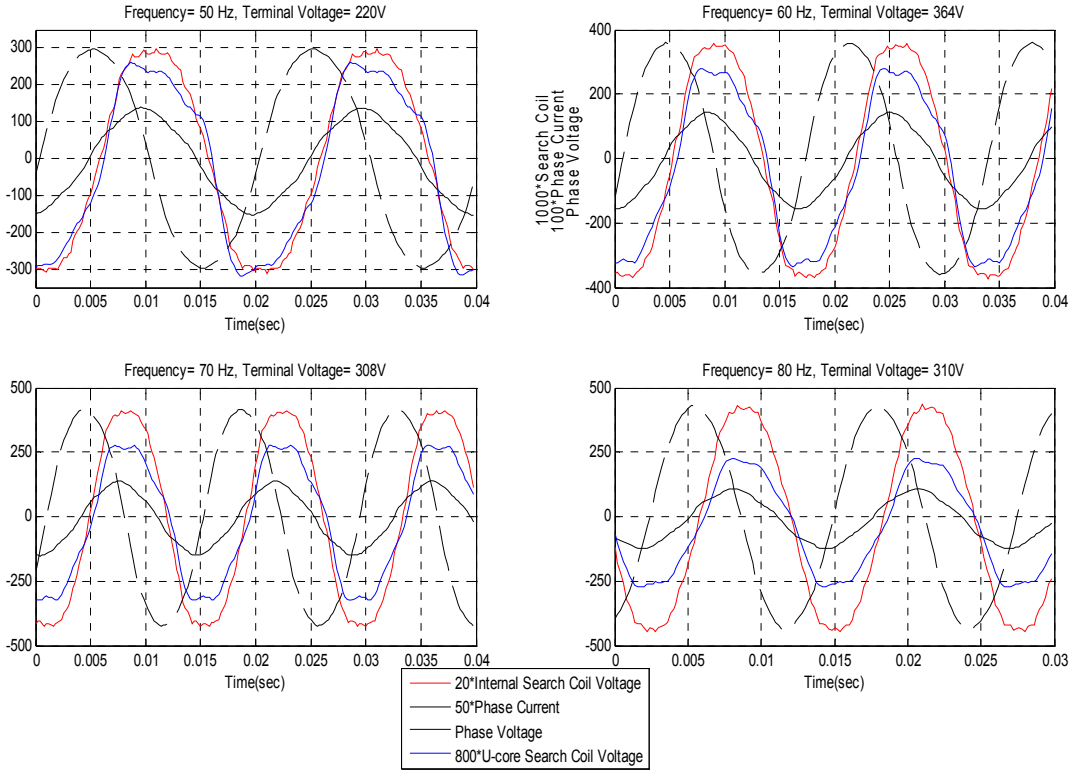

Fig. D-2 Waveforms of internal and external search coil with various stator frequencies (50 - 80 Hz) at no load

In the following graphs, the experimental data are represented together for a better understanding of induced search coil voltages with varying frequency at different load conditions. The lines connecting experiment data are plotted using parabolic interpolation.

Graphs are plotted for each load conditions as follows;

II) Induced external and internal search coil voltage magnitudes (rms)

III) Phase differences of the induced voltages and phase currents with respect to phase voltages (degree)

IV) Applied phase voltage and phase current magnitudes (rms)

V) Phase differences of the induced search coil voltages with respect to phase currents (degree)

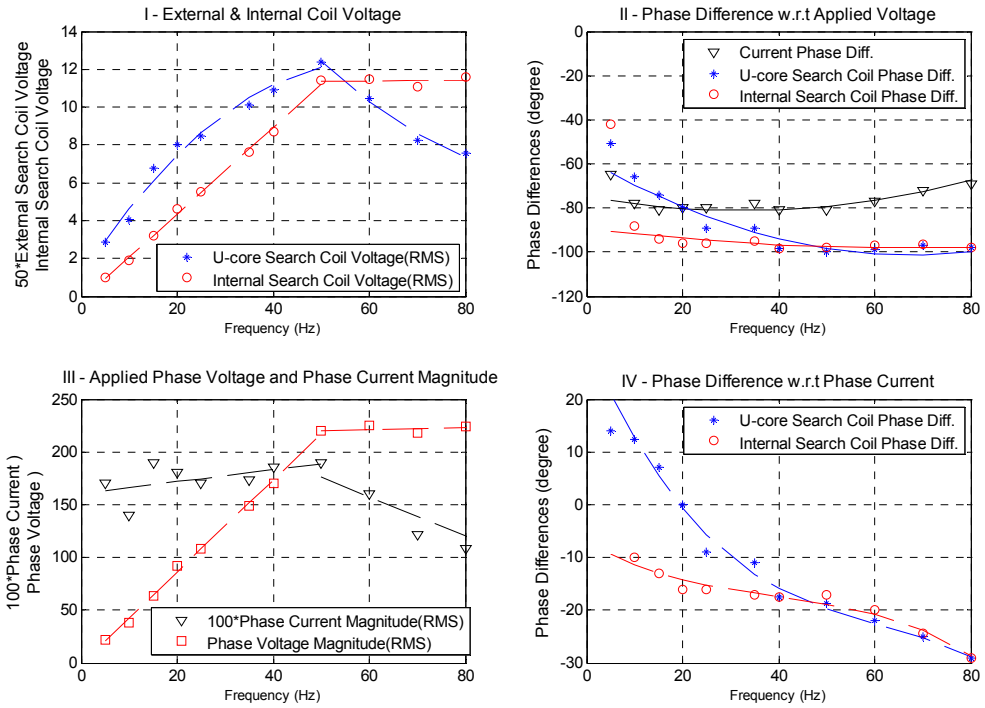

Fig. D-3 No load test at varying frequencies

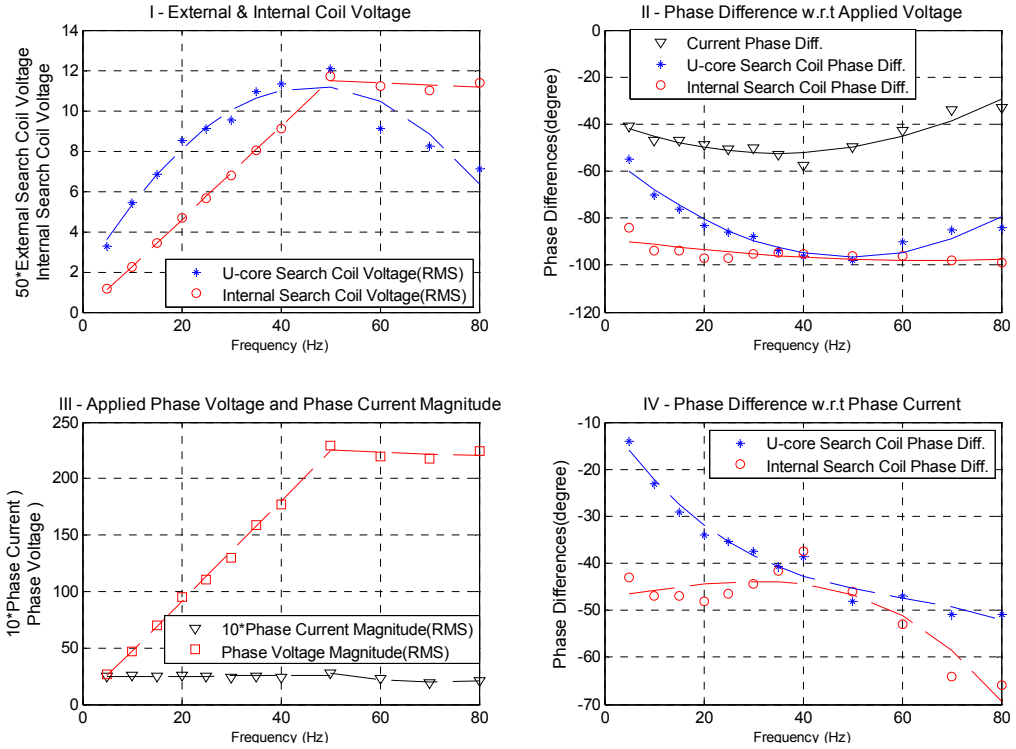

Fig. D-4 Half load test at varying frequencies

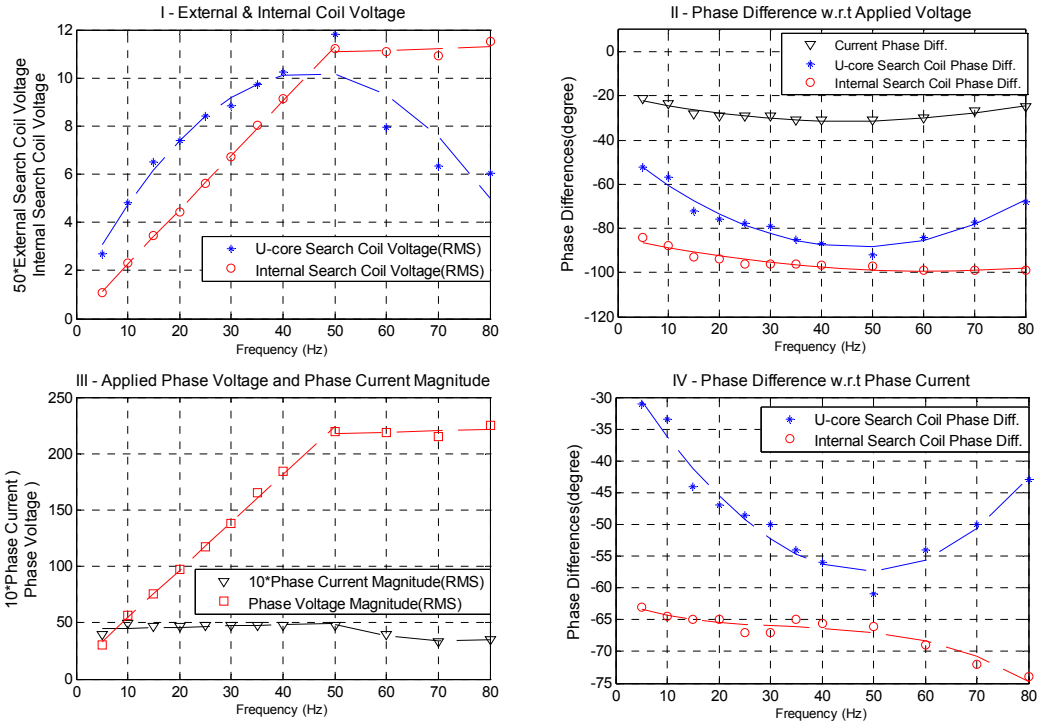

Fig. D-5 Full load test at varying frequencies

In order to see clearly, how the induced search coil voltages varies with the load; both no load, half load and full load condition data given in previous figures are collected together on the same graphs in Fig. D-6.

Graphs are plotted for as follows;

I) Induced internal search coil voltage magnitude (rms)

II) Phase difference of the internal coil induced voltages with respect to phase voltage (degree)

III) Induced external search coil voltage magnitude (rms)

IV) Phase difference of the external coil induced voltages with respect to phase voltage (degree)

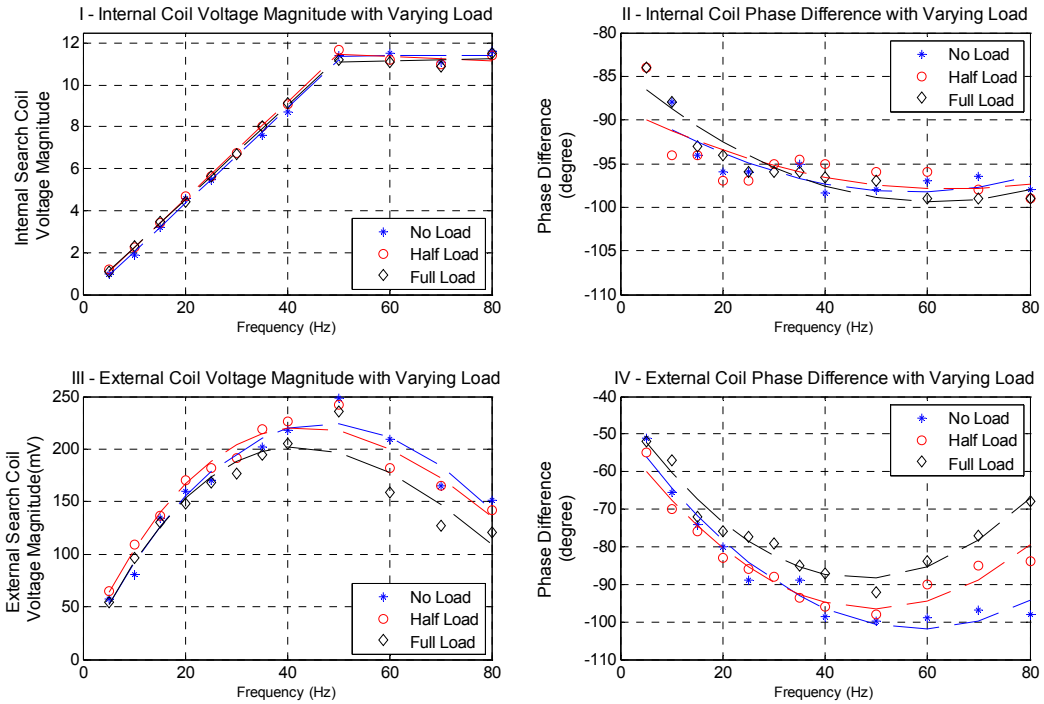

Fig. D-6 No load, half load and full load experiments with varying frequencies

The experiment data of the magnitude of fundamental and 3rd order harmonics of the induced external search coil voltage is presented in the following tables.

Table D-4 Estimated fundamental component magnitude of external search coil voltage for no load, half load and full load

Freq. (Hz)	No Load	Half Load	Full Load
10	0,14 /-62^0	0,16/-63^0	0,13/-63^0
15	0,21/-73^0	0,19/-73^0	0,18/-69^0
20	0,25/-80^0	0,23/-77^0	0,21/-76^0
30	0,24/-85^0	0,27/-88^0	0,25/-83^0
40	0,34/-96^0	0,32/-99^0	0,29/-86^0
50	0,37/-96^0	0,33/-101^0	0,30/-90^0
60	0,29/-93^0	0,24/-91^0	0,23/-79^0
70	0,24/-98^0	0,20/-89^0	0,18/-75^0
80	0,21/-94^0	0,18/-87^0	0,17/-62^0

Table D-5 Estimated 3rd order harmonic of external search coil voltage for no load, half load and full load

Freq. (Hz)	No Load	Half Load	Full Load
10	0,075 /-78^0	0,098/-76^0	0,073/-63^0
15	0,113 /-88^0	0,092/-87^0	0,090/-63^0
20	0,111 /-95^0	0,096/-90^0	0,090/-63^0
30	0,053 /-103^0	0,076/-101^0	0,077/-63^0
40	0,070 /-112^0	0,070/-113^0	0,067/-63^0
50	0,059 /-114^0	0,057/-117^0	0,053/-63^0
60	0,032 /-106^0	0,028/-113^0	0,028/-63^0
70	0,019 /-113^0	0,020/-110^0	0,016/-63^0
80	0,014 /-110	0,011/-112^0	0,010/-63^0

Table D-6 Induced external and internal search coil voltages for single phase excitation

	Phase Current (A)	Phase Voltage (V)	Internal Coil Voltage (mV)	External Coil Voltage (mV)
PHASE A	1	11	105 / -176^o	25 / -173^o
	2	20.6	198 / -177^o	44 / -179^o
	3	29.7	295 / -175^o	63 / -175^o
PHASE B	1	10.8	3.7 /? ^{o}	9.3 / -161 ^{o}
	2	19.7	4/ ?^{o}	17.1/ -157
	3	30.1	5.7/ -180^o	20 / -153
PHASE C	1	10.8	398 / +14	6 / +16
	2	20	770 / +14	11 / +23
	3	29.8	1150 / +13	15.4 / +31

APPENDIX E

HARDWARE PCB

In this part, PCB layouts of the designed hardware circuitry are given. The designed circuit consists of two boards; isolation board and measurement board.

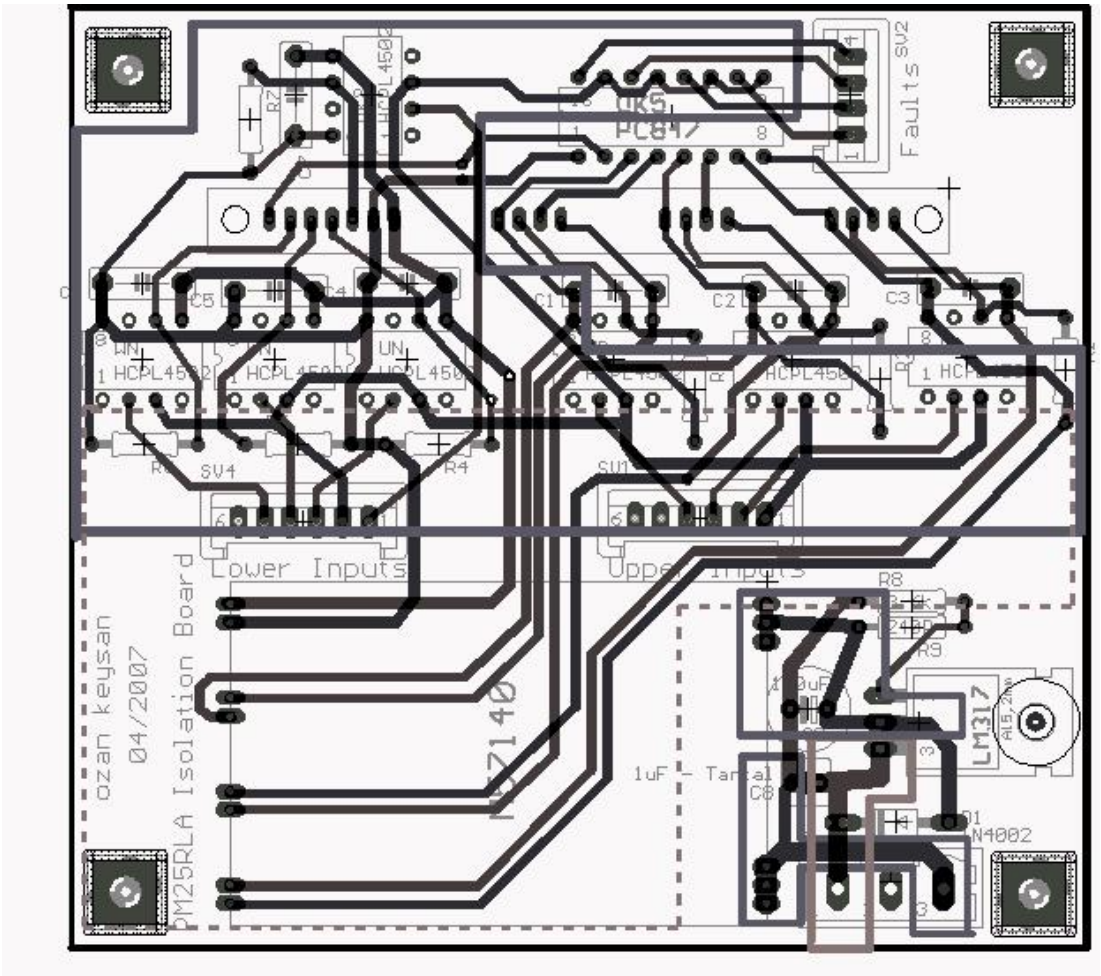

Fig. E-1 PCB layout of the isolation board

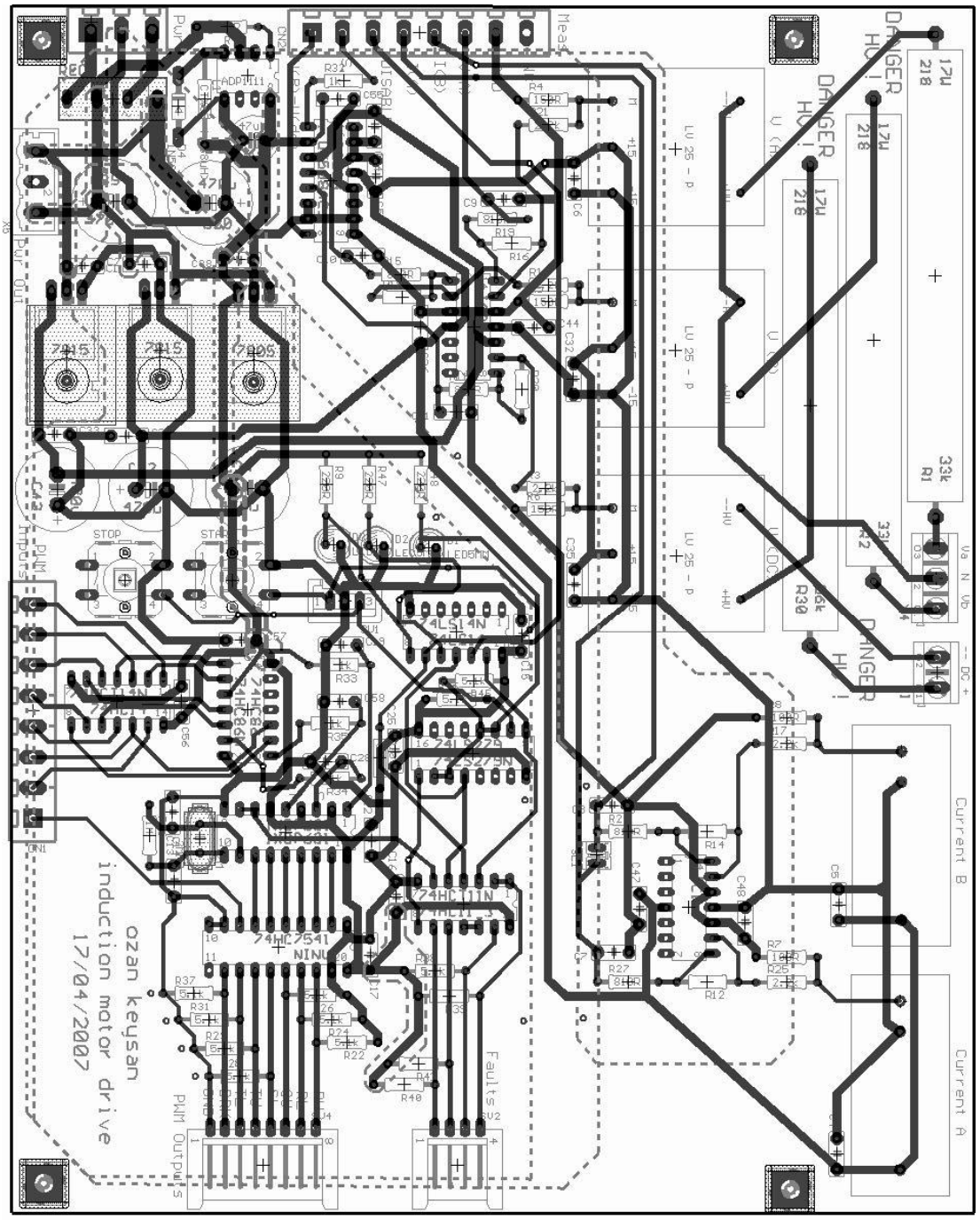

Fig. E-2 PCB layout of the data acquisition and measurement board

APPENDIX F

FIR FILTER BASICS

In this study one-dimensional digital FIR (Finite Impulse Response) filters are used. The filter is called finite impulse response because it settles to zero in a finite number of sample intervals [52]. A N^{th} order FIR filter can be defined with the difference equation or in convolution form (F-1).

$$y[n] = b_0x[n] + b_1x[n-1] + \cdots + b_nx[n-N] \qquad \text{(F-1)}$$

$$y[n] = \sum_{i=0}^{N} b_i x[n-i]$$

Where, y[n] is the output of the filter, x[n] is the input signal and b_i are the filter coefficients [52]. In Fig. F-1, the block diagram for a FIR filter is presented.

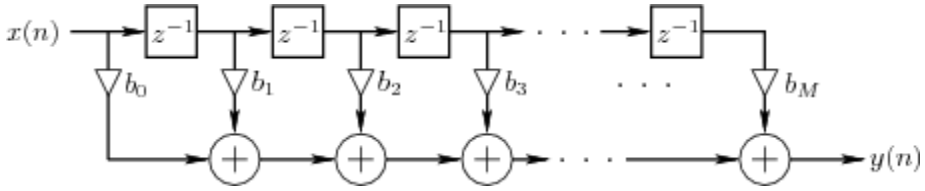

Fig. F-1 – The typical block diagram of a FIR filter

The filter constants (b_i) of a band-pass filter designed with MATLAB Filter Design Tool, with center frequency of 1150 Hz and 200 Hz bandwidth is as follows;

b[i] = [0.050, -0.070, 0.056, 0.014, -0.069, -0.094, -0.048, 0.019, 0.047, 0.015,
-0.040, -0.058, 0.017, 0.041, 0.056, 0.009, 0.050, -0.057, -0.004, 0.054
0.054, -0.004, -0.057, -0.050, 0.009, 0.056, 0.041, -0.017, -0.058, -0.040
0.015, 0.047, 0.019, -0.048, -0.094, -0.069, 0.014, 0.056, -0.070, 0.050]